The Role of Chemistry and Strut Porosity and the Influence of Serum Proteins in Modulating Cellular Response to Bone Graft Substitutes

by

Viviana Castagna

MSci Pharmaceutical Chemistry with Honours

For the fulfilment of the degree of

Doctor of Philosophy

Supervision

Dr. Karin A. Hing

Professor Alice C. Sullivan

Queen Mary University of London

School of Engineering and Material Science

Abstract

The objective of this thesis was to investigate the role of hydroxyapatite and silicate-substituted hydroxyapatite synthetic bone graft substitute (SBG) material properties in modulating the processes of protein adsorption and desorption, and their combined role in the subsequent regulation of cell attachment, proliferation and differentiation on the surfaces of these materials *in vitro*.

As a result of their purported role in promoting osteogenic behaviour *in vivo* the materials parameters selected for investigation were chemistry (stoichiometric hydroxyapatite (HA) versus 0.8wt% silicate-substituted hydroxyapatite (SA)) and strut porosity (20% versus 30% strut porosity). Cell attachment and response to different SBG was assessed to samples in the 'as received' condition as well as after a series of sequentially varied pre-treatments with solutions of phosphate buffered saline or cell culture media either unsupplemented or in combination with mixed serum proteins and/or Fibronectin (Fn). This enabled investigation of the effect of sample chemistry and strut porosity on mixed serum protein interactions and Fn adsorption under both competitive and non-competitive conditions, and the study of subsequent regulation of cell attachment and response as a consequence of pre-treatment.

Results showed that serum protein interactions were key to modulation of cell response to chemistry, and there was evidence that for Fn this may be related to conformational changes in the adsorbed protein rather than its level of enrichment in the protein interlayer.

In terms of the materials properties investigated strut porosity was found to be the most dominant factor in the regulation of cell response, where SBG with 30% strut porosity promoted human mesenchymal stem cell (hMSC) osteoblastic differentiation. Moreover hMSC response to SBG with 30% strut porosity seemed to be less sensitive to pre-treatment.

In conclusion, the results of these experiments indicate that strut porosity more directly influences the cellular response to HA and SA BGS than chemistry *in vitro*. Moreover, the role that Fn and other serum proteins have in regulating this response is dependent on the physiological environment and BGS chemistry.

Acknowledgements

I would like to thank my supervisors Dr Karin Hing and Professor Alice Sullivan for all their support and guidance throughout these four years. Through their supervision I was able to widen my knowledge and my perspective and approach to science. I will always be grateful of the opportunity that I have been given.

I would also like to thank my family for being, even if from far, always supportive and understanding throughout these hard years, and also a thank you to my special cousin Elodie, for having always been there, no matters what.

A final thank you goes also to my PhD colleagues Krystelle Mafina, Alan Parish and Nav Chana, for having made every day full of work, a cheerful day.

Statement of Originality

I confirm that all the work presented in this thesis is my own.

The experimental work presented in Chapters 4, 5 and 7 was performed within the School of Engineering and Materials at Queen Mary University of London while the experimental work presented in Chapter 6 was performed as a PhD student visiting Prof Barbara Boyan within the Biomedical Engineering Department at the Georgia Institute of Technology (USA).

Ms V Castagna

1 Table of Contents

List of Figures

List of Tables

1 Literature Review

1.1 Introduction

When tissues or organs have been so severely diseased or lost by cancer, congenital anomaly, or trauma that conventional pharmaceutical treatments are no more applicable, artificial organs (including tissues) or organ transplantation are the first choice to reconstruct the devastated tissues or organs. However, these surgical treatments have been facing a number of challenges at the moment (shortage of donor organs, presence of infectious agents to further complicate the transplants, immune rejection, and lastly very high costs). The term 'tissue engineering' was created about three decades ago to represent a new concept that focuses on regeneration of neotissues from cells with the support of biomaterials and growth factors. It is a multidisciplinary field involving biology, medicine and engineering with the aim to improve the health and quality of life of people by restoring, maintaining or improving tissue and organ functions.

It is raised from a dramatic improvement in the fields of biochemistry, molecular biology, genetics and material science and uses synthetic or naturally derived engineering biomaterials to replace damaged or defective tissues and organs such as bone and skin.

Tissue engineering can have either a therapeutic or a diagnostic application:

-therapeutic when the tissue is either grown in a patient or outside the patient and transplanted;

-diagnostic when the tissue is made in vitro and used for testing drug metabolism, uptake, toxicity or pathogenicity.

The specific tissue can be engineered in one of two ways:

- *In vivo:* stimulating the body's own regeneration response with the appropriate biomaterial
- *Ex vivo:* cells are expanded in culture, attached to a scaffold and then re-implanted into the host.

The way by which tissue engineering can reach its aim is by putting together several advanced technologies: large-scale culturing of human or animal cells

(like skin, bone, muscle, marrow, stem cells) may provide substitutes to replace damaged components in humans; natural or synthetic materials can be moulded into a “scaffold” that when implanted in the body allows the body’s own cells to grown and form new tissues while the scaffold is gradually adsorbed or removed; biomolecules as angiogenic factors, growth factors, differentiation factors and bone morphogenetic proteins to further stimulate the organ/tissue to growth. Biomedical engineering utilizes these basic three tools either simultaneously or not.

Examples of early tissue engineering studies include Wakitani that reported the repair of rabbit articular surfaces with allograft chondrocytes embedded in collagen gel (Wakitani et al., 1989) and the ones from Vacanti, in which he studied the cell transplantation using bioabsorbable synthetic polymers as matrices (Vacanti et al., 1988).

The reason why tissue engineering has become such a developed field is because it potentially reduces medical costs and offers great improvements in medical care for hundreds of thousands of patients annually.

For example organ transplants alone present many opportunities because of the significant shortage of donor organs. More than 10,000 people have died during the past five years while waiting for an organ transplant. Infectious agents such as hepatitis C and HIV further complicate the organ transplants, and recipients generally must remain on costly immunosuppressive drugs for the balance of their lives. Outcome studies have shown that the survival rates for major organ transplants are poor despite their high cost. "Engineered" replacement organs could sidestep many of the hazards and problems associated with donor organs, and at lower cost.

It is estimated that the cost of an implantable artificial liver, plus surgical procedures and follow-up could lead to a total saving of $720 million a year only in the US, with a higher survival rate and better quality of life for the patients. In fact, a tissue-engineered artificial liver is currently under development for temporary use (outside the body) until a permanent donor organ becomes available. Ultimately, it could become an implantable device totally replacing the need for donor organs if the remaining technical obstacles can be overcome.

Other equally promising applications include replacement of lost skin due to severe burns or chronic ulcers; replacement or repair of defective or damaged bones, cartilage, connective tissue, or intervertebral discs; replacement of worn and poorly functioning tissues such as aged muscles or corneas; replacement of damaged blood vessels; and restoration of cells that produce critical enzymes, hormones, and other metabolites.

However, though artificial organs and tissues have been improved by remarkable advances in the biomedical engineering in the past decade, they still need better biocompatibility and biofunctionality. Tissue engineers are still working hard on some of the big current challenges in the field such as:

- Making sure that immune acceptance is created. This problem is less pronounced with autologus cells, but allogenetic cells are needed when there is a need to make the engineered product widely available for routine use. It will be just as susceptible to immune response as allogeneic organ or tissue transplants and generally require immunosoppression
- Large scale production of tissue engineered products
- Preservation of the products so that it has a long shelf-life
- Ability to generate large, vascularised tissues that can easily integrate into the host's circulatory system.

1.2 Bone Tissue Engineering

As previously said, one of the early promising applications of tissue engineering was within the replacement, or repair, of defective or damaged bones. Soon after was then born Bone Tissue Engineering: an emerging interdisciplinary field which seeks to apply the principles of biology and engineering to address the needs for the development of viable substitutes that restore and maintain the function of human bone tissues. This form of therapy differs from standard drug therapy or permanent implants in that the engineered product can be:

-partially integrated within the patient, leading to a remodelling of the natural bone tissue;

-completely integrated within the patient, leading instead to a complete replacement of the natural bone tissue.

In both the cases, there is a potentially permanent and specific cure of the disease state.

Bone is a remarkable organ playing key roles in critical functions in human physiology including protection, movement and support of other important organs, blood production, mineral storage and homeostasis, blood pH regulation, multiple progenitor cells housing and others.

The importance of this tissue for the health of the whole body is highlighted by the presence of different and various bone-related diseases, like osteoarthritis, osteomyelitis and osteoporosis, and genetic abnormalities, like osteogenesis imperfecta. These represent only some of the cases in which the functional defect of the bone reflects pathological consequences in the body. If we also consider the relevance of traumatic injuries, orthopaedic surgeries and tumour resections it is clear how the clinical and economic impact of bone defects' treatments is worldwide astounding.

For example, the number of total joint arthroplasties and revision surgeries in the US has increased from 700,000 in 1998 to over 1.1 million in 2005. Medical expenses relating to fracture, reattachment, and replacement of hip and knee joint was estimated to be over $20 billion (USD) in 2003, and predicted to increase to over $74 (USD) billion by the year 2015 (Kurtz et al., 2007).

The safest and best way bone can healis by self-regeneration, which can occur as bone has an intrinsic ability to physiologically regenerate itself. However, for several reasons, sometimes injured or diseased bone may not be capable of repairing itself. In these cases the reconstruction of bone defects resulting from trauma, tumour, infections, biochemical disorders, or abnormal skeletal development is a clinical situation in which surgical intervention is required. The types of graft materials available to treat such problems essentially include autologous bone (from the patient), allogeneic bone (from a donor), demineralised bone matrices, as well as a wide range of synthetic biomaterials such as metals, ceramics, polymers, and composites.

Until recently, the use of autologous bone grafts has been the number one choice for bone repair and regeneration (Damien and Parsons, 1991)(Yaszemski et al., 1996) (Coombes and Meikle, 1994). A patient's own bone lacks immunogenicity and provides bone-forming cells, which are directly delivered at the implant site. Moreover, autologous bone grafts recruit mesenchymal cells and induce them to differentiate into osteogenic cells through exposure to osteoinductive growth factors (Lane et al., 1999).

Although there are many advantages to using autologous bone, there are major drawbacks to the harvesting procedure, and for centuries there has been a search for alternatives.

1.3 Bone structure and composition

Bone is a complex, highly organized and specialized connective tissue that is continuously being broken down and restructured in response to such influences as structural stress or the body's requirement for calcium.

It is characterized physically by the fact that it is a tissue hard, rigid and strong, and microscopically by the presence of relatively few cells and much intercellular substance formed of collagen fibers and inorganic stiffening substances.

It is important to understand this complex structure in detail in order to comprehend how the complex process of bone healing occurs when fractures heal. Furthermore, only by understanding the biomechanical and biological properties of bone it's then possible to develop bone grafts or bone substitutes able to reconstruct large defects of human bone.

1.3.1 Macroscopic analysis

The skeleton serves a variety of functions. The bones of the skeleton provide structural support for the rest of the body, permit movement and locomotion by providing levers for the muscles, protect vital internal organs and structures, provide maintenance of mineral homeostasis and acid-base balance, serve as a reservoir of growth factors and cytokines, and provide the environment for hematopoiesis within the marrow spaces (Taichman, 2005).

Bones are divided into four types based on their shape: long, short, flat and irregular bones. In the present paragraph, I will focus on the anatomy and physiology of long bones.

Long bones have various regions within them: we can identify two end regions called **epiphyses,** two corn-shaped **metaphyses** below them and one middle region called **diaphysis**; the region where the epiphysis and the diaphysis meet is a disk-shaped region called **epiphyseal disk** (Figure 1-1).

As the bone is a hard tissue, to make contact between other bones at the level of the joints it is coated at the end of each epiphysis with **articular cartilage**: this is a coating of hyaline cartilage which contains mostly collagen (primarily type II), glycosaminoglycans, water, glycoproteins and hyaluronic acid.

Except at joints, all bones are covered in a thin membrane called **periosteum**which is made up of dense connective tissue which contains a lot of collagenous fibers and also many cells (Figure 1-1). The periosteum is tightly attached to the outer cortical surface of bone by thick collagenous fibers, called **Sharpeys' fibers**, which extend into underlying bone tissue.

The **endosteum** is a membranous structure covering the inner surface of cortical bone, trabecular bone, and the blood vessel canals (Volkman's canals) present in bone. The endosteum is in contact with the bone marrow space (which can be either red marrow where blood is made or yellow marrow where fat is deposited), trabecular bone, and blood vessel canals and contains blood vessels, osteoblasts, and osteoclasts.

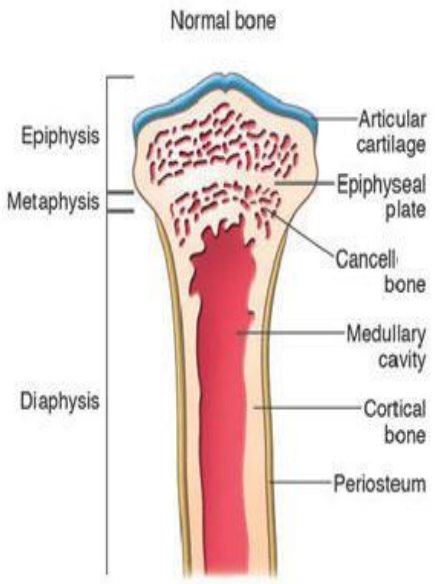

Figure 1-1*: **The different regions and characteristics of long bones*** **(Glorieux, 2005)**

Macroscopically it is possible to identify two structurally different types of bone (Tortora and Derrickson, 2008):

• **Cortical** (or compact) bone: it forms the hard outer, smooth layer of bones. It accounts for the 80% of the total bone mass of an adult skeleton and gives bones their white, solid appearance. This structure resists to tensile stresses (Figure 1-2).

• **Cancellous** (or spongy, or trabecular) bone: highly porous, it represents the inner part of mature bones and, even if accounts for the remaining 20% of total bone mass, has almost ten times the surface area of cortical bone. This structure resists compression stresses (Figure 1-2).

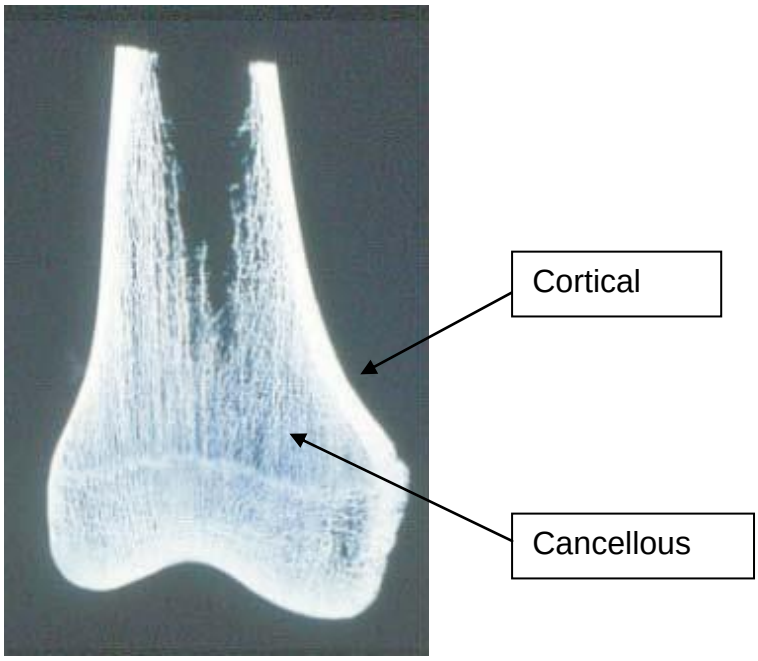

Figure 1-2 ***Radiological appearance of cancellous and cortical bone***

The adult human skeleton is composed of 80% cortical bone and 20% cancellous bone on the overall mass, however the last one has nearly ten times the surface area of the cortical bone (Eriksen et al., 1994). The diaphysis is composed primarily of dense cortical bone, whereas the metaphysis and epiphysis are composed of trabecular meshwork bone surrounded by a relatively thin shell of dense cortical bone.

Cortical or compact bone is dense and solid and surrounds the marrow space. Both cortical and cancellous bone are composed of **osteons**. Cortical osteons, also called **Haversian systems** (Tortora and Derrickson, 2008)**,** represent the fundamental functional unit of much compact bone (Figure 1-3). Each Haversian System is cylindrical in shape, is approximately 400 mm long, 200 mm wide and 0.2 mm in diameter. They form a branching network within the

cortical bone running parallel to the long axis of the diaphysis. The walls of Haversian systems are formed of concentric **lamellae**, which in the centre present the **Haversian canal**. This contains blood vessels, nerves and loose connective tissue. Surrounding each canal are 4–20 concentric lamellae of collagen fibres. The Haversian canals are round or oval in cross-section. They generally run in a longitudinal direction (Figure 1-3). Between adjoining osteons, there are angular intervals that are occupied by **interstitial lamellae**. These lamellae are remnants of osteons that have been mostly destroyed. Near the surface of the compact bone, the lamellae are arranged parallel to the surface; these are called **circumferential lamellae**.

Each osteon communicates with the marrow cavity, the periosteum and with each other through transverse or oblique canals: the **Volkmann's canals** (Tortora and Derrickson, 2008) (Figure 1-3). The **osteocytes** are arranged circumferentially around the central canal in parallel with the lamellae and are interconnected by fine processes of osteocyte cytoplasm: the **filopodia**. The osteocytes are housed in **lacunae** interconnected by **canaliculi** containing these fine cytoplasmic processes.

Irregular areas of compact bone are present between the Haversian Systems: **interstitial lamellae**. These are remnants of previous Haversian systems which have been remodelled.

Each osteon is separated from its neighbour and from interstial lamellae by a **cement line** which stains darkly with Haematoxtylin. The outermost and innermost layers of cortical bone contain no Haversian canals, and the lamellae are arranged parallel with the periosteal and endosteal surfaces to form the so-called **circumferential lamellae** (outer and inner circumferential lamellae).

Cancellous or spongy bone consists of a series of interconnecting plates of bone: the **trabeculae** (Tortora and Derrickson, 2008) (Figure 1-3). Each bone trabecula contains collagen fibres arranged in parallel lamellae. Trabeculae are similar to osteons in that both have osteocytes in lacunae that lie between calcified lamellae. As in osteons, canaliculi present in trabeculae provide connections between osteocytes. However, since each trabecula is only a few

cell layers think, each osteocyte is able to exchange nutrients with nearby blood vessels. Thus, no central canal is necessary.

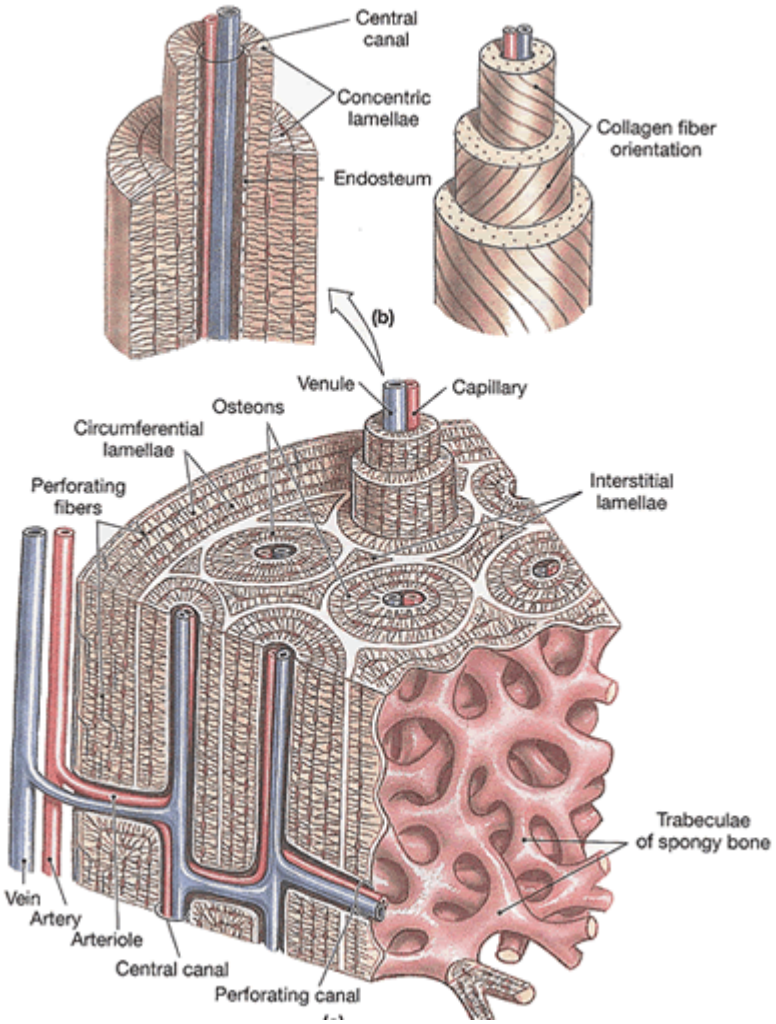

Figure 1-3*: **Hierarchical structure of a long bone***

1.3.2 Microscopic analysis

At the microscopic level, bone consists of:

- **bone cells**
- **extracellular matrix** { **organic** / **inorganic**

The majority of bone is made of the bone matrix which has inorganic and organic parts. The inorganic part is composed of poorly crystalline salts and bone mineral crystals. The organic part is composed of collagen fibrils and non-collagenous proteins.

The rest of the bone is made up of bone cells, which are classified in three different types: osteoblasts, osteoclasts and osteocytes (

Figure 1-4).

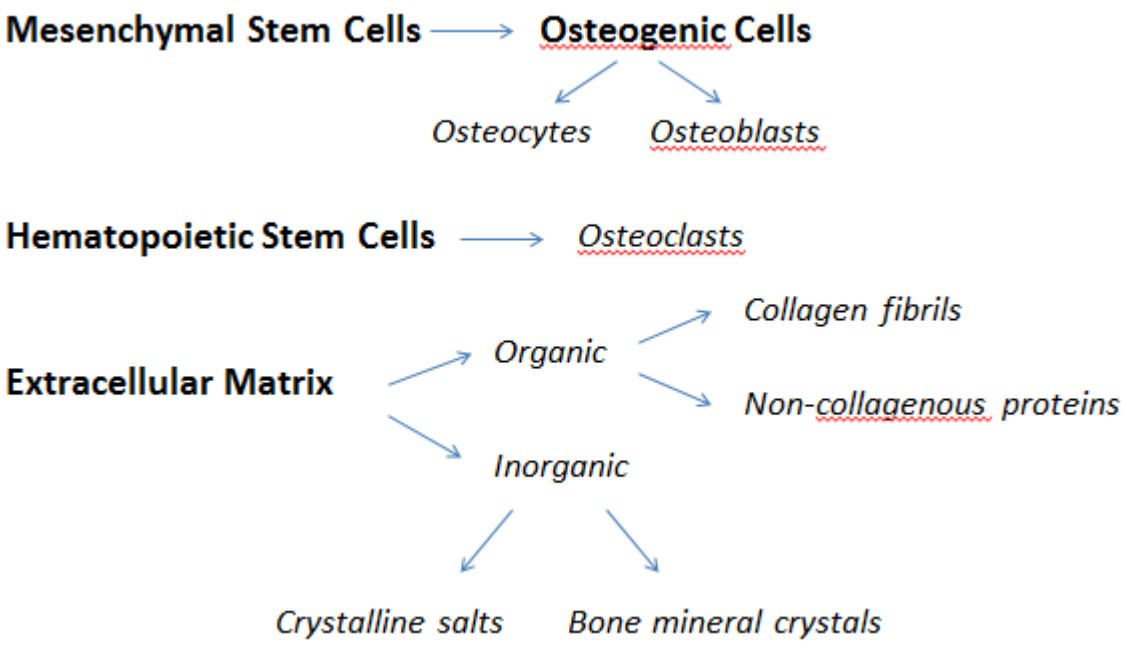

Figure 1-4: Microscopic composition of normal bone

1.3.3 Bone cells

Bone is a type of tissue in constant remodeling. To be able to do this, it needs different kind of cells finely regulated to give the right ratio of building up/breaking down of bone.

The primary source of bone cells is the **Bone Marrow**, which contains mesenchymal stem cells (MSCs) and hematopoietic stem cells (HSCs) that take part in important physiological processes.

Mesenchymal stem cells: The main source of MSCs, as said, is the bone marrow. They are progenitors of different cells type, which also give rise to and maintain:

- the osteoblasts that synthesize new bone matrix on bone forming surfaces;
- the osteocytes within bone matrix that support bone structure;
- cartilaginous cells (chondrocytes), fat, muscle and fibrous connective tissues

They reside in the loose connective tissue between trabeculae, along vascular channels, and in the condensed fibrous tissue covering the outside of the bone (Pittenger et al., 1999)

Osteoblasts: being the bone forming cells, they directly participate to the new bone formation. The bone is essentially enveloped by the osteoblasts, since the cells are in close contact with one another and tight junctions and gap junctions have been observed. Thus, the osteoblastic layer controls the transport of materials from the extracellular space to the osteoid seam and mineralization front. When quiescent they present a flattered morphology, while when active they present a cubical one. Ultra structurally, osteoblasts feature a complement of organelles which is characteristic of cells actively involved in protein synthesis. They have abundant endoplasmic reticulum and numerous ribosomes, and the Golgi apparatus and mitochondria are quite prominent. Procollagen molecules are produced by the ribosomes and extruded into the extracellular space, but only along the surface that faces bone.

Their proteolysis and polymerization within the extracellular space result in the formation of collagen fibrils. The combination of these intracellular and extracellular events leads to the production of the osteoid seam. As previously mentioned, proteoglycans are also present in the extracellular matrix: they are packaged in the Golgi apparatus, and vesicles containing these products migrate to the surface of the cell and release their contents by exocytosis. The combination of proteoglycans and collagen fibers results in the production of a mineralizable matrix for which these cells are responsible (Young, 1963).

When active, osteoblasts show high alkaline phosphatase activity. Alkaline phosphatase is thought to act as a pyrophosphatase and may be involved in the initiation of the mineralization process.

Osteocytes: Approximately 10% of the osteoblastic population becomes enclosed in the developing matrix: when this happen, cells are then referred to as osteocytes. They have structural features very similar to when they were osteoblasts, but the endoplasmic reticulum may not be so profuse. As the cells become more deeply embedded in the mineralized bone matrix, their cytoplasmic volume reduces, as does their complement of cytoplasmic organelles. They occupy the lacunae in the bone matrix and possess long, thin cytoplasmic processes (the **filopodia**) located in thin, cylindrical spaces or canals in the bone matrix (the **canaliculi**). Tight gap junctions are present at this level: both from the osteocytes deeper towards the inside of the bone, and from the osteoblasts more superficially towards the external part of the bone. These junctions are present in order to regulate the flow of mineral ions from the extracellular fluid to the osteocytes passing through the osteoblasts, from the osteocytes to the extracellular fluid surrounding them, and finally from this fluid to the mineralized bone matrix. Thus, the large surface area provided by the osteocytic population results in a regulatory

mechanism for the exchange of mineral ions between the extracellular fluid and bone, by means of the canalicular system (Bonewald, 1999).

Osteocytes do not normally express alkaline phosphatise but do express osteocalcin, cell adhesion receptor for hyaluronate, and several matrix proteins that support intercellular adhesion and regulate the exchange of mineral in the bone fluid within lacunae.

The primary function of the osteocyte-osteoblast lining cell syncytium is mechanosensation (Rubin and Lanyon, 1987). Osteocytes transducer stress signals from bending of bone into biologic activity. Following stimuli from external forces, the flow of canalicular fluid induces a variety of responses within osteocytes. Rapid fluxes of bone calcium across filipodial gap junctions, for example, are believed to stimulate transmission of information between osteoblasts on the bone surface and osteocytes within the bone (Jørgensen et al., 2003). Moreover, it has been evaluated the possibility that osteocytes could remove and replace bone, process known as “osteocytic osteolysis”, which assumes that also this cell type, together with osteoclasts, could participate in the remodelling process (Liu et al., 2012)(Qing et al., 2012).

Chondrocytes: They are the only cells found in cartilage. They produce and maintain the cartilaginous matrix, which consists mainly of **collagen** (type II) and **proteoglycans.** They also are fundamental for a number of functions within the cartilage, for example facilitating the exchange of fluids through the gelatinous layers which make up cartilage. Because cartilage lacks vascularisation, it relies on this exchange to receive nutrients and eliminate waste materials (Culav et al., 1999).

These cells are risen from the bone marrow: after stem cells differentiate into cartilage cells, they start out as chondroblasts that actively produce chondrin (primary substance in cartilage) to

build up and repair cartilage. Once a chondroblast becomes totally surrounded, it is a mature chondrocyte.

Fully mature chondrocytes tend to be round, and they may cluster together in small groups within the network of the cartilage. They are not capable of cell division (DeLise et al., 2000).

Bone marrow contains not only mesechymal stem cells but also hematopoietic stem cell population that gives rise to osteoclast cells and blood cell lineages.

The function of these precursor cells is of fundamental importance for the proper differentiation in each specific cell lineage in the bone.

Osteoclasts: Osteoclasts are found in sites where bone has been remodelled. They are large, multi-nucleated cells formed by fusion of monocytes that lie on, or near, bone surface in shallow depressions called the **Howship's lacunae**.

The size and number of nuclei in osteoclasts vary, but each nucleus usually is associated with a perinuclear Golgi apparatus, in which Golgi vesicles are found in all stages of development. The cytoplasm is filled with vacuoles and small vesicles. There is little endoplasmic reticulum and few ribosomes, and mitochondria are present in much greater number than in osteoblasts. The zone of contact of the plasma membrane with the bone surface consists of two areas: the ruffled border and the sealing area. The ruffled border comprises finger-like membranous folds that extend varying distances into the cytoplasm, while the sealing area is characterized by a very dense homogeneous cytoplasm that surrounds the site of active bone resorption, namely, the ruffled border (Vaananen et al., 2000).

Bone resorption depends on osteoclast secretion of hydrogen ions and cathepsin K enzyme. H^+ ions acidify the resorption compartment beneath osteoclasts to dissolve the mineral component of bone matrix, whereas cathepsin K digests the

proteinaceous matrix, which is mostly composed of type I collagen.

Binding of osteoclasts to bone matrix peptides (*via* β1 family of integrin receptors in the osteoclast membrane) causes them to become polarized. During this event the osteoclast resorbing surface develops a ruffled border that, when acidified, forms vesicles which contain matrix metalloproteinases and cathepsin K. These vesicles, transported *via* microtubules, are then fused with the membrane. The cell's ruffled border secretes H^+ ions *via* H^+-ATPase and chloride channels, and causes exocytosis of cathepsin K and other enzymes in extracellular matrix (Teitelbaum et al., 1995).

Upon contact with bone matrix, the fibrillar actin cytoskeleton of the osteoclast organizes into an actin ring, which promotes formation of the sealing zone around the periphery of osteoclast attachment to the matrix. The sealing zone surrounds and isolates the acidified resorption compartment from the surrounding bone surface (Vaananen et al., 2000). Disruption of either the ruffled border or actin ring blocks bone resorption.

1.3.4 Bone matrix

As previously mentioned, osteoblasts synthesize the bone matrix, which is the material located between the cells. This intercellular substance contains large quantities of both proteins (around 30%) and inorganic components (around 70%) (Tortora and Derrickson, 2008). Their presence and combination provides the bone with its typical mechanical properties such as elasticity, toughness, hardness.

Organic matter: its weight is composed by 85% to 90% of collagenous proteins (Brodsky and Persikov, 2005), which consist of type I collagen fibers embedded in the ground substance containing proteoglycans and glycoproteins. There are also trace amounts of collagen type III, V and FACIT at certain stages of bone formation. FACIT collagen is a member of the family of Fibril-Associated Collagens with Interrupted Triple Helices, a non-fibrillar collagen which serves as molecular bridge important for the organization and stability of extracellular matrices. Members of this family include collagens IX, XII, XIV, XIX, XX, and XXI. The collagen fibers are made up of bundles of fibrils to resist pulling forces: it's thanks to these fibers that bone presents its typical characteristics of flexibility, bending resistance, elasticity and resistance to tension stress (Van Apeldoorn et al., 2005).

The remaining 10% to 15% of organic matter consists of non-collagenous proteins. Osteoblasts synthesize and secrete as much non-collagenous proteins as collagen on a molar basis. The non-collagenous proteins are divided broadly into several categories, including proteoglycans, glycosylated proteins, glycosylated proteins with potential cell-attachment activities, and γ-carboxylated (gla) proteins. The roles of each of the bone proteins are not well defined at present, and many seem to serve multiple functions, including regulation of bone mineral deposition and turnover and regulation of bone cell activity. The most prevalent non-collagenous protein in bone is osteonectin, accounting for approximately 2% of total protein in normal bone.

Osteonectin is thought to affect osteoblasts growth and/or proliferation, and matrix mineralization (Tortora and Derrickson, 2008).

Inorganic matter: The mineral content of bone is a Calcium/Phosphate with structure similar to hydroxyapatite [$Ca_{10}(PO_4)_6(OH)_2$], with trace amounts of different ions like carbonate, magnesium, sodium, or potassium. Compared with geologic hydroxyapatite crystals, bone hydroxyapatite crystals are smaller, measuring only approximately 200 Å in their largest dimension. These small, poorly crystalline crystals are more soluble than geologic hydroxyapatite crystals, characteristic which allows them to more easily support mineral metabolism (Robinson, 1952). The inorganic components give to the bone essential characteristics like hardness, rigidity, load-bearing strength and resistance in compression stress (Van Apeldoorn et al., 2005).

Inorganic matrix maturation is associated with expression of alkaline phosphatase and several non-collagenous proteins, including osteocalcin, osteopontin, and bone sialoprotein. It is thought that these calcium- and phosphate-binding proteins help regulate ordered deposition of mineral by regulating the amount and size of hydroxyapatite crystals formed.

The process of matrix formation is facilitated by the presence of extracellular matrix vesicles secreted by osteoblasts: these vesicles serve as protected microenvironments in which calcium and phosphate ions can reach a sufficiently high concentration in order to promote crystal's precipitation and consequently bone formation. In the extracellular fluid this wouldn't normally happen because this environment is not normally supersaturated with calcium phosphate ions. These extracellular matrix vesicles contain a nucleational core that is composed of proteins and a complex of acidic phospholipids, calcium, and inorganic phosphate, which promote hydroxyapatite crystals' precipitation.

As bone matures, hydroxyapatite crystals enlarge and reduce their level of impurities. Crystal enlargement occurs by both crystal growth and aggregation. Bone matrix macromolecules may facilitate initial crystal nucleation by sequestering mineral ions to increase local concentrations of calcium and/or phosphorus, or by facilitating heterogeneous nucleation. Macromolecules also bind to growing crystals' surfaces to influence the size, shape, and number of crystals formed (Landis, 1995).

1.4 Pattern of growth, modeling and remodeling

To understand in which way a bone-graft could be of help in the case of severe bone injury is necessary to understand which are the physiological processes for grow and remodeling of normal bone.
It is therefore important to underline the different aspects between bone growth and bone modeling and remodeling.

Even before bone growth, precisely during the fetal development of the skeletal system, two types of bone histogenesis namely intra-membranous ossification and endochondral ossification occur (Palastanga et al., 2006).
Intra-Membranous Ossification occurs in flat bones such as the skull or the scapula. In this process, the bone is developed from a condensation of mesenchymal tissue: the ossification centre. The cells within this tissue differentiate directly into osteoblasts which spontaneously synthesize osteoids which then undergo mineralization.
Endochondral Ossification occurs in long bones and short bones. This process involves initial formation of cartilage and later replacement by bone. A part for the fetal development of the skeletal system, this process is also essential for the elongation of long bones and the natural healing of bone fractures.
During endochondral ossification, some transcription factors (Sox9, Sox5 and/or Sox6) are expressed and are involved in the induction of chondrocytes in the growth plate (de Crombrugghe et al., 2001). The pre-hypertrophic

chondrocytes mature into hypertrophic chondrocytes, which lay down a matrix rich in Collagen X and secrete VEGF (Gerber et al., 1999). VEGF promotes the invasion of blood vessels from the perichondrium, bringing in both the bone forming osteoblasts and the bone resorbing osteoclasts. The hypertrophic chondrocytes then undergo apoptosis, and are replaced by trabecular bone and bone marrow.

Bone growth occurs during childhood and adolescence, and it is both longitudinal and radial. Longitudinal growth occurs at the growth plates, where cartilage proliferates in the epiphyseal and metaphyseal areas of long bones, before subsequently undergoing mineralization to form primary new bone.

Bone modelling is the process in which bones change their shape, letting the skeleton being gradually adjusted in response to biological or mechanical forces. Wolff's law describes the observation that long bones change shape to accommodate stresses placed on them (Wolff, 1870). These biological and/or mechanical stresses basically activate the simultaneous action of osteoblasts and osteoclasts which, by not-coupled bone formation and resorption processes, will cause a change in bone axis. Bone modelling is less frequent than remodelling in adults, and may be increased during some pathologies such as hypoparathyroidism (Ubara et al., 2003), renal osteodystrophy (Ubara et al., 2005), or treatment with anabolic agents (Lindsay et al., 2006).

Bone remodelling is the process by which bone is renewed to maintain its strength and mineral homeostasis. Remodelling involves removal of discrete packets of old bone, replacement of these packets with newly synthesized proteinaceous matrix, and subsequent mineralization of the matrix to form new bone. The remodelling process resorbs old bone and forms new bone in order to prevent accumulation of bone micro damage. Remodelling begins before birth and continues until death. The bone remodelling unit is composed of a tightly coupled group of osteoclasts and osteoblasts that sequentially carry out the processes of resorption and bone formation (Burr, 2002)(Parfitt, 2002).
The remodelling process is essentially the same in cortical and trabecular bone, and is composed of four steps: activation, resorption, reversal and

formation. Remodelling sites may develop randomly but are also targeted to areas that require repair.

Activation involves recruitment and activation of mononuclear monocyte-macrophage osteoclast precursors from the circulation (Roodman, 1999), lifting of the endosteum that contains the lining cells off the bone surface, and fusion of multiple mononuclear cells to form multinucleated preosteoclasts. Preosteoclasts bind to bone matrix via interactions between integrin receptors on their cell membranes and RGD-containing peptides in matrix proteins, to form annular sealing zones around bone-resorbing compartments beneath multinucleated osteoclasts.

Osteoclast-mediated bone resorption takes only approximately 2 to 4 weeks for each remodeling cycle. Resorbing osteoclasts secrete hydrogen ions via H^+-ATPase proton pumps and chloride channels on their cell membranes. These ions are pumped into the resorbing compartment in order to lower the pH to a level as low as 4.5, which will help mobilize bone mineral (Silver et al., 1988). A part for acting via a chemical attack, osteoclasts also secrete biological molecules like tartrate-resistant acid phosphatase, cathepsin K, matrix metalloproteinase 9, and gelatinase in order to digest the organic matrix (Delaissé et al., 2003). These molecules are secreted from cytoplasmic lysosomes. The resorption phase is completed by mononuclear cells after the multinucleated osteoclasts undergo apoptosis (Eriksen, 1986).

The reversal phase represents the transition from bone resorption to bone formation. At the completion of bone resorption, resorption cavities contain a variety of mononuclear cells, including monocytes, osteocytes released from bone matrix, and preosteoblasts recruited to begin new bone formation. The coupling signals linking the end of bone resorption to the beginning of bone formation are as yet unknown. Proposed coupling signal candidates include bone matrix-derived factors such as TGF, IGF-1, IGF-2, bone morphogenetic proteins, PDGF, and fibroblast growth factor (Bonewald and Mundy, 1990)(Hock et al., 1988) (Locklin et al., 1999). The reversal phase has also

been proposed to be mediated by the strain gradient in the lacunae (Smit et al., 2002) and by the osteoclasts themselves (Martin and Sims, 2005).

Bone formation takes approximately 4 to 6 months to complete. Osteoblasts synthesize new collagenous organic matrix and regulate mineralization of matrix by releasing small, membrane-bound matrix vesicles that concentrate calcium and phosphate, and enzymatically destroy mineralization inhibitors such as pyrophosphate or proteoglycans (Anderson, 2003). Osteoblasts surrounded by and buried within matrix become osteocytes with an extensive canalicular network connecting them to bone surface lining cells, osteoblasts, and other osteocytes. The osteocyte network within bone serves as a functional syncytium. At the completion of bone formation, approximately 50 to 70% of osteoblasts undergo apoptosis, with the rest becoming osteocytes or bone-lining cells.

The final result of each bone remodeling cycle is the production of a new osteon with the aimed preservation of bone mechanical strength and biological functions and ions homeostasis. The relatively low adult cortical bone turnover rate of 2% to 3% per year is adequate to maintain biomechanical strength of bone. The rate of trabecular bone turnover is higher, more than required for maintenance of mechanical strength, indicating that trabecular bone turnover is more important for mineral metabolism. Increased demand for calcium or phosphorus may require increased bone remodelling units, but, in many cases, this demand may be met by increased activity of existing osteoclasts. Ongoing bone remodeling activity ensures a continuous supply of newly formed bone that has relatively low mineral content and is able to exchange ions more easily with the extracellular fluid.

During fracture healing a modified version of endochondral ossification often occurs, which is characterised by a 5-step process:

-Firstly, the injury to the periosteum and to local soft tissue promotes the formation of an haematoma (blood clot). The periosteum is the fibrous membrane that covers most bone surfaces containing blood vessels which

nourish the bone and also act as an attachment point for tendons and muscles.

-As a consequence of this disruption in the blood supply, osteocytes nearest to the fracture die, resulting in local necrosis of the bone around the fracture. Simultaneously, there is a demand for the repair of the bone, the stabilization of the damaged area and the removal of the dead tissue.

-To remove tissue debris and to rapidly express extracellular matrix, the bone requires the activity of macrophages and fibroblasts, and osteoblast and chondrocytes respectively.

In addition, mesenchymal stem cells are recruited to differentiate into osteoprogenitor cells and periosteum.

-This leads to an apparent thickening of the periosteum and the production of a callus around the fracture site. The callus is a bony and cartilaginous formation across a bone fracture which happens during bone repair. Those osteoprogenitor cells that lie close to undamaged bone (and are thus within reach of a ready supply of oxygen) differentiate into osteoblasts and form an osteoid which is rapidly mineralized into bone, while those farther away become chondroblasts and form cartilage. Angiogenesis is induced concurrently, capillaries are formed, and osteoclasts and osteoprogenitor cells invade now the cartilaginous callus.

-The cartilaginous material is resorbed and new bone is deposited. The woven bone (immature bone, in which collagen fibers are arranged in irregular random arrays and contains smaller amounts of mineral substance) is then remodelled into lamellar bone (in which the tubular lamellae are formed, characterized by parallel spirally arranged collagen fibers) and the process is completed by the return of normal bone marrow within cancellous regions (Mackie et al., 2008).

1.5 The importance of calcium in bone homeostasis

Calcium is one of the most important ions present in the body and the most abundant (Intakes and others, 1997). It plays fundamental roles in many different cellular functions and is essential for the activity of different proteins, enzymes, pumps. Some examples are its role in blood clotting, in stabilizing blood pressure, in the contribution to the normal brain functions, or for the communications between cells. Because of its vital role in many different activities, the body has its own calcium “reservoir” which is represented by bones: here is where calcium intake is stored, and from where it is collected when the body is in need, all of this in the processes of old bone resorption and new bone formation. To mediate this events there are specific hormones, which finely regulate the levels of calcium in the blood to be readily available for the cells to help them to perform various fundamental activities such as: the regulation of the amount of glucose entering inside the cells, the release of chemicals needed for the signal transmissions between nerves and target cells, the process of muscle cell contraction, or the support to the movement of sperm into an egg to fertilize it. The body can do this in three different ways: by decreasing the urinary excretion of calcium from the kidneys, by adjusting the absorption of calcium from the diet, and by withdrawing calcium from bones (Intakes and others, 1997). These hormones are: Parathyroid Hormone (PTH), Calcitriol and Calcitonin. Seen the major role that calcium plays in the body and that bone represent its main calcium “reservoir”, it’s clear how the presence of this ion can affect processes like bone formation and resorption. Therefore, different studies have been looking at how calcium affects the cell response during bone formation. It has been extensively shown that the presence of calcium supports cell proliferation and differentiation in bone remodelling, and that this could be an effect both direct and indirect through the activity of monocytes. Moreover, the presence of bone graft substitutes to support the bone formation process is thought to help bone remodelling through ionic exchange between the graft’s surface and the physiological environment.

1.6 Key proteins involved in bone remodelling The biological bone-markers

In the physiological bone environment different proteins and enzymes have been identified to have a fundamental role in various bone development processes, such as bone formation, modelling, remodelling, and bone resoprtion. These molecules have been extensively studied in order to understand their correlation with bone physiological processes, and nowadays represent fundamental biological markers used to gather new insights into the biological response to bone graft materials used for bone regeneration.

This paragraph introduces the bone markers which have been used during the experiments presented in this thesis and focuses on their biological functions.

1.6.1 Alkaline phosphatase

Alkaline phosphatise (ALP) is a protein of the proteoglycan membrane bounded enzymes group, found in different tissues, such as placenta, kidneys, intestines, and most importantly liver and bone (Weiss et al., 1986). Bone specific ALP is localized in the outer plasma membrane connected to membrane inositol phosphate by a phosphatidyl-glycan bridge. It is synthesized by osteoblasts in specific vesicles which also contain high amounts of inorganic phosphate and is then anchored in the areas of bone growth (Anderson, 2003). ALP is considered an early differentiation marker for bone formation, as it has been confirmed its essential role in co-operating inorganic phosphate and calcium ions in order to form apatite crystals (van Straalen et al., 1991).

1.6.2 Osteocalcin

Osteocalcin (OCN) is a non-collagenous protein synthesized from the osteoblasts and it is a widely used biomarker for bone turnover. Its transcription is regulated by 1,25-dihydroxy-Vitamin D3 (which makes this

vitamin essential for healthy bones) and after transcription its mRNA is translated in pre-proosteocalcin. Then, through a γ-carboxylation in 3 different points by vitamin K1, it reaches its final and stable structure (Lee et al., 2000).
OCN is an essential protein involved in the mineralization of bone and calcium homeostasis. Moreover, it has also been shown to act as a hormone in the body, causing pancreatic beta cells to release more insulin, and at the same time to stimulate the release of the hormone adiponectin from adipose cells which increases sensitivity to insulin (Lee et al., 2007).
In bones, even if its precise function remains elusive, it has been proven that higher serum levels of osteocalcin are well related with increase in bone mineral density (BMD), or with pathologies which present increased bone or osteoid formation. For this reason it has been used as a preliminary marker to test the effectiveness of drugs for bone formation (Teriparatide, (Chen et al., 2005)) or of antiresorptive agents (bisphosphonates or hormone replacement therapies, (Chen et al., 1996)). The link between OCN and BMD is thought to be related to the fact that this protein presents, on its negatively charged surface, five calcium ions in a complementary position with those in hydroxyapatite. Using this recognition mechanism OCN could potentially modulate the crystal morphology and formation of hydroxyapatite (Hoang et al., 2003). For the same reasons OCN is nowadays widely used also to study BGS effect on bone formation.

1.6.3 Osteoprotegerin

Osteoprotegerin (OPG) is a cytokine receptor for the RANKL (Receptor activator of nuclear factor kappa-B ligand) and is often used as a marker for bone turnover. RANKL is a transmembrane ligand expressed on osteoblasts/stromal cells that binds to RANK, a transmembrane receptor on hemopoietic osteoclast precursor cells. The interaction of RANK and RANKL initiates a signaling and gene expression cascade that results in the differentiation and maturation of osteoclast precursor cells to active osteoclasts capable of resorbing bone (Wada et al., 2006). OPG was found to be able to bind to RANKL and blocks its interaction with RANK, therefore inhibiting the development of osteoclasts and indirectly the bone resorption

process. In general, upregulation of RANKL is associated with downregulation of OPG, or at least lower induction of OPG, so that the ratio of RANKL to OPG changes in favour of osteoclastogenesis. Many reports have supported the assertion that the RANKL/OPG ratio is a major determinant of bone mass (LC and M, 2004).

1.6.4 C-terminal propeptide of the type-1 collagen

CICP represents the C-terminal propeptide of type-1 collagen, which is related to the final Collagen production. Collagen type-I is indicative for the collagen production in vivo. As the primary organic constituent of bone, type-I collagen levels have been linked to bone growth and formation. Elevated levels of CICP have been shown in diseases associated with high levels of bone turnover including Paget's disease (Simon et al., 1984), hyperthyroidism, primary hyperparathyroidism and renal osteodystrophia. Slightly elevated levels of CICP have also been documented in some women in early menopause (Ebeling et al., 1996). For its correlation with type-1 collagen levels it is also widely used as a marker for studies of BGS-mediated osteogenesis (Guth et al., 2006a, Feng et al., 2013).

1.6.5 Vascular endothelial growth factor

Vascular endothelial growth factor (VEGF) is a key regulator in the process of angiogenesis. It is a specific mitogen for vascular endothelial cells and its biological effects are mediated by specific tyrosine kinase receptors. The VEGF family consists of seven members, of which VEGF-A is the most abundant and the most used in investigational studies (Thomas, 1996). During bone growth, development, remodeling and repair, the process of angiogenesis is closely correlated to the one of osteogenesis (Rabie, 1997) in both intramembranous and endochondral ossification (Emad et al., 2006)(Rabie et al., 2007). In these events the hypoxia-inducible factor, induced by decrease of oxygen tension, is one of the key upstream regulators of VEGF.

The mechanism how VEGF regulates endochondrial ossification is by regulating blood vessel invasion (neovascularisation): these vessels can bring to the wound site progenitor mesenchymal stem cells which can later differentiate into osteoblasts and start the osteogenetic process ((Rabie and Hägg, 2002). Actually, different studies have shown the effect that growth factors have in regulating osteoblast differentiation and bone formation, and their expression of VEGF. Some examples are vitamin D3, TGF-β, BMP-4, BMP-6, BMP-7 (Wang et al., 1996) (Saadeh et al., 1999) (Deckers et al., 2002). Moreover, the presence of a blood supply confers to the wound site also the essential delivery of oxygen and nutrients essential for cells to develop and tissue formation. Apart for physiological remodelling processes, VEGF was found to be involved also in fracture healing: its activity was found to be essential for the conversion of soft cartilaginous callus to a hard bony callus and mineralisation in response to bone injury (Geiger et al., 2005).

Different studies report the important role of VEGF also in chondrocytes differentiation and survival, osteoclasts recruitment and osteoblasts cell proliferation and differentiation. Gerber for example reports a decrease in formation of trabecular bone, slower blood vessels development and massive expansion of hypertrophic zones in growth plates after VEGF inhibition (Gerber et al., 1999). Other reports show the role of VEGF not only in osteoclasts recruitment but also in their differentiation (Nakagawa et al., 2000) and stimulation of their activity (Carano and Filvaroff, 2003).

For all of these reasons, VEGF is nowadays considered a marker for angiogenesis and it is used to evaluate improved new bone formation.

1.7 Bone grafting

This chapter will explain why it is necessary to focus and invest in the development of advanced bone grafting materials, why synthetic bone scaffolds are needed and the advantages of their uses.

Worldwide, an osteoporotic fracture is estimated to occur every 3 seconds (Johnell and Kanis, 2006). Osteoporosis is estimated to affect 200 million women worldwide: one-tenth of women aged 60, one-fifth of women aged 70, two-fifth of women aged 80 and two-thirds of women aged 90 (Kanis et al., 2007). By 2050, the worldwide incidence of hip fracture in men is estimated to increase by 310% and 240% in women (Gullberg et al., 1997). In white women, the lifetime risk of hip fracture is 1 in 6 compared with a 1 in 9 risk of a diagnosis of breast cancer (Cummings and Melton, 2002). Furthermore, only in Europe the total direct costs were estimated at €31.7 billion (£21 billion) which are expected to increase to €76.7 billion (£51 billion) in 2050 based on the expected changes in the demography (Kanis et al., 2007). In UK, 1 in 2 women and 1 in 5 men will suffer a fracture after the age of 50 (Van Staa et al., 2001) and the cost of treating all osteoporotic fractures in postmenopausal women has been predicted to increase to more than £2 billion by 2020 (Burge et al., 2001). These statistics highlight how much osteoporosis and bone fractures represent a worldwide economic clinical issue with extremely high estimated growth rates.

It is well known that bone is a remarkable living tissue capable of maintaining optimal shape and structure throughout life via a continual process of renewal. This ability makes bone able to respond to changes in its bio-mechanical environment through the process of remodelling, enabling to maintain an optimal balance between form and function. However, bone requires a constant supply of oxygen and nutrients; can suffer from pathological conditions; and is subject to degeneration as a result of age and/or diseases. In most of these cases, patient comfort and bone function can only be restored by surgical reconstruction.

1.8 History of bone grafting

Bone grafting is the procedure of replacing missing bone with material from either the patient's own body (autografting) or that of a donor (allografting), and was first established in the 1800s (Meeder and Eggers, 1994) (Sanan and Haines, 1997). As well as replacing missing bone, the grafts are being used to augment the defect site by encouraging new bone growth into the actual defective site. This new bone should eventually replace the graft material within the site and maintain an optimal balance between its form and function.

The first documented attempt at bone tissue engineering was made in 1668 by the Dutch surgeon Job van Meek'ren, who described the filling of a bony defect in a soldier's cranium with a piece of skull from a dog (De LongJr et al., 2007). Interestingly, this bone graft was removed 2 years later at the patient's request so that he could be allowed back into his church, which had excommunicated him because of the xenotransplant.

Regarding autografting, even though the first described autologous bone grafting procedure was performed by Fred Albee in 1915 using part of the tibia for spinal fusion, the first demonstration of actual osteoinduction was shown by the Swedish surgeon Levander in 1930. He prepared alcohol extracts of bone and then injected them into muscle, noting bone production (Desai, 2007).

1.9 Biomaterials used in bone grafting

Synthetic bone scaffolds are used to fuse joints to prevent excessive movement, to repair broken bones that present too much bone loss, or to repair injured bone that has not healed by itself. The advantages of using bone scaffolds compared to either auto- or allograft are different, for example elimination of disease transmission risk; fewer surgical procedures; reduced risk of infection or immunogenicity; and abundant availability of synthetic scaffold materials.

Bone graft substitutes are made of biomaterials, for which different definitions have been proposed: a biomaterial is used to make a device to replace a part or function of the body (Hench, 1998), or is any natural or synthetic material that has an interface with living tissue or is in contact with biological fluids

(Buck et al., 1989). Biomaterials can be classified in many different ways. **Error! Reference source not found.** lists the most used biomaterials for bone grafting comparing their advantages and disadvantages, and giving examples of real life applications.

Table 1-1: ***Biomaterials used in the body***

Materials	Advantages	Disadvantages	Examples
Metals (Ti and its alloys, Co-Cr alloys, stainless steel)	Strong, tough, ductile	May corrode, dense, difficult to make	Joint replacements, bone plates and screws, dental root implants
Polymers (nylon, silicone rubber, polyethylene polyester, poly methyl methacrylates)	Easy to fabricate, resilient	Not strong, deforms with time, may wear or degrade	Sutures, blood vessels, hip socket, bone cement, ear, nose, soft tissues
Ceramics (calcium phosphates and glasses, carbon, alumina, zirconia)	Biocompatible, strong in compression	Brittle, low toughness (except alumina and zirconia), difficult to make	Dental, femoral head of hip replacement, coating of dental and orthopaedic implants
Composites (HA with polyethylene, wire or fibre reinforced bone cement)	Tailor-made, strong	Difficult to make	Ossicles, heart valves

Material properties and characteristics of biomaterials make them more appropriate for specific biological applications rather than others. For example, materials used for bone replacement need to exhibit first of all important

factors like toughness and compressive strength, while a ligament replacement material must possess primarily flexibility and tensile strength characteristics.

1.9.1 Biomaterial properties

The first characteristic that a material for biological applications should possess is **biocompatibility**. For a material to be biocompatible, it needs to have the ability to be implanted in a living tissue without being toxic, cause injury or immunological rejection. Another characteristic that needs to be considered is its **bioactivity**. A bioactive material stimulates a biological effect when in contact with the surrounding tissue. Larry Hench defines materials as bioactive when they illicit a certain biological response at their interface, which results in the formation of a bond between the tissue and the material (Hench, 1998). Hench *et al.* developed Bioglass™ in 1969. This was the first type of man-made material which could bond with bone and connective tissue for bone repair. Biocompatibility of the material, and in many cases bioactivity of the material, will determine most of the success of the new bone graft.

Other important material properties for bone grafting are **osteoconductivity**, **osteoinductivity** and **osteointegration**.

Osteoconduction occurs when new bone apposition is supported by a scaffold structure on whose surface cells can adhere and grow.

Osteoinduction is the process by which osteogenesis is induced. It occurs when bone is produced in an ectopic site, such as muscle or skin, and is given by the stimulatory effect of the implant on the local host tissue, causing differentiation of uncommitted stem cells into bone forming cells.

Osteointegration is the stable anchorage of an implant, achieved by direct bone-to-implant contact (Albrektsson and Johansson, 2001).

Bone graft materials can be defined as “any material alone or in combination with other materials, which promotes bone healing by providing osteoconductive and osteoinductive activity to the repair site” (Bauer and Muschler, 2000).

A number of approaches have been used to treat osseous defects by attempting to stimulate bone via the use of bone grafts. From the materials perspective it can be broadly categorised into two main groups: natural and synthetic biomaterials.

1.9.2 Natural bone grafts

There are three types of natural bone grafts that are being currently used. These include autografts, allografts and xenografts.

The current accepted gold standard in bone grafting is **autografts** (Olkarinen and Korhonen, 1979)(Burchardt, 1987). One of the primary reasons is the fact that it is osteoinductive and osteoconductive. It is the bone tissue harvested from and implanted in the same individual, it contains the patient's own cells and growth factors and therefore transmission of infections and immunogenic reactions are minimal. Moreover, autologous bone grafts recruit mesenchymal stem cells and induce them to differentiate into osteogenic cells through exposure to osteoinductive growth factors (Giannoudis et al., 2005).
Despite these advantages and many others related to the use of autologous bone grafts, there are also major drawbacks. Their use has been limited to the treatment of small osseous defects. The extra surgery involved in harvesting autologous bone causes morbidity at the donor site (Brown and Cruess, 1982) (Koole, 1994), post-operative continuous pain (Arrington et al., 1996) and can cause also hypersensitivity, pelvic instability (Coventry and Tapper, 1972), infections and paresthesia (Cowley and Anderson, 1983). These complications affect 10% to 30% of the patients. Moreover, the amount of bone that can be collected is limited.

In cases of large osseous defects, allografts and xenografts have been used as bone substitutes: they are both osteoconductive and provide the necessary mechanical support.
Allograft is the bone tissue harvested from a donor and implanted in another patient. The use of **Xenografts** is a method by which the graft is taken from another species for the insertion into a patient.

The use of allografts increased dramatically from 5,000-10,000 cases in 1985 to almost 150,000 cases in 1996 (Boyce et al., 1999), and nowadays, they are the most commonly used bone grafts in cases of large defects. However, both allografts and xenografts, unlike autografts, lack in osteoinductive properties, are associated with incidence of disease transmission (both within and across species barriers) and can potentially trigger a host immune response (Buck et al., 1989).

Nevertheless, the quality of allografts is worse than that of autologous grafts. Allografts have a poor degree of cellularity, less revascularisation, and a higher resorption rate compared to autologous grafts (Yaszemski et al., 1996), resulting in a slower rate of new bone tissue formation, as observed in several studies (Oklund et al., 1986) (Oikarinen and Korhonen, 1979). In addition, the immunogenic potential of these allografts and the risks of virus transmission to the recipient are serious disadvantages (Strong et al., 1996). Although processing techniques such as demineralisation, freeze-drying, and irradiation have been shown to reduce the patient's immune response, processing also alters the structure of the graft and reduces its potential to induce bone healing (osteoinductivity). A number of cases have in fact been cited in which the human immunodeficiency virus and hepatitis C were transmitted through the transplantation (Tomford et al., 1995). In another study it was reported the higher rate of fracture after implantation which could be due to the structural change in the cross linking of the collagen after the irradiation of the allograft (Lietman et al., 2000).

1.9.3 Synthetic bone grafts

All the above grafting procedures have their limitations and therefore a number of synthetic bone graft biomaterials have been developed and are in use clinically with mixed success. Synthetic bone grafts form a credible alternative in the treatment of osseous defects, particularly in cases where the autografts are in limited supply or the defects are particularly large. Bone grafts are widely used in different areas of rehabilitation surgery, as dentistry or orthopedics. All of these materials are biocompatible, most are osteoconductive and some claim to be osteoinductive. Furthermore, synthetic

bone graft substitutes offer structural reproducibility and consistency, and unlike allografts and xenografts, present no threat of disease transmission (Moore et al., 2001).

Many studies show that bioactive materials, such as calcium phosphate ceramics, form direct bonds with the surrounding bone tissue (process known as “bioactive fixation”) and that bone-graft composition and surface characteristics impact on osteoblasts metabolism and affect tissue healing (Jarcho, 1981).

Ideally, the main characteristics that a bone graft biomaterial should have are:

- Biocompatibility
- Absence of immune rejections
- Osteoconductive properties
- Inductive effect through superficial endogenous protein adsorption
- The capacity to speed up the physiological healing processes
- The capacity to prevent or modulate inflammation and infection reactions
- Be totally resorbable
- Complement bone mechanical and physiological functions

Moreover, the graft should not only replace the missing tissue, but encourage new bone ingrowth into the grafted area, thereby reinforcing the repaired area and forming a living bridge between the existing bone and the graft material with the newly formed tissue.
With time, this new tissue should penetrate and replace much of the graft thanks to the resorbable properties of some of the currently used bone graft substitutes.

1.9.3.1 Bioceramics: Calcium Phosphate

Considering the limited utility of non-degrading synthetic bone scaffolds or fixation devices, the only realistic options for bulk biomaterial selection are ceramics and polymers.

Ceramics that have found a use in biological systems are referred as bioceramics. They are inorganic, non-metallic compounds which can either be bioactive or bioinert. Although, there are uncertainities about their osteoinductive capacity, they certainly possess osteoconductive abilities as well as a remarkable ability to bind directly to bone (Hollinger and Battistone, 1986) (Hämmerle et al., 1997).

Biodegradable polymers and ceramics, however, generally lack in their mechanical properties. Ceramics fail mechanically due to their brittleness, tensile and compressive strengths (ceramics are hard materials with small elongation to failure), whereas in polymers there is a deficiency in the compressive strengths and Young's modulus compared with native bone tissue (polymers are typically too ''soft'') (Murugan and Ramakrishna, 2005).

The primary constituent (60%) of bone is calcium–phosphate (CaP) minerals, specifically non-stoichiometric hydroxyapatite (LeGeros, 1994). Dozens of calcium–phosphate formulations have been developed and investigated for their bioactivity (i.e., tricalcium-phosphate (TCP), biphasic calcium phosphate (BCP), hydroxyapatite (HA), and bioglass ceramics (BGC)).

CaP biomaterials offer outstanding properties: similarity in composition to bone mineral; bioactivity (ability to form bone apatite-like material or carbonate hydroxyapatite on their surfaces) (Manjubala et al., 2002); ability to promote cellular function and expression leading to formation of a uniquely strong bone-CaP biomaterial interface (Ducheyne and Qiu, 1999); and osteoconductivity (ability to provide the appropriate scaffold or template for bone formation).

In addition, CaP biomaterials with appropriate three-dimensional geometry are able to bind and concentrate endogenous bone morphogenetic proteins in circulation, and may become osteoinductive (capable of osteogenesis) (Fellah et al., 2008).

The most common types of calcium–phosphate (CaP) materials investigated for synthetic bone scaffold development are: hydroxyapatite (HA), tricalcium phosphate (TCP), biphasic calcium phosphates (BCP), and bio-glasses. On the basis of the composition and stoichiometry of a calcium–phosphate ceramic, important physical properties such as degradation rate, modulus, dissolution and fracture strength can be obtained (Klein et al., 1983) (Gauthier et al., 1999)(Ducheyne, 1987) (Royer et al., 1993).
Research on TCP materials, however, has revealed that their degradation rate is too rapid *in vivo*, while synthetic versions of HA degrade too slowly to allow native tissue integration. This phenomenon motivated the development of BCP and bio-glasses which have tuneable (to some degree) degradation rates based on the relative magnitude of TCP (more commonly β-TCP) and HA in a composite ceramic (Kohri et al., 1993)(Kwon et al., 2002)(Kwon et al., 2003).

Wtihin the range of CaP biomaterials, particular attention was paid to stoichiometric synthetic Hydroxyapatite (HA), which has been widely used as a bone grafting substitute due to its chemical similarity to the mineral component found in bone and teeth and to the absence of immune-reaction.
It is the most commonly used CaP within the fields of dentistry and orthopaedic surgery, and was firstly commercialised in the mid-seventies independently by Jarcho, Groot and Aoki (Hench and Wilson, 1993).

Nowadays hydroxyapatite has several uses, not only as a replacement material but also as a coating for the metallic acetabular cups and hip stems. HA coatings have been shown, in fact, to improve the initial biological fixation of the metal implants, and to promote bone remodelling and early osseous integration at the bone-prosthesis interface (Zheng et al., 2000) (Oonishi, 1991).

1.9.3.1.1 HA properties

HA belongs to a group of compounds called “apatite”, all of which have a similar crystal structure but different compositions. In particular, crystalline HA has a hexagonal structure unit cell as shown in **Error! Reference source not**

found. with a space group, $P6_3/m$, made up of PO^{3-}_4 tetrahedra, and CaO_6 and CaO_7 polyhedra with channels containing the hydroxyl anions running parallel to the c-axis, where its general empirical formula is $Ca_{10}(PO_4)_6(OH)_2$.

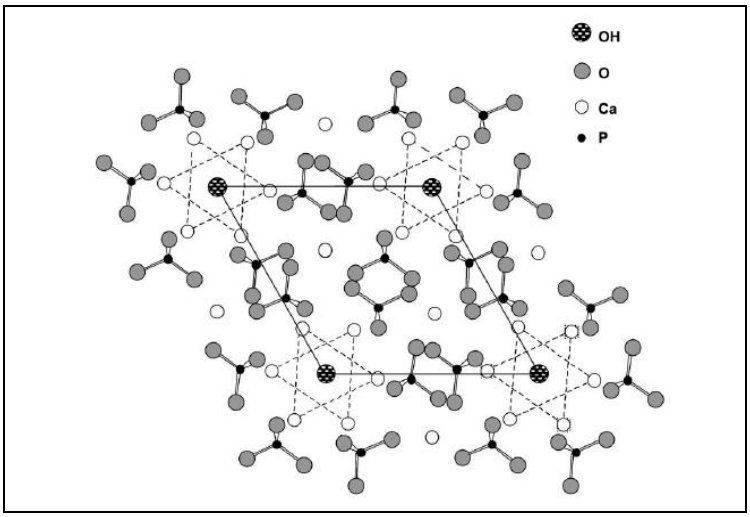

Figure 1-5: Crystal Structure of Hydroxyapatite (Cazalbou et al., 2004)

Hydroxyapatite is a hydrated calcium phosphate that is similar to the mineral component of bone (Cazalbou et al., 2004). HA has been shown to be biocompatible and to promote adsorption of serum proteins, and osteoblast adhesion and migration/infiltration *in vitro* (Kilpadi et al., 2001)(Hott et al., 1997). Moreover, it has a unique capability of binding to natural bone through biochemical bonding, which promotes the interaction between host bone and grafted material (Tracy and Doremus, 1984).

Unfortunately, HA is scarcely bioresorbable, and it fails in terms of mechanical properties. It shows a relatively higher Young's Modulus than cortical bone, therefore making it stiffer. Additionally, HA has a very low tensile and compressive strength, which make this material more susceptible to breaks as compared to bone (see**Error! Reference source not found.**).

Table 1-2: Mechanical properties of Cortical Bone and synthetic HA (Murugan and Ramakrishna, 2005)

	Young's modulus (GPa)	**Tensile Strength** (MPa)	**Compressive Strength** (MPa)	**Fracture Toughness** (MPa $m^{1/2}$)	**Density** (g/cm^3)
Cortical Bone	14-20	50-150	170-193	2-12	18-22
HA	80-100	0.05	0.4-0.9	0.7-1.2	3.16

Furthermore the resorption rate of HA compared to other CaP materials is very low, thus making its remodelling potential weaker, the rehabilitation time longer and the probability for the implant to fail higher (Murugan and Ramakrishna, 2005).

HA has a long history of use as a bone graft substitute. Since early '50s many studies and investigations were carried out testing HA in either animals or humans models (Ray and Ward Jr., 1951). However, its use in clinic started only in the 70s (Jarcho et al., 1976), and since then a different number of fabrication methodologies, and synthetic forms of HA, have been reported. Nowadays HA covers a wide range of clinical applications such as repair of long bone defects; spinal fusions; cranioplasty; vertebral fusions; non union bone fractures; but also dental surgery, as a coating agent on biometallic implants and for drug delivery. The low compressive strength and fracture toughness, however, make HA use limited in orthopaedic applications with a low load-bearing implantation.

Even though HA presents some unique characteristics, research is still devoting a lot of effort trying to develop a material with better mechanical properties and bioresorbable characteristics. In order to improve HA fracture toughness, for example, researchers are studying the incorporation of biocompatible reinforcement agents or of matrix materials, incorporated within the HA structure. One matrix material widely studied is collagen, which would not interfere with the biocompatibility of HA (Kikuchi et al., 2004).

The other direction where research is looking is the fabrication of HA combined with another ceramic in order to increase its low resorption rate.

Some ceramic composites examples are HA/TCP alone (with different ratios) or combined with autogenous bone. These modifications have the potential to provide a ceramic biomaterial with improved functionality and faster resorption without losing its osteoconductive properties (Sulaiman et al., 2013a)(Jalota et al., 2006).

1.9.3.1.2 The biological relevance of silicon

As previously mentioned, bone mineral is mainly composed of non-stoichiometric HA. However, the inorganic part of bone is also enriched with a few trace elements, which include carbonate, citrate, sodium, magnesium, and trace amounts of silicate, fluoride, chloride, and potassium (see **Error! Reference source not found.**). The prime role of minerals is to provide toughness, rigidity, and sustain bone's metabolic functions (LeGeros, 1994).

Table 1-3: Inorganic composition of bone

Inorganic phase	HA	Carbonate	Citrate	Sodium	Magnesium
Wt%	~60	~4	~0.9	~0.7	0.5

Numerous studies have identified biomaterial surface chemistry as crucial in directing subsequent bioactivity at the implant interface (Best et al., 1997)(Hing, 2008). Therefore, in order to enhance HA behaviour, researchers have devoted efforts in trying to reproduce as closely as possible the bone's mineral phase in the HA structure (Jha et al., 1997)(Gibson and Bonfield, 2002) (Ikeuchi et al., 2003). Depending on which substitution takes place, there can be an effect on different material properties like surface structure, crystal morphology, crystallinity, thermal stability, solubility and charge of HA, which could either positively or negatively influence its biological response.

In this sense, an interesting way to improve the bioactivity of HA is the addition of silicon to the apatite structure, taken into account the influence of this

element on the bioactivity of bioactive glasses and glass-ceramics (Hench and Wilson, 1993) (Ohura et al., 1991).
In addition, several studies have proposed the considerable importance of silicon on bone formation and growth (Carlisle, 1970)(Carlisle, 1981) at *in vitro* and *in vivo* conditions.

Silicate ions are of particular interest as it is believed to have a physiological role in bone formation with evidence of its influence on bone mineralisation, and found to be crucial to bone development since the 1970s, when Carlisle showed the detection of silicon ions *in vivo* (up to 0.5wt%) in the young bone of mice and rats, suggesting that these ions have an important role in the bone calcification process (Carlisle, 1972).
In 1972, Schwarz and Milne demonstrated that a silicon deficient diet in rats retarded the growth and disturbed the development of bone structures (Schwarz and Milne, 1972). They particularly saw a change in the skull size and also the architecture of the bone within these rats. The authors, therefore, suggested that silicon plays an important role in the binding of bone structures due to the stability of the Si-O-Si bonds present.
One of the most important findings of Schwarz was in 1977, when he discovered an enzyme, which had the capability to remove silicic acid from a synthetic bond form, silicase (Schwarz, 1978). The enzyme is membrane bound and is found in the pancreas, stomach and in the kidneys but at a lower concentration. The enzyme is stable and can be heated to temperatures of $100^{o}C$ without losing activity for at least 10 minutes. Schwarz also proposed a correlation between the effects of silicon and bone disease along with wound healing and atherosclerosis

Later on Carlisle presented a study on chicks that further concluded the importance of silicon in the mineralisation of bone. She also was successful in showing that silicon plays a role in the growth and development of bone, connective tissue metabolism and bone calcification process (Carlisle, 1978). She showed that the chicks, with a silicon deficiency, had distorted skeletal development, less flexible legs, smaller skull and also flatter bones.

Using electron microprobe, Carlisle also demonstrated that silicon was concentrated in the cytoplasm of osteoblast cells in young bones. Therefore, there is a direct relation between the concentration of silicon and the amount of calcification taking place. The study showed that after an increase in calcium, there was a decrease in silicon, especially when the levels of calcium reached the values that are seen in bone mineral.

The maximum amount of silicon was shown when the Ca/P ratio was 0.7, however the amount decreased very quickly when the Ca/P ratio increased to 1.67.

Moreover, the detection of new apatite layers formed on the surface of many glasses and glass ceramics after only a few hours in simulated body fluids further supported the idea of incorporating Si into the HA structure (Arcos et al., 2002).

Therefore, the incorporation of silicate ions (silicon as an element) in the apatite structure was suggested, studied, and confirmed as an improvement to the bioactivity of these biomaterials.

1.9.3.1.3 Silicate substituted Hydroxyapatite (SA)

Since the bioactive process is regarded as a surface process between the implant and the surrounding living tissue, the chemical changes that the HA surface undergoes due to the incorporation of silicon must be highlighted.

Therefore many groups focused on X-ray photoelectron spectroscopy (XPS) and zeta potential (ZP) measurements in order to clarify the rate of incorporation of silicon in the HA structure. If it was either incorporated as SiO_4^{4-} by the substitution of PO_4^{3-} or retained at the grain boundaries as polymeric SiO_2 species.

Botelho *et al* confirmed, by using XPS, that in the HA structure silicon exists as a tetrahedral silicate SiO_4 group rather than in a polymeric form of SiO_2 for silicon amounts of up to 1.2wt% (Botelho et al., 2002).

Balas *et al* achieved similar results and reported the polymerisation of the silicate species at the surface for silicon contents higher than 1.6wt%. The ZP measurements showed that at physiological pH, surface charge was

significantly lowered by the presence of silicate groups; therefore a faster apatite layer formation would follow (Balas et al., 2003a).
Also, Botelho reported that the incorporation of silicon into the HA lattice induced a more negative surface charge (Botelho et al., 2002).
In vitro studies by Gibson *et al*. demonstrated that the incorporation of Si into the phase-pure HA stimulates the osteoblast-like cell activity compared with stoichiometric HA; and enhances the formation of a surface apatite layer in an artificial physiological solution (Gibson et al., 2009).
An *in vivo* study by Patel *et al*., comparing bone apposition to HA and Si-HA ceramic implants, demonstrated bone apposition to be significantly increased at the surface of Si-HA ceramics (Patel et al., 2002).

Other studies focused instead on the optimal silicon substitution rate in the HA lattice. A study conducted by Hing *et al* investigated the influence of varying levels of silicon content (0, 0.2, 0.4, 0.8 and 1.5wt %) on the rate, quality and volume of bone apposition within porous SA scaffolds *in vivo* (Hing et al., 2006a). These results showed an optimal biological response achieved with the 0.8wt% group.
The enhanced biological activity of silicate-substitute HA bone grafts materials is constantly confirmed by different studies, performed both *in vitro* and *in vivo,* which makes this biomaterial to be considered one of the best substituted HA grafts used in orthopaedics (Botelho et al., 2005, (Guth et al., 2006a) (Gibson et al., 2002a) (Balas et al., 2003a)(Guth et al., 2006a).

Despite the relevant biological effect, the mechanisms by which Si increases the *in vitro* and *in vivo* bioactivity of calcium phosphate bone grafts are still unresolved. However, several hypotheses have been proposed.
When passive mechanisms are involved, it is supposed not to be the chemical nature of Si in itself responsible for the effect, but rather the influence of physio-chemical changes due to the presence of Si; some of these can be, for example, changes in grain size (Porter et al., 2004), or surface charge and hydrophobicity that may lead to changes in protein conformation at the material surface. Otherwise, active mechanisms, i.e. Si release could be responsible for these changes; if Si is not included in the crystallographic

structure of Si-substituted HA, but is present as a soluble compound, Si ions can be released and “seen” by cells in a bioavailable form which may interact directly with cell metabolism or osteogenic proteins, peptides or enzymes. Cells metabolism will be, therefore, directly affected (Balas et al., 2003a)(Botelho et al., 2005a) .

1.9.3.2 Porous CaP biomaterials

Bone cells and matrix proteins are sensitive not only to chemical changes, but also to other properties of the material such as bulk geometry, surface geometry and topography.

The elaborate hierarchical geometric structure of bone, in fact, is critical not only for the macroscopic mechanical properties of bone, but also for progenitor and bone cells survival and functionality at the micro and nano-scale. Because of the direct apposition and binding of the ECM proteins and cell cytoskeleton through cell receptors, cells sense and respond to the physical properties of the matrix by converting mechanical cues into intracellular chemical signals which drive activities such as gene expression, protein production, and general phenotypic behaviour (Lutolf and Hubbell, 2005)(Galbraith et al., 2002). Therefore, a primary goal in bone scaffold design is to mimic the unique micro and nano-scale characteristics of bone.

In recent years, it has been well established by the literature, the relevant role that material porosity plays on bone cells behaviour (Bruijn et al., 1999)(Desai, 2000).

Different studies have shown that porous hydroxyapatite grafts are able to massively enhance the biological response compared to non-porous HA (Klawitter and Hulbert, 1971)(Campion et al., 2011) (Patel et al., 2002).

These studies showed that the level of porosity in the bulk structure of a CaP graft is able to differently influence the biological response. In particular, the *in vivo* studies from Hing and Campion demonstrated an increased level of microporosity may improve the bioactivity of porous HA scaffolds and accelerate osteointegration (Campion et al., 2011)(Hing et al., 2004).

Another study by Hing, investigating the *in vivo* influence of microporosity on early osseointegration and final bone volume within porous HA, showed that in the longer term the dominating factor effecting osseointegration was the influence of strut porosity rather than only total porosity (Hing et al., 2005). These results indicate that manipulation of the levels of microporosity within a bone graft substitute can be used to accelerate osseointegration and elevate the equilibrium volume of bone. Researchers have also demonstrated that in phase pure porous hydroxyapatite scaffolds, with equivalent levels of total-porosity, the presence of microporosity altered the pattern and dynamics of osteointegration: HA bone grafts with increased levels of microporosity promoted the apposition of greater volumes of new bone in a more dense morphology and at earlier time points (Hing et al., 2004).

It is believed that this improved bioactivity is due to the ability of porous materials to permit effective vascularization within the graft, nutrient delivery and bone ingrowth. These events are all fundamental for the development of any new tissue in the body, thus are essential for the induced bone formation of any synthetic bone implant. These events are shown in different studies where capillary penetration in scaffolds with different strut porosity grades was detected, suggesting that the rate of development of the vascular network is linked to the strut porosity variation (Karageorgiou and Kaplan, 2005).

1.9.3.3 Roughness of CaP biomaterials

Together with surface charge, surface chemistry, topography and porosity, another parameter that has been proved to be “sensed” by cells, therefore, affecting their response is surface roughness. A number of studies have demonstrated that cell attachment is highly dependent on surface roughness, and it seems there is some evidence that this mechanism is synergic to the surface physiochemistry mechanism. Therefore, there is evidence that the bioactivity of the implant can be affected by both morphology (the roughness of the surface) and chemistry (the presence or not of Si) and, furthermore, that these parameters can have a synergic effect.

Surface roughness and its effect on cell response have been therefore long studied. The roughness of a material can generally be obtained by either chemical treatments (acid etching) or mechanical treatments (by polishing).
The first studied looked at surface roughness effect on relatively inert materials like titanium (Ti), both *in vitro* (Martin et al., 1995)(Olivares-Navarrete et al., 2012) and *in vivo* (Buser et al., 2004)(Klokkevold et al., 1997). However, there have been few systematic studies on hydroxyapatite and its derivatives (Rouahi et al., 2006) (Dos Santos et al., 2008).

On Ti implants, studies demonstrated that surface roughness affects the rate of bone contact with the material, and that the synthesis of extracellular matrix and subsequent mineralization were enhanced by an increase in surface roughness (Groessner-Schreiber and Tuan, 1992). In another study, however, higher surface roughness decreased osteocalcin and ALP activity as compared to smooth surfaces, suggesting that bone cells phenotype can be differently controlled by surface pre-treatments (Stanford et al., 1994).
Because of the different responses obtained by the various studies on surface roughness of Ti implants, other works looked at the effect of surface roughness on the response of variably differentiated cells. These studies showed that this response could be dependent on the cell maturation state, which is an interesting concept in terms of wound healing, where the first cells to interact with a material are likely to be undifferentiated mesenchymal cells, rather than differentiated osteoblasts (Martin et al., 1995)(Schwartz et al., 1996).

Regarding the effect that surface roughness has on cell response from HA bone grafts, fewer studies have been done. What they show is a milder effect of surface roughness on cell proliferation and not a significant effect on cell differentiation as compared to titanium implants. In particular, ALP activity seemed to not being affected by changes in roughness ((Missirlis, 2000) (Korovessis and Deligianni, 2002)), which instead affected significantly protein adsorption (especially Fn and BSA (Rouahi et al., 2006)), cell attachment (Missirlis, 2000) and cell proliferation ((Missirlis, 2000) (Korovessis and Deligianni, 2002)).

For either Ti implants or HA bone grafts, the reason why surface topography may affect cell responses is that the cells can consequently assume a variety of morphologies upon attachment. These differences in morphologies, mediated by different arrangements of the cytoskeleton, serve as an intracellular signal that provides information for new gene transcription and translation (Pockwinse et al., 1992)(Owen et al., 1991).

1.10 The biological response to biomaterials

The replacement of injured or diseased tissues with devices made from materials that are not of biologic origin is the central approach in current biomaterials science and clinical practice. The prevalence of this approach is due largely to the fact that these materials are not attacked by the immune system, unlike donor tissues or organs. This fundamental difference arises from the presence of immunologically recognizable biologic motifs on donor tissue and their absence on synthetic materials. The basis for these reactions is the adsorption of adhesion proteins to the surface of the biomaterials that are recognized by various cell-adhesion receptors, the most important of which are the integrins, present on most cells. Conversely, the favourable adsorption of adhesion proteins to the biomaterial can convert it into a biologically recognizable material. The interaction of adhesion receptors on the cells with adhesion proteins on the materials surface thus constitutes a major cellular recognition system for biomaterials. Therefore, the role of adsorbed adhesion proteins in mediating cellular interactions with biomaterials is of primary importance regarding the biological response to biomaterials.

1.10.1 Cell-Biomaterial Interface

When a biomaterial is in contact with a living tissue, proteins from the surrounding body fluids will be spontaneously adsorbed onto its surfaces within few seconds; in seconds to minutes, a protein monolayer is formed well before cells finally arrive at the material surface (Anselme, 2000).

It is through this adsorbed layer that cells sense foreign surfaces through the cellular trans-membranous receptors such as integrins.

The adsorbed protein layer is then able to influence the cellular development by determining cell attachment (Rouahi et al., 2006)(McFarland et al., 2000)(Thomas et al., 1997)(van Wachem et al., 1987) (Yang et al., 2003), morphology (Kilpadi et al., 2001) (Gugala and Gogolewski, 2004), proliferation and laterly differentiation (Sogo et al., 2007) (Wilson et al., 2005).
These cell-biomaterial interactions are considered to be significant towards the osteointegration event, which is also dependent by the sensitivity to the surface physiochemistry of the biomaterials (including features such as topography, surface charge, surface energy, and wetability) (Wilson et al., 2005) (Bagambisa et al., 1994).
The cellular behaviour (thus cellular response) can therefore be controlled by affecting the protein layer, which in turn can be controlled by "playing" with the material surface characteristics.

In particular, molecules including collagen (Hennessy et al., 2009), cell adhesive proteins such as fibronectin (Grinnell and Feld, 1982), laminin (Dennis et al., 1992), vitronectin (Thomas et al., 1997), and peptide sequences like the RGD motif (Itoh et al., 2002) have been shown to be adsorbed onto the surface of CaP bone grafts and to mediate cell attachment. However, the extent to which each of these factors contributes to the control of this layer of surface-bound proteins is not fully understood, although clearly being of major importance to biocompatibility.

Data from many studies suggest that one of the reasons calcium phosphates, such as hydroxyapatite, promote better bone formation *in vivo* compared to many other materials (Geesink, 2002), is because HA is more efficient in adsorbing adhesive proteins from the patient's body fluids (Kilpadi et al., 2001)(Matsuura et al., 2000).
Moreover these adhesion proteins are adsorbed on the materials surface in conformations that support the binding of human mesenchymal stem cells (Kilpadi et al., 2001), a type of pluripotent cell that is then encourage to differentiate into osteoblasts (Conget and Minguell, 1999).

1.10.1.1 Fibronectin

One of the most important proteins involved in the cell-biomaterial interaction is fibronectin (Fn). Fn is a high-molecular weight extracellular matrix glycoprotein that binds to membrane receptor proteins called integrins, a group of transmembrane glycoproteins widespread especially in osteoblasts cells (Hynes, 1990).

Fibronectin is one of the most important adhesion proteins of the extracellular matrix (ECM) and osteoblastic cells, in different *in vitro* studies, have shown to depend on adsorbed fibronectin for the initial adhesion and spreading on various materials (Howlett et al., 1994), including HA (Kilpadi et al., 2001)(Hynes, 1990)(Anselme, 2000).

Fibronectin's structure is rod-like and composed of three different types of homologous, repeating modules, Types I, II, and III. These modules, though all part of the same amino acid chain, can be envisioned as "beads on a string," each one joined to its neighbours by short linkers (Potts and Campbell, 1994). Twelve type I modules make up the amino-terminal and carboxy-terminal region of the molecule, and are involved mainly in fibrin and collagen binding. Only two type II modules are found in FN. They are instrumental in binding collagen. The most abundant module in fibronectin is Type III, which contains the RGD recognition sequence for Fn-receptor integrins, along with binding sites for heparin. Depending on the tissue type and/or cellular conditions, the fibronectin molecule is made up of 15-17 type III modules (Baron et al., 1992).

Fibronectin exists in two main forms: 1) as an insoluble glycoprotein dimer that serves as a linker in the ECM, and 2) as a soluble disulphide-linked dimer found in the plasma (plasma Fn). The plasma form is synthesized by hepatocytes, and the ECM form is made by fibroblasts, chondrocytes, endothelial cells, macrophages, as well as certain epithelial cells (Paolella et al., 1993).

Fn is involved in many cellular processes, such as tissue repair, embryogenesis, blood clotting, and cell migration/adhesion (Hynes, 1990). The importance of fibronectin in cell migration events during embryogenesis has been documented in several contexts (George et al., 1993), e.g.: 1)

mesodermal cell migration during gastrulation (an early phase of animal embryo development) can be blocked by injection of Arg-Gly-Asp (RGD) tripeptides that block cellular FN receptors (integrins); 2) injection of anti-FN antibodies into chick embryos blocks migration of precardiac cells to the embryonic midline, and 3) the patterns of FN deposition in developing vertebrate limbs determines the patterns of precartilage cell adhesion to the ECM, thereby specifying limb-specific patterns of chondrogenesis.

Furthermore, Fibronectin can act as a general cell adhesion molecule by anchoring cells to collagen or proteoglycan substrates. But most importantly Fn can also serve to mediate cellular interactions by acting as a bridge between different components of the extracellular matrix and membrane-bound Fn receptors on cell surfaces (Carsons, 1989).

Due to its role in mediating intercellular interactions, it has been proved that Fn plays an active role also in the processes that modulate the interactions between bone graft biomaterials and cells. This modulation makes it possible the translation from the biomaterial's surface properties to consequent cell response in terms of cell attachment, spreading, proliferation and differentiation (Grinnell and Feld, 1982)(Schönmeyr et al., 2008a)(Sogo et al., 2007)(El-Ghannam et al., 1999)(García et al., 1999) (Deligianni et al., 2005).

Moreover, ample evidence exists that Fn undergoes conformational changes upon adsorption on the biomaterial's surface, and that its cell binding domain is sensitive to this conformation, therefore sensitive to surface's characteristics (Iuliano et al., 1993) (Michael et al., 2003)(García et al., 1999a).

1.10.1.2 Assessment of Fibronectin Adsorption

There are relatively few studies published regarding the adsorption of pure fibronectin onto HA and SA scaffolds.

An interesting study conducted by Guth *et al.* in 2010 (Guth et al., 2010a) showed that Fn adsorption was significantly greater on SA discs compared to HA only under specific conditions. In the experiment that investigated the Fn adsorption in C-MEM with increasing concentrations of FCS (10–50%), on the SA and HA discs Fn adsorption did not increase with increasing concentration

of FCS and the quantity of Fn on the SA discs was lower in the medium containing 50% FCS than in the medium containing 20% FCS. This suggests that, as the solution's protein concentration increases to supra-physiological levels, either the relatively large molecular weight of the Fn may lead to a reduction in Fn adsorption through a decrease in its mobility, or the Fn is more susceptible to displacement because of the higher protein concentration.

A number of other studies have looked directly to the importance of the Fn protein layer regarding general cellular attachment, spreading, development. Schonmeyr *et al.* demonstrated that the attachment and proliferation of bone-forming cells on HA is significantly increased when pre-treated with Fn+fetal calf serum. Though, this difference is less profound and not significant *in vivo* (Schönmeyr et al., 2008b). The Deligianni group in 2005 showed that Fn pre-adsorption on smooth and rough HA substratum increases the number of attached osteoblasts at 40% and 62% respectively (Deligianni et al., 2005). None of these works, however, had previously evaluated the true protein behaviour on different biomaterials, to then be able to associate it with the cellular response.

Previously to any cell work; it thus appears to be fundamental to understand when, and in which way, the binding of fibronectin on the implant surface can be regulated by biomaterial characteristics such as chemistry, topography and porosity.

2 Techniques for the quantification characterization of analytes

The methods used to quantify proteins and cells, and to study protein's conformational changes, were based on collection and analysis of quantitative data. In this section the principles of operation of these techniques are described.

2.1.1 Fluorescence spectroscopy

Fluorescence spectroscopy is a type of electromagnetic spectroscopy which analyzes fluorescence from a sample.

Fluorescence can occur in certain molecules (generally polyaromatic hydrocarbons or heterocycles) called "fluorophores" or "fluorescent dyes". This technique is an important investigational tool in many areas of analytical science, due to its extremely high sensitivity and selectivity. With many uses across a broad range of chemical, biochemical and medical research, it has become an essential investigational technique allowing detailed, real-time observation of the structure and dynamics of intact biological systems with extremely high resolution.

The method consists in analysing the molecules of the analyte by exciting them with an irradiation of a specific wavelength, which excites the electrons of the molecule. This excitation causes these molecules to emit light, whose wavelength is unique of that specific molecule or compound.

The advantages of using fluorescence techniques are intrinsic sensitivity, suitable time scale, non-invasive nature, and minimum perturbation (Lakowicz, 2007)(Valeur and Berberan-Santos, 2013). In addition, the ability to incorporate fluorophores in a site-specific manner makes fluorescence approaches very powerful in biological research (Cohen et al., 2002).

2.1.1.1 Principles

Fluorescence is the result of a three-stage process that occurs in a fluorescent dye.

At room temperature most molecules occupy the lowest vibrational (energetic) level of the ground electronic state. When they are hit by a photon of a specific wavelength, they can absorb the energy of that photon and get into an excited state. Upon relaxation from that excited state, the same molecule releases a photon: this process is called fluorescence emission. The energy of the photon that is released is always lower than that one of the photon that was absorbed. Therefore the photon that excites the dye always has a smaller wavelength than the photon that gets emitted (Lakowicz, 2007).

The process responsible for the fluorescence of a fluorophore is illustrated by the simple electronic-state diagram (Jablonski diagram) shown in **Error! Reference source not found.**Figure 2-1:

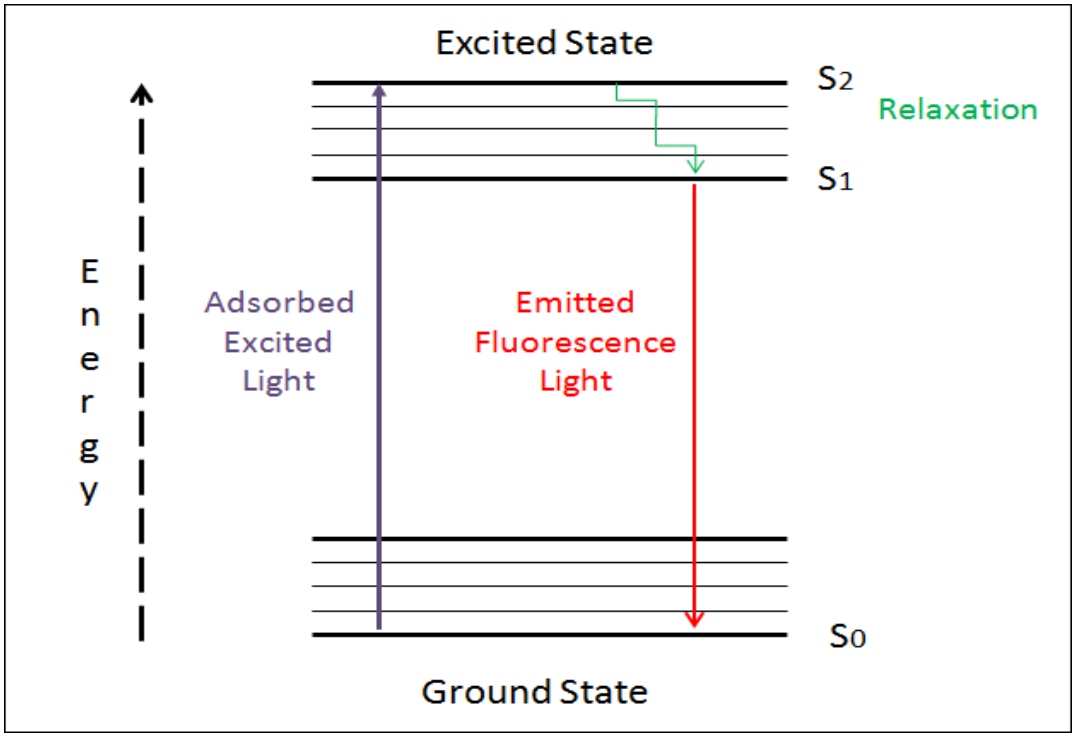

Figure 2-1: Jablonski diagram illustrating the transitions between electronic energy levels.

As previously said, the fluorescence process consists of three different steps:

- Stage 1: Excitation
- Stage 2: Excited-State Lifetime
- Stage 3: Fluorescence emission

Stage 1: Excitation. A photon of certain energy is supplied by an external source (such as an incandescent lamp or a laser) and absorbed by the fluorophore, creating an excited electronic singlet state (S_2).

Stage 2: Excited-State Lifetime. The excited state exists for a finite time (usually 1-10 nanoseconds) during which the fluorophore undergoes conformational changes and is subject to a multitude of possible interactions with its molecular environment. These processes have two possible consequences. First, the energy of S_2 is partially dissipated, yielding a relaxed singlet excited state from which fluorescence emission originates (S_1). Second, not all the molecules initially excited by absorption, return to the ground state (S_0) by fluorescence emission. Other processes such as collisional quenching, fluorescence resonance energy transfer (FRET) and intersystem crossing may also depopulate S_1. The fluorescence quantum yield, which is the ratio of the number of fluorescence protons emitted to the number of photons absorbed, is a measure of the relative extent to which the process of fluorescence occurs.

Stage 3: Fluorescence emission. A photon is emitted, enabling the fluorophore to return to its ground state S_0. Due to the energy dissipation during the excited-state lifetime, the energy of this photon is lower, and therefore of longer wavelength, than the excitation photon. The difference in energy (or wavelength) is called the “Stokes shift”. The Stokes shift (**Error! Reference source not found.**), discovered by the Irish Sir George Gabriel Stokes (**Error! Reference source not found.**b) in 1852 (Stokes, 1852), is fundamental to the sensitivity of fluorescence techniques because it allows emission photons to be detected against a low background, and isolated from excitation photons.

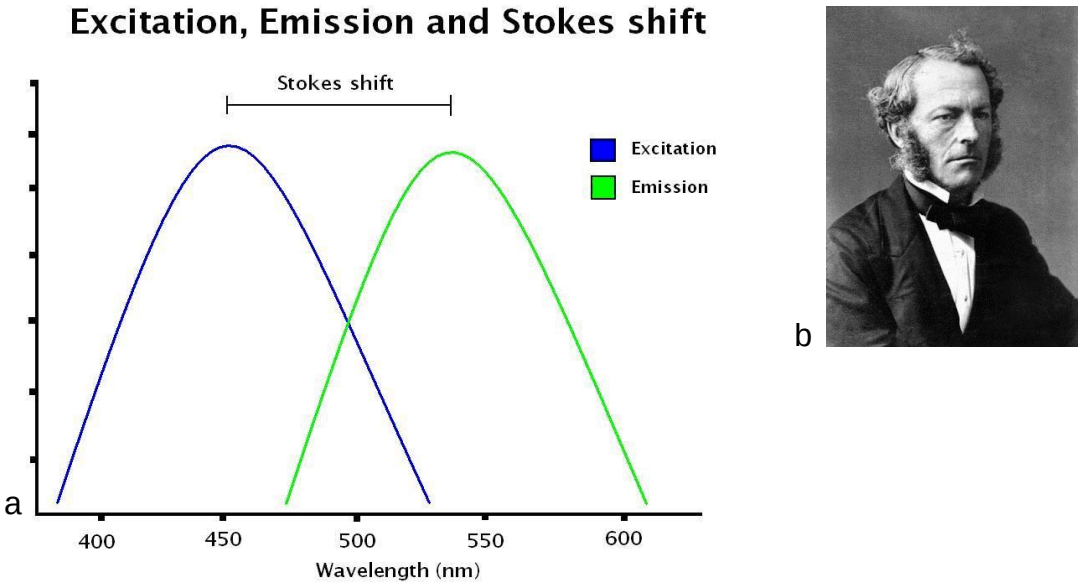

Figure 2-2: a) An idealized chart showing the processes of Fluorescence excitation, Fluorescence emission and the Stokes shift (Riddle, 2006) b) Sir George Gabriel Stokes.

The entire fluorescence process is cyclical (unless the fluorophore is irreversibly destroyed in the excited state) and the same fluorophore can be repeatedly excited and detected.

Furthermore, for polyatomic molecules in solution, the discrete electronic transitions represented in Figure 2-1are replaced by rather broad energy spectra. The fluorescence spectrum of a polyatomic dye, in fact, is characterized not by only one, but by a range of wavelengths around a peak, that will form the “excitation spectrum”. The same can be said for the emission, with a specific “emission spectrum”. Excitation and emission spectrum are characteristic for each fluorescent dye.

2.1.1.2 Instrumentation

The instrument that enables fluorescence analysis is the “Fluorescence detector”. The fluorescence detector is essentially made by four different elements:

- A **light source** to provide excitation;
- A **fluorophore**;

- **Wavelengths filters** to isolate emission photons from excitations photons;
- **A detector** that registers emission photons and produce recordable output, usually as an electrical signal.

Fluorescence instruments can be divided, on the basis of their specific application, in four different types:

- **Spectrofluorometers and microplate readers** measure the average properties of bulk samples;
- **Fluorescence microscopes** resolve fluorescence as a function of spatial coordinates in two dimensions for microscopic objects;
- **Fluorescent scanners** (including microarray readers) resolve fluorescence as a function of spatial coordinates in two dimension for macroscopic objects;
- **Flow cytometers** measure fluorescence per cell in a flowing stream, allowing subpopulations within a large sample to be identified and quantificated.

The instrument that has been used for the experiments of the following chapters is a microplate reader (FLUOstar OPTIMA, BMG Labtech,Figure 2-3) that, as a typical fluorometer, contains an excitation source, sample cell, excitation monochromator and fluorescence detector (Figure 2-4).

Molecules in solution are usually excited by uv light and the excitation source is usually a deuterium or xenon lamp.
Broad-band light from a lamp passes through a monochromator, which selects only the light of a specific wavelength. This excitation light is adsorbed from the fluorescent dye, and the fluorescence emission from the dye is dispersed by another monochromator. Finally it is detected by a photomultipler tube. Scanning the excitation monochromator gives the excitation spectrum and scanning the fluorescence monochromator gives the fluorescence spectrum.

Figure 2-3: FLUOstar OPTIMA, example of microplate reader used for fluorescence and optical density analysis.

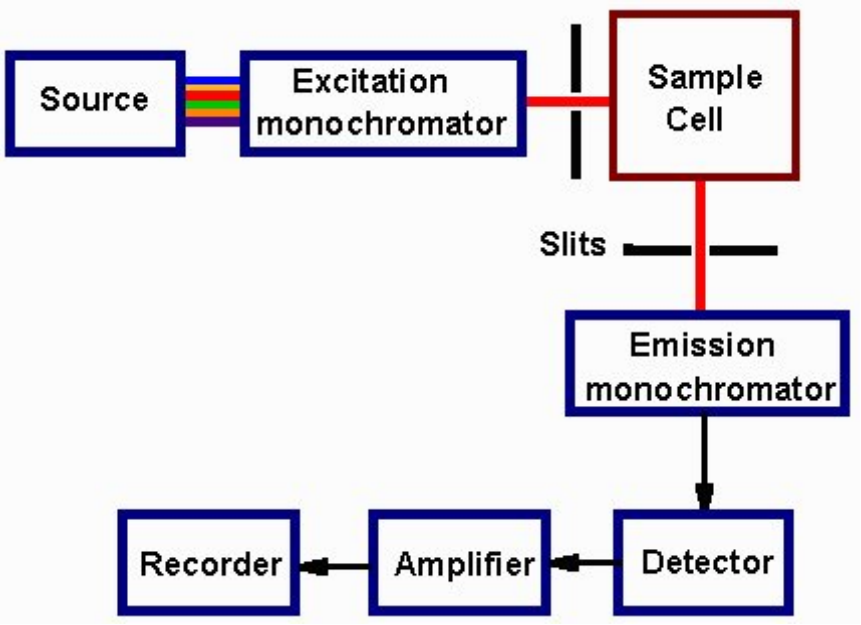

Figure 2-4*: Fluorimeter schematic*

The outcome is measured in Intensity of Fluorescence.

This technique is most accurate at very low concentrations, where the intensity of the fluorescence (I_f) is related to the intensity of the incident radiation (I_o), expressed as follows:

$$I_F = 2.3 I_0 \varepsilon_\lambda c d Q$$

Equation 2.1

where c is the concentration of the fluorophore solution, d is the light path in cm, ε_λ is the molar extinction coefficient for the absorbing material at wavelength (λ) in $dm^3 mol^{-1} cm^{-1}$, and *Q* is the quantum yield.

2.1.1.3 Fluorophores in biological sciences

A fluorophore is a type of fluorescent dye that can be used to mark proteins, tissues or cells for examination by fluorescence spectroscopy or microscopy.

As previously said, a fluorophore works by absorbing energy of a specific wavelength region (commonly referred as “Excitation Range”), and re-emitting that energy at another specific wavelength region (commonly referred as “Emission Range”). The Excitation and Emission Ranges are specific of each fluorophore, because are dictated by its chemical structure and influenced by its environment (Lakowicz, 2007).

In general, a fluorophore will be excited by high energy light (wavelengths in the ultraviolet, violet, or blue region spectrum), and will emit fluorescence with slightly lower energy (wavelengths in the green, red, or near IR region of the spectrum, Figure 2-5).

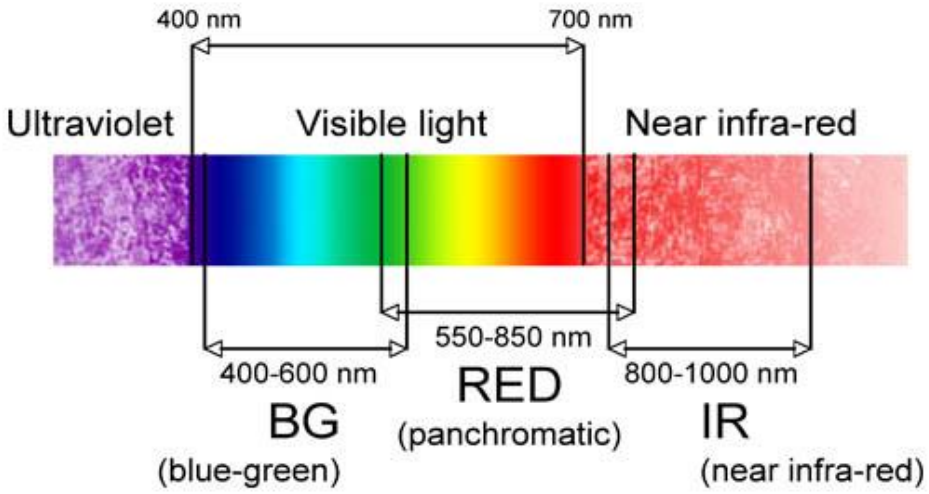

Figure 2-5*: Regions of the spectrum*

Each fluorophore has a wavelength at which it absorbs energy most efficiently, referred as the “Peak Excitation”, and a corresponding wavelength at which the maximum amount of adsorbed energy is re-emitted, referred as the “Peak Emission”. Selecting individual filters with the maximum amount of transmission at each of those wavelengths will ensure brilliant fluorescent images or great fluorescence analysis.

A typical fluorophore widely used in biological research, and which was used in the experiments in Chapter4, is **Sulforhodamine 101** (SR101) (Figure 2-7):

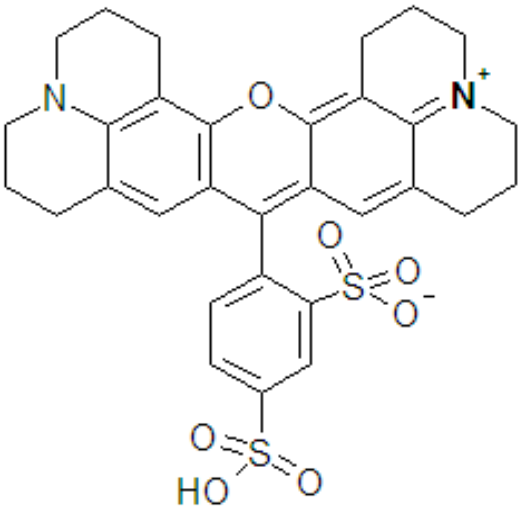

Figure 2-6*: Sulforhodamine 101 structure*

SR101 is a water-soluble, solfonic-derivated red fluorescent dye, that shows excitation and emission peaks respectively at ≈586 and ≈605 nm (Figure 2-8):

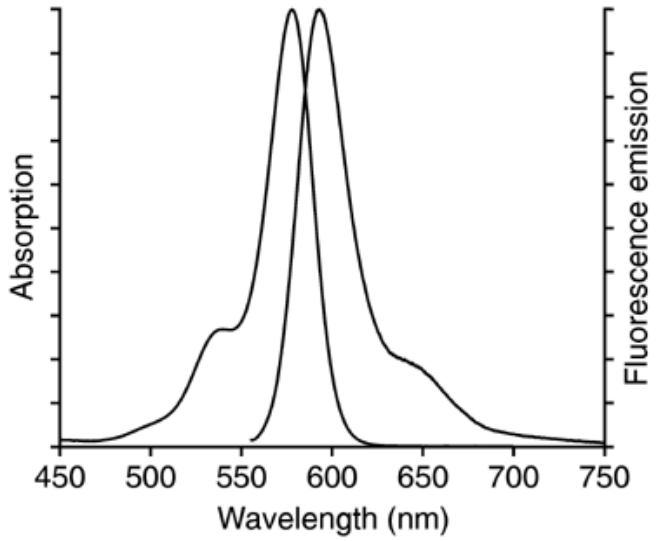

Figure 2-7 *Excitation-Emission spectrum of SR101*

Another widely used fluorophore is **Fluorescein isothiocyanate** (FITC). It is a derivate of a fluorescein molecule, functionalised with an isothiocyanate reactive group replacing a hydrogen atom on the bottom ring of the structure (Figure 2-8).

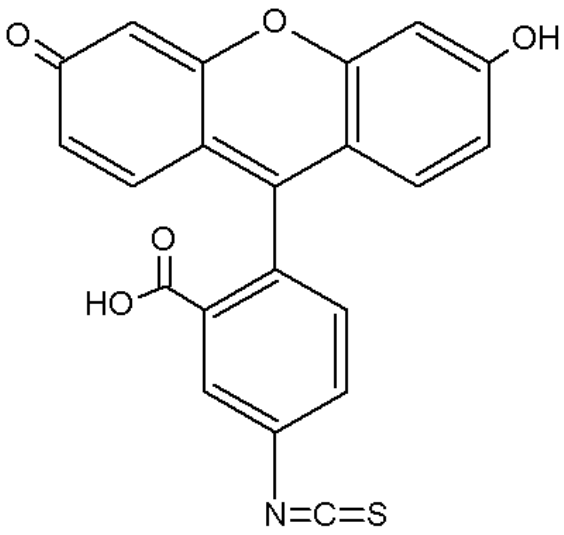

Figure 2-8 ***Fluorescein isothiocyanate structure.***

FITC is used especially for protein labelling (e.g. antibodies), for fluorescence microscopy, flow cytometry and immunofluorescence-based assays such as Western Blotting and ELISA. It has an excitation and an emission wavelength at ≈495 nm at ≈520 nm respectively (Figure 2-9).

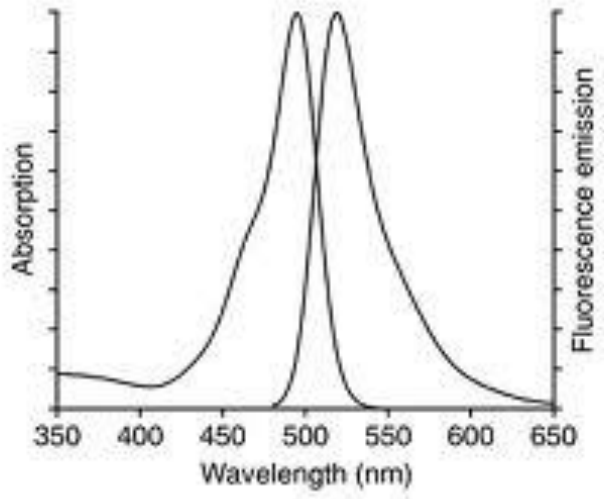

Figure 2-9*: Excitation-Emission spectrum of FITC and CMFDA*

A fluorophore which is commonly used for short and long term tracing of living cells is the green-fluorescent chloromethyl derivatives of **Fluorescein diacetate** (CMFDA) (Figure 2-10):

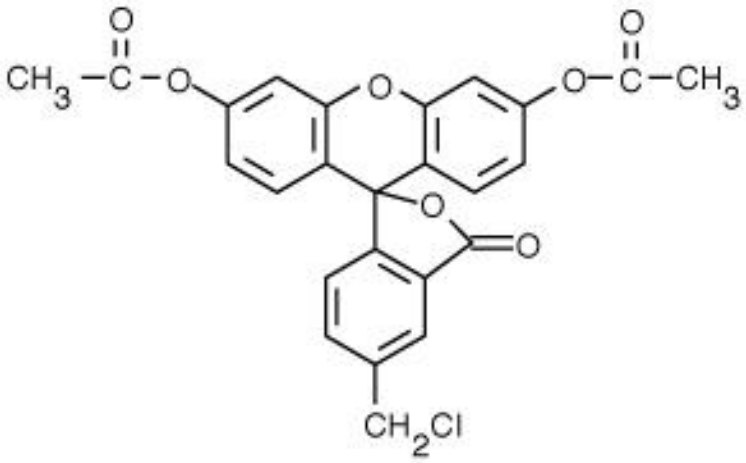

Figure 2-10*: 5-chloromethylfluorescein diacetate structure*

Showing emission and excitation respectively at ≈493 nm and ≈517 nm, the spectrum of CMFDA is identical to the one of FITC (Figure 2-9).

This fluorophore has the ability to freely diffuse through the membranes of live cells and, once inside, to be cleaved by an esterase into a fluorescent derivate. It can then react with thiol groups on proteins and peptides to form aldehyde-fixable conjugates (Figure 2-11).

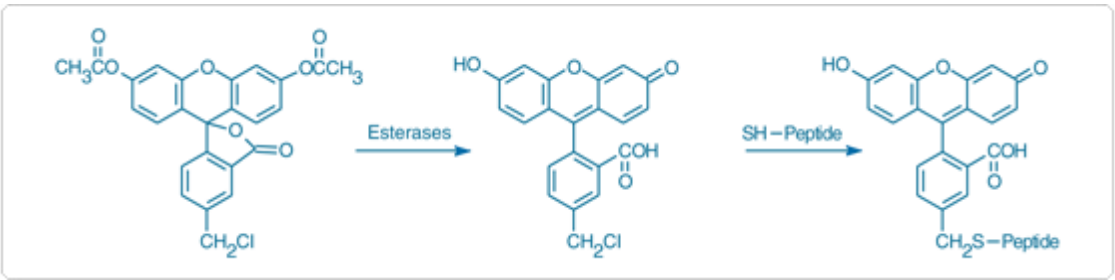

Figure 2-11 Intracellular reactions of CMDFA: firstly an esterase hydrolysis converts non-fluorescent CMFDA to fluorescent 5-chloromethylfluorescein, than it reacts with thiols on proteins and peptides

2.1.2 Circular Dichroism

Chirality is the property of some compounds to rotate the plane of polarisation of monochromatic light that passes through them. It is due to the particular disposition of the atoms in the molecule, which let the compound be non-superimposable on its mirror image.

Circular dichroism (CD) is the different adsorption of right and left circular polarized lights through a chiral molecule. The chiral characteristic of some compounds, in fact, makes this subsequently difference in adsorption helpful to define their specific molecular structure, and to recognise the exact compound.

CD is a spectroscopic technique which has applications in a variety of modern research fields, ranging from biochemistry to inorganic chemistry. Such widespread use of the technique arises from its essential property of providing structural information that cannot be acquired by other means. One other laudable feature of CD is its being a quick, easy technique that makes analysis a matter of minutes.

Circular dichroism is widely used especially for studying protein and nucleic acid conformation. It represents the difference in their absorption of left and right circularly polarized light, and can be therefore considered as the their absorption spectrum measured with left circularly polarized light minus the absorption spectrum measured with right circularly polarized light (Nafie et al., 1976).

However, this difference is so minute that can't be measured simply by difference with an ordinary UV spectrometer, but it is needed a specific instrument known as "CD Spectrometer", "Spectropolarimeter", or "Dichrograph".

2.1.3 CD Spectrometer

A CD spectrometer is made up of different sections (Figure 2-12):

-a source of light

-a monochromator

-a photoelastic modulator

-a photomultipler detector

Light from an intense source passes through a polarization modulator to the photomultiplier detector. This light had been monochromaticly polarized by the monochromator.

The polarization modulator induces a periodic variation in the polarization of the light beam through all ellipticities from left circular through elliptical, unchanged linear, and elliptical to right circular. During this cycle the intensity of the light beam does not vary.

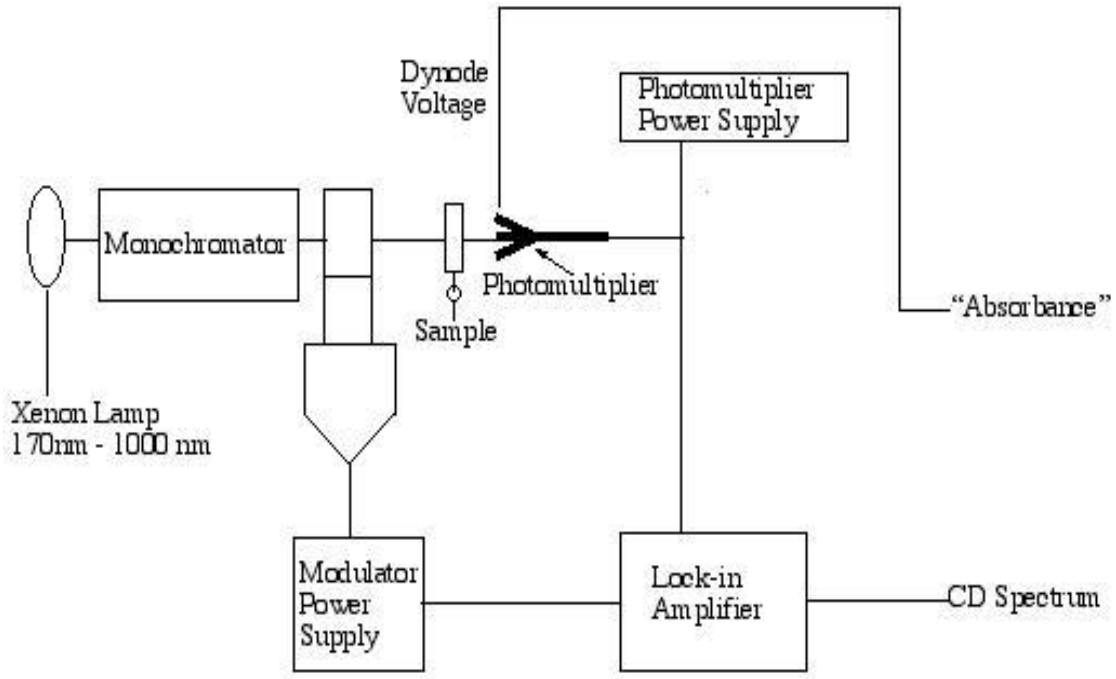

Figure 2-12*: CD spectrometer*

When an optically active (or chiral) sample is analysed, if it absorbs at the specific wavelength used, it gives a preferential absorption during one of the polarization periods and the intensity of the transmitted light will now, therefore, vary during the modulation cycle.

This variation of intensity is directly related to the circular dichroism of the sample at the specific wavelength used. Successive detections at different wavelengths lead to the generation of the full CD spectrum of the sample.

A picture of the instrument is given inFigure 2-13.

Figure 2-13 ***A typical CD spectrometer***

2.1.3.1 Principle of operation

In the CD spectrometer the sample is placed in a cuvette and a beam of light is passed through the sample. The light (electromagnetic waves) coming from the source is subjected to circular polarization, meaning that its plane of polarization is made to rotate either clockwise (right circular polarization) or anti-clockwise (left circular polarization) with time while propagating).

The sample is firstly irradiated with left rotating polarized light, and the absorption is determined byEquation 2.2:

$$A_l = \varepsilon_l c l$$

Equation 2.2

where ε_l is the molar extinction coefficient for left circularly polarized light, c is the molar concentration of the analyte and l is the pathlength (the cuvette width in cm).

A second irradiation is performed with right polarized light. The absorption then is determined byEquation 2.3:

$$Ar = \varepsilon_r c l$$

Equation 2.3

Now, due to the intrinsic asymmetry of chiral molecules, they will interact with circularly polarized light differently according to the direction of rotation. There will be a tendency to absorb more from one of the two rotation directions.

From the Beer's law (Beer, 1852), the differential molar extinction coefficient Δε, which is the difference between absorption of left and right circularly polarized light, is then obtained fromEquation 2.4:

$$\Delta\varepsilon = \varepsilon_l - \varepsilon_r = (A_l - A_r)/cl = \Delta A/cl$$

Equation 2.4

where ΔA is the differential absorbance between left circularly polarized (A_l) and right circularly polarized light (A_r); c is the concentration in moles per litre; and l is the cuvette pathlength in centimetres.

The difference in absorption can be related to difference in extinction, Δε, byEquation 2.5:

$$\Delta\varepsilon = \varepsilon_l - \varepsilon_r$$

Equation 2.5

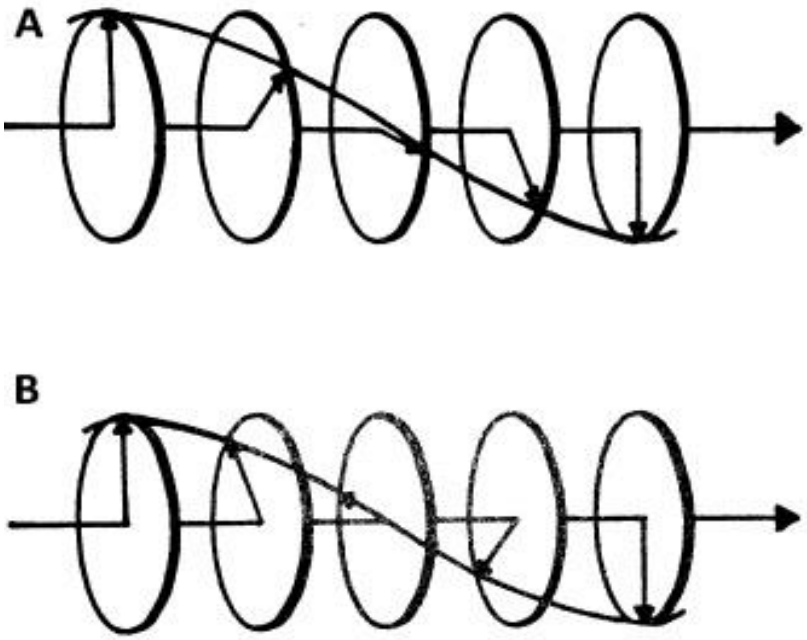

Figure 2-14 Schematic representation of right circularly polarized (a) and left circularly polarized (b) light.

Usually, due to historical reasons the CD is reported not only as difference in absorption or extinction coefficients, but also as degree of ellipticity, [θ].

The relationship between [θ] and Δε is given byEquation 2.6:

$$[\theta] = 3{,}298\ \Delta\varepsilon$$

Equation 2.6

Since the absorption is monitored in a range of wavelengths, the output is a plot of [θ] versus wavelength or Δε versus wavelength.

2.1.3.2 Applications

As previously said, in order to exhibit CD a sample must be optically active, which means that the molecule can't be superimposable on its mirror image (Figure 2-15).

The existence of such chiral molecules is critical to the chemical aspects of living systems.

As the chirality of each monomer in biological macrostructures (such as nucleic acids, peptides and proteins) is determinant for their functions and biological and biochemical processes, the determination of their stereochemistry is extremely important.

Only X-ray crystallography offers means of achieving this with complete certainty. However, pure crystals of biological samples, fundamental to perform X-ray analysis, are often either difficult or not convenient to reproduce.

Circular dichroism is an easy and fast alternative to X-ray crystallography. It is a direct consequence of the absolute spatial aspect of molecular shape.

The CD spectra associated with the conformation (secondary structure) of a biological macromolecule is related to the optical activity imposed by the optically active monomer units. Therefore, the contribution of each optically active monomer will influence the final CD spectrum of the macromolecule.

In principle, the sign and the magnitude of a CD band deriving from a particular transition needs to be correlated with the analyte structure. It involves theoretical calculations and the comparison of the CD of the compound under study with that of a well chosen compound of previously established stereochemistry.

The **far-UV** (<240 nm) region of the CD spectrum can reveal important characteristics of the secondary structure of proteins. CD spectra can in fact be useful to estimate the fraction of a molecule that is in the alpha-helix, beta-sheet, beta-turn, or any other (e.g. random coil) conformation (Whitmore and Wallace, 2008)(Greenfield, 2007).

CD cannot, however, say where a particular conformation detected is located within the molecule, or even absolutely predict its amount in the molecule. Despite this, CD is a valuable tool, especially for showing changes in conformation. It can, for instance, be used to study how the secondary structure of a molecule changes as a function of temperature or of the concentration of denaturing agents. CD can therefore reveal important thermodynamic informations about the molecule that cannot otherwise be easily obtained (Sreerama et al., 2000).

The **near-UV CD** (>250 nm) region of the CD spectrum provides informations on the protein's tertiary structure. The signals obtained in the 250–300 nm region are due to the absorption, dipole orientation and nature of the surrounding environment of the phenylalanine, tyrosine, cysteine (or S-S disulfide bridges) and tryptophan amino acids. Differently from the far-UV CD, the near-UV CD spectrum cannot determine any particular 3D structure. Rather, near-UV CD spectra provide structural informations on the nature of the prosthetic groups in proteins, e.g., the heme groups in hemoglobin and cytochrome c (Sreerama et al., 2001).

Visible CD spectroscopy is a very powerful technique to study metal–protein interactions and can resolve individual d–d electronic transitions as separate bands. CD spectra in the visible light region are only produced when a metal ion is in a chiral state, thus, free metal ions in solution are not detected. This has the advantage of only observing the protein-bound metal, so pH dependence and stoichiometries are readily obtained (Rupp and Weser, 1978).

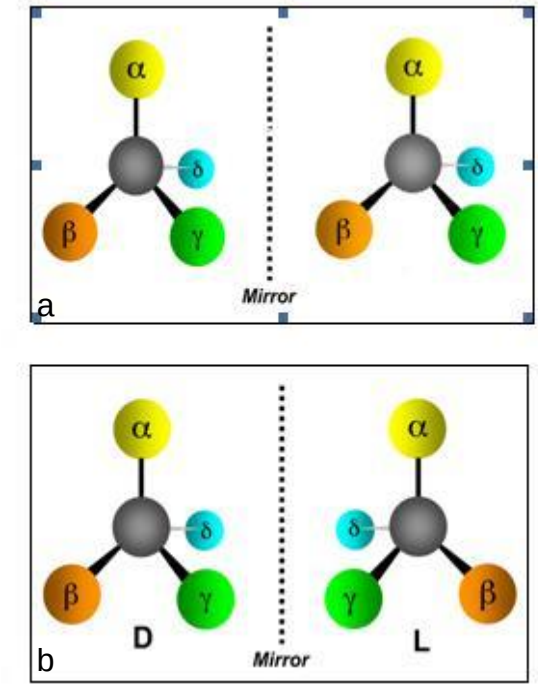

Figure 2-15: Example of (a) two achiral compounds and (b) two chiral compounds

2.1.3.3 Protein Secondary Structure analysis by CD

When analyzing biological macromolecules by CD, the informations obtained refers to the chirality of the backbone of the molecule: this is related to the amide-amide (in proteins) or base-base (in nucleic acids) interactions.

The simplest method of extracting secondary structure content from CD data is to assume that a spectrum is a linear combination of CD spectra of each contributing secondary structure type (e.g., "pure" alpha helix, "pure" beta strand etc.) weighted by its abundance in the polypeptide conformation. The major drawback of this approach is that there are no standard reference CD spectra for "pure" secondary structures. Synthetic homopolypeptides used to obtain reference spectra are in general poor models for the secondary structures found in proteins.
For example, the CD of an alpha helix has been shown to be length dependent and no homopolypeptide system has been found that is a good example of the beta sheet structure found in proteins.

In response to these shortcomings, several methods have been developed which analyze the experimental CD spectra using a database of reference protein CD spectra, containing known amounts of secondary structures (Provencher and Gloeckner, 1981)(Manavalan and Johnson Jr, 1987)(Sreerama and Woody, 1994).

The basic chromophore of the polypeptide backbone is the amide group that has two electron absorptions: a π-π^* transition, giving a strong absorption around 190 nm, and an n-π^* transition giving a weak absorption around 210 nm (often masked by the π-π^*). This defines the spectral range between 250-170 nm for protein's secondary structure analysis. These two transitions become optically active under the influence of the substituents on the asymmetric α-carbon atom in a free amino acid amide (Figure 2-16).

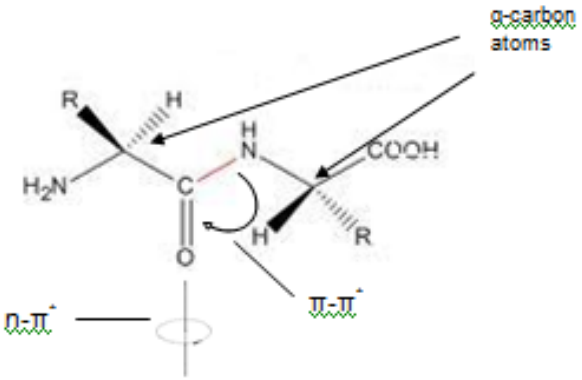

Figure 2-16: The monomer unit: optical activity induced by the groups attached at the centre of chirality

The optical activity derived from coupling chromophores is related to the relative orientations of the transition moments, hence, the secondary structure (conformation) of the polypeptide chain.

Unfortunately, a reliable calculation of the CD associated with a specific protein structure from first principles remains difficult. However, as different conformations have different amide-amide orientations, hence different CD spectra (Figure 2-17), X-ray of known proteins structures can be treated as fingerprints to correlate to the CD spectra of the compound of interest.

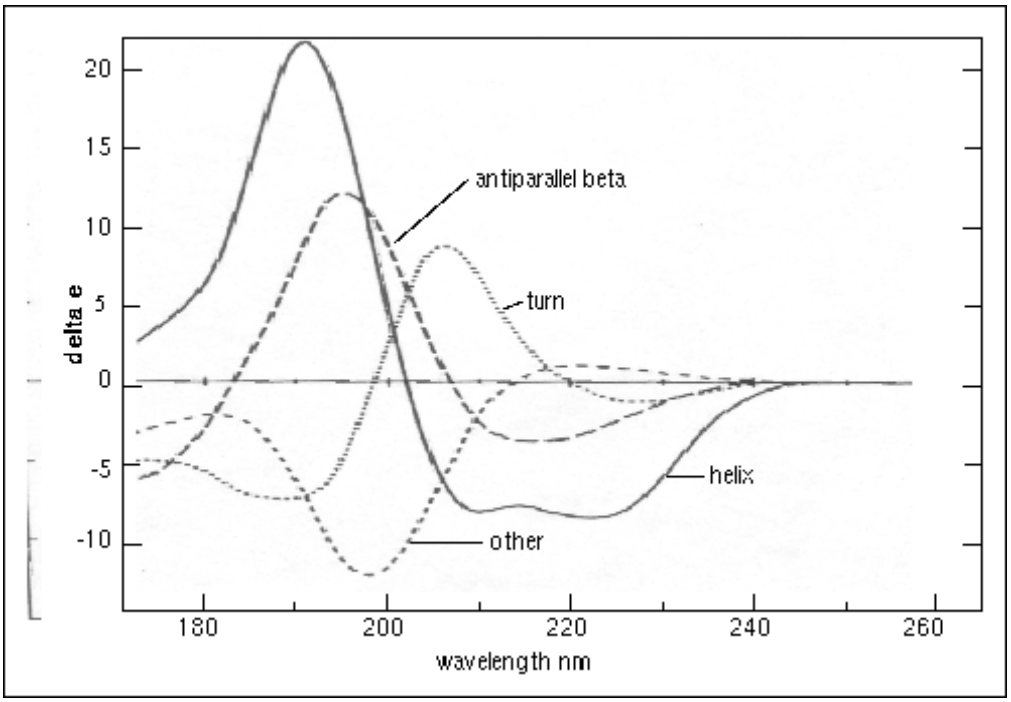

Figure 2-17: Circular dichroism spectra of "pure" secondary structures (Brahms and Brahms, 1980).

2.1.3.4 Advantages and limitations

As any other method, CD has its own advantages and limitations compared to related techniques.

As previously said, another technique which helps to understand the exact secondary structure of peptides, proteins and nucleic acids is the X-ray spectroscopy: this analysis is very precise, giving an accurate understanding informations about compound's structures. However it is an expensive technique, and has some limitations due to the preparation of the sample's crystals.

Another related technique is Nuclear Magnetic Resonance (NMR). Advantages of this technique are: ability to get informations for assigning a unique structure; very powerful technique for atomic level analysis, providing essential informations about chemical bonds; possibility to estimate chemical composition by performing quantitative data analysis. However, there are also some limitations: the size of the sample (it is need in the range of mg); the experiments are not as quick to perform as for the CD; special conditions are required to differentiate between different enantiomers; and there is also a limit to its sensitivity, whereas CD can work also with very small concentrations of the sample.

2.1.4 Colourimetry

Colourimetry involves the measurement of a compound or group of compounds present in a complex mixture by making use of the property that when light passes through a particular solution, some wavelengths are absorbed more than others (Mu and Plummer, 1988). It is a method widely used for determining the concentration of compounds, and when the compounds themselves are not coloured, they can be made to absorb light in the visible region by reaction with suitable reagents (Gordon, 1995). These reactions can be very specific and sensitive.

The depth of colour is proportional to the concentration of the compound being measured, while the amount of light absorbed is proportional to the intensity of

colour and hence the concentration (Mu and Plummer, 1988). This is expressed in terms of the Beer-Lambert law:

$$A = \varepsilon cl;\ A = log_{10}\frac{I_o}{I}$$

Equation 2.7

where *A* is the absorbance, I_o is the incident beam and *I* is the emerging beam; ε is the molar extinction coefficient, *c* is the concentration of the compound in solution and *l* is the optical pathway in cm.

There are several colourimetric assays available to analyse protein's concentrations. The most common ones are: the "Lowry method", also known as "Folin-Ciocalteau" method (which also includes the "Biuret reaction"), the "BCA reagent" (bicinchoninic acid) method and the "Coomassie brilliant blue" method, also known as the "Bradford" method (Gordon, 1995). Each one has a distinct working wavelength, which are 660, 562 and 595 nm, respectively.

Figure 2-18shows a schematic principle of any colourimetric analysis.

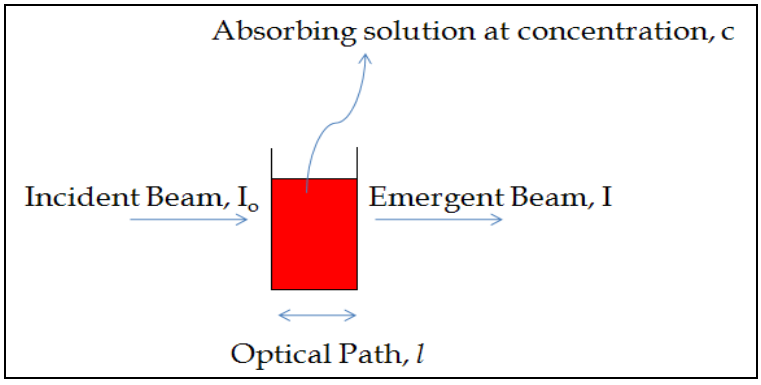

Figure 2-18: Schematic of the colourimetric analysis

2.1.5 Enzyme-linked immunosorbent assay

Enzyme-linked immunosorbent assay (ELISA) uses colourimetric analysis to quantify a specific analyte from a mixed solution. It is a plate-based assay

designed for detecting and quantifying molecules like peptides, proteins, antibodies and hormones.

Despite the relatively high costs per analysis, this method presents the advantage to be able to quantify a specific compound (usually a protein) from a mixture solution. This capacity is due to the unique use of an enzyme linked to an antibody or antigen to detect the analyte.

There are mainly three different types of ELISA assays: Direct, Indirect and Sandwich. In the present studies protein's quantifications were analyzed by Sandwich ELISA assays: in this method, it is measured the amount of antigen between two layers of antibodies. The antigen needs to present two antigenic sites capable of binding antibodies (Figure 2-19).

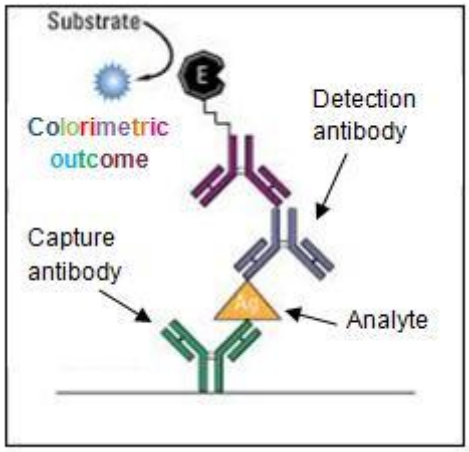

Figure 2-19: schematic of a sandwich ELISA assay

In the present studies different proteins were quantified by sandwich ELISA: Osteocalcin, Osteoprotegerin, CICP and VEGF.

2.2 Techniques for the characterization of materials

In this section, the characterisation techniques for calcium phosphate biomaterials will be briefly described in terms of principle, data expected and meaning to the information collected.

2.2.1 Brunauer–Emmett–Teller (BET)

The Brunauer-Emmett-Teller theory owns the name to its developers which, in 1938, published the first article about the BET theory in the Journal of the American Chemical Society (Brunauer et al., 1938).

The BET method is a very common technique used to determine the specific surface area of a material. Its theory is based on the Langmuir theory of Isotherms, and enables calculation of the surface area of powders or particles by analyzing the physical adsorption of a gas on the surface of the sample.

During a surface area analysis by BET (Figure 2-20), the samples are firstly dried either by heat under vacuum or by nitrogen purging. Adsorption of nitrogen is then followed at a temperature of 77 K, which leads to the so-called adsorption isotherm. The consequent pressure changes due to the adsorption of the gas on the surface of the samples are then monitored with high precision and accurate transducers and then, using a software, related to the surface area of the materials, including open macro and micropores.

The capacity of the BET method to determine the specific external surface area and also the open porosity of macroporous and microporous materials make this technique widely used not only in research for the study of artificial bone biomaterials, absorbents, sintering studies, gas filtration and others, but also in industrial applications like healthcare, pharmaceuticals, cosmetics, nanotechnology, medical devices, and many more.

Figure 2-20: Instrument for the determination of surface area by BET in the IRC centre at QMUL (Micromeritics, UK)

2.2.2 X-ray Diffractomery (XRD)

XRD involves the scattering of X-rays with λ ~ 1 Å by the repeating elements of a crystal lattice resulting in a diffraction from the crystal planes. It is used for determining the crystal structure of a specimen.

Bragg's Law indicates that diffraction is only observed when a set of planes make a very specific angle with the incoming X-ray beam (Balasubramaniam, 2007)(Cantor, 1980) (Figure 2-21). This angle depends on the inter-plane spacing d, which itself depends on the size of the atoms which make up the structure. During XRD, diffraction is measured for a range of different angles theta (θ). Figure 2-22shows the schematic of a powder diffractometer.

The amount of beam scattered depends also on the atomic number of the element present in the sample (specimen). The crystallographic directions and planes are expressed in Miller indices, where (x,y,z) indicates the location of an atom, and hkl indicates the direction from (0,0,0) to (x,y,z) (Park and Lakes, 2007).

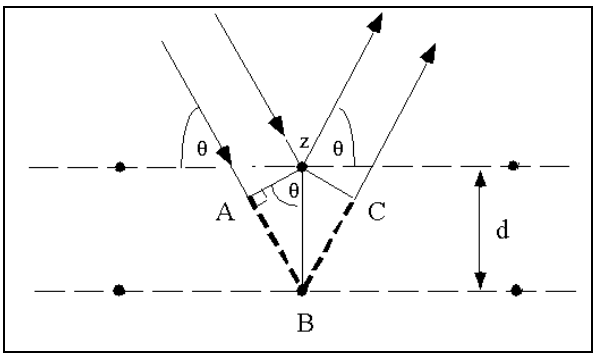

Figure 2-21: Schematic diagram of Bragg's Law

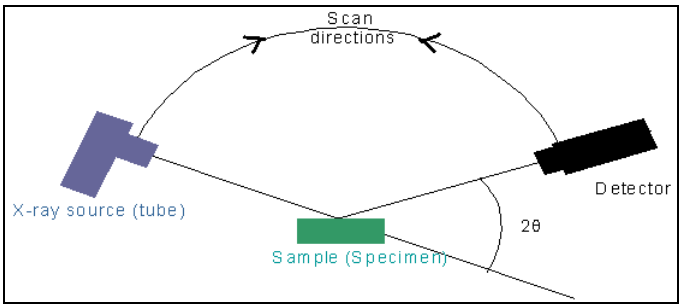

Figure 2-22: Schematic of a Powder Diffractometer

$$n\lambda = 2d_{hkl}Sin\theta_{hkl}$$

Equation 2.8

This relationship is further explained *via* Bragg's equation inEquation 2.8, where the path difference between coherently reflected beams is related to the d-spacing between the crystal planes, d_{hkl}, and the particular Bragg angle, θ_{hkl}, at which reflections from these planes are observed, the latter is detected and recorded against intensity as a XRD pattern.

2.2.3 Fourier Transform Infrared - Photoacoustic Spectroscopy (FITR-PAS)

Photoacoustic spectroscopy (PAS) is commonly used in the analysis of a variety of materials. It is a non-destructive technique that is applicable to almost all types of samples, powders, films and polymers. It offers minimal or

no sample preparation and the possibility to perform depth-profiling experiments. PAS can be used for both qualitative and quantitative analysis.

In PAS, the transformation of an optical event to an acoustic one occurs. Initially, modulated light is absorbed by the sample located in a sealed chamber. The non-radiative decay of this absorbed light produces a modulated transfer of heat to the surface of the sample. This modulated thermal gradient produces pressure waves in the gas (helium, He) inside the cell that can be detected by the attached microphone (Figure 2-23). This microphone signal, when plotted as a function of wavelength, will give a spectrum proportional to the absorption (or transmittance, or photo-acoustic unit) spectrum of the sample.

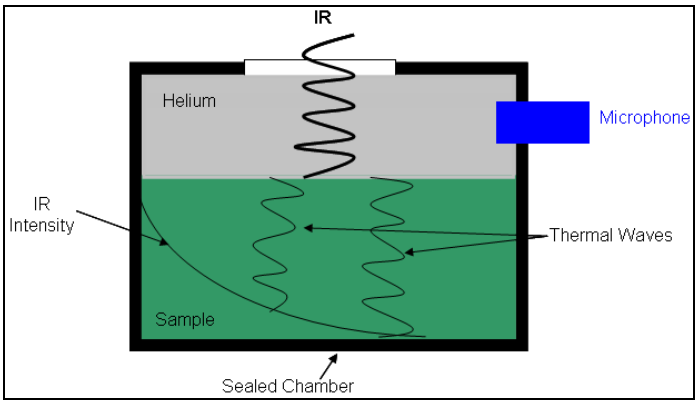

Figure 2-23: Depiction of a Photoacoustic Spectrometer (PAS) signal

For PAS experiment conditions, a FT-IR spectrometer capable of operating in both continuous scan mode and in step-scan mode is used. A photo-acoustic cell is used as an accessory for containing the sample within the sample chamber. Helium gas is used as the transfer medium in the cell and to purge water vapour and carbon dioxide. A 60 % carbon black-filled polymer is often used as a reference sample.

2.2.4 Scanning Electron Microscopy (SEM)

SEM is a technique that uses electrons instead of light to form an image. A probe is used to scan the surface of the object under investigation. SEM has a large depth of field, which allows more of a specimen to be in focus at one time.

It also has a high resolution with more control over the magnification due to the use of electromagnets rather than lenses, as a result, producing clear images. (Figure 2-24,Figure 2-25).

The method is suitable for specimens with conductive surfaces. For imaging only of specimens, preparation of the surface needs to be made, where the specimen is coated with gold

Figure 2-24: SEM Instrument in Nanovision Centre at QMUL (F.E.I., UK)

Further experiments/analysis, such as *energy dispersive spectroscopy (EDS)* can be used in conjunction with SEM to obtain elemental composition of the material under investigation. *EDS* is a microanalysis technique that is performed by measuring the energy and intensity distribution of X-ray signals generated by a focused electron beam on the sample material (Goldstein et al., 2003).

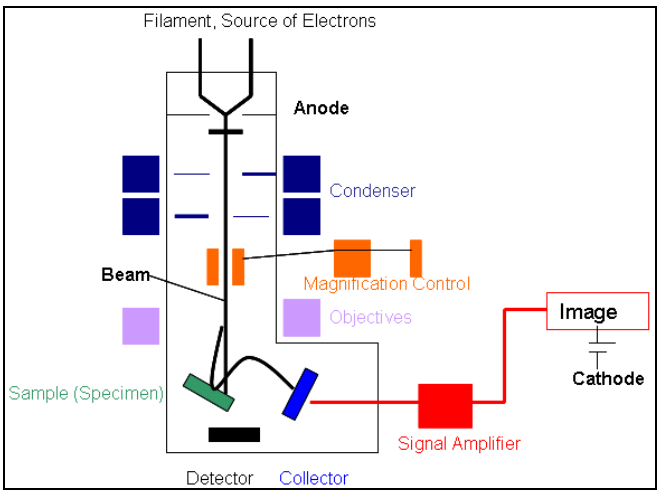

Figure 2-25: Schematic of an SEM instrument (Rochow and Tucker, 1994)

The surface of the object is scanned with the electron beam point by point, whereby the resultant signals are then fed to the amplifier. Various signals can be collected by the amplifier such as secondary electrons, back-scattered electrons, incident beam, visible light and X-rays. All can be monitored separately or simultaneously by the means of the appropriate detector. SEM thus constructs a pattern or map of the chosen resultant signals that can be interpreted as an image of the object under investigation.

2.2.5 Laser Confocal Microscopy (LCM)

LCM uses a laser beam to obtain high resolution images and 3-D reconstructions. This laser beam firstly passes through a light source aperture, and then is focused into a small focal volume on the surface of the specimen. A beam splitter separates portions of the light and, after passing a pinhole, the light intensity is detected by a photodetection device (like a photomultipler tube) transforming the light signal in electrical signal, recorded by a computer (Figure 2-26).

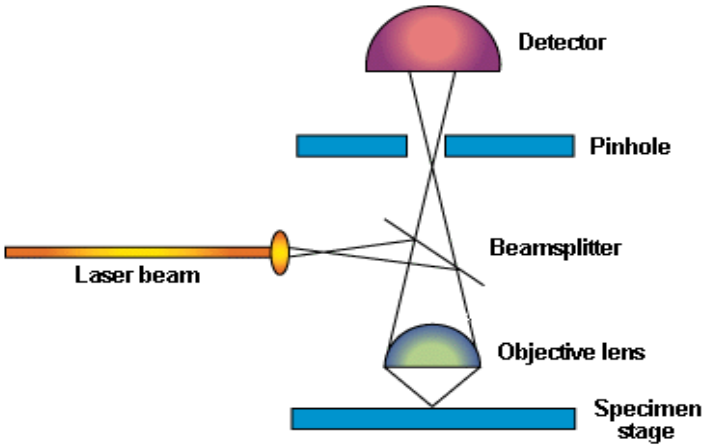

Figure 2-26: Schematic of a Laser Confocal Microscope

Images are acquired point-by-point, and with the help of the software it is possible to obtain three-dimensional reconstructions of topographically complex specimens. Its key feature is the ability to reproduce in-focus images of thick specimens at various depths.

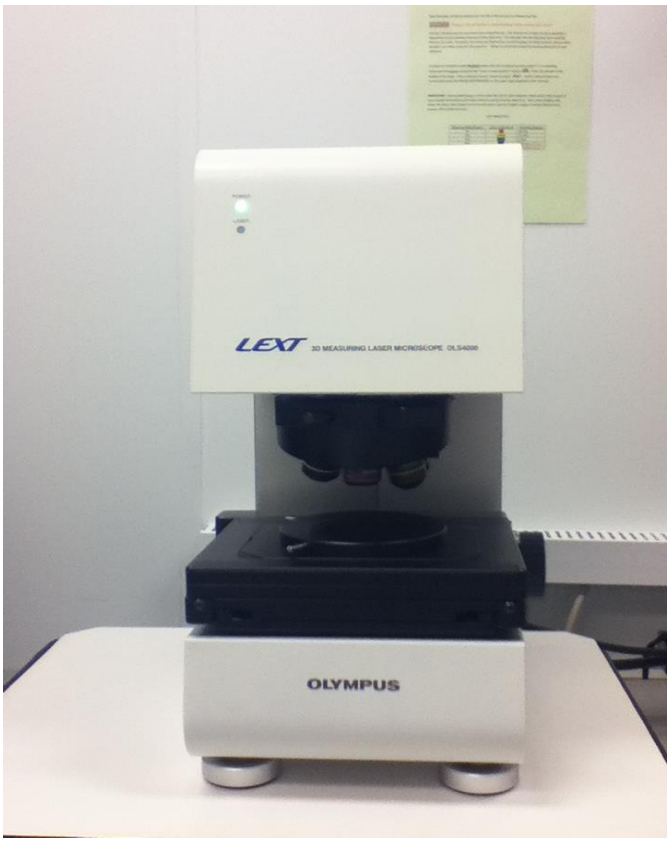

Figure 2-27: LCM instrument at the Marcus Nanotechnology Centre at GeorgiaTech (Olympus, Japan)

This characteristic makes LCM particularly useful for the analysis of thick biological samples. Moreover, it also enables LCM to detect with high definition features, up to the nanometer level, of particular 3D features on inorganic specimens like acute-angled slopes, or differences in surface roughness. In the present studies, LCM was used to characterize the surface roughness of different specimens before and after chemical and mechanical treatments.

2.2.6 X-ray Photoelectron Spectroscopy (XPS)

XPS is a technique that enables the determination of the elemental composition of the surface of a material. It is widely used in different industries, like cosmetics, fabrics, biomedical or packaging, and it is routinely used to determine the type and the quantity of the elements present up to a depth of 1-12 nm of the material surface, any chemical contamination, the chemical state of the elements and their bonding.

In XPS the sample is illuminated with soft (1.5kV) X-ray radiation in an ultrahigh vacuum. The photoelectric effect caused by the X-rays leads to the production of photoelectrons, the energy spectrum of which can be determined in a beta-ray spectrometer. This energy spectrum permits to determine the composition of the sample. The Einstein equation (Equation 2.9) is used to calculate the energies of the photoelectrons (E_b) knowing the photon energy (hv) and the energies of the emitted photoelectrons (E_k).

$$E_k = hv - E_b$$

Equation 2.9

Because the binding energies of the electron orbitals in atoms are known, the position of the peaks in the spectrum allows identifying the atomic composition of the sample surface.

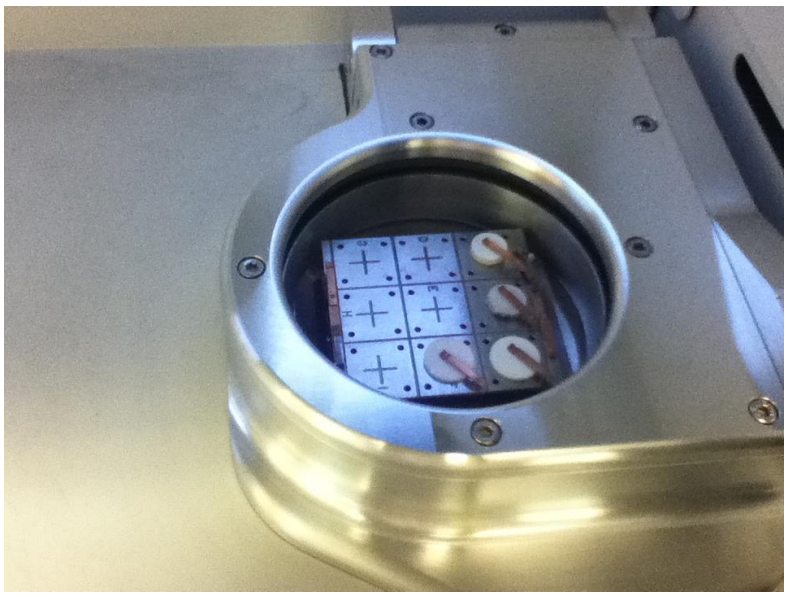

Figure 2-28: Sample chamber of the XPS instrument at the Marcus Nanotechnology Centre at GeorgiaTech (Thermo Scientific, USA)

In the present studies, XPS was used to characterize semi-quantitatively the surface chemical composition of different specimens before and after chemical and mechanical treatments.

3 Synthesis and characterization of materials

3.1 Background

Several studies have shown the importance of materials surface physiochemical properties such as surface roughness (Missirlis, 2000), surface area (Campion et al., 2011), surface charge (Bodhak et al., 2009), porosity (Hing et al., 1999a) and chemistry (Gibson*, et al.* 2002; Hing 2005) in directing the biological response.

These studies seem to suggest that each factor affects the bioactivity and thus biocompatibility of the material *in vivo* and *in vitro* in different ways (Ducheyne, 1987). For example, a Ca/P ratio of 1.67 is the optimum ratio to which stoichiometric HA forms as a one phase product, which was also found to be true when forming Silicate-substituted hydroxyapatite (SA) (Hing et al., 1998)(Gibson et al., 1999a) where enhanced bioactivity was achieved (Patel et al., 2002). Lower or higher ratios resulted in impurities, which often lead to poorly calcined or sintered samples (Gibson et al., 2001), that changed the biomaterials' surface area and charge, the packing of the crystallites, the roughness, and the density, which subsequently have an effect on the adsorption property of the proteins to that surface (Rashid et al., 2008).

Thus, it is of great importance to characterise HA and SA samples so that microstructure is similar and is therefore possible to compare results of protein and cell behaviours with defined material's structural features.

3.2 Experimental Methodology

SA and stoichiometric hydroxyapatite (HA) powders were synthesised at Apatech^{TM} Ltd. They were processed so as to achieve dense discs with matched densities and surface morphologies between the SA and HA specimens.

Porous granules were received directly from Apatech^{TM} Ltd in different granule's sizes and strut porosity.

3.2.1 Material Synthesis

3.2.1.1 Dense Disc (DD) Samples Preparation

Phase-pure, stoichiometric HA and 2.6wt % silicate-substituted SA powder (containing 0.8wt % Si) were synthesized by Apatech Ltd. An aqueous precipitation route was used to synthesize HA and SA powders, as previously shown by Akao and Gibson respectively (Akao et al., 1981), (Gibson et al., 1999a). However, in order to obtain exactly 0.8% Si substitution of stoichiometric HA, the exact number of moles used to synthesize the SA powder followed the protocol shown in the study of Hing et *al*. (Hing et al., 2006a)

Dense discs (DD) were prepared by pressing 1.00 g of either HA or SA powder in a 16 mm diameter steel die. The force used was 1.75 ton pressure, corresponding to powders pressed at loads of 18KN (around 90.9 MPa).

The discs were then sintered in Carbolite Furnaces (RHF1600 or RHF1400, Carbolite, UK) at temperatures ranging from 1200°C to 1375°C for SA, and from 1150°C to 1300°C for HA. The ramp rate was 2.5°C per minute, dwell time of 120 minutes and cooling rate of 10 °C per minute to ambient temperature.

3.3 Material Characterisation

3.3.1 X-ray Diffractometry (XRD)

XRD patterns were obtained using a Siemens Xpert-Pro diffractometer. The samples were required to be <1mm, they were placed in a sampling holder and scanned continuously by a graphite detector from 20° to 70° 2θ, at a scanning speed of 1°/min 2θ at a minimum step size of 0.02° 2θ and a count time of 2.5 seconds. The monochromatic Cu-K radiation was used at wavelengths of Ka_1 = 1.540598 nm and Ka_2 = 1.544426 nm with an intensity ratio of 0.5.

Crystallography Parameters were obtained using the XRD patterns in conjunction with 3 programs. Xpert HighScore Plus software along with the ICDD database was used to obtain the crystallographic parameters, and peak

list with the Miller indices of known stoichiometric HA. Pickpx2 software (developed in-house, UK) enabled *xrdml* and *uxd* files of the XRD data to be converted into corresponding 2-theta values and their d-spacing along with peak intensities. And the UnitCellWin software (developed by T.J.B. Holland (Holland and Redfern 1997), UK) evaluated all information (Miller indices and 2-theta data) and calculated the crystallographic parameters ($a = b \neq c$ and cell volume).

3.3.2 Fourier Transform Infrared Spectroscopy (FTIR)

FTIR-Photoacoustic spectroscopy (PAS) spectra were obtained using a Thermo Nicolet 8700 spectrometer in conjunction with a PA Cell-MTEC Model 200 with KRS-5 sample chamber window. Spectra were obtained at a resolution of 4 cm^{-1}, averaging 128 scans, operating from 4000 to 400 cm^{-1}. The sample chamber of the PAS cell was purged with helium gas prior to analysis.

3.3.3 Surface Area Analysis & Porosimetry

A micromeritrics FlowPrep060 degaser (Gemini II 2370, Micromeritics, UK) multipoint analyser was used to measure the surface area of granular samples < 1 mm size via BET method.

Surface area values were obtained using helium (He) at 15 psi with an evacuation rate of 300 mmHg/min. Prior to the analysis samples were dried at 200 ^{o}C overnight with nitrogen (N_2) at 15 psi.

Strut porosity of the porous granules was confirmed by embedding porous specimens in resin mixture with a 5.2 resin/hardener ratio (EpoFix, Struers, UK) and left to slowly set for 8 hours. The specimens were then polished on diamond paper from P400 to P1600, and then imaged using SEM. The strut porosity was then determined using ImageJ 1.44i (National Institute of Health, USA).

3.3.4 Scanning Electron Microscopy (SEM) and Energy Dispersive Spectroscopy (EDS)

Surface microstructure and morphology was qualitatively assessed by scanning electron microscopy (SEM) using an Ultra 60 field emission (FE) microscope (Carl Zeiss SMT Ltd., Cambridge, UK). The Hummer Sputtering System was used to prepare non-conductive samples by coating those with Au/Pd. Once coated, the samples were then mounted on aluminum studs and analyzed for their surface characteristics from the micro to the nano scale using the Zeiss Ultra60 FE-SEM, with an accelerating voltage of 5KeV and a working distance between 4.6 and 11.1 mm.

A INSPECT F (FEI, UK) field emission gun scanning electron microscope (FE-SEM) equipped with an energy dispersive X-ray spectrometer (EDS) was used to observe morphology and determine elemental distribution of silicon (Si) at a high resolution and accelerating voltage of 10 kV.

3.3.5 Density and porosity ratio measurements

Apparent density, real density and total porosity were obtained using a method based on the Archimedes principle of water displacement.

The specimens were weighed in a dry condition (W_{dry}) in triplicate using an analytical plus electronic balance™ (Ohaus, Leicester, UK). The specimens were then placed in boiling deionised water for 30 minutes (60 minutes for porous samples) to ensure all open pores were filled with water and left to cool, still submerged in water. The specimens were then weighed using the density AP solids kit (Ohaus, Leicester, UK), three times submerged in deionised water (W_{sub}) of known temperature, and then three times in the wet state (W_{sat}). The apparent and real densities of specimens were calculated using Equation 3.1 and Equation 3.2 respectively. The former takes into account both the open and closed porosity of the material, while the latter only considers closed pores.

$$Apparent\ density = \left\{ \frac{W_{dry}}{W_{sat} - W_{sub}} \right\} \rho H_2O$$

Equation 3.1

$$Real\ density = \left\{ \frac{W_{dry}}{W_{dry} - W_{sub}} \right\} \rho H_2O$$

Equation 3.2

Where ρH_2O is the density of de-ionised water and *W* is weight.

$$Total\ Porosity\ (TP) = \left[1 - \left(\frac{Apparent\ Density}{\rho HA} \right) \right] \times 100$$

Equation 3.3

Equation 3.3 was used to determine the total porosity. The apparent density includes both open and closed porosity in the volume of the material, whereas the real density includes only the closed porosity.

3.3.6 Statistical Analysis

For analysis of materials densities, surface area and total and strut porosities the sample size was n=3, and mean and standard deviation were calculated for each sample.

3.4 Results

3.4.1 Material chemistry

3.4.1.1 X-ray Diffractometry (XRD)

Phase purity and the presence of silicate and phosphate groups were confirmed using XRD and FTIR respectively. XRD (Figure 3-1) confirmed the phase purity of both the HA and SA samples. There was no presence of either *β-TCP* or CaO impurities, as they should be observed at around 31.2 ^{o} and 37.8 ^{o}, respectively (Hing et al., 1998). These impurities may form within the samples as a result of decomposition during the sintering process which makes the Ca/P ratio either greater or lower than the stoichiometric molar ratio of 1.67 (Hing et al., 1998), (Gibson et al., 1999a). The peaks shown are

narrow and sharp which indicate a high level of crystallinity for all the compositions.

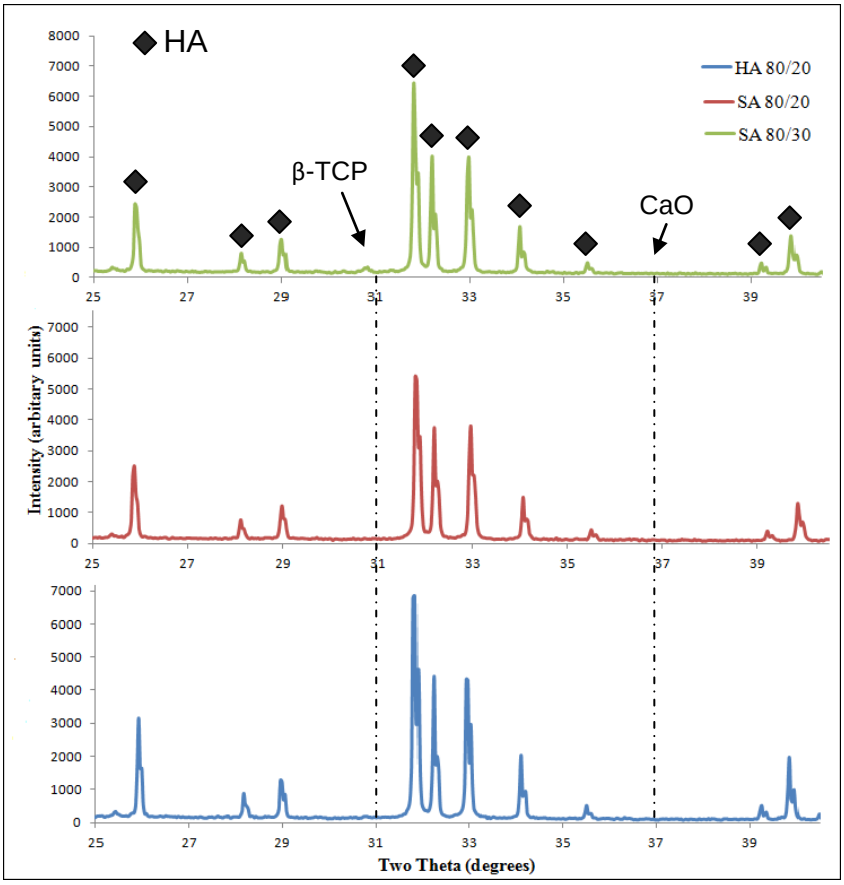

Figure 3-1: XRD patterns of HA and SA porous granules

3.4.1.2 FTIR analysis

Following the XRD analysis, FTIR was performed to analyze the presence of phosphate and silicate groups (Figure 3-2). In both HA and SA samples there is a noticeable sharp peak present at 3570cm^{-1} which corresponds to the presence of OH groups. The band heights of the peak is found to be slightly higher at ~6PA (photoacoustic) in SA 80/30 than SA 80/20 and HA 80/20 where it is found to be ~4PA.

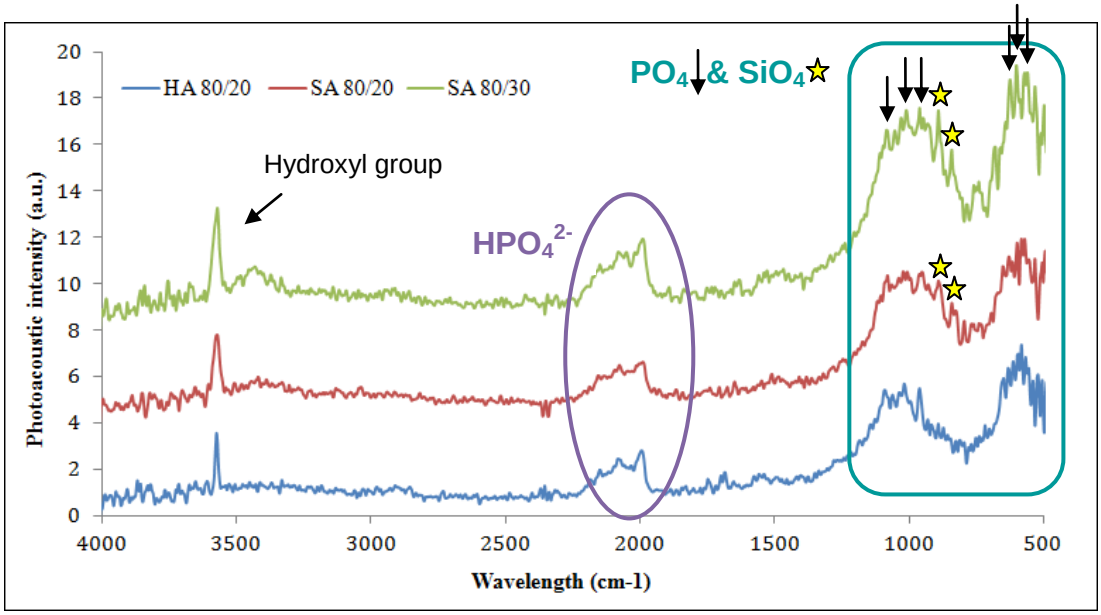

Figure 3-2: FTIR spectra of HAG80/20, SAG80/20 and SAG80/30 between 1000 and 500 cm^{-1}

All the spectra also show a broad peak ~1100cm^{-1}, which indicates the presence of phosphate groups. The phosphate symmetric stretching vibration (ν_3 and ν_1 bands) are characterised by 3 peaks present at 1089cm^{-1}, 1032cm^{-1} and 962cm^{-1}, which again are more defined and intense in sample SA80/30. The phosphate bending vibration (ν_4 bands) is again characterised by 3 peaks present at 631cm^{-1}, 606cm^{-1} and 559cm^{-1}. In the two SA samples spectrums two peaks present at ~880cm^{-1} determine the presence of SiO_4^{4-} groups with the Si-O vibration. Finally the spectra for the HA and SA samples show broad peaks present between 2000cm^{-1} – 2200cm^{-1} these peaks may correspond to surface absorbed HPO_4^{2-} groups (Gibson et al., 1999a) (Hing et al., 2006a).

3.4.2 EDS analysis

The EDS analysis showed the content of element present on the surface of the samples under investigation in terms of weight and atomic percentages. Table 3-1 shows the elemental distribution as a percentage on the surfaces of the two biomaterials. On SAG80/20 and SAG80/30 was detected a percentage of Si of 0.75 and 0.77 % respectively, while none for HAG80/20.

Table 3-1: Weight and atomic percentage of elements present in HA and SA PG analyzed by EDS

	HAG80/20		SAG80/20		SAG80/30	
Element	**Weight%**	**Atomic%**	**Weight%**	**Atomic%**	**Weight%**	**Atomic%**
C	9.74	16.57	10.08	17.25	10.35	18.96
O	45.84	58.52	44.42	57.09	34.89	48.00
Si	-	-	0.75	0.40	0.77	0.53
P	15.15	9.99	14.34	9.65	17.20	12.29
Ca	29.27	14.92	30.41	15.60	36.80	20.21

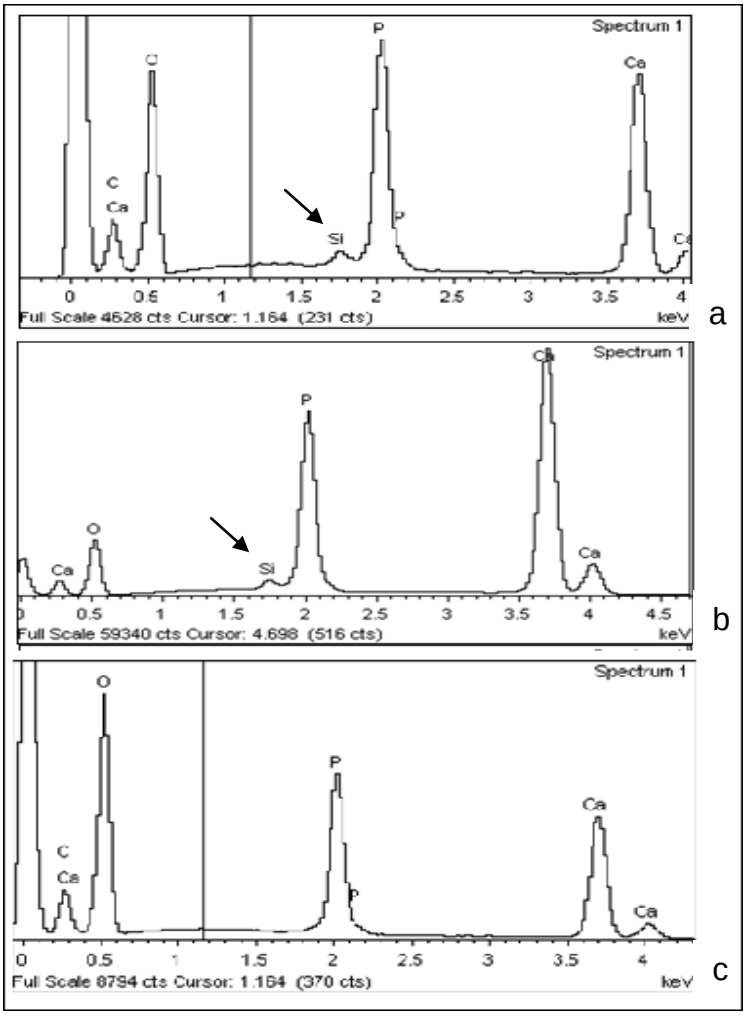

Figure 3-3: EDS spectra of (a) SAG80/30, (b) SAG80/20, and (c) HAG80/20

Figure 3-3 shows the EDS spectra of each sample, clearly showing the absence (c) and presence (a and b) of the silicon as an element in the biomaterials' surface of HA80/20, SAG80/20 and SAG80/30 respectively. No other peaks appear other than Oxygen, Calcium and Phosphate.

3.4.3 Sample morphology

3.4.3.1 Density and Porosity measurements

All the samples were investigated for their apparent and real densities and total porosity (TP) using the Archimedes' principle (Table 3-2).

On DD, results showed very similar apparent and real densities and also a very similar level of total porosity between HA and SA.

On PG, the results showed lower both apparent and real densities from the two SA porous granules compared to HA. The TP was also lower on HAG80/20 compared to the two SAG. The apparent and real densities, as well as the TP % were, however, very similar between the two SA samples.

Table 3-2: Table of densities and percentage of porosities using Archimede's Principle of water displacement for HAG 80/20, SAG 80/20 and SAG 80/30

Material	Apparent Density (g/cm^3)	Real Density (g/cm^3)	TP %
HAD	2.85±0.2	3.10±0.3	9.1±0.1
SAD	2.81±0.4	3.09±0.2	9.2±0.08
HAG 80/20	0.71±0.05	2.82±0.08	77.6±0.9
SAG 80/20	0.56±0.06	2.72±0.1	79.3±0.7
SAG 80/30	0.55±0.04	2.76±0.2	80.2±0.6

3.4.3.2 Surface area analysis

B.E.T. analysis was performed on porous granules of HA 80/20, SA 80/20 and SA 80/30. The results showed a grater surface area on the SA 80/30 sample compared to the others, probably due to the higher percentage of strut

porosity. HA and SA 80/20 showed a very similar surface area between each other shown from Table 3-3.

Table 3-3: Table of surface area using B.E.T.

Material	Sample Weight (g)	Surface area (m^2/g)
HAG 80/20	2.02	0.24±0.07
SAG 80/20	2.52	0.24±0.09
SAG 80/30	2.19	0.27±0.1

3.4.3.3 SEM analysis

SEM images were used to analyze the morphology and microstructure of the samples. Figure 3-4: SEM images of (a) HA and (b) SA dense discs, gold coated shows HA and SA dense discs analyzed at a 30,000X magnification, showing no signs of degradation, a crystalline structure and the presence of clear grain boundaries. Figure 3-5a, b and c shows the PG samples analyzed at a magnification of 24,000X: grain boundaries are still visible on the surface of the porous samples and similar to those seen on dense discs.

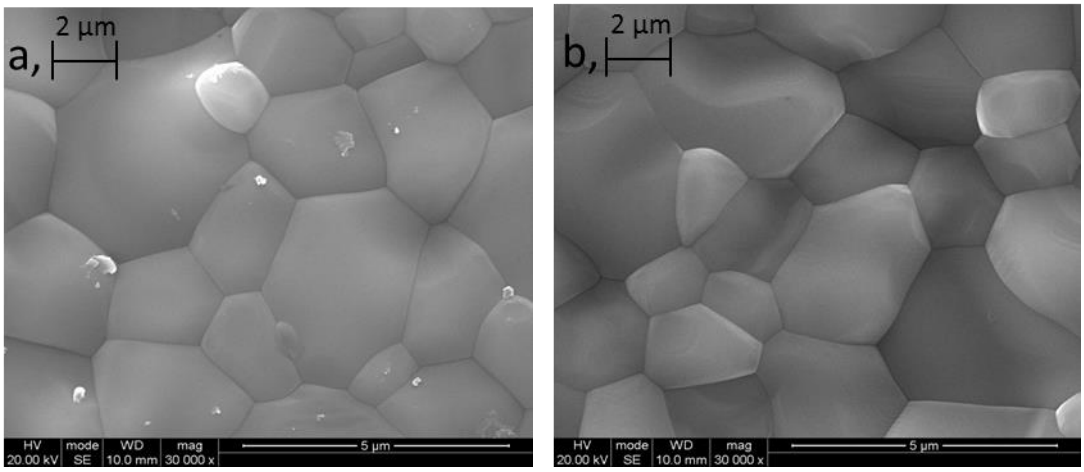

Figure 3-4: SEM images of (a) HA and (b) SA dense discs, gold coated

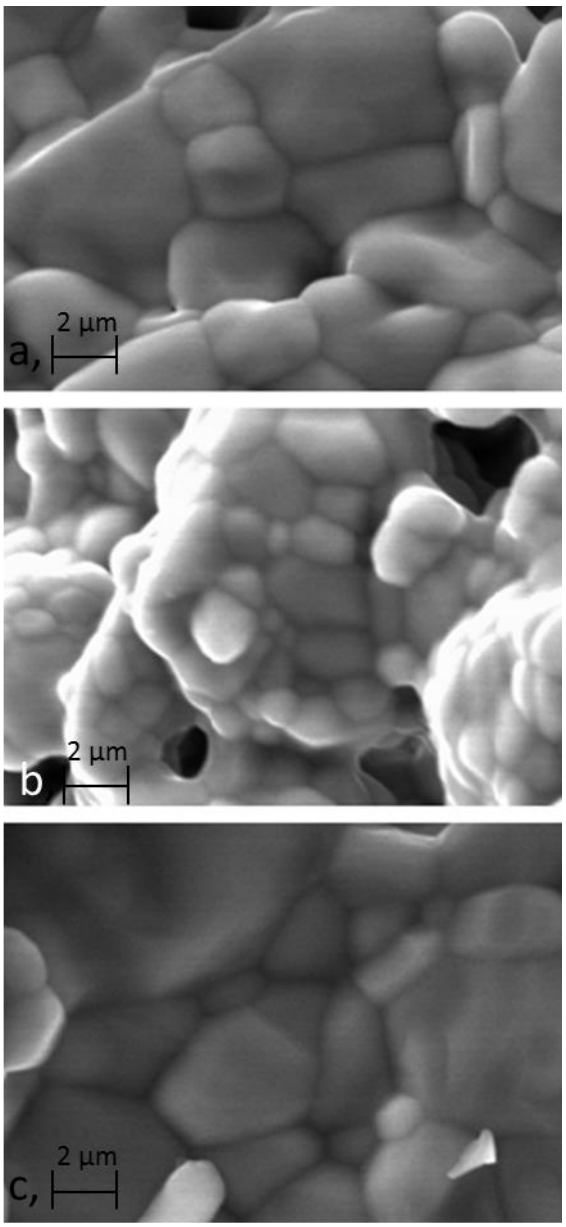

Figure 3-5: SEM images of (a) HAG80/20, (b) SAG80/20 and (c) SAG80/30, gold coated

Pore interconnectivity was determined via samples embedded in resin, polished and imaged by SEM. The strut porosity was observed as in Figure 3-6, Figure 3-7 and Figure 3-8 respectively for HAG80/20, SAG80/20 and SAG80/30, and quantified as shown in Table 3-4.

Table 3-4: Strut porosity of the samples analyzed via thresholds

Sample	Strut Porosity %
HAG80/20	18.4 (±0.7)
SAG80/20	19.8 (±0.3)
SAG80/30	31.8 (±0.3)

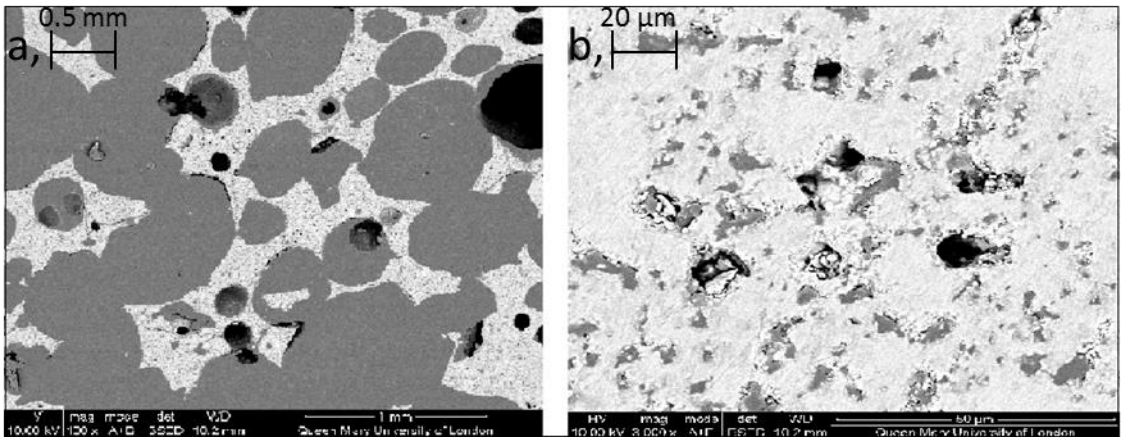

Figure 3-6: SEM images of porous HAG80/20 embedded in resin and polished used to determine the strut porosity at (a) 100 and (b) 3000 magnification

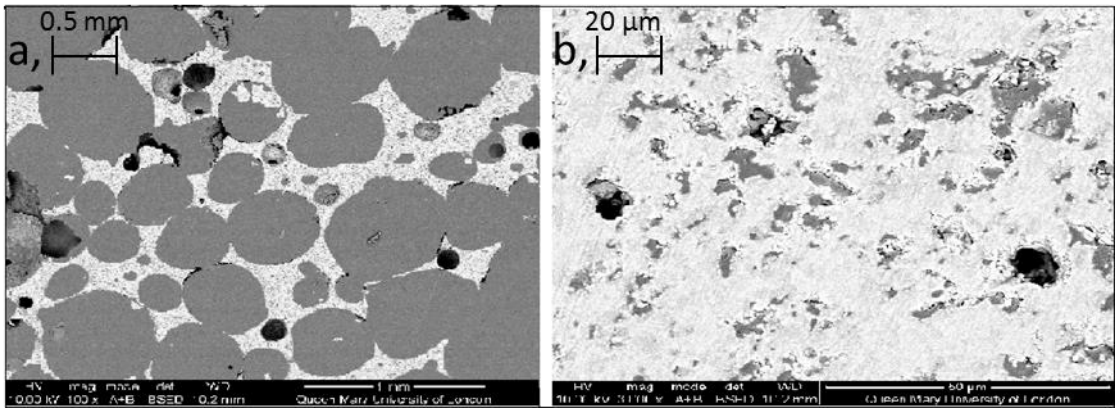

Figure 3-7: SEM images of porous SAG80/20 embedded in resin and polished used to determine the strut porosity at (a) 100 and (b) 3000 magnification

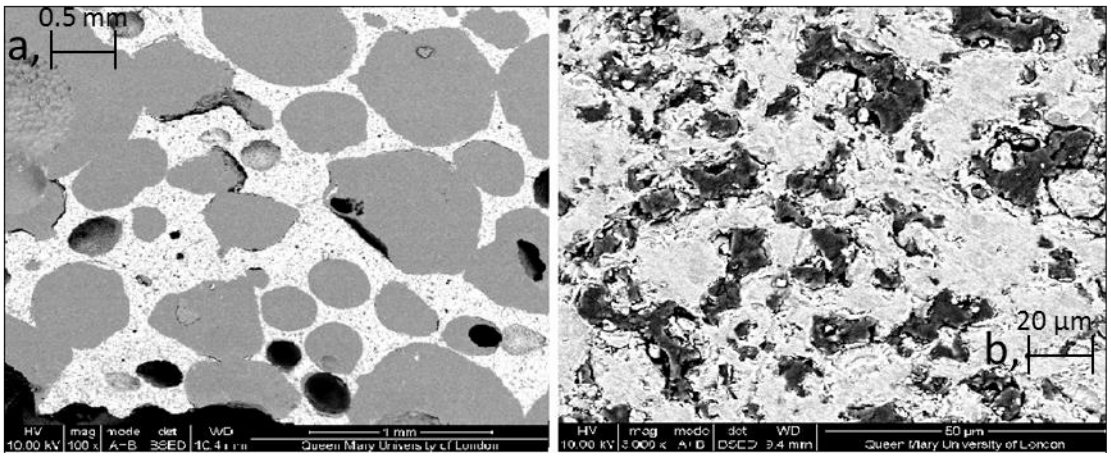

Figure 3-8: SEM images of porous SAG80/30 embedded in resin and polished used to determine the strut porosity at (a) 100 and (b) 3000 magnification

3.5 Discussion

The results of the analysis described in this chapter confirm the chemical, morphological and structural characteristics of the samples as they were expected to be found.

XRD data was successful in showing no additional phases to HA (Figure 3-1) The differences in the intensity of the XRD pattern from HA to SA were known to be due to the presence of silicon (Si), as silicon is known to act as a sintering aid, which results in SA samples having lower crystallinity at the same calcination temperature than HA (Gibson et al., 2002, Kim et al., 2003). Hence, lower intensity was observed. Also, as indicated on the respective figure, no secondary phases such as CaO or β-TCP were detected. These phases would have risen from the impurities present on decomposition of SA whilst being sintered: in fact, if silicon was not entirely being incorporated in the HA structure, it would have led to an increase or decrease in the molar CaP ratio of 1.67 which would have given rise CaO or β-TCP within the diffraction patterns.

FTIR analysis (Figure 3-2) was able to identify phosphate peaks of ν_3, ν_1 and ν_4 in both HA and SA samples and the presence of silicon in the SA samples. There were no carbonate peaks detected therefore suggesting that the SA samples had silicate ions substituted for the phosphate ions. Results show a broader spectrum for the SA material, probably due to the loss of the hydroxyl through the substitution compared to HA, as shown at the full range of 4000 to 400 cm-1, which was expected and agreed with by others.(Balas et al., 2003, Gibson et al., 1999, Hing et al., 2006, Thian et al., 2006) For the characteristic phosphate and silicate group peak position, the assignments made agreed with those found in the work of Gibson, Best *et al.* (Gibson et al., 1999), where the peak positions observed showed phosphate peaks at 950, 890 and 840 cm-1 in SA compared to HA between 960 and 1100 cm-1, which have moved due to the presence of silicate. Further confirmed by peak assignment found in the work of Hing *et al.*(Hing et al., 2006) and Thian *et al.* (Thian et al., 2006).

EDS analysis was conducted on SA80/20, SA80/30 and HA80/20 samples in order to verify the levels at which calcium, phosphate and silicon were present (Figure 3-3 and Table 3-1). It was reassuring to see that there were high wt% of calcium and phosphate present in all samples. The wt% of silicon that was detected in SA80/20 and SA80/30 was 0.75wt% and 0.77wt% respectively. The reason behind the lower wt% of silicon in both samples could be that after the sintering process, the silicon could be hidden behind the carbon that is present therefore not all of the silicon was able to be detected by EDS analysis.

.

Densities measurements (Table 3-2) showed the real density being higher compared to the apparent density and the density of the porous samples lower than the calculated density of the dense discs. This observed lower density was already expected, especially from the porous samples (PG) which present close porosity; moreover, was also found by others (Hing et al., 1999) for the porous specimens, which were cylindrical in shape with a length of 8.8 mm and a diameter of 4.6 mm.
Using the Archimedes‟ principle also allowed for the total porosity of the samples to be determined at an average 80 % for all samples, which was as expected. This would represent the macroporosity of the samples *via* density and SEM (in mm), while the microporosity (the strut) can be visualised using SEM (in μm), but sometimes also measured using intrusion porosimetry (Rosengren et al., 2002)

Surface area measurements by BET (Table 3-3) showed a slightly higher surface area on the SAG80/30 compared to the other two samples, probably due to its higher percentage of strut porosity. The introduction to porosity should not affect the surface chemistry of the samples compared to the powder or dense disc specimens, as in principle only the interconnectivity would have increased (Shors and Holmes, 1993) which was observed here also.

Finally, strut porosity of the PG was analyzed and measured via ImageJ software of SEM images of the resin-embedded and polished samples (Table 3-4). It was shown to be ~20% for HAG and one of the two SAG, and ~30% for the second SAG.

These analyses confirmed the chemical and morphological characteristics of the samples, thus enabling the study of the effects that each of this features plays in regulating protein adsorption and cell attachment, proliferation and differentiation on bone graft substitutes.

4 Fn adsorption and desorption on HA and SA discs and porous granules in different conditions

4.1 Introduction

On contact with living tissue, the first event that takes place at an implant interface is the adsorption of a layer of proteins.

This layer will act as an intermediary to promote subsequent cell attachment, proliferation and differentiation, and thus in bone graft substitutes is associated with new bone formation and bone healing (Sawyer et al., 2005), (Fujisawa et al., 1997), (Hersel et al., 2003) (Roessler et al., 2001), (El-Ghannam et al., 1999) (Itoh et al., 2002).

Therefore the surface properties of the material such as wettability (Bodhak et al., 2009), surface charge (MacDonald et al., 2002a), surface roughness (Missirlis, 2000), (Hayashi et al., 1994), material porosity (Bignon et al., 2003), (Karageorgiou and Kaplan, 2005) (Annaz et al., 2004) and surface chemistry (Scotchford et al., 1998), (Zreiqat et al., 2005) (Zreiqat et al., 1999a) through their ability to regulate the quantity, speciation and conformation of the protein layer, have been increasingly recognised as important for promoting bone growth.

Cell-biomaterial interactions are therefore mediated by, and dependent on, this protein layer, which consequently becomes fundamental in terms of controlling and regulating the process of osteointegration through the bone graft implant.

Despite the recognised significance, there are still controversies in the behaviour of extracellular adhesion proteins regarding the adsorption, dynamics and protein layer composition on HA and SA implants. It is still not clear how the differences in material properties influence this behaviour, and also how a physiological environment (presence of proteins, peptides and growth factors) can affect, positively or negatively, the formation of the protein layer and its characteristics.

The work presented in this chapter is concerned with the investigation of the absorption/desorption processes of Fn on dense and porous stoichiometric hydroxyapatite and silicate-substituted hydroxyapatite (containing 0.8wt% Si) samples, under physiological (with the presence of competitive proteins) and non physiological (without competitive proteins) conditions.

The physiological level of Fn in Fetal Bovine Serum (FCS) has been estimated to be ~300 μg ml^{-1} (Grinnell and Phan, 1983, Mosher, 1984) . In the present study, two different levels of Fn (one close to the physiological, and one lower than this) were tested on HA and SA dense discs and porous granules with different strut porosity. Being the mechanisms of action of Fn still unclear in certain settings, these two speficic Fn levels were used in order to:

- investigate if changes from the physiological concentration influence its activity, and
- to determine if the specific quantity of this protein at the site of action is fundamental in promoting its function.

Experiments were carried out in Eagle Minimal Essential Medium (MEM) with and without the addition of 10% of (FCS).

The other purpose of this study was to investigate the effects of material porosity and chemical composition and the presence of competitive serum proteins on the adsorption pattern of Fn to bone graft biomaterials.

4.2 Materials and Methods

4.2.1 Materials

Both dense discs (DD, 1 gram) and porous granules samples (PG, 0.5 grams) were used in these adsorption experiments. Two chemistries, stoichiometric hydroxyapatite (HA) and 0.8wt% Si silicate-substituted hydroxyapatite (SA) were used. All porous granules had a total porosity of 80% and strut porosity of either 20% or 30% (Chapter 3).

4.2.2 Scanning Electron Microscopy analysis

Analysis of the samples surface after Fn adsorption was performed using a scanning electron microscope. Dense Discs and Porous Granules were mounted on aluminium studs and carbon coated. The images were taken using a magnitude range of 50,000X-60,000X for DD and 14,000X-16,000X, 20.00 KeV and 9.4 to 15.9 mm working distance.

4.2.3 Protein staining

The protein fibronectin was supplied from Calbiochem, in aliquots of 5 mg at a concentration of 1.01 mg/ml. Aliquots of 1.0 ml were stored in 1.5 ml eppendorf tubes, labelled and frozen.

Fibronectin was labelled with the fluorophore Sulphorodamine 101 (SR101, Figure 2-6, from Acros Organics) following the procedure described by Mafina *et al.* (Mafina et al., 2013). SR101 shows optimal fluorescence excitation at 576 nm and emission at 620 nm (Figure 2-7).

The fluorophore was diluted in Minimum Essential Medium Eagle Modified (MEM, Sigma-Aldrich) to achieve a final concentration of 1.048 mg/ml. This solution (SR101, 1 ml in MEM, 1.727×10^{-6} M) and Dicyclohexylcarbodiimid solution (DCC, 1 ml, 30 mg/ml) were mixed and incubated for 5 minutes at 37 °C. The pH was checked during activation and maintained at 5 adding NaOH (1M) drop wise.

Fibronectin solution (1 ml, 1 mg/ml, 2.2×10^{-9} moles) was added to the reaction mixture and incubated at 37 °C for 4 hours in darkness. The reaction was stopped by adding sodium acetate (AcONa, 24.6 mg, 0.1 M) and incubated for at 37 °C 1 hour (Figure 4-1).

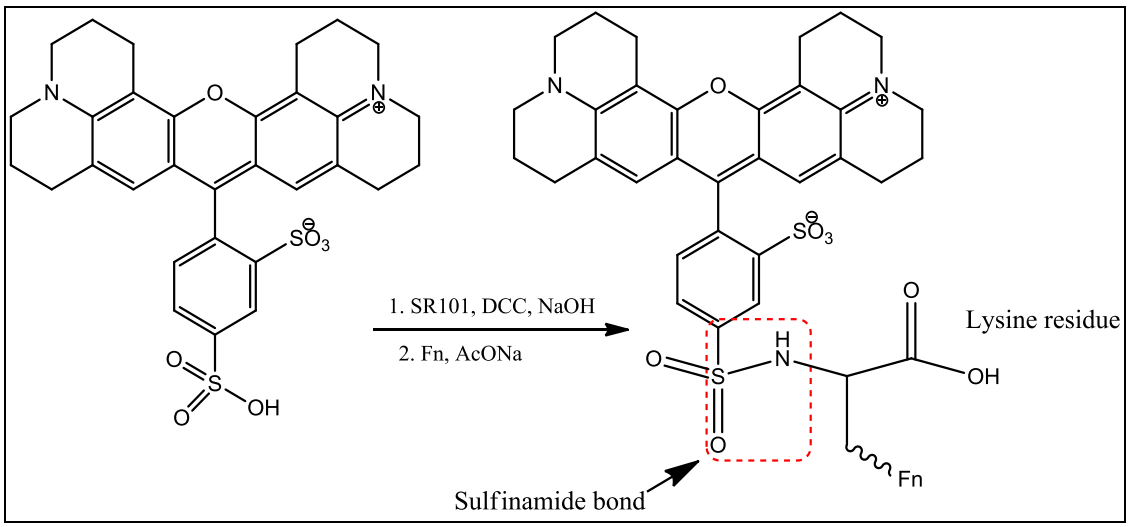

Figure 4-1: Coupling reaction scheme of the FN with SR101

Fluorophore-protein conjugate was separated from free fluorophore by dialysis directly against MEM, for 24 hours (Harlow and Lane, 1988) using dialysis tubes (SpectrumLabs, UK).

Dilutions with MEM stock resulted in final Fn-SR101 concentrations of 0.250 mg/ml (Fn2) and 0.100 mg/ml (Fn1) (Figure 4-2). Verification of the exact protein concentration in the two solutions was made by weighting the freeze-dried samples of the MEM solution and of the two Fn-SR101 solutions.

The same procedure was followed for the preparation of the Fn-SR101 solution in MEM with 10 % of Fetal Bovine Serum (FCS, Sigma-Aldrich) which was added to the MEM stock solution that has then been used to make all the dilutions.

The medium was without phenol red to avoid interference with the protein-SR101 fluorescence analysis.

Figure 4-2*: Fn-SR101 solution at the concentration of 0.250 mg/ml*

4.2.4 Protein Adsorption/Desorption

Protein adsorption experiments were performed on dense discs (HA and SA) and porous granules (HAG80/20, SAG80/20 and SAG80/30). Each sample was incubated in a vial at 37 °C, and 1.5 ml of fibronectin-SR101 solution of each of the 2 different concentrations was added (Fn2: 0.250 mg/ml and Fn1: 0.100 mg/ml).

Within a total incubation time of 1 hour, 0.1 ml aliquots were taken for analysis after 1, 5, 10, 15, 30 and 60 minutes to access fibronectin adsorption via depletion (Figure 4-3).

Samples were washed (with MEM) and re-suspended in 1.5 ml of fresh MEM (or MEM + 10 % FCS) and 0.1 ml aliquots were then taken after 1, 10, 60 minutes, 4 and 24 hours to access fibronectin desorption from the graft.

4.2.5 Fluorescence analysis

Quadruplicate samples (n=4) of the supernatant were transferred into a 96-well plate filled with 200 µl of MEM and 20 µl of sample aliquot in each well. Fluorescence intensity of the solutions was measured at an excitation wavelength of 544 nm and an emission wavelength of 590 nm, using

FLUOstar galaxy^{TM} and its associated software (BMG Labtech Ltd., Aylesbury, UK).

Moreover, additional experiments were performed in which the fluorescence intensity of known concentrations of labelled fibronectin were analysed, to provide calibration curves in both the MEM and the MEM + 10 % FCS solutions (from 0 µg/ml to 16.65 µg/ml) protein concentrations.

This calibration was then used to calculate the amount of protein present in the unknown samples, in order to determine the amount of protein adsorbed on each sample at different time points.

Figure 4-3*: Collecting of aliquots for Fn adsorption analysis*

4.2.6 Circular Dichroism

Circular dichroism analysis was performed on Fn solutions in MEM, at a concentration of 0.1 mg/ml ($2.27x10^{-7}$ M). Three samples of 1 ml were prepared: one placed in contact with HA for 15 minutes, one with SA for 15 minutes and one as prepared. Circular dichroism was also performed on a solution of pure MEM, to be used as a blank. The cuvette path length was 0.1 cm.

The analysis of the data was performed using the Dichroweb application (Whitmore and Wallace, 2004) (Whitmore and Wallace, 2008), available on-line for analysis of Circular Dichroism spectra. This application enables

collection of structural information about the protein sample by comparing its spectra with a library of standard spectra (whom secondary structure is gained from X-ray crystallography) available in the server.

The software used for the analysis of the structural changes of Fn was CDSSTR (reference set 7).

4.2.7 Statistical Analisys

The sample size for each DD and PG material was n=3. Variations in responses of Fn adsorption and desorption between chemistries (HA vs SA), morphologies (DD vs PG), strut porosities (20% vs 30%), or Fn concentrations (Fn1 vs Fn2) were assessed statistically by using a one-way analysis of variance. Differences were evaluated by using Bonferroni post testing. All statistical tests were run by using KaleidaGraph statistical software (v 4.0, Synergy Software, Reading, PA, USA) at a significance level of α=0.05.

4.3 Results

4.3.1 Material's characterization

The characterization of the materials is shown in Chapter 3.

4.3.2 Scanning Electron Microscopy analysis

SEM images show Fn adsorption on DD and PG of HA and SA samples after 60 min of Fn solution incubation and 24 hrs of desorption. In Figure 4-4 it is possible to detect the lower amount of protein adsorbed on DD (a, b) compared to the PG (c, d, e). Whereas in Figure 4-5 are shown the images of two PG with different strut porosity: (a) 80/30 and (b) 80/20.

4.3.3 Fibronectin adsorption

The calibration curves showed a good correlation between fluorescence intensity and protein concentration (Appendix, Figure 9-1 for the experiment in MEM and Figure 9-2 for the experiment in MEM+10% FCS).

Both the calibrations showed a quite linear relationship between the two variables, giving further support to the technique that has been used. The calibration in MEM+10% FCS, furthermore, showed a higher fluorescence intensity compared to the one obtained from experiments in MEM.

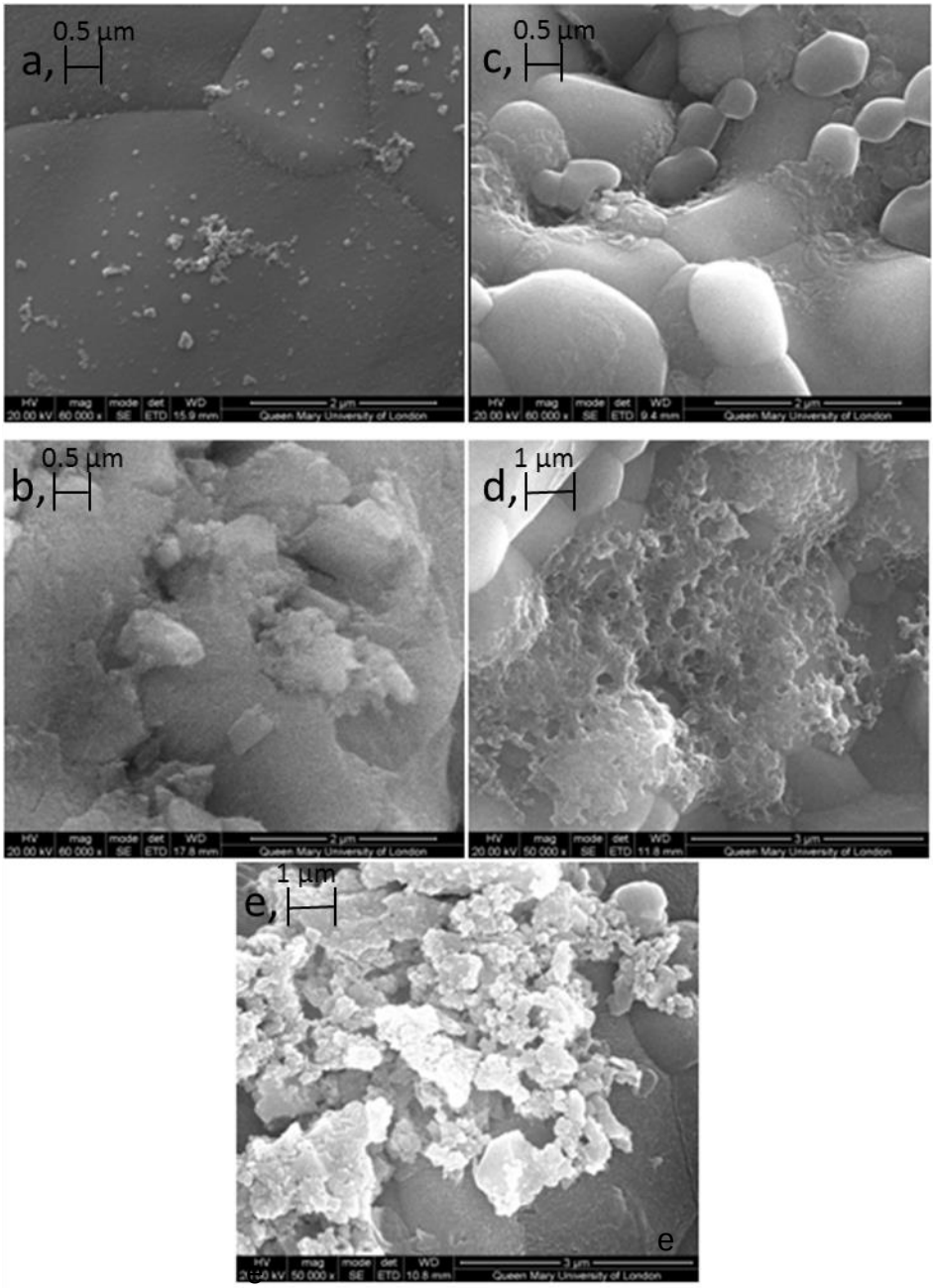

Figure 4-4: Scanning electron image showing Fn adsorbed on the surface of (a) HA and (b) SA DD, and (c) HA 80/20, (d) SA 80/20 and (e) SA 80/30 PG.

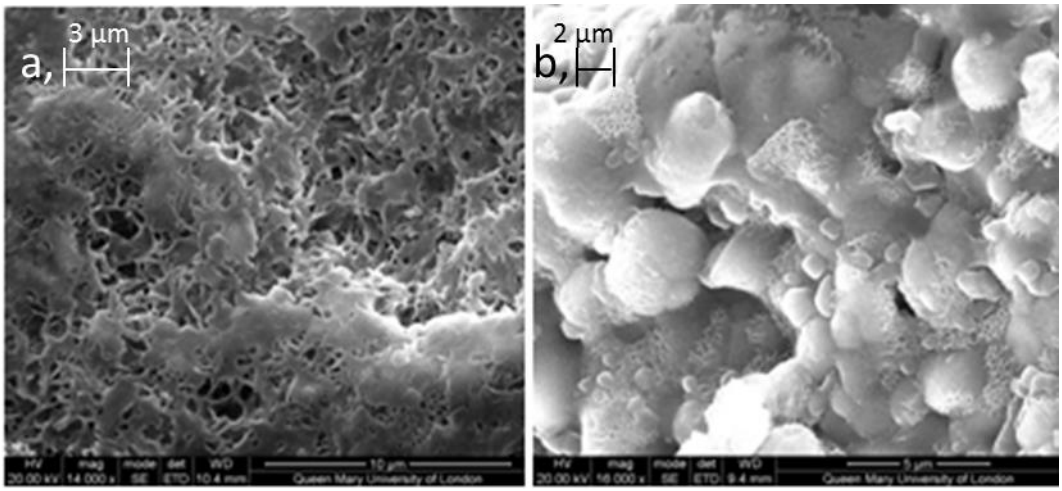

Figure 4-5: Scanning electron image showing the differences in strut porosity between (a) SAG 80/30 and (b)SAG 80/20.

4.3.3.1 Adsorption on dense discs

The amount of Fn adsorbed on the samples was calculated subtracting the amount detected in the solution analyzed at each time point from the amount in the original solution. Results of Fn adsorption on DD are shown from Figure 4-6 to Figure 4-14

Hydroxyapatite dense discs (HAD) and Silicate-substituted hydroxyapatite dense discs (SAD) showed a similar pattern of Fn adsorption in the MEM solution (Figure 4-6a, b for the two concentrations used). In this condition SA showed more Fn adsorption compared to HA, however significantly different only after 15 minutes of adsorption at the lower concentration of Fn used (Fn1) (Figure 4-6b)

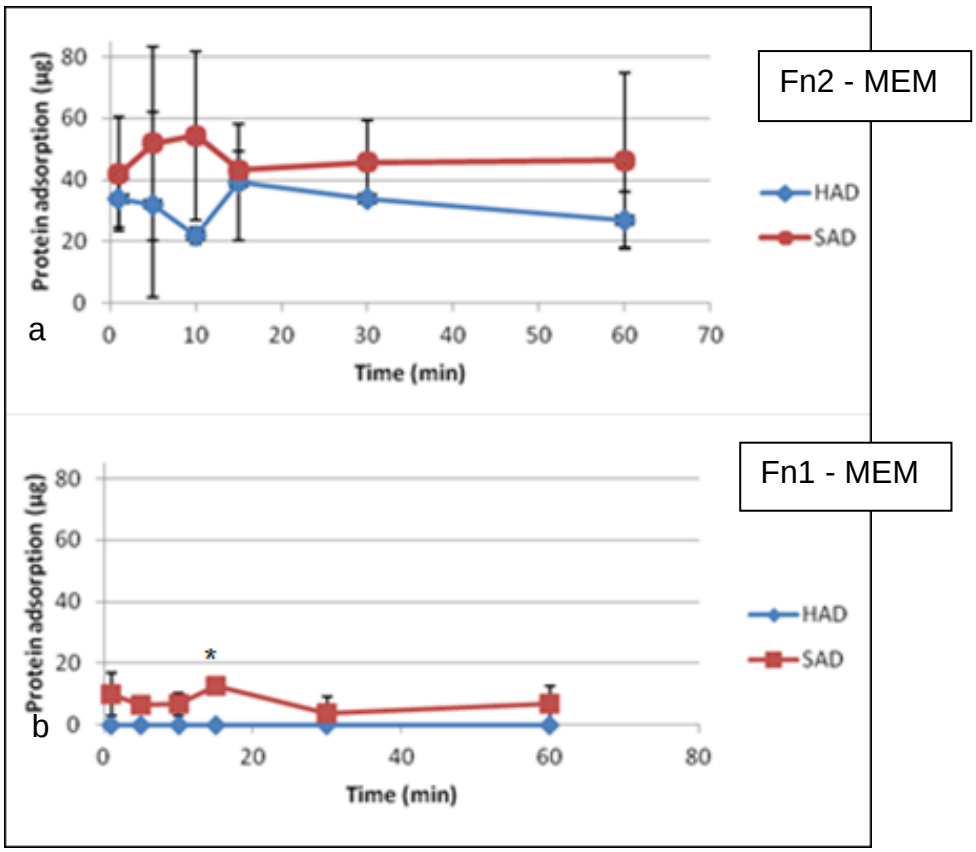

Figure 4-6 SR101-Fn adsorption on HAD and SAD in MEM at concentrations of (a) 0.250 mg/ml Fn, and (b) 0.100 mg/ml Fn (*p<0.05 SAD vs HAD after 15 min)

However, with the addition of FCS to the environment and so the introduction of competitive protein species (Figure 4-7a,b), it can be seen that at high Fn concentration the protein adsorption is very similar between the two samples but at low concentration HA adsorbed more protein than SA, significantly different at almost all the time points, reversing the observations without FCS (Figure 4-6b). This suggests that both Fn concentration and the presence of competitive species have a significant effect on the relative adsorption profiles of HA and SA.

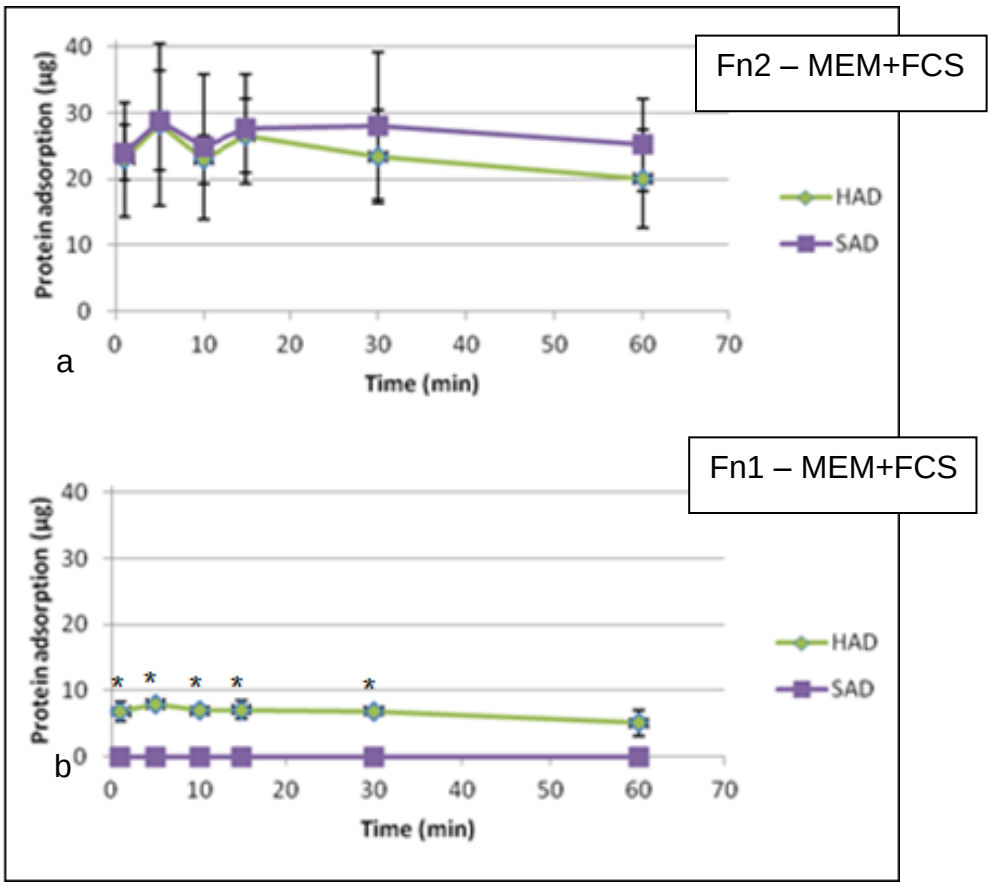

Figure 4-7: SR101-Fn adsorption on HAD and SAD in MEM+10% of FCS at concentrations of (a) 0.250 mg/ml Fn, and (b) 0.100 mg/ml Fn (*p<0.05 HAD vs SAD after 1, 5, 10, 15 and 30 min)

Focusing on the effect of the introduction of competitive species for each sample chemistry, Figure 4-8 shows that at high concentrations, HA is not influenced by competitive species, while at low concentrations the presence of serum proteins significantly enhances Fn adsorption on HA (Figure 4-8b).

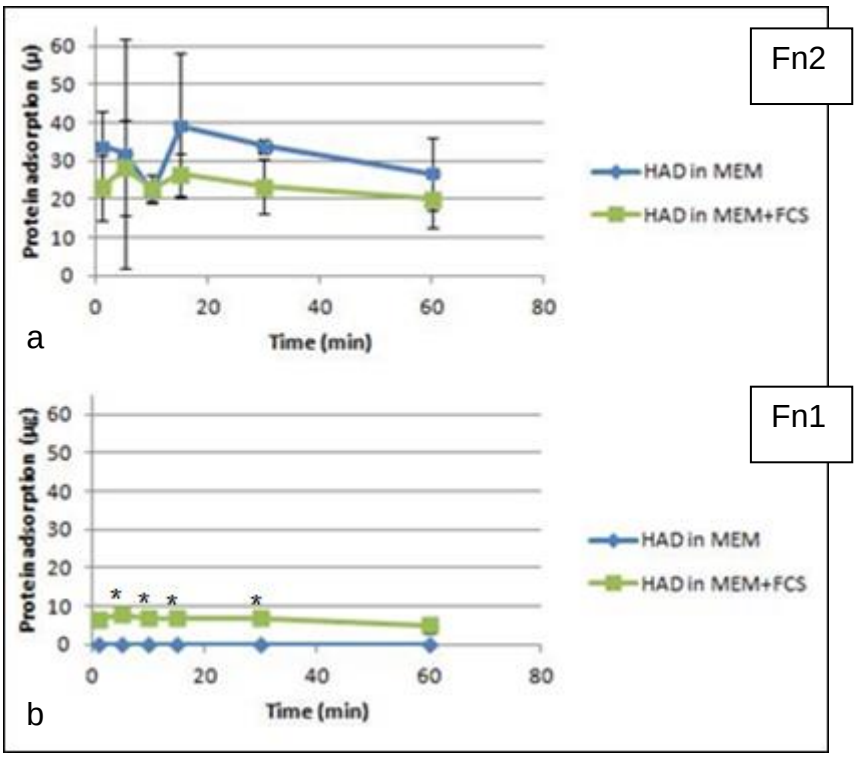

Figure 4-8: SR101-Fn adsorption on HAD in MEM and MEM+10% of FCS at concentrations of (a) 0.250 mg/ml Fn, and (b) 0.100 mg/ml Fn (*p<0.05 HAD in MEM+FCS vs HAD in MEM after 1, 5, 10, 15 and 30 min)

In contrast, Figure 4-9 demonstrates that at high and low concentrations Fn adsorption on SA is reduced by serum proteins. This effect is particularly enhanced at low concentrations where the presence of competitive species almost blocks Fn adsorption on SA (significant only after 15 min using low Fn concentrations) (Figure 4-9Figure 4-8b).

These results clearly suggest that the presence of the serum is critical to the adsorption of Fn on the samples.

After the analysis of this data it was decided that the adsorption/desorption experiments on the porous granule samples should be continued only in the MEM+10% FCS solution as this most closely resembled the physiological environment.

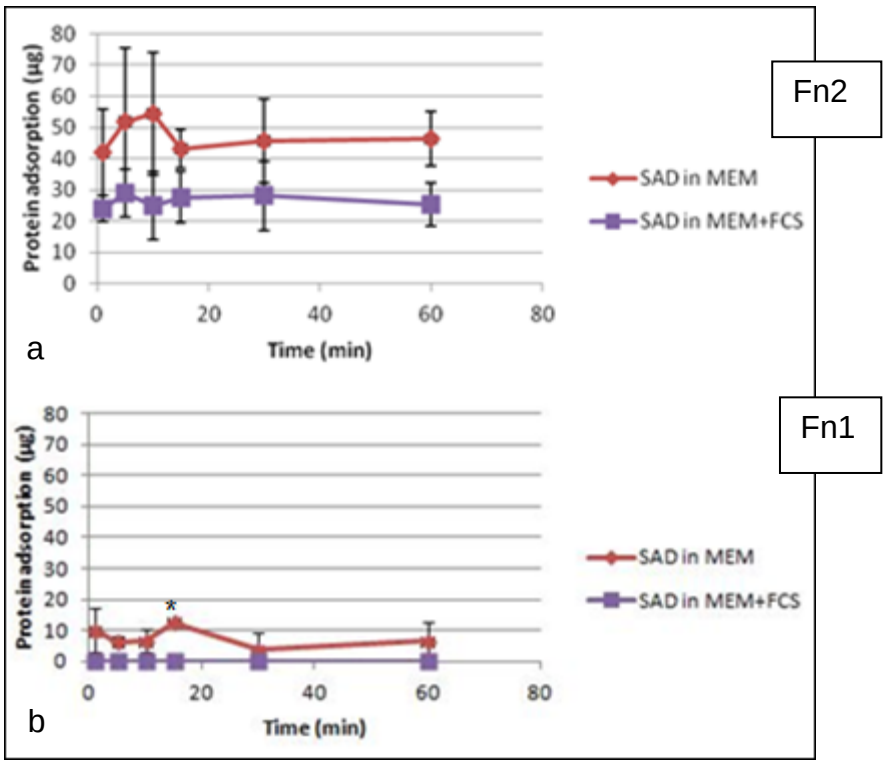

Figure 4-9: SR101-Fn adsorption on SAD in MEM and MEM+10% of FCS at concentrations of (a) 0.250 mg/ml Fn, and (b) 0.100 mg/ml Fn (*p<0.05 SAD in MEM vs SAD in MEM+FCS)

4.3.3.2 Fn adsorption on granules

Following the same method, the adsorption of Fn was analyzed on three different porous granules (PG) samples: HAG80/20, SAG80/20 and SAG80/30 (see Chapter 3 for full details of the materials) using only the solution MEM+10% of FCS.

Results of Fn adsorption on PG are shown in Figure 4-10: with the higher (physiological) concentration of Fn (Fn2), SA was observed to adsorb more Fn than HA after 60min, while there was significant fluctuation in Fn adsorbed to HA at earlier time points. Moreover, the difference in strut porosity in the two SA samples (20% and 30%) did not appear to significantly influence the quantity of protein adsorbed.

Statistical analysis of the data is shown in Figure 4-11.

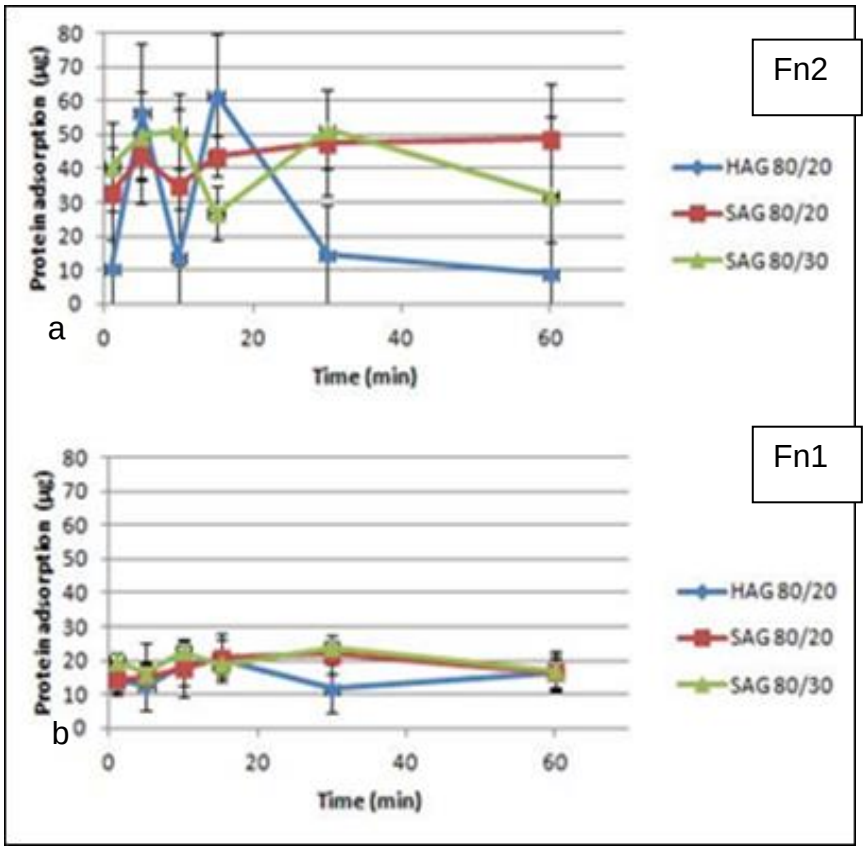

Figure 4-10: SR101-Fn adsorption on HAG 80/20, SAG 80/20 and SAG 80/30 in MEM+10% of FCS at concentrations of (a) 0.250 mg/ml Fn, and (b) 0.100 mg/ml Fn

Both SAG80/20 and SAG80/30 adsorbed significantly more Fn than HAG80/20 after 1, 10 and 30 minutes (Figure 4-11a, c, e), SAG80/20 only adsorbed more Fn than HAG80/20 also after 60 min (Figure 4-11f) and HAG80/20 and SAG08/20 more than SAG80/30 after 15 min (Figure 4-11d).

The quantity of Fn adsorbed at lower concentration (Figure 4-10b) did not vary significantly with either granule chemistry or porosity.

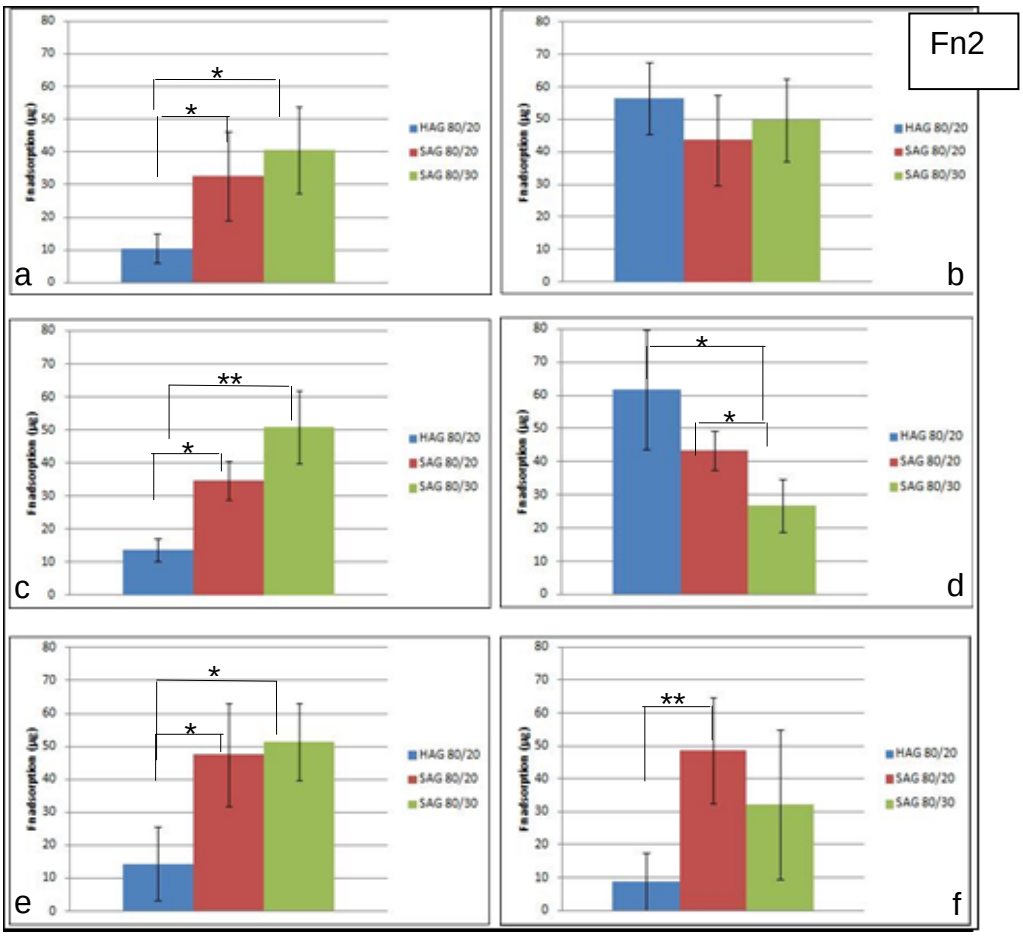

Figure 4-11: Amount (µg) of Fn adsorbed on HAG 80/20, SAG 80/20 and SAG 80/30 at 0.250 mg/ml Fn concentration after (a)1, (b)5, (c)10, (d)15, (e)30, and (f) 60 minutes (*p<0.05, **p<0.005)

In Figure 4-12a-d are shown the adsorption profiles of the samples with the same chemical composition and in the same solutions but with different topography (dense discs (DD) vs porous granules (PG)). For the HA chemistry, the porous granules showed a higher amount of Fn adsorbed at both the Fn concentration solutions, with significant differences found after 5 and 15 min from 0.250m mg/ml of Fn (Figure 4-12a) and after 10, 15 and 60 min from 0.100 mg/ml of Fn solution (Figure 4-12b). For the SA chemistry, this difference in adsorption between DD and PG was more emphasized, and significantly different after 1, 5 and 10 min only from SAG80/30, and after 15 min from SAG80/20, with the higher Fn concentration solution (0.250 mg/ml, Figure 4-12c). While for the lower Fn concentration solution (Fn1) there was significantly less Fn adsorbed to SA DD at all time points as compared to SAG80/20 and SAG80/30 (Figure 4-12d).

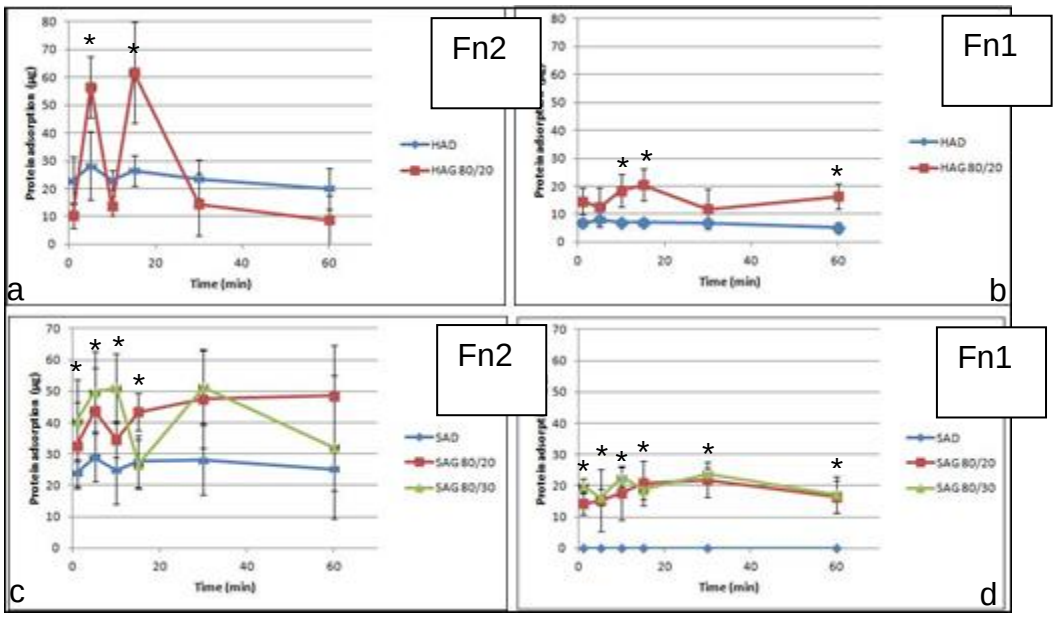

Figure 4-12: SR101-Fn adsorption in MEM+10% FCS on (a) HAD and HAG 80/20 at (a) 0.250 mg/ml, (b) HAD and HAG 80/20 at 0.100 mg/ml, (c) SAD, SAG 80/20 and SAG 80/30 at 0.250 mg/ml and (d) SAD, SAG 80/20 and SAG 80/30 at 0.100 mg/ml. (*p<0.05)

Another interesting interpretation of the data would also be to look at it in terms of % of Fn adsorbed relative to the initial concentration used, which is either 0.250 (Fn2) or 0.100 (Fn1) mg/ml. This would enable to see how Fn adsorption changes as a function of its concentration. Figure 4-13 shows the percentage of Fn adsorbed to the samples from MEM and MEM+10%FCS solutions for the DD, and from the MEM+10%FCS solution for the granules, with the two Fn concentration solutions, 0.250 mg/ml and 0.100 mg/ml after 1, 5 and 10 minutes. Figure 4-14 shows the same results after 15, 30 and 60 minutes.

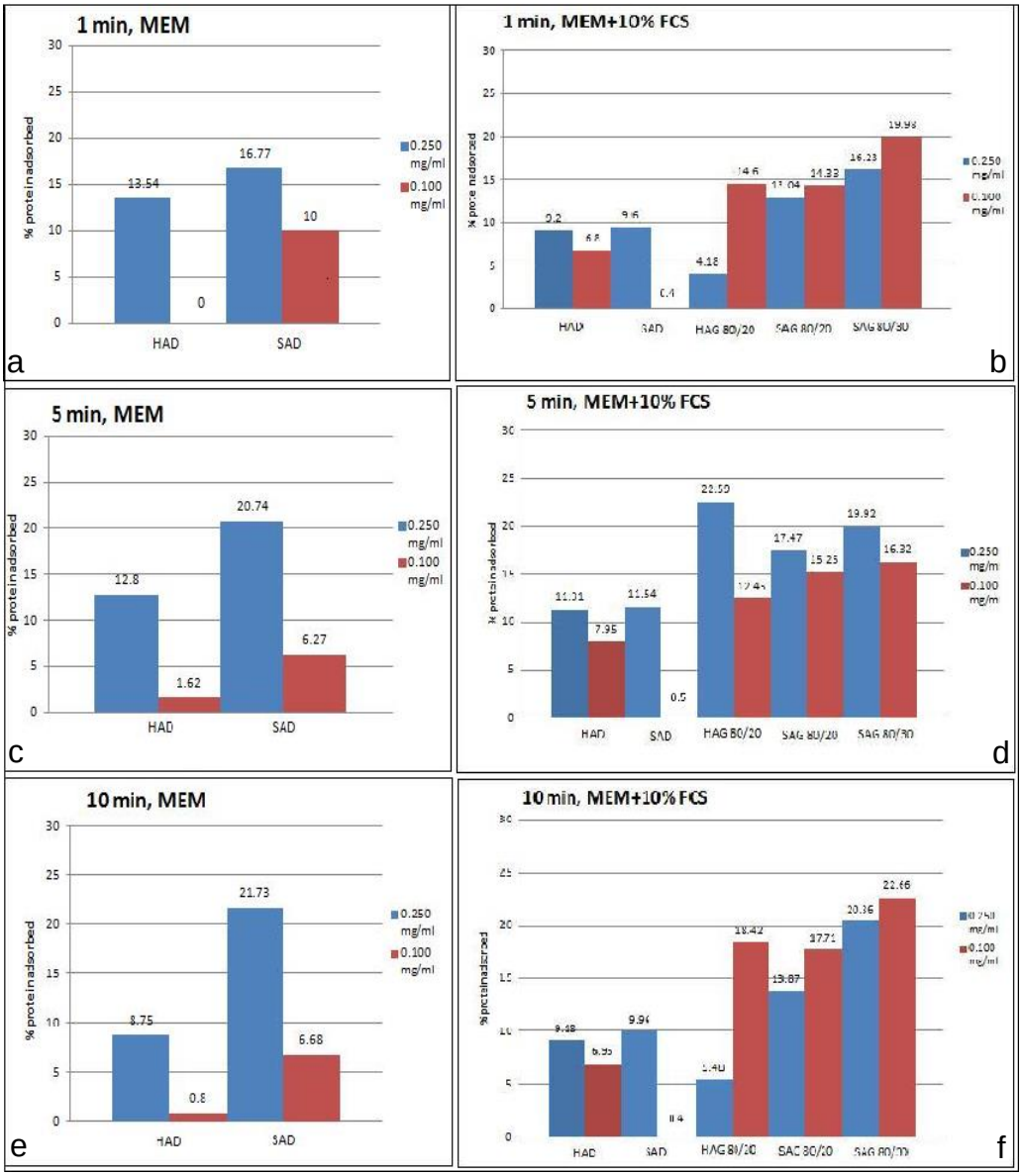

Figure 4-13: percentage of Fn adsorbed on DD in MEM in physiological (0.250 mg/ml) and sub-physiological (0.100 mg/ml) concentrations of Fn solutions after (a)1, (c) 5, (e)10 minutes, and PG in MEM+10% FCS in physiological (0.250 mg/ml) and sub-physiological (0.100 mg/ml) concentrations of Fn solutions after (b)1, (d)5, (f)10 minutes

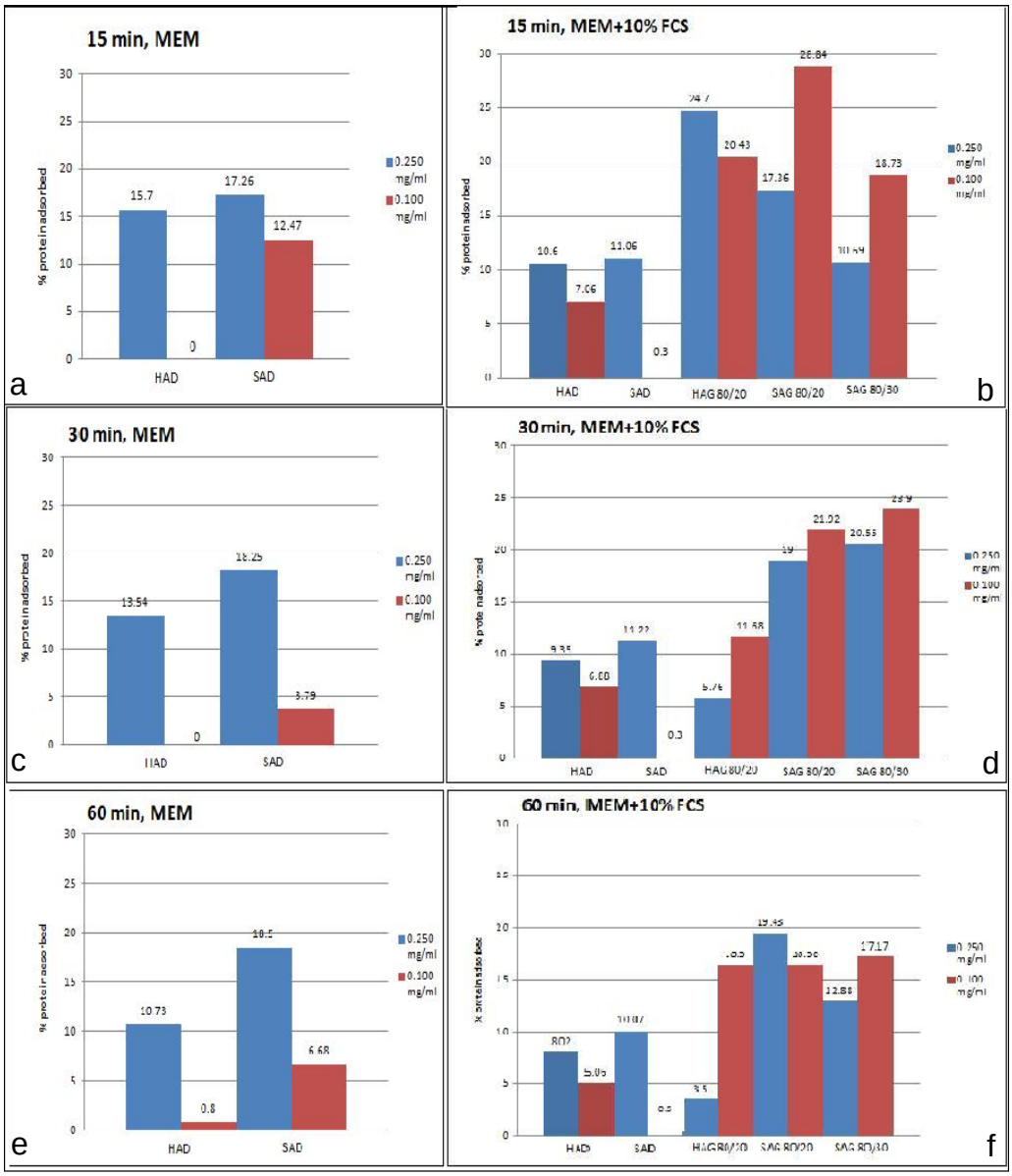

Figure 4-14: percentage of Fn adsorbed on DD in MEM in physiological (0.250 mg/ml) and sub-physiological (0.100 mg/ml) concentrations of Fn solutions after (a)15, (c)30, and (e) 60 minutes, and percentages of Fn adsorbed on DD and PG in MEM+10% FCS in physiological (0.250 mg/ml) and sub-physiological (0.100 mg/ml) concentrations of Fn solutions after(b)15, (d)30, and (f) 60 minutes.

This evaluation suggests that for DD the adsorption of Fn was relatively higher in the 0.250 mg/ml solution at all the time points compared to the 0.100 mg/ml solution in both MEM (Figure 4-13a, c, e and Figure 4-14a, c, e) and MEM+10% FCS (Figure 4-13b, d, f and Figure 4-14b, d, f). However, for PG a relatively higher amount of Fn was adsorbed from the lower concentration solution apart from the 5 min time point, and for HAG80/20 after 15 min and SAG80/20 after 60 min (Figure 4-13b, d, f and Figure 4-14b, d, f).

4.3.3.3 Fn desorption from dense discs

Also the desorption studies have been performed in MEM on DD, and in MEM+10% FCS on DD and PG. The same two Fn concentration solutions (Fn1 and Fn2) were used for all the samples. The data was generated by quantification of the protein amount analyzed in the aliquots (taken after the re-suspension in fresh MEM or MEM+10% FCS), at each desorption time points, which were: 1 min, 10 min, 60 min, 4 hr and 24hr.

In MEM (Figure 4-15a, b) the trends between HAD and SAD were the same at both higher and lower concentration of Fn, with the protein being more readily desorbed from HA compared to SA. Furthermore Fn desorption showed to be significantly higher on HA than on SA after 24 hours, from Fn2 (Figure 4-15a) and after 60 minutes from Fn1 (Figure 4-15b).

Figure 4-16a, b shows Fn desorption from the MEM+10% FCS solution. Data shows that at both higher and lower Fn concentration solutions, Fn desorption was very similar for both HA and SA, showing a high Fn release peaking after only 1 min (significantly higher from HAD in Fn2), and then finding a lower and steady equilibrium level after 10 min. No more desorption was found after this time point.

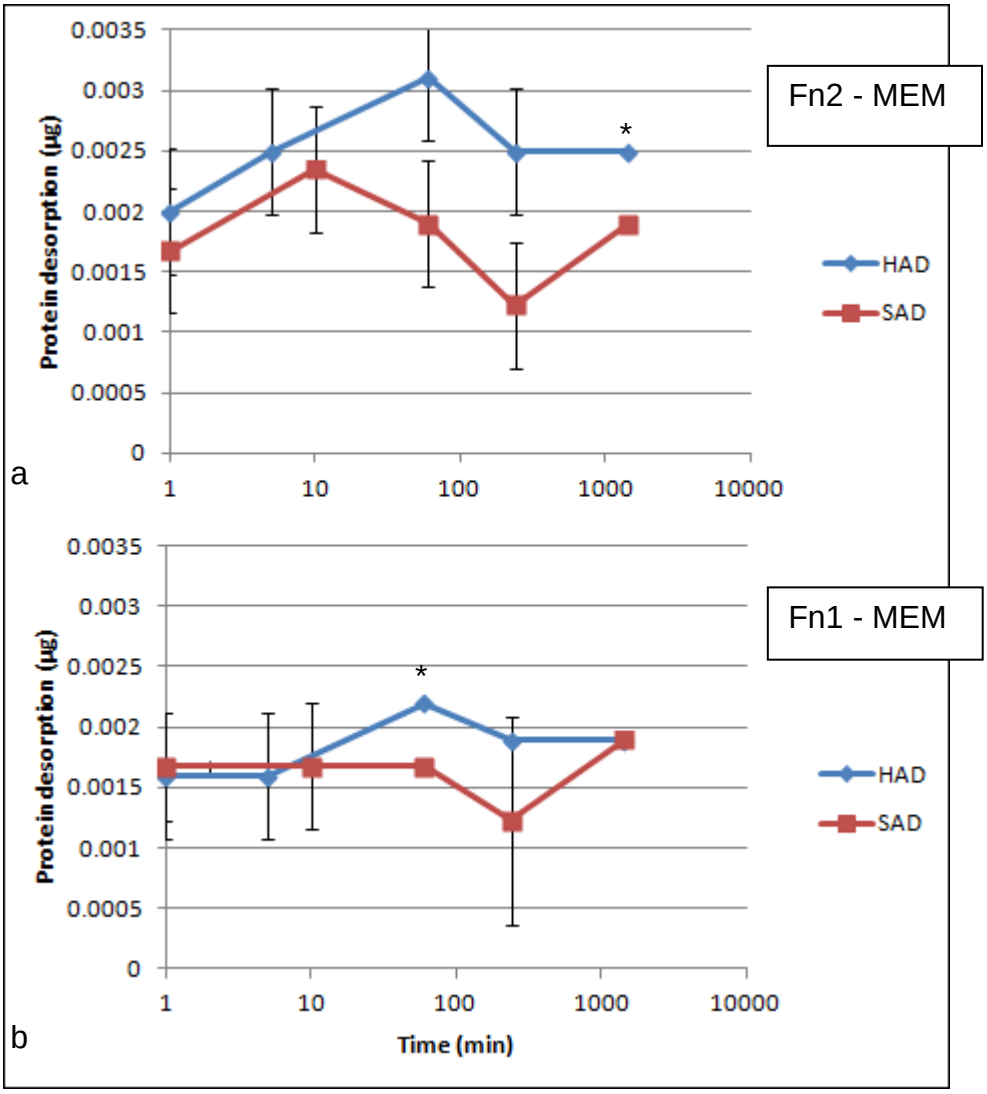

Figure 4-15: SR101-Fn desorption on HAD and SAD in MEM at concentration of (a) 0.250 mg/ml Fn, and (b) 0.100 mg/ml Fn (*p<0.05).

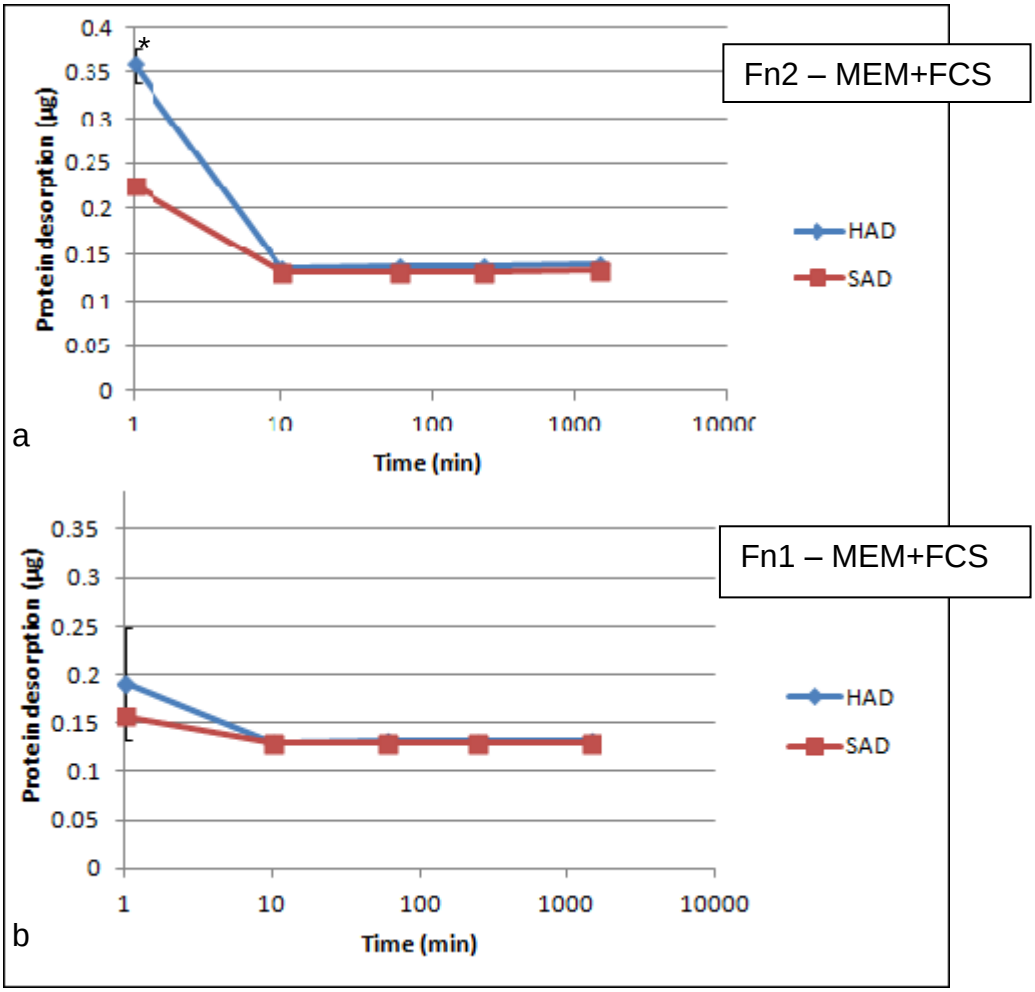

Figure 4-16: SR101-Fn desorption on HAD and SAD in MEM+10% FCS at concentration of (a) 0.250 mg/ml Fn, and (b) 0.100 mg/ml Fn (*p<0.05).

The analysis of the desorption comparing the same chemistry in the MEM and MEM+10% FCS solutions are shown in Figure 4-17 and Figure 4-18. This data shows that, for both HA and SA DD, the presence of FCS during adsorption/desorption increases the desorption of Fn from HAD and SAD, with a peak after just one minute. After the first minute, however, in either MEM or MEM+FCS there isn't any further release of Fn.

This difference was statistically significant from both HAD and SAD using either higher (Figure 4-17a and Figure 4-18a respectively), or lower (Figure 4-17b and Figure 4-18b respectively) Fn concentration solutions. The presence of an early peak and a subsequent lower level of desorption suggests that Fn is readily and quickly released at first in the new fresh solution, and that after 10 min could be re-adsorbed again on the graft surface.

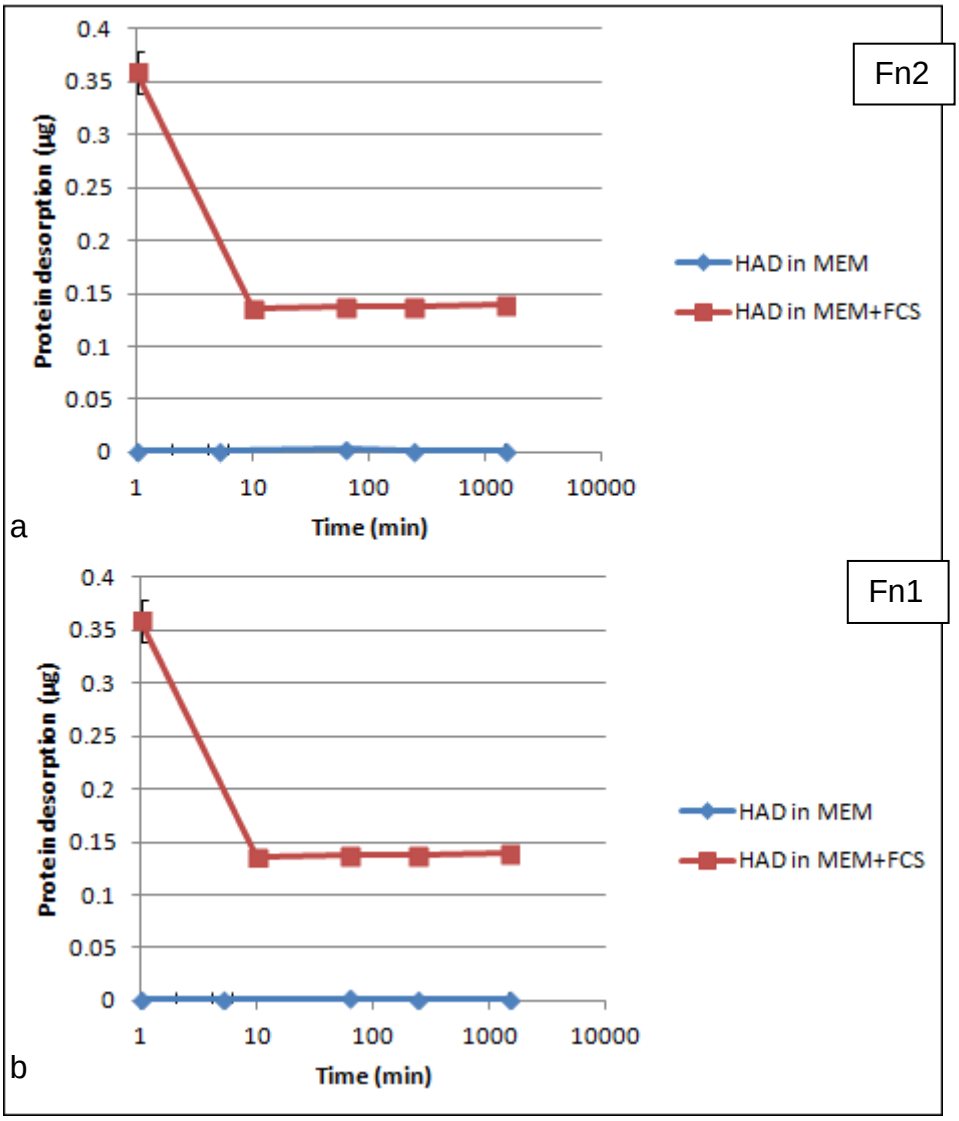

Figure 4-17: SR101-Fn desorption on HAD in MEM and MEM+10% of FCS at concentration of (a) 0.250 mg/ml Fn and (b) 0.100 mg/ml Fn (HAD in MEM $p<0.0001$ vs HAD in MEM+FCS at all the time points)

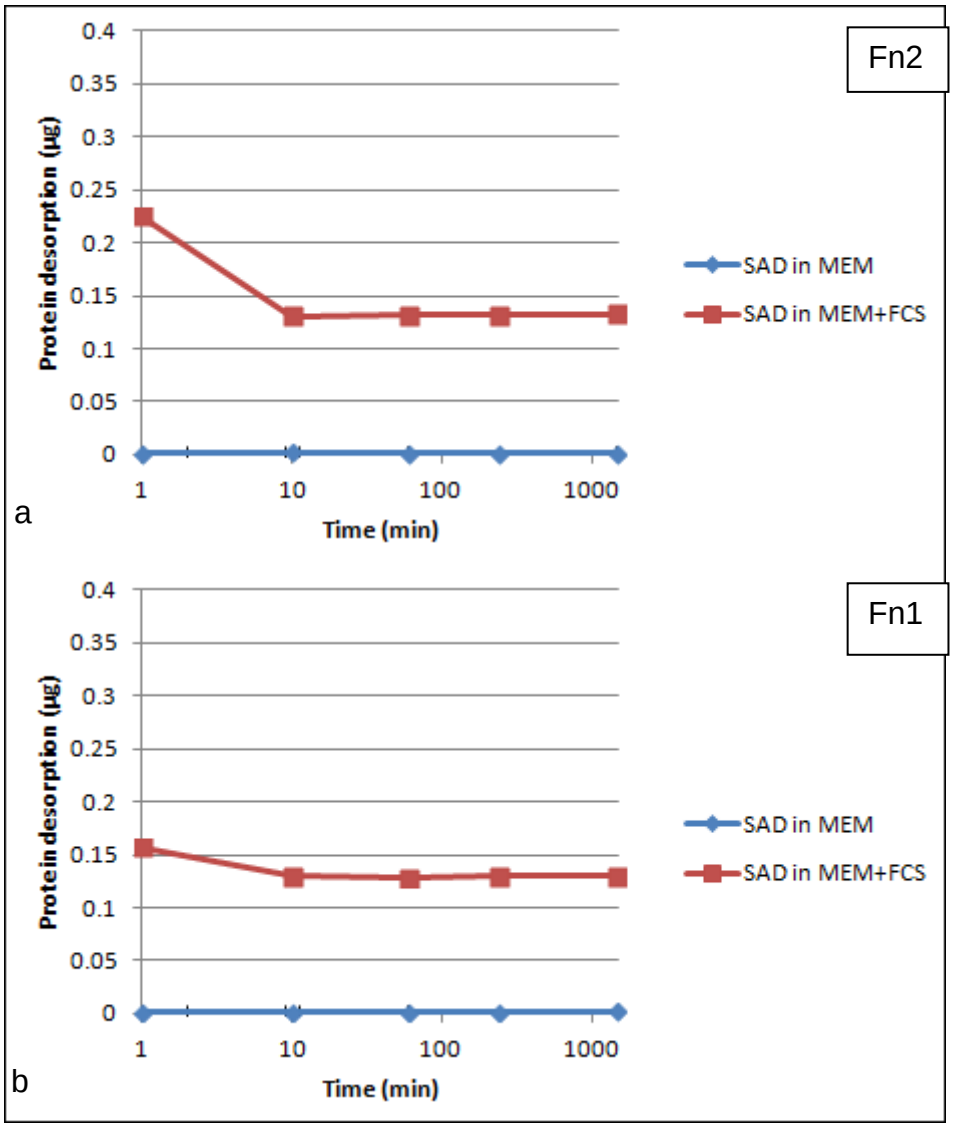

Figure 4-18: SR101-Fn desorption on SAD in MEM and MEM+10% of FCS at concentration of (a) 0.250 mg/ml Fn and (b) 0.100 mg/ml Fn (SAD in MEM p<0.0001 vs SAD in MEM+FCS at all the time points)

4.3.3.4 Fn desorption from granules

Figure 4-19a, b shows the data obtained from the study of Fn desorption from porous HA and SA granules. The three samples showed a very similar desorption trend at both the two Fn concentration solutions.

As for the DD, PG showed an early peak of desorption after only 1 min, and then a lower and steady equilibrium level and no more Fn desorption. Fn desorption was slightly higher from SAG80/20 compared to SAG80/30 and HAG80/20 at both the Fn concentration solutions.

Evaluating the influence that sample topography has on Fn desorption, Figure 4-20a-d shows levels of protein desorbed between HAD and HAG80/20, and between SAD, SAG80/20 and SAG80/30. The results show a significant higher amount of Fn desorbed from the PG compared to the DD, for both HA and SA, and at both the two Fn solutions.

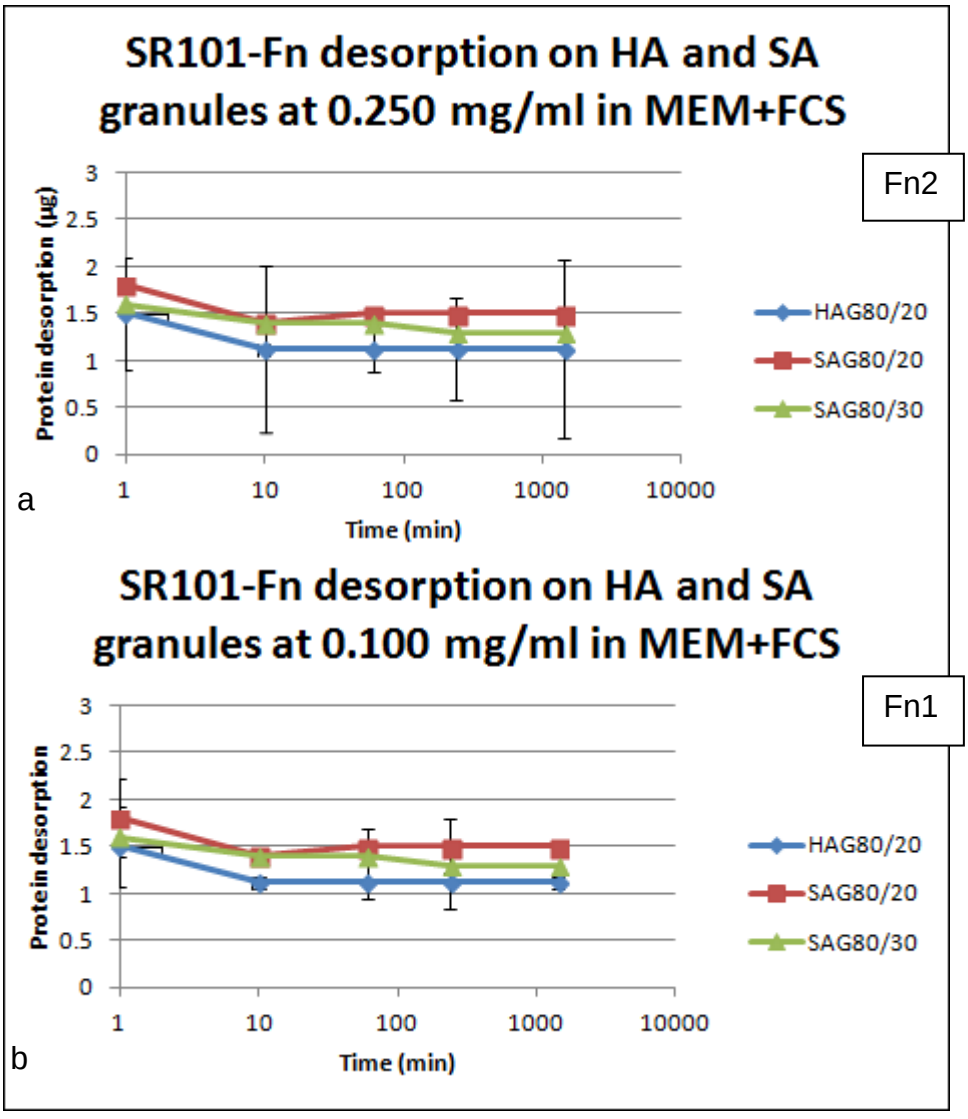

Figure 4-19: SR101-Fn desorption on HAG 80/20, SAG 80/20 and SAG 80/30 in MEM+10% of FCS at concentration of (a) 0.250 mg/ml Fn and (b) 0.100 mg/ml

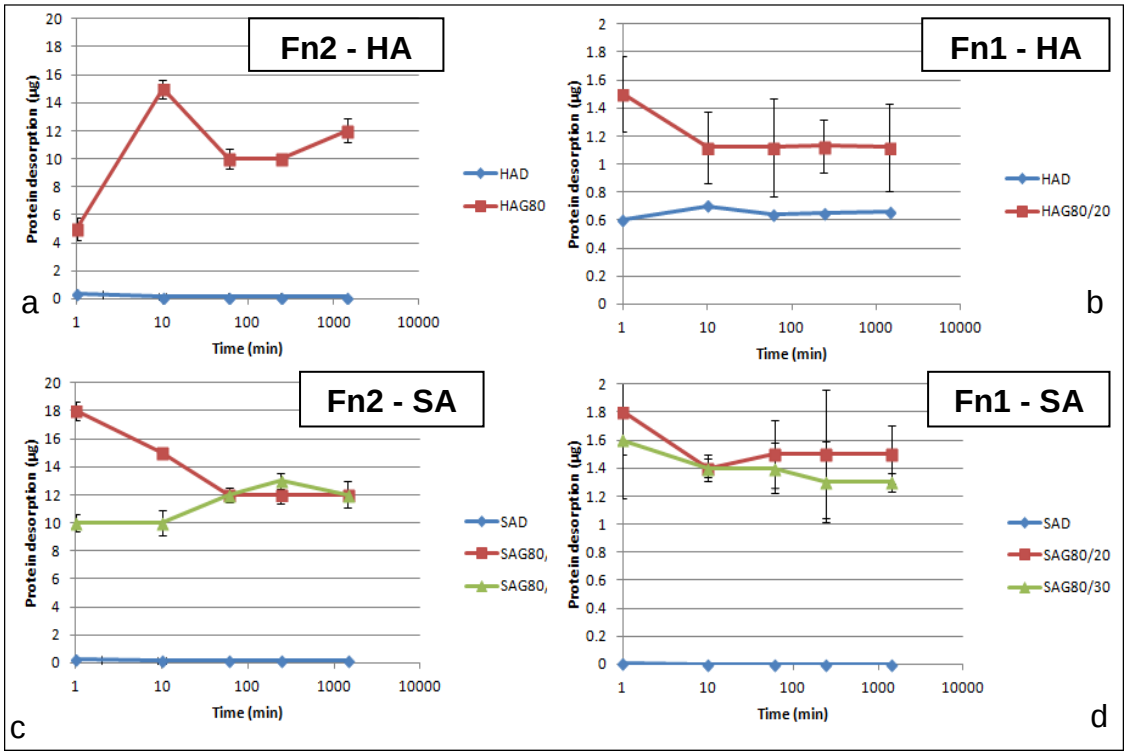

Figure 4-20: SR101-Fn desorption in MEM+10% FCS on (a) HAD and HAG 80/20 at 0.250 mg/ml FN, (b) HAD and HAG 80/20 at 0.100 mg/ml Fn, (c) SAD, SAG 80/20 and SAG 80/30 at 0.250 mg/ml Fn and (d) SAD, SAG 80/20 and SAG 80/30 at 0.100 mg/ml Fn (HAD $p<0.0001$ vs HAG and SAD $p<0.0001$ vs SAG80/20 and SAG80/30 at both the Fn concentration solutions)

Figure 4-21a-j shows the percentage of Fn desorbed relatively to the amount adsorbed at each time point.

Comparing the two Fn concentration solutions, it is showed that from DD Fn was desorbed more from the lower concentration solution than the higher one, except for HA after 60min, were the desorption was higher from the 0.250 mg/ml Fn solution (Figure 4-21e).

From PG, while the two materials with 20% strut porosity showed the same trend, the SAG80/30 sample showed a relatively higher desorption of Fn from the 0.250 mg/ml Fn concentration solution, at all the time points.

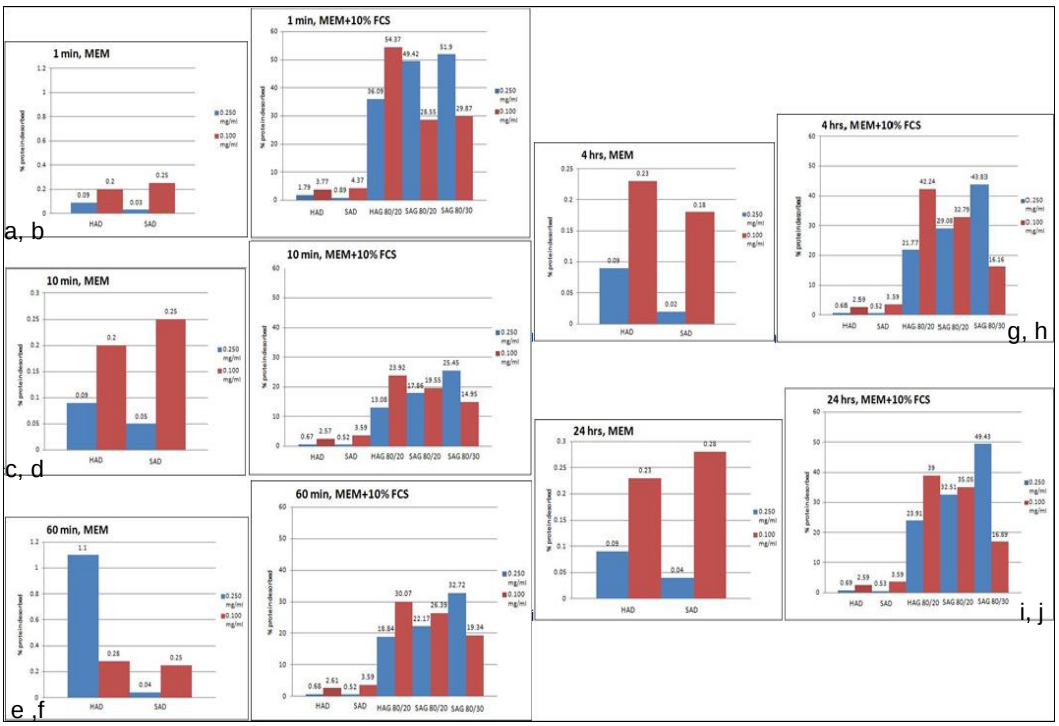

Figure 4-21: Percentage of desorption of Fn from the samples as a function of the amount adsorbed for the higher (0.250 mg/ml Fn) and lower (0.100 mg/m Fn) Fn concentration on DD in MEM after (a) 1, (c) 10, (e) 60, (g) 240, and (i) 1440 minutes and on DD and PG in MEM+10% FCS after (b) 1, (d) 10, (f) 60, (h) 240 and (j) 1440 minutes

4.3.1 Circular Dichroism

The CD spectra of Fn solutions in Figure 4-22a shows the differences in the ellipticity (Δε) between the three samples, in function of the wavelength. The details of the differences in the secondary structure can be more easily seen between 205 and 260 nm in Figure 4-22b.

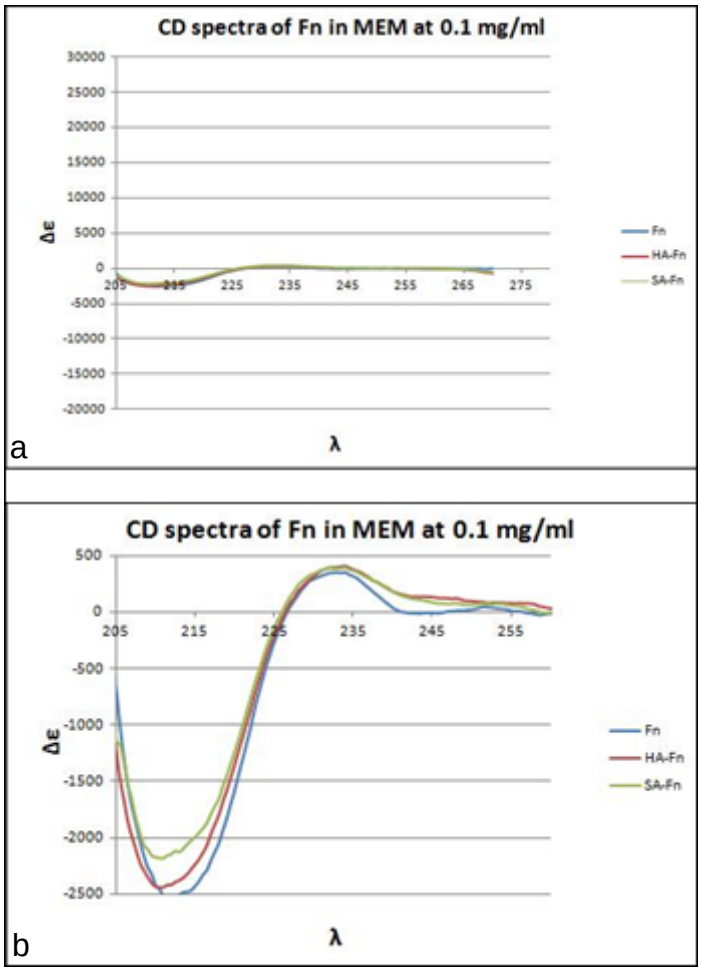

Figure 4-22: (a) CD spectra of the three Fn solutions in MEM and (b) details of the different Δε relevant for the secondary structure for the three solutions of Fn

Figure 4-23a,b shows the spectra of HA-Fn (Fn solution after contact with HAD for 15 min) and SA-Fn (Fn solution after contact with SAD for 15 min) in MEM after subtraction of Fn spectra. It is clear that there are differences in the adsorption of left and right circular polarised light between the three samples, therefore in their secondary structure.

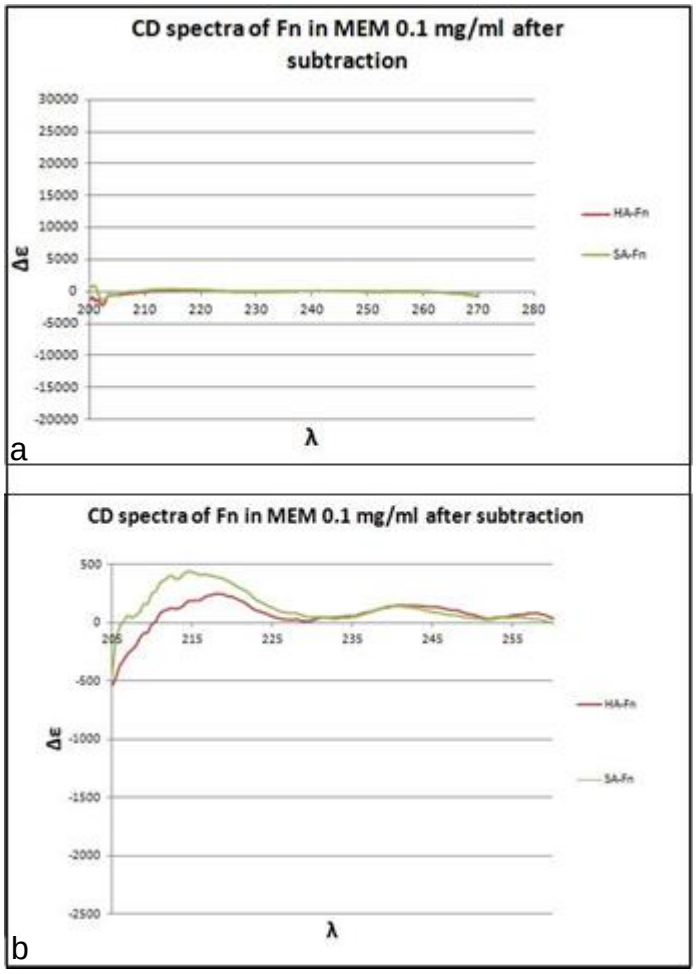

Figure 4-23: ***(a)CD spectra of the three Fn solutions after subtraction of Fn-MEM to the HA-Fn and SA-Fn spectra and (b) details of the differences***

The analysis of the data, using the programme CDSSTR of Dichroweb, showed a NRMSD (Normalized Residual Mean Square Difference) of 0.058, 0.064 and 0.056 respectively for Fn in MEM (Fn), Fn in MEM after contact with HAD (HA-Fn), and Fn in MEM after contact with SAD (SA-Fn). NRMSD characterizes the performances of secondary structure calculations, and represents the root mean square deviations between the crystal and CD estimates of the secondary structure content. The overall NRMSD is determined by considering all secondary fractions collectively. Lower values of NRMSD indicate less discrepancy between the calculated and crystallographic data. Therefore it is generally accepted that NRMSD measures the reliability of the method.

The relative secondary structure content (α-helix, β-strand, turns and unordered) of each sample solution was then predicted. The results are shown

in Table 4-1, and suggest that there is some structural change in Fn on contact with both HA and SA:

Table 4-1: relative secondary structure of the three Fn solutions

	α-helix	β-sheet	Turns	Unordered	Strand segments %	NRMSD
Fn	0	0.56	0.16	0.3	8.518%	0.058
HA-Fn	0	0.54	0.22	0.25	9.825%	0.064
SA-Fn	0	0.64	0.11	0.26	9.385%	0.056

4.4 Discussion

4.4.1 The effect of Fn concentration

In the study of protein adsorption the use of different protein concentration solutions can help to understand the nature of any dominant protein-biomaterial interaction. If the same adsorption of protein from solutions of different concentrations is observed, it suggests that the mechanism of action is not dependent on the concentration (i.e. there can be a saturation of the binding sites on the surface of the implants so that the adsorption doesn't increase above a certain level, even with a higher protein concentration solution). Equally, if from different concentration solutions different adsorption trends are observed, it can indicate that affinity to a surface for a particular protein is concentration dependent. This level of understanding provides insight into: firstly, what may happen in the dynamic physiological environment as compared to in well controlled static conditions in the laboratory; secondly, what may be the optimal concentration to obtain maximum adsorption; thirdly, the possible mechanisms of actions behind protein adsorption to a specific material.

The results from the study using dense discs (DD) showed that adsorption of Fn was always relatively higher in the higher (physiological) concentration solution (Fn2, Figure 4-13, Figure 4-14). This difference ranged between 8-16% (% of the initial concentration of Fn in the solution) on HA in MEM but only 2-3% on HA in MEM+10% FCS; and between 5-15% on SA in MEM and 9-11% on SA in MEM+10% FCS.

The results obtained in the MEM solution on DD showed a correlation between Fn concentration and Fn adsorption. Furthermore, the higher percentage of adsorption from the 0.250 mg/ml solution suggested that Fn binding sites were not saturated. The presence of serum proteins did not change this pattern of behaviour: adsorption was still higher from the 0.250 mg/ml Fn solution, but the degree of difference between the two concentration solutions was reduced on both HA and SA DD, suggesting that when there are competitive species in the environment, they compete with Fn and have a greater inhibitory effect on Fn adsorption at higher concentrations.

In contrast, on porous granules (PG) a greater amount of Fn was adsorbed from the lower concentration solution than the higher one (Figure 4-13, Figure 4-14). This difference, however, was more pronounced on HAG 80/20 (ranging between 6-13%) than SAG 80/20 (ranging between 1-9%) and SAG 80/30 (ranging between 2.3-8%). These differences in relative Fn adsorption support the hypothesis, previously reported, that geometric/topographic characteristics of the implant influence the process of Fn adsorption (Bruijn et al., 1999).

These results can be compared with a previous study by Guth *et al*. (Guth et al., 2010a) where an increasing amount of fetal calf serum (FCS) inhibited the total adsorption of Fn. This study was conducted on microporous HA and SA discs, and the amount of Fn adsorbed on the discs was evaluated after using concentrations of 10%, 20% and 50% FCS in the medium. Similarly to the results showed in the present study on the PG, increasing the amount of FCS from 20% to 50% in the medium resulted in a lower amount of Fn adsorbed on the surface of the implants. This could suggest that, as the concentration of Fn in the solution increased, the large molecular weight of Fn may have led to a reduction in its mobility, especially when exposed to a more intricate porous surface as compared to a more open and smoother surface as found on DD. Another hypothesis could be that Fn becomes more susceptible to displacement by the other proteins in the serum as its (Fn) concentration in solution increases.

Regarding the desorption of Fn, results of the present study showed the same effect of Fn concentrations on DD and 80/20 PG (both HA and SA), but a different one on SAG80/30. In particular, a higher amount of Fn was found to be desorbed from the lower Fn concentration solution (Fn1) at all the time points from HA and SA DD, HAG 80/20, and SAG 80/20. Differently, desorption from SAG 80/30 was higher from the solution with the higher amount of Fn (Fn2, Figure 4-21).

The evidence of how important the concentration of Fn is in directing the adsorption to bioactive surfaces, points out how fundamental it is to develop adsorption/desorption experiments using concentration of the protein as close as possible to the physiological one at the implant interface. However, most of the Fn adsorption studies previously done on different surfaces were performed using either Fn already present in the serum (whom concentration can't be exactly determined) or adding Fn to the solution in concentrations ranging between 1-20 µg/ml (Gugala and Gogolewski, 2004), (Kilpadi et al., 2001), (Scotchford et al., 2002a), (McFarland et al., 2000), far from the physiological one of 300µg/ml (Mosher and Williams, 1978).
Moreover, the evidence that Fn adsorption from a competitive environment is not a phenomenon driven by the amount of Fn in the surrounding media supports the hypothesis that a possible change of conformation of the protein occurs upon its adsorption on the implant.

4.4.2 The effect of a competitive environment

The interaction between a material's surface and proteins is a multi step process, influenced by different factors. This event is the most rapid to occur after the implantation of the material, even faster than cellular attachment. Also, as different kinds of serum proteins compete for adsorption through available binding sites on the surface of the implant, protein adsorption is recognised to be a competitive process. Which proteins preferentially adsorb from the mixture of the serum to this limited number of binding sites will depend, at least, on their relative concentrations and on their surface affinities (Fabrizius-Homan and Cooper, 1991), (Horbett, 1996a).

Which protein species drive the initial phase of protein adsorption probably depends on their relative concentration; over time, however, or after the coating approaches monolayer, the adsorption is then regulated by the so called "Vroman effect" (Vroman and Adams, 1986): in the absence of cellular interactions the composition of the adsorbed protein layer will change as faster and more abundant diffusing molecules (e.g. albumin) are displaced by proteins with a higher affinity for the surface.

Every time a study aims to clarify which are the possible events happening in the body in a particular condition or situation, it is fundamental to try and mimic the *in vivo* environment (in terms of temperature, conditions, etc) as closely as possible. In the present study therefore it was decided to perform adsorption/desorption experiments of Fn on bone graft surfaces in the presence of serum proteins, in order to investigate the mechanisms of Fn adsorption to different chemistry and morphology of hydroxyapatite surfaces in a competitive (and most similar to the physiological) environment.

Looking at the results in terms of absolute adsorption, under competitive conditions the adsorption of Fn was significantly higher on HA compared to SA DD from the 0.100mg/ml concentration solution (Figure 4-7b), while in contrast Fn adsorption was highest on SA DD (but not significantly) from the 0.250mg/ml concentration solution (Figure 4-7a). Under non competitive conditions there was a trend towards greater levels of Fn adsorption on SAD with higher absolute levels of Fn adsorbed from the 0.250 mg/ml concentration solution (Figure 4-6).

This indicates that the presence of competitive species in the environment significantly influences the biological response of bone graft substitutes in terms of protein adsorption, and that the precise nature of this effect depends on both the concentration of the protein and the chemistry of the bone graft.

These observations suggest that from pure Fn solutions, Fn has a greater affinity to silicate substituted HA than stoichiometric hydroxyapatite surfaces from both Fn1 and Fn2 concentrations. However the presence of serum proteins changed this effect, resulting in greater affinity of Fn to HA from lower Fn1 concentration solution. This effect could be due to a relatively high affinity of serum proteins for SA as compared to HA, which would provide greater competition with Fn at the surface of SA DD and prevent its adsorption.
This effect is abolished by increasing the relative concentration of Fn.

These results show that Fn adsorption from a competitive environment is a complex process, dependent not only on bulk Fn concentration but also

relative surface affinities. Similar studies where Fn adsorption/desorption was evaluated with and without competitive species are limited (McFarland et al., 2000), but many researchers have studied Fn adsorption to different materials from either FCS or from a pure solution. In one of these studies the adsorption of Fn from FCS was studied on different material surfaces, and Fn was shown to have a statistically relevant higher adsorption on HA than on titanium or on steel (Kilpadi et al., 2001).

The behaviour of Fn in terms of adsorption on patterned surfaces was investigated by McFarland *et al*: they showed that Fn was able to adsorb on the surface from pure solution but not from FCS giving, as in this study, further evidence of the influence that the competitive environment has on Fn adsorption at the implant surface (McFarland et al., 2000). However, it must be taken into consideration that the concentration of Fn used in the McFarland study was very low, at 20 µg/ml.

Another investigation of Fn in a competitive environment demonstrated how serum Fn, adsorbed on microporous HA and SA discs, was sensitive not only to the presence of other serum proteins but also to its total amount in the solution: in particular an increase in total concentration of serum proteins (therefore also Fn) from 20 to 50% had a detrimental effect of Fn adsorption (Guth et al., 2010a).

In addition to these results, there is also some evidence that Fn, despite being recognised as the archetypal cell adhesive protein, may have a diminished role in situations of adsorption from complex mixtures due to its low competitive activity (Underwood and Bennett, 1989).

Another relevant study involved adsorption of Fn on hydrophobic and hydrophilic tissue culture surfaces. When the relative amount of Fn adsorbed from serum solutions to these different surfaces was analysed at different serum concentrations, and interestingly the amount of Fn adsorbed increased with serum concentration up to 0.1% and then decreased progressively until, at 10% serum, there was little Fn adsorbed on the dishes (Grinnell and Feld, 1982). Moreover, as most tissue culture is carried out with 10% of serum, looking at these results it seems unlikely that it is the amount of Fn adsorbed

from the serum that is responsible for promoting subsequent cell attachment and spreading.

Regarding Fn desorption from dense discs the present results showed a fast release to both the MEM and MEM+10% FCS solutions at very early time points, which rapidly slows to minimal net release by 10 minutes (Figure 4-17, Figure 4-18). Interestingly, desorption from MEM+10% FCS was always significantly higher than from MEM on both HA and SA DD.
Looking at the percentage of Fn desorption relatively to the amount adsorbed, from MEM+10% FCS it was always higher than from MEM for HA and SA DD at all the time points with the exception of 60 minutes on HA (Figure 4-21).
These results suggest that competitive proteins promote a faster and more abundant release of Fn from the binding sites, independently of the chemistry of the samples.

4.4.3 The effect of chemistry

The chemistry of the material implanted has been recognised to be of fundamental importance in directing cell behaviour on bone graft materials (Guth et al., 2010b) (Sulaiman et al., 2013), (Ghanaati et al., 2012a) (Zreiqat et al., 1999b). There have been many theories proposed to explain this, including the influence that variation in charge density has directly on the cell population or the influence that surface charge has on the quality and quantity of proteins adsorbed on its surface, which then will appropriately mediate cell behaviour and biological activity.
Moreover it has been proposed that a relevant role is also played by the dissolution or exchange of ions from the material to the surrounding environment which can also influence cell behaviour. For instance it has been proposed that Si has the ability to bind with oxygen when it is dissolved, forming a silicate network on the surface of an implant which can be capable of binding proteins more tightly and, in turn, promoting better cell attachment (Schwarz, 1974).
Alternatively, in a study which investigated the dissolution of Silicon from microporous SA and its effect on osteoblasts behaviour, results showed that

cells were sensitive to the presence and the availability of Si ions in solution, which directly affected ALP expression and activity, (Guth et al., 2006b).

One of the aim of the present experiment was to understand whether or not Fn has higher affinity for stoichiometric hydroxyapatite or silicate substituted hydroxyapatite, and if changes in the geometry and topography of the implants alters this affinity.

On DD in MEM Fn showed higher affinity for SA than HA from both the Fn concentration solutions, and this effect was more pronounced from the 0.100 mg/ml solution (Figure 4-13, Figure 4-14); In serum containing media, this trend continued with the 0.250 mg/ml Fn concentration solution (Figure 4-7a), However with the low Fn concentration solution, the adsorption trend changed, and HA showed a significantly higher Fn adsorption than SA (Figure 4-7b).
The evidence that the higher affinity of the protein for SA is abolished with the presence of the serum suggests that the affinity of Fn and other serum proteins is higher for the silicate substituted rather than the stoichiometric HA, and also that the relative affinity of individual protein species is highly dependent on their individual concentrations when in the presence of competitive species. Therefore, it is possible to hypothesize either that the affinity of Fn for both the implant surfaces is lower than the one of the other competitive species in the serum, or that other serum proteins have higher affinity for SA than Fn, but non for HA, thus giving a relatively higher Fn adsorption affinity to HA.
Moreover, the evidence that the effect of serum proteins did not significantly affect Fn affinity when using the 0.250 mg/ml Fn concentration solution (Figure 4-7a), suggests that Fn concentration influences its own adsorption, and that the affinity of Fn and serum proteins for HA and SA is sensitive to their relative concentration.
On the granules samples the experiment was carried out only in the MEM+10% FCS. Looking at the results using 0.100 mg/ml of Fn solution (Figure 4-10b), the absence of a significant difference between the two chemistries suggests, again, an effect of Fn concentration on regulation of its own affinity and adsorption to bone grafts.

In the high Fn concentration solution, however, the adsorption of the protein was generally higher on the two SAG samples (a part for the 5 and 15 minutes time points, Figure 4-11a), with the adsorption on HAG showing a more variable trend.

The reason behind the apparent affinity of Fibronectin to SA (more hydrophobic and more negatively charged) compared to HA (more hydrophobic and less negatively charged), could be related to a combination of differences in the physic-chemical characteristics of the two materials, such as wettability, surface charge and indirect effects due to the presence of the silicate ions (Rashid et al., 2008).

The wettability (hydrophobicity or hydrophilicity) of a material refers to its ability to bind with water molecules. Because water is the most abundant component in the human body, its properties, characteristics and especially its role in mediating cellular processes have to be taken into consideration while evaluating the interactions between proteins and implant surface. On hydrophobic surfaces, even if there is an entropic penalty when water molecules self-associate together to minimize contact with it (Vogler, 1998), at the same time they have the advantage to be more favourable to the process of dehydration, which is fundamental for a protein to absorb, as both the protein and the surface must partially dehydrate before being able to make contact (Norde, 1996), (Haynes and Norde, 1994). Conversely, the displacement of water from a hydrophilic surface presents an energy barrier that needs to be exceeded.

In the light of these evaluations, protein adsorption on hydrophobic surfaces looks to be more thermodynamically favourable than on hydrophilic ones. However, there is some evidence that adsorption does occur on hydrophilic surfaces when charge interactions or protein conformation changes provide the driving force.

The role of surface charge in protein adsorption is complex and still not completely clear. It is believed that opposite charges will be mutually attracted, but this event is not the only one taking place at the implant surface, with different circumstances happening concomitantly.
First of all the presence of water molecules shields the charge of the material surface (Hanein et al., 1993); furthermore, this charge is modulated by the pH and counterbalanced by small ions present in the close environment (Brash and Horbett, 1995). Finally, the charge on a surface is minimized at its isoelectric point: a pH below this creates a positive charge and a pH above a negative charge, resulting in the formation of an electrical layer, the composition of which is dependent on entropy and on opposing charge neutralisation (Israelachvili and Wennerström, 1996). For all of these reasons, it is hard to predict the precise effect that surface charge has on protein adsorption.

Despite a number of different studies that have looked at the effect of material properties on protein adsorption and Fn adsorption on different surfaces (Dos Santos et al., 2008)(Guth et al., 2010a) (Zhu et al., 2009), it appears that the mechanisms that control this interaction are still not completely clear. For example some studies show enhanced adsorption of Fn on polarized or positively charged groups (Steele et al., 1995), while some others found more Fn adsorbed on negatively charged surfaces (Scotchford et al., 2002b). Conversely, in 2002 MacDonald et al. (MacDonald et al., 2002b), analysing the adsorption of human plasma Fn on modified titanium dioxide particles, suggested that hydrophobicity plays a major role in enhancing Fn adsorption on the substrates, supported probably by an increased change in conformation compared to hydrophilic surfaces.

In the light of all of these evaluations it is possible to hypothesize that the higher adsorption of Fn showed in this study for the silicon substituted implant, can be related to the presence of the Si, which changes the surface charge and the wettability, to support a more thermodynamically favourable protein adsorption.

The higher Fn adsorption seen on HA in MEM+10% FCS using low Fn concentration solutions, could have been supported by a greater relative affinity that Fn could have for this chemistry compared to other serum proteins, which was not detected from the higher Fn concentration solution because of steric constraints.

One event that it is widely hypothesized to act as a driving force in promoting protein adsorption on more hydrophilic surfaces is its possible change of conformation. This is because a change in conformation can indeed help to increase the entropy of the system (Horbett, 1996b) (Norde and Giacomelli, 2000). These structural changes in the adsorbed protein help to increase the bond mobility and thus potentially increase the contact with the surface. Many studies have reported structural changes in different proteins upon adsorption to surfaces, and they demonstrated that the adsorbed proteins, upon conformational change, retain their ordered secondary structure which gives them their specific function (Norde and Giacomelli, 2000) (Norde and Giacomelli, 1999) (Giacomelli and Norde, 2001).
However, even if the secondary structure is retained, its rearrangement and changes in its orientation can still modulate the activity of the protein. Some studies for example reported that impaired or enhanced activity of proteins as Fn, upon adsorption, can be related to conformational changes (Horbett, 1994) (Horbett, 1999). Furthermore, some studies showed the reduced cell binding functionality of Fn in soluble form, which can suggest that its increase in binding activity can only happen after a surface-mediated conformational change (Klebe et al., 1981a) (Schwarz and Juliano, 1984). These findings can also be compared to some other studies which showed that Fn coatings on hydrophilic tissue culture polystyrene enhanced bone-derived cell adhesion (Steele et al., 1993) and osteoblastic differentiation (Stephansson et al., 2002) compared with identical amounts on hydrophobic polystyrene. The higher cell adhesion and differentiation are possibly due to either a conformational change of the protein towards a more active state, or to a higher amount of protein adsorbed, which is possible because of the more active conformation.

These observations can be correlated to the results obtained from the MEM+10% FCS solution (using 0.100 mg/ml Fn solutions) in the present study: a higher amount of Fn was adsorbed on the more hydrophilic surface (HA) and, as showed by the circular dichroism analysis, a change of conformation happened after contact with these surfaces. This change of conformation could support the higher protein adsorption on HA compared to the more hydrophobic SA. The results of the circular dichroism analysis in fact show changes in the secondary structure of Fn in the 3 different solutions of the protein dissolved in MEM: before and after contact with HA or SA surfaces. Furthermore, some other studies demonstrated that Fn adsorbed on hydrophobic surfaces shows a reduction in cell-adhesive functions compared to when it is adsorbed on hydrophilic ones, where instead it shows its highest functionality (Jönsson et al., 1982) (Lewandowska et al., 1989).

Regarding the desorption of Fn from the DD or PG, results showed a higher protein desorption from HA than SA in the MEM solution and in MEM+10% FCS in Fn2 solution, while no significant difference was observed in the MEM+10% FCS in Fn1 solution (Figure 4-15, Figure 4-16). Though, the trends were still similar in all of them: a peak of release within the first ten minutes, which suggests that Fn may be re-adsorbed on the surface of the materials, and then a dynamic equilibrium maintained.

Desorption studies from PG results showed a non-significant difference in Fn desorption between HA and SA PG (Figure 4-19), giving further evidence to the fact that the presence of serum proteins tends to abolish the preferential behaviour that Fn showed towards HA or SA when using the MEM solution.

4.4.4 The effect of sample morphology

Many studies have investigated the influence of porosity of calcium phosphate substrates on cell proliferation, differentiation, protein expression and synthesis *in vitro* (Bignon et al., 2003) and osteoinduction *in vivo* (Yuan et al., 1998) (Toth et al., 1993) (Klein et al., 1994).

Other authors reported how differences in the material topography can influence serum proteins adsorption and indirectly also the biological response of the bone graft (Zhu et al., 2009) (El-Ghannam et al., 1999).

The results of this study enabled us to compare Fn adsorption and desorption between materials with different topography (dense discs and porous granules) but with the same chemical composition (HA or SA), media used (MEM+10% FCS) and Fn concentration used (0.250 mg/ml or 0.100 mg/ml).

At first sight it appears clear that porous granules show more protein adsorbed compared to dense discs, for both HA and SA. In particular a and b shows that on the HA the PG adsorbed significantly more Fn than the DD (after 5 and 15 min for the high Fn concentration solution and after 10, 15 and 30 min for the lower Fn concentration solution). On SA the results are similar, as shown from Figure 4-12c and d, where the PGs adsorbed significantly more Fn than the DD (after 1, 5, 10 and 15 min using the high Fn concentration solution, and after all the time points analyzed using the lower Fn concentration solution).

The higher levels of Fn adsorbed on the porous samples, for both HA and SA, is probably due to a combination of factors: firstly, the presence of the micro porosity increases the surface area of the implant, giving the protein more space to assume its favourable conformation and more surface on which to be adsorbed, as well as increasing the roughness, the presence of a microporous structure through which offers Fn a three-dimensional surface which may also facilitate the adsorption of the protein.

Similar observations have already been made by of Zhu et al. where two biphasic calcium-phosphate ceramics (one dense and one porous) exhibited different abilities to bind serum proteins: the porous material adsorbed a lot more serum proteins compared to the dense one, in both *in vitro* and *in vivo* studies (Zhu et al., 2009). However, as these studies were concerned with the effect of pore size, no tests were performed to measure the percentage of porosity in the samples, which makes it difficult to understand the effect of porosity, and also to directly compare those results with the present study. Similarly Rouahi *et al.* worked directly on HA substrates, studying the influence of microporosity on protein adsorption to bone scaffolds: the amount of BSA and Fn adsorbed on microporous HA was more than three times (analyzed by

SDS-PAGE) and more than 10-times higher (analyzed by temperature-programmed desorption) than adsorption to non-microporous HA (Rouahi et al., 2006).

Regarding the desorption of Fn from samples with different morphologies, the granules showed an absolute higher level of protein desorbed compared to the discs at both the concentrations, on both HA and SA. In particular, the release from the granules was not only higher in value but also more rapid compared to discs (Figure 4-20). Furthermore the difference was more pronounced in the physiological solution (Fn2, 0.250mg/ml) than the sub-physiological (Fn1, 0.100mg/ml) Fn concentration.

To obtain a clear understanding of the influence of morphology in protein desorption relative to the amount of the protein adsorbed, is useful to look at the results in terms of percentages of relative desorption of Fn from the samples. All the samples exhibited a higher release of protein from the PG compared to the DD (Figure 4-21). Using high Fn concentrations, SAG 80/30 showed the highest release but using the lower Fn concentration this sample showed the lowest Fn desorption within the three PG samples, whereas HAG 80/20 exhibited the highest.

Some *in vivo* studies demonstrated the higher osteogenetic potential of silicon-substituted HA with a high strut porosity percentage (Hing et al., 2004) (Campion et al., 2011) (Coathup et al., 2012)(Patel et al., 2002).

The work from Campion *et al*. showed how important the regulation of the strut porosity is, more than total porosity, for a bone graft for osteointegration, especially through an early process of neovascularisation.

Another work from Hing *et al*. reported that the distribution of porosity volume between the macro and the micro structure of the implant influences the process of osteointegration through permeability and angiogenesis processes, and that in long term, it is more the strut than the total porosity that influences this mechanism (Hing et al., 2005).

Considering Fn adsorption on Silicate substituted HA PGs SAG80/20 and SAG80/30 as a function of strut porosity, where strut porosity is the fraction of porosity within the scaffold struts, the present results of protein adsorption

don’t show a significant difference in Fn adsorption between the two different strut porosity percentages (20% and 30%). The desorption however was found to be relatively higher from the 30% strut porosity rather than the 20% (Figure 4-21), suggesting that the 20% retains Fn more tightly than the 30% sample, perhaps indicating a conformational variation.

Moreover these results suggest also that the greater biological activity with higher percentages of strut porosity observed *in vivo*, are unlikely to be due to a higher amount of Fn adsorbed on the surface of the biomaterials. One possible explanation could be a change of conformation of Fn to a more active state once adsorbed on biomaterials with higher strut porosity, supporting the higher relevance of protein conformation rather than protein amount for the biological response.

4.5 Conclusions

This study was performed to assess Fn behaviour on bone scaffolds. To test how Fn adsorption and desorption processes are influenced by selected factors and features of the test environment and presentation of the morphology of the material which have been previously hypothesised to affect Fn protein adsorption to bone graft substitutes. These features include the chemistry of the material, the presence of a competitive environment, different concentrations of the protein studied and differences in morphology of the material.

The chemistry of the material was found to affect protein adsorption only relatively: the presence of silicate in the hydroxyapatite crystal lattice was found to enhance Fn adsorption, either without the presence of competitive species or when Fn concentration was higher. However, in the presence of competitive species and when Fn concentration was lower, Fn adsorption was found to be higher on HA. Also, without serum proteins Fn desorption was lower in the silicon substituted HA, which suggests that SA binds proteins more tightly than HA. However the presence of serum proteins was found to make the Fn desorption very similar between HA and SA after the first 10 minutes.

The presence of the competitive species is confirmed to influence protein adsorption and desorption: Fn always presented a lower adsorption in the presence of serum proteins, which confirms the previous findings that Fn may have a lower affinity for HA and SA compared to the other serum proteins.

The concentration of Fn in the local environment site is relevant to influencing its behaviour. The differences in its adsorption using the two different concentrations suggest that the binding sites are not saturated at low concentration and when performing *in vitro* studies, it is important to use physiological concentrations of the protein if the data is to be correlated with behaviour *in vivo*.

Specimen morphology is a feature of the material that has been recognised to influence protein adsorption and desorption. These results confirm that the presence of strut or micro porosity enhances Fn adsorption compared to dense surfaces; however a higher percentage of strut porosity did not appear to significantly enhance any further adsorption. Also, the preference of Fn to bind to Silicate substituted hydroxyapatite is preserved in porous granules samples.

Finally, Circular Dichroism experiments confirmed that Fn undergoes a change of conformation after contact with both HA and SA biomaterials.

5 Investigtion of Osteoblast attachment to hydroxyapatite and silicate-substituted hydroxyapatite dense discs and porous granules with and without pre-conditioning with Fn

In light of the findings of Chapter 4, where Fibronectin (Fn) adsorption and desorption to HA and SA was found to be influenced by the presence of a competitive environment, the morphology and chemistry of the material, and to be dependent on its own concentration, the next series of experiments was focused on the study of cell adhesion to HA and SA discs and porous scaffolds with and without pre-conditioning with Fn. The rationale behind these experiments being to investigate whether or not it was possible to correlate cell adhesion with Fn adsorption and to clarify if, and to what extent, the chemical properties and morphological features of bone graft substitute scaffolds promote osteoblast attachment through their influence on the quantity or quality of Fn adsorbed.

5.1 Experimental methodology

The experiment was divided in two parts:

- Analysis of cell adhesion with no pre-treatment and with pre-treatment with either serum containing media (SCM) or sub-physiological concentration of Fn in SCM (Fn1), at three different time points on porous granules (PG)
- Analysis of cell adhesion with no pre-treatment and with pre-treatment with either SCM, sub-physiological concentration of Fn in Phosphate Buffer Saline (Fn1 PBS) and SCM (Fn1 SCM), and physiological concentration of Fn in PBS (Fn2 PBS) and SCM (Fn2 SCM), at 60 minutes and on dense discs (DD) and PG

5.1.1 Cell culture media and test specimens

A human osteosarcoma cell-line (MG63) was used for this experiment. Cells were expanded *in vitro* using MEM containing 10% of Foetal Calf Serum

(FCS), 1% Penicillin /Streptomycin (PEN/STREP), 1% L-Glutamine (L-Glu) (SCM) (Sigma Aldrich, UK).

The samples tested possessed 3 different morphological forms as follows (See Chapter 3 for full specimen details):

- 12mm diameter (1g) dense discs of phase pure stoichiometric hydroxyapatite (**HAD**) or silicate-substituted hydroxyapatite (with 0.8wt% Si) (**SAD**),
- 0.5g porous granules, 1-2mm in size, with 80% total porosity and 20% strut porosity of phase pure stoichiometric hydroxyapatite (**HAG 80/20**) or silicate-substituted hydroxyapatite (with 0.8wt% Si) (**SAG 80/20**)
- 0.5g porous granules, 1-2mm in size, with 80% total porosity and 30% strut porosity of phase pure silicate-substituted hydroxyapatite (with 0.8wt% Si) (**SAG 80/30**).

Prior to experiments all samples were sterilized under UV light, discs were transferred to a 24-well plate, granules to a 48-well plate.

5.1.2 Quantification of cell attachment

In order to quantify the amount of cells on the samples, a cell tracker dye (the green CMFDA, Figure 2-10) was used to stain and then analyze the cells via fluorescence analysis. Calibrations curves were obtained using known numbers of labelled cells. Cells were labelled using a 2µM cell tracker dye solution (10 ml for a T75 flask) which, along with PBS (Sigma) and SCM (Lonza), was warmed up to 37°C in a water bath. The SCM from a T75 flask of confluent MG63 was then removed and replaced with 10ml of warm cell tracker solution which was then incubated for 40 minutes to allow the dye to pass through the cell membrane., The cell tracker solution was then removed, and replaced with 10ml of SCM and incubated for a further 40 mins to enable serum proteins to activate the dye through modification of the chloromethyl group. After incubation the SCM was removed, the cell layer washed with fresh, sterile PBS and the labelled cells trypsinized to enable cell counting. The trypsinization process involved a 3 minute incubation at 37°C with a 1.5ml solution of Trypsin-EDTA (Sigma-Aldrich) after which cells were checked for detachment under a microscope prior to addition of 1.5ml fresh SCM to the

flask and transfer of the resultant cells/trypsin/SCM solution to a conical centrifuge tube which was then spun down for 5 minutes at 1800 rpm.

After centrifugation and removal of supernatant, the cell pellet was diluted in fresh SCM and appropriate dilutions were made to make up a known, 1:2 dilution series of labelled MG63 cells in SCM.

Table 5-1 shows the dilutions and relative cell concentrations used to generate cell tracker dye calibration curves. Basically, serial dilutions were made from a 10^6 cell/ml solution, then the same volume of 0.1% Triton X-100 was added to each concentration, allowed to sit at 37°C for 20 minutes and then sonicated for 60 seconds/well. Then 0.3ml of this solution was added, in triplicates, to a white 96-well plate for fluorescence reading. A line of best fit was obtained between fluorescence intensity and cell number, and the equation used to calculate the number of cells in unknown samples from fluorescence intensity readings.

Table 5-1: Cell concentrations and cell number in the suspensions made to calibrate the cell tracker dye

No	Initial cell concentration (cell/ml)	Cell concentration after Triton X-100 addition (cell/ml)	Known Cell number
1	1000000	500000	150000
2	500000	250000	75000
3	250000	125000	37500
4	125000	62500	18750
5	62500	31250	9375
6	31250	15600	4680
7	15600	7800	2340
8	0	0	0

5.1.3 Investigation of cell attachment to pre-conditioned porous granules with time

The aim of this experiment was to monitor cell adhesion over time to HAG80/30, SAG80/20 and SAG80/30, under various different conditions, as outlined in Table 5-2, in order to select an appropriate time point for the full study.

After sterilization under UV light, samples were randomly selected to either the BARE, SCM, or Fn1 treatment groups (Table 5-2). Samples were run in triplicate at each of the three different time points (30, 60 and 90 minutes).

Table 5-2: Pre-conditioning treatment, sample type and study time-points

Pre-conditioning Treatment	Sample	Cell exposure
BARE (No Conditioning)	HAG80/20 SAG80/20 SAG80/30	30, 60 or 90 min at 37°C, 95% Humidity, 5% CO_2
SCM (60 min at 37°C in MEM supplemented with 10% Bovine Serum)		
Fn1 (60 min at 37°C in SCM supplemented with 0.10mg/ml Fn)		

After one hour, conditioning solutions were aspirated and samples washed with PBS before addition of the cell suspension (1ml of a $5x10^5$ cell/ml suspension); then they were left in an incubator for the specific set incubation time.

At the end of each experiment the cell suspension was removed from the samples and discarded, samples were washed twice (to remove non adherent cells which may have been trapped in open porosity) with fresh sterile PBS. A solution of SCM/Triton X-100 in a 70/30 ratio was added to permeabilize cells for 20 minutes at room temperature.

The solution from each well was then transferred into an eppendorf tube, vortexed and 0.3ml of it transferred in triplicate into a white 96-well plate for fluorescence analysis using the FLOStar OPTIMA fluorometer (Figure 2-3).

5.1.4 Investigation of cell attachment following pre-conditioning with Fn supplemented in PBS or SCM

Based on the results of the time course study, a 60 minutes incubation period was selected for analysis of cell attachment from suspension. DD and PG were subjected to a range of pre-conditioning treatments using either SCM or PBS as substrate media supplemented with either 0.10 mg/ml Fn (Fn1) or 0.25 mg/ml Fn (Fn2) (Table 5-3). The aim being to determine whether the simultaneous presence of serum proteins and amino acids found in SCM altered Fn adsorption and any subsequent influence on cell attachment. Additionally HA and SA dense discs were analysed: HAD and SAD. The experimental plan was as shown in Table 5-3.

Table 5-3: Pre-conditioning treatment and sample details.

Pre-Conditioning Treatment	Sample	Cell exposure
BARE (No Conditioning)	HAD SAD HAG80/20 SAG80/20 SAG80/30	60 min at 37°C 95% Humidity, 5% CO_2
SCM (60 min at 37°C in MEM supplemented with 10% Bovine Serum)		
Fn1 PBS (60 min at 37°C in PBS supplemented with 0.10mg/ml Fn)		
Fn2 PBS (60 min at 37°C in PBS supplemented with 0.25mg/ml Fn)		
Fn1 SCM (60 min at 37°C in SCM supplemented with 0.10mg/ml Fn)		
Fn2 SCM (60 min at 37°C in SCM supplemented with 0.25mg/ml Fn)		

After conditioning, samples were incubated with 1ml of a $5x10^5$ cell/ml cell suspension and then analysed following the same protocol described in section 5.1.3.

5.1.5 Statistical Analisys

The sample size for each DD and PG material was n=3. Variations in responses of cell attachment between chemistries (HA vs SA), strut porosities (20% vs 30%), or pre-treatments (SCM, Fn1 PBS, Fn2 PBS, Fn1 SCM, Fn2 SCM) were assessed statistically by using a one-way analysis of variance. Differences were evaluated by using Bonferroni post testing. All statistical tests were run by using KaleidaGraph statistical software (v 4.0, Synergy Software, Reading, PA, USA) at a significance level of α=0.05.

5.2 Results

5.2.1 Investigation of cell attachment to pre-conditioned porous granules with time

Figure 5-1 shows the number of cells attached to HAG80/20 samples from the BARE, SCM and Fn1 treatment groups after incubation for periods of 30, 60 and 90 minutes. There were significantly less cells attached to SCM conditioned samples as compared to BARE samples, irrespective of incubation time. At 30 min the conditioning with Fn1 promoted the highest cell attachment compared to BARE and SCM, however this effect diminished at later time points showing instead BARE samples to have significantly more cells attached compared to both SCM and Fn1 at 60 min and 90 min.

In all the figures the colour refers to the group with the significantly higher value, and the symbols represent: p<0.05 vs * BARE, ^ SCM, $ Fn1, p<0.005 vs ** BARE, ^^ SCM, $$ Fn1, p<0.0001 vs ^^^ SCM

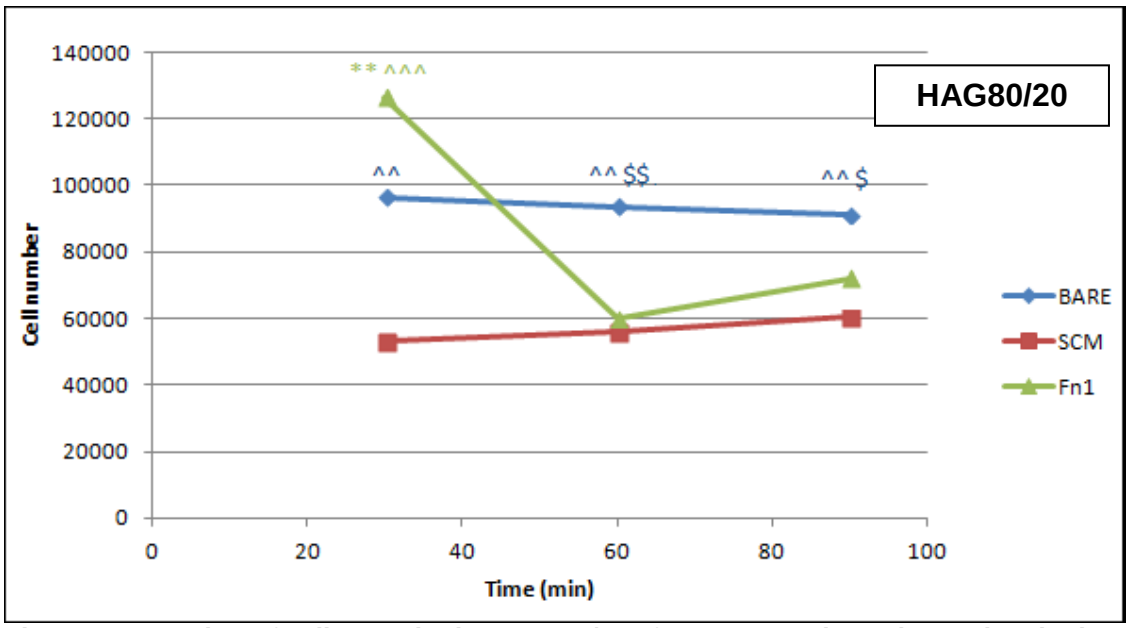

Figure 5-1: number of cells attached to HAG80/20 after 30, 60 and 90 minutes incubation from BARE, SCM and Fn1 treatment groups.

Figure 5-2 shows the number of cells attached to SAG80/20 samples from the BARE, SCM and Fn1 treatment groups after incubation for periods of 30, 60 and 90 minutes. As for HAG80/20, also on SAG80/20 there were less cells attached to the SCM treatment group irrespective of incubation time, but for this sample this difference was only significant after 30 and 60 minutes of incubation. There was no significant difference in cell attachment number between the BARE and Fn1 treatment groups at any time point. Significantly more cells were attached to samples from the Fn1 treatment group as compared to the SCM treatment group after incubation for 30 and 60 minutes.

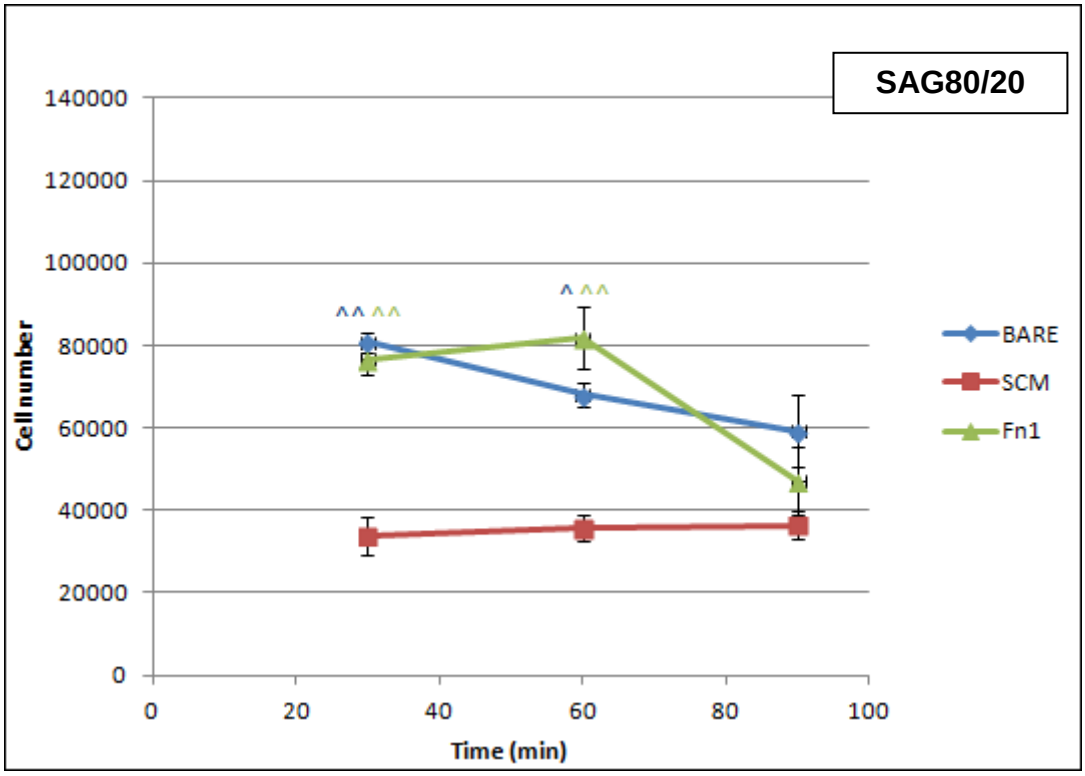

Figure 5-2: number of cells attached to SAG80/20 after 30, 60 and 90 minutes incubation from BARE, SCM and Fn1 treatment groups.

Figure 5-3 shows the number of cells attached to SAG80/30 samples from the BARE, SCM and Fn1 treatment groups after incubation for periods of 30, 60 and 90 minutes. In contrast to samples with a low strut porosity (SAG80/20, Figure 5-2

Figure 5-2: number of cells attached to SAG80/20 after 30, 60 and 90 minutes incubation from BARE, SCM and Fn1 treatment groups.

) and low strut porosity and different chemistry (HAG80/20, Figure 5-1) SCM didn't result in a significant lower cell attachment as compared to BARE and Fn1 pre-conditioned samples, but was actually significantly higher compared to BARE after both 30 and 60 minutes. Moreover, after 60 minutes cell attachment on SCM treated samples was significantly higher also compared to Fn1. After 90 minutes there was no significant difference in number of attached cells between the samples. After 30 minutes cell attachment to Fn1 treated samples was significantly higher than those attached to BARE samples, but by 60 minutes there was no significant difference.

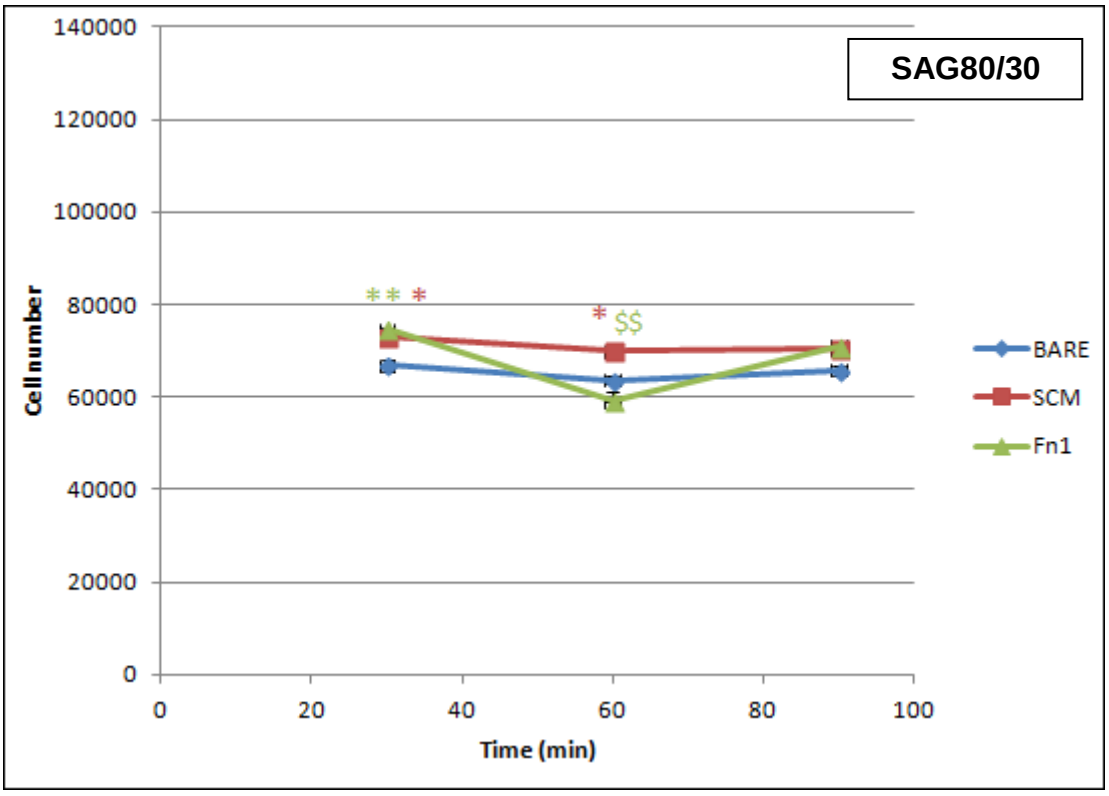

Figure 5-3: number of cells attached to SAG80/30 after 30, 60 and 90 minutes incubation from BARE, SCM and Fn1 treatment groups

Figure 5-4: number of cells attached to HAG80/20, SAG80/20 and SAG80/30 after 30, 60 and 90 minutes incubation from BARE

shows the number of cells attached to BARE HAG80/20, SAG80/20 and SAG80/30 samples after incubation for periods of 30, 60 and 90 minutes. At each time point analyzed the HAG80/20 showed a significantly higher number

of cells attached as compared to SAG80/20 and SAG80/30 at all the time points. The only other significant difference was shown by SAG80/20 vs SAG80/30 at 30 minutes.

In all the figures the colour refers to the group with the significantly higher value, and the symbols represent: p<0.05 vs * HAG80/20, ^ SAG80/20, $ SAG80/30, p<0.005 vs ** HAG80/20, ^^ SAG80/20, $$ SAG80/30.

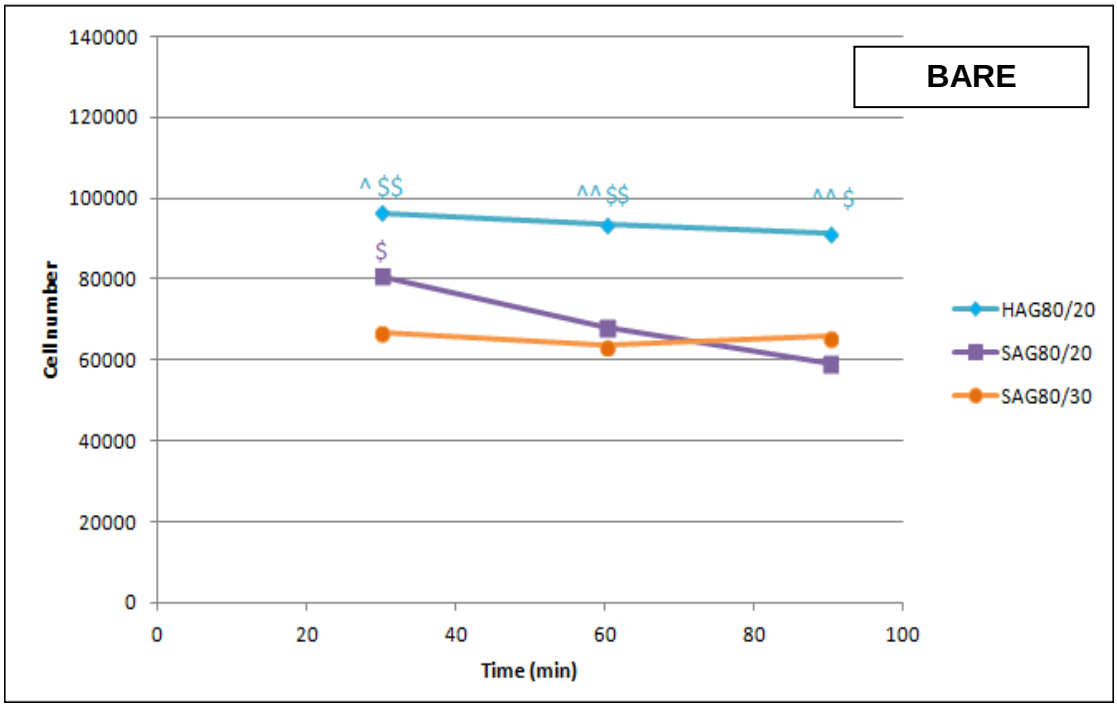

Figure 5-4: number of cells attached to HAG80/20, SAG80/20 and SAG80/30 after 30, 60 and 90 minutes incubation from BARE

Figure 5-5 shows the number of cells attached to SCM pre-conditioned HAG80/20, SAG80/20 and SAG80/30 samples after incubation for periods of 30, 60 and 90 minutes. At all the time points SAG80/30 showed to attach significantly more cells than HAG80/20 (p<0.05) and SAG80/20 (p<0.005).

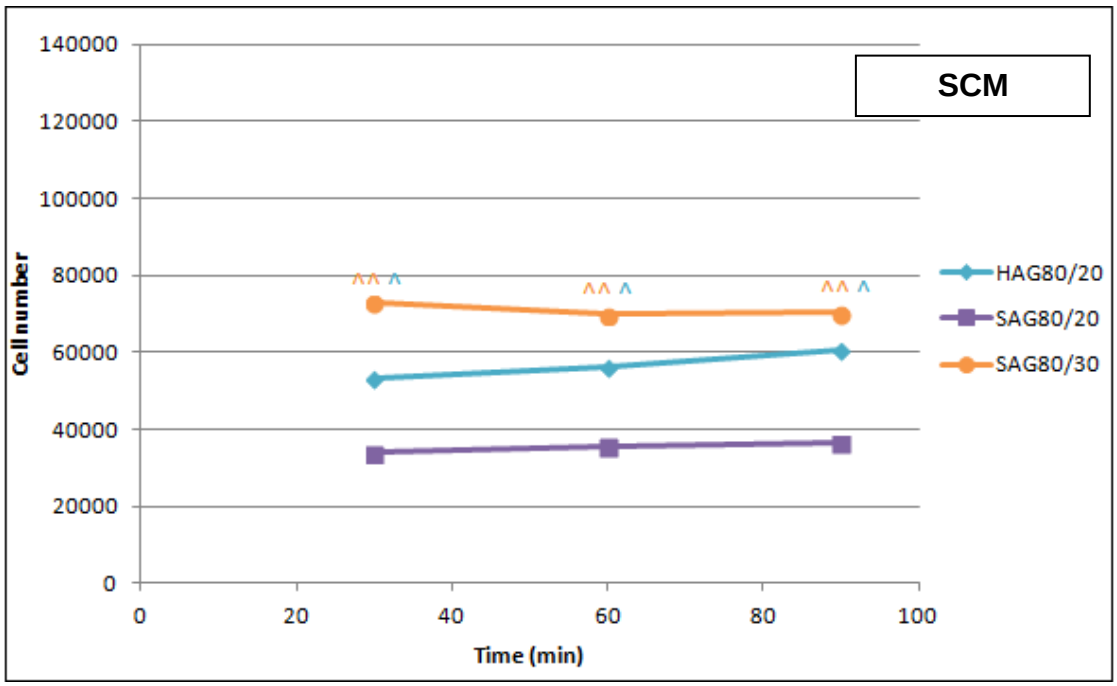

Figure 5-5: number of cells attached to HAG80/20, SAG80/20 and SAG80/30 after 30, 60 and 90 minutes incubation from SCM

Figure 5-6 shows the number of cells attached to HAG80/20, SAG80/20 and SAG80/30 samples from the Fn1 pre-treatment group after incubation for periods of 30, 60 and 90 minutes. With this pre-treatment, HAG80/20 supported a significantly higher number of cells attached at 30 min (as compared to both SAG80/20 and SAG80/30) and 90 minutes (as compared to SAG80/20), while after 60 minutes was significantly lower than SAG80/20. Moreover, SAG80/30 showed to attach significantly more cells than SAG80/20 after 90 minutes, but also significantly lower than this sample after 60 minutes. These results basically show fluctuations in cell attachment after pre-treatment of the samples with Fn1 solution.

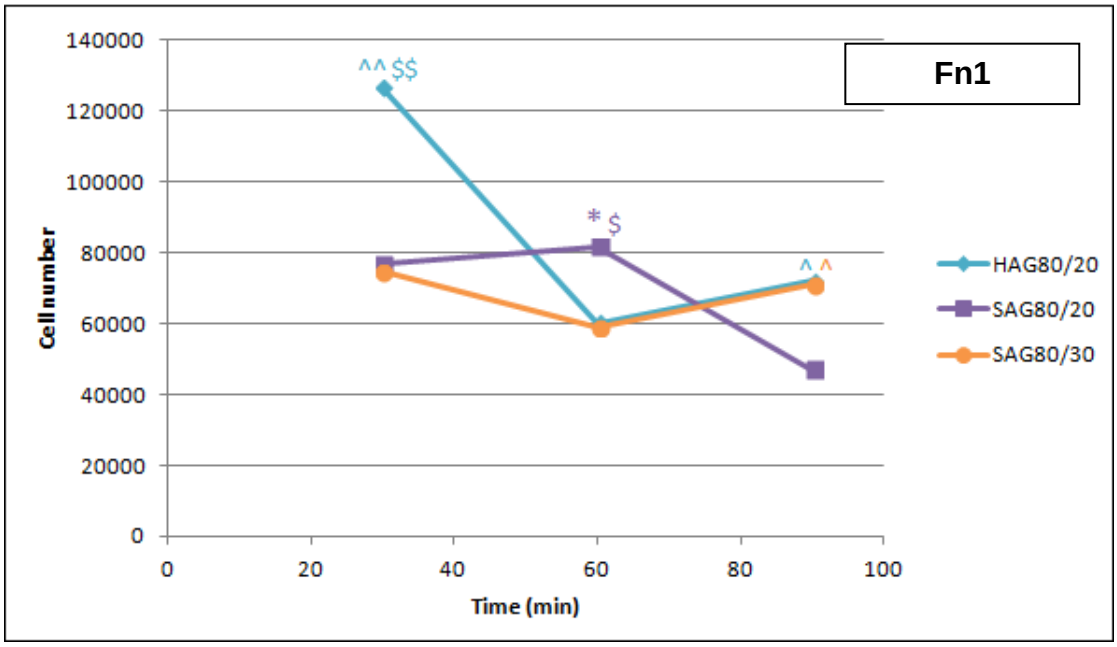

Figure 5-6: number of cells attached to HAG80/20, SAG80/20 and SAG80/30 after 30, 60 and 90 minutes incubation from Fn1

5.2.2 Investigation of cell attachment following pre-conditioning with Fn supplemented in PBS or SCM

In the second part of experiments cell adhesion was analyzed on dense discs and porous granules. As can be seen in Figure 5-7, the cell attached on HAD, even if higher on BARE, Fn1 and Fn2 in PBS treatments was not significantly different between the groups.

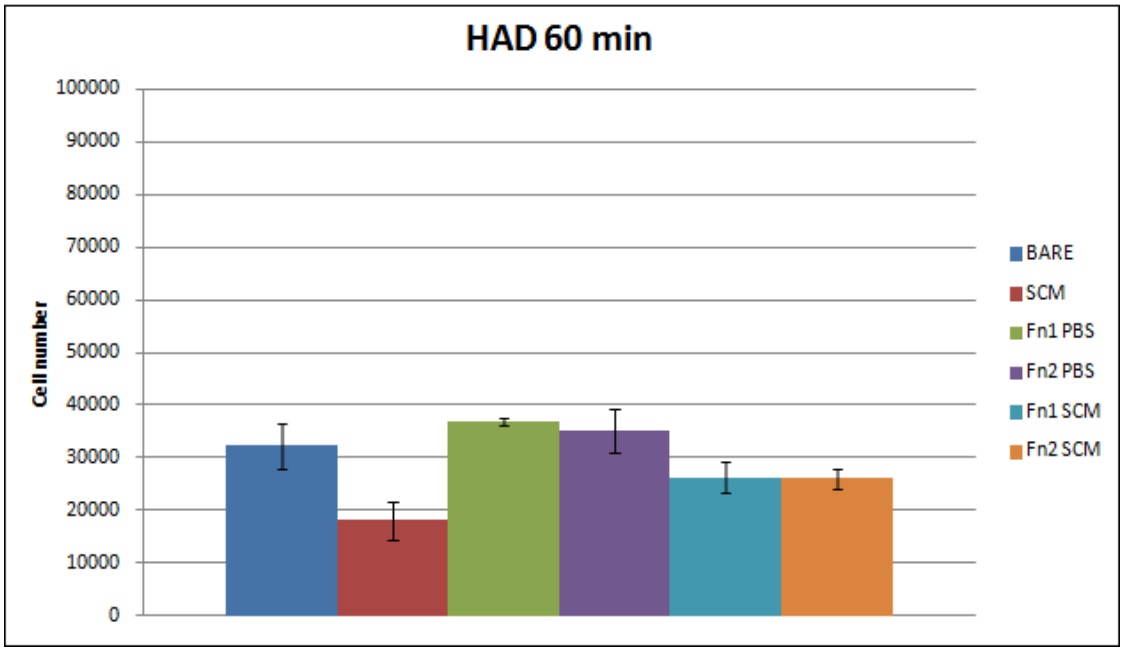

Figure 5-7: number of cells attached to HAD after 60 minutes using BARE, SCM, Fn1 and Fn2 in PBS, and Fn1 and Fn2 in SCM pre-treatments.

Figure 5-8shows the number of cells attached to SAD after SCM, Fn1 or Fn2 in PBS, Fn1 or Fn2 in SCM pre-treatments, or on BARE samples. The trend was similar to the one on HAD (Figure 5-7**Error! Reference source not found.**) however, on SAD the number of cells attached was significantly higher ($p<0.05$) on Fn2 in PBS compared to Fn2 in SCM.

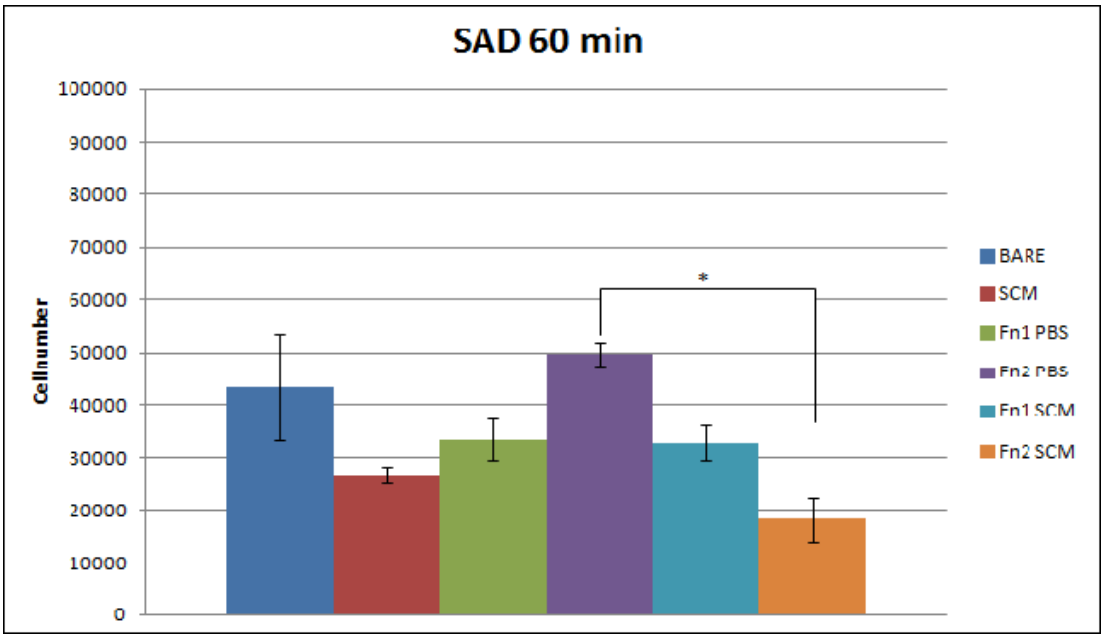

Figure 5-8: number of cells attached to SAD after 60 minutes using BARE, SCM, Fn1 and Fn2 in PBS, and Fn1 and Fn2 in SCM pre-treatments.

Figure 5-9 shows the number of cells attached on HAG80/20 after SCM, Fn1 or Fn2 in PBS, Fn1 or Fn2 in SCM pre-treatments, or on BARE samples. The results show that the cell number didn't change substantially between conditions, however there was a significant difference ($p<0.05$) between BARE and Fn2 in SCM pre-treatments.

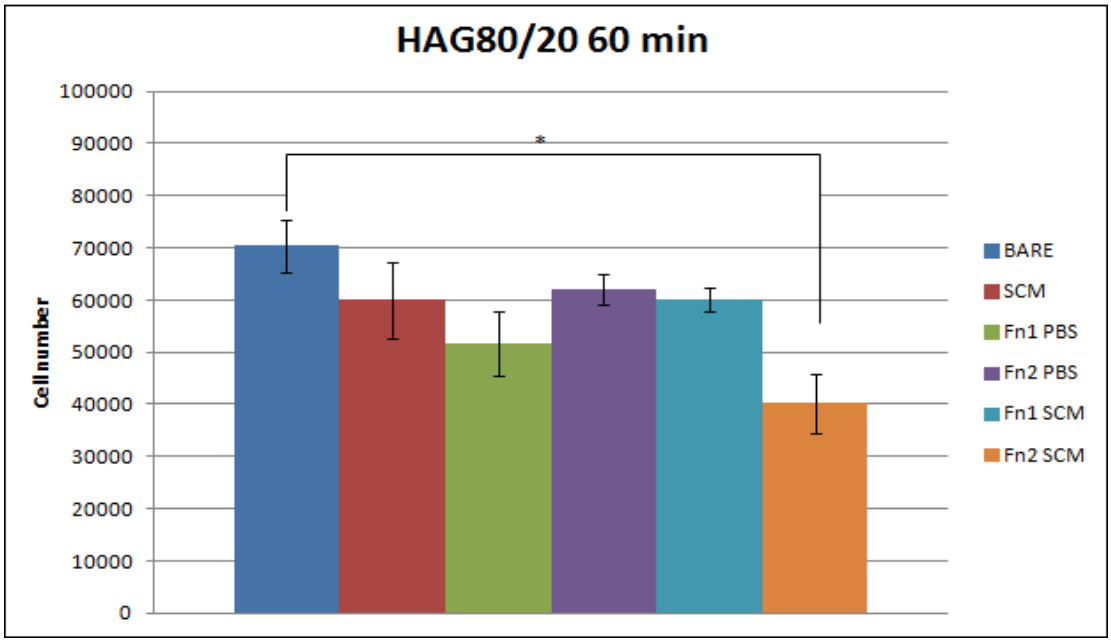

Figure 5-9: number of cells attached to HAG80/20 after 60 minutes using BARE, SCM, Fn1 and Fn2 in PBS, and Fn1 and Fn2 in SCM pre-treatments.

Figure 5-10 shows the results of cell attachment on SAG80/20. The Fn1 in SCM pre-treatment showed the highest number of cell attached, significantly higher compared to BARE, SCM and Fn2 in SCM. Moreover, also Fn2 in PBS showed a significantly higher number of cells attached to SAG80/20 compared to Fn2 SCM.

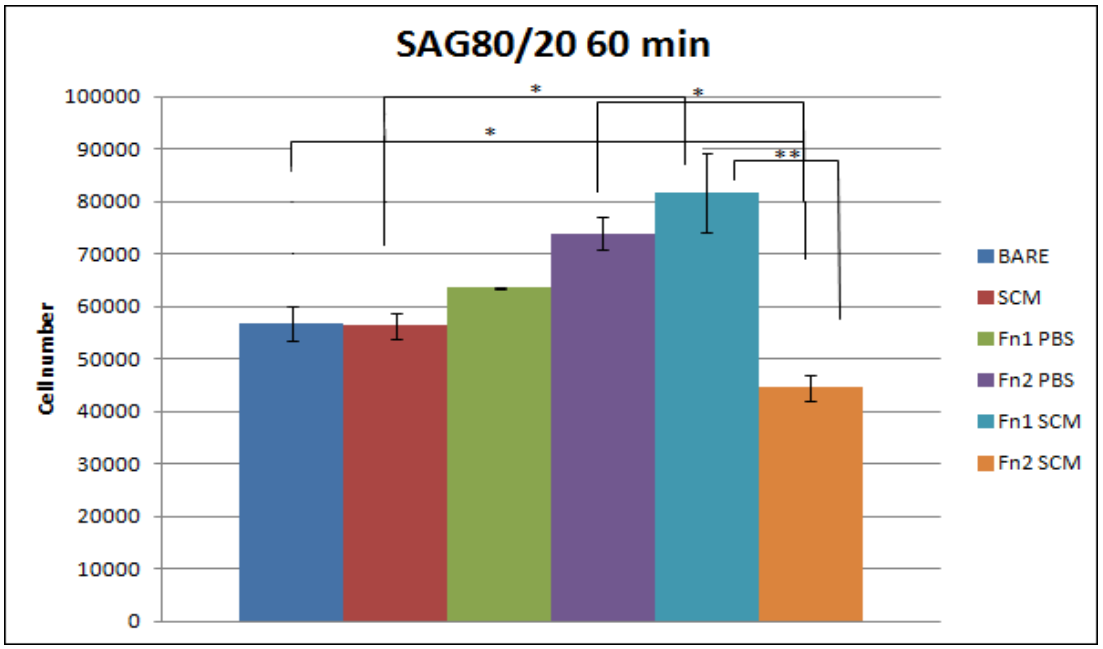

Figure 5-10: number of cells attached to SAG80/20 after 60 minutes using BARE, SCM, Fn1 and Fn2 in PBS, and Fn1 and Fn2 in SCM pre-treatments.

Figure 5-11 shows the number of cells attached on SAG80/30 after SCM, Fn1 or Fn2 in PBS, Fn1 or Fn2 in SCM pre-treatments, or on BARE samples. On this sample both the pre-treatments of Fn in SCM showed a lower cell attachment compared to the other treatments. In contrast to the SAG80/20 sample in fact (Figure 5-10), SAG80/30 showed a significantly higher number of cells on BARE, Fn1 PBS and Fn2 PBS compared to Fn1 SCM, and a significantly lower number of cells on Fn2 SCM compared to all the other treatment groups ($p<0.005$ and $p<0.0001$ respectively).

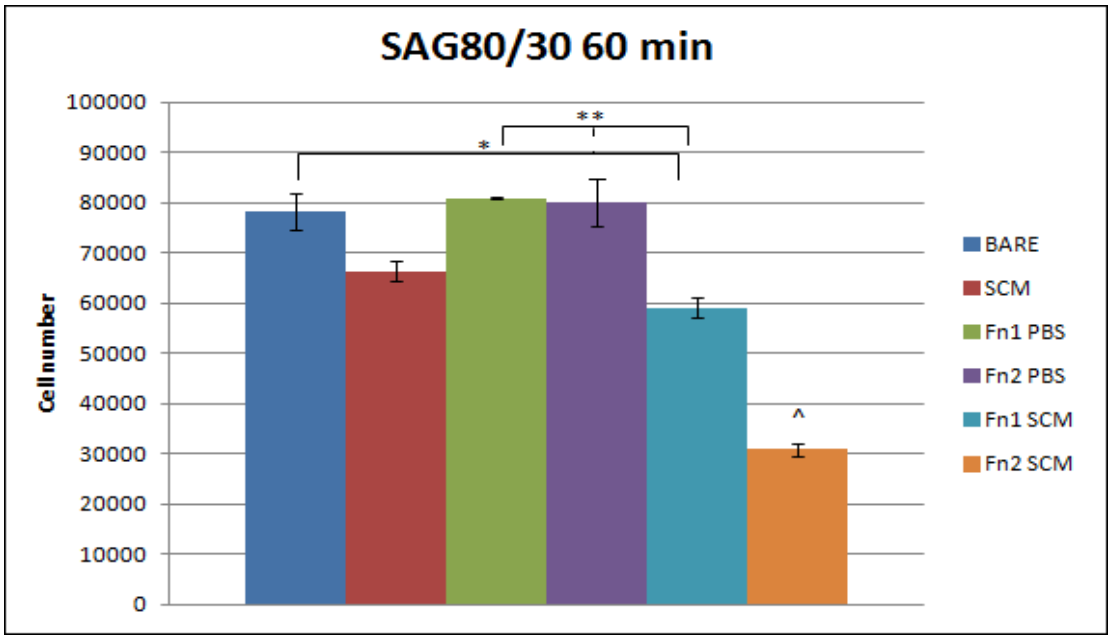

Figure 5-11: number of cells attached to SAG80/30 after 60 minutes using BARE, SCM, Fn1 and Fn2 in PBS, and Fn1 and Fn2 in SCM pre-treatments (*p<0.05, **p<0.005).

Moreover, to be able to compare the effect that chemistry has in mediating cell attachment in the different conditions studied, the number of cells attached was compared between HAG80/20 and SAG80/20 for each pre-treatment. Figure 5-12 shows that the presence of Fn, in any solution (PBS or SCM) and at any concentration (Fn1 or Fn2), increased the number of cells attached on SAG80/20 compared to HAG80/20, while cell attachment to HAG80/20 was higher as compared to SAG80/20 only on BARE and on SCM treated samples. These differences were statistically significant only on SA after Fn2 PBS and Fn1 SCM pre-treatment groups.

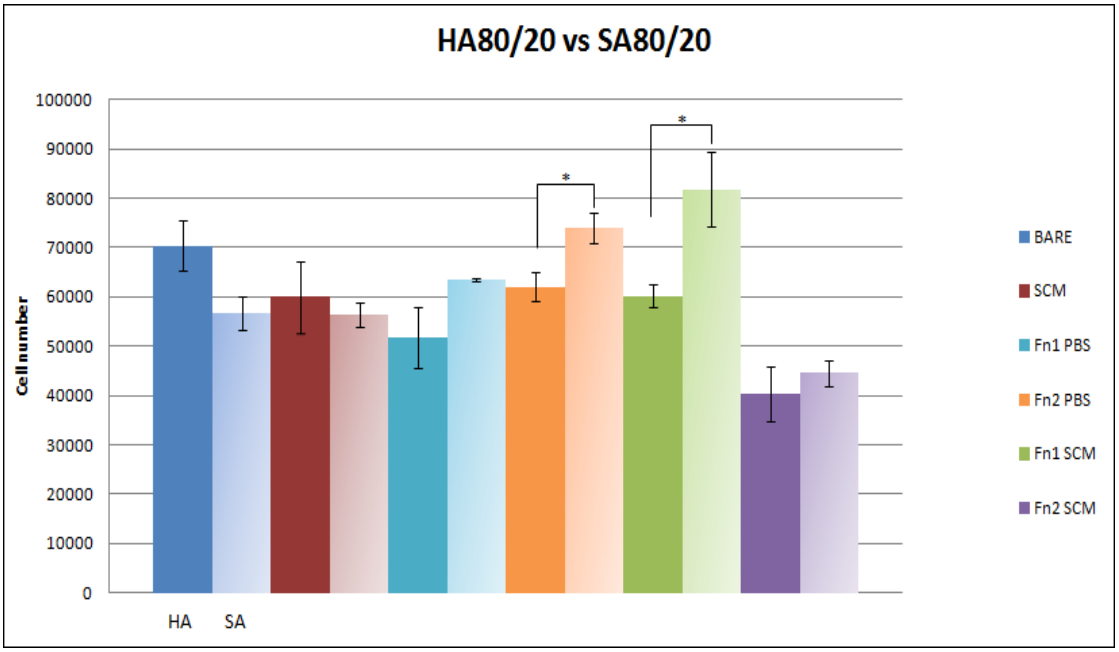

Figure 5-12: number of cells attached to HAG80/20 and SAG80/20 after 60 minutes using BARE, SCM, Fn1 and Fn2 in PBS and Fn1 and Fn2 in SCM pre-treatments.

Figure 5-13 shows the number of cells attached to SAG80/20 and SAG80/30 with each pre-treatment and compares the 20% strut porosity with the 30% strut porosity of SA granules. Interestingly, the 30% strut porosity supported significant higher cell attachment to BARE, SCM and Fn1 PBS treated samples, while a solution of Fn in SCM (no matter the Fn concentration) resulted in a significant increase in the number of cells on the 20% strut porosity sample compared to the 30% one.

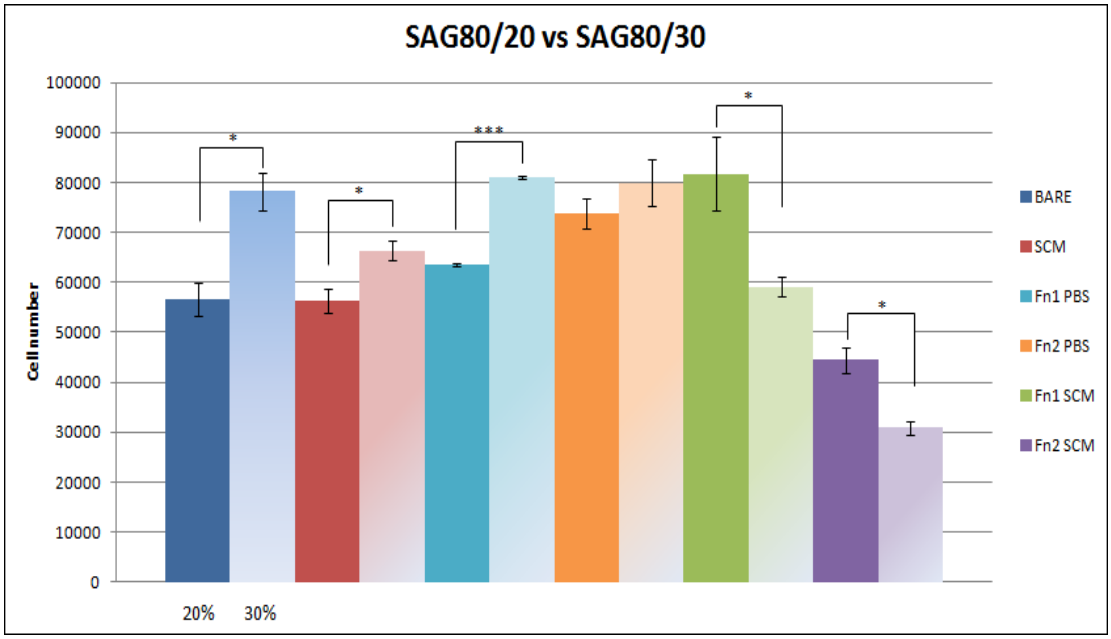

Figure 5-13: number of cells attached to SAG80/20 and SAG80/30 after 60 minutes using BARE, SCM, Fn1 and Fn2 in PBS and Fn1 and Fn2 in SCM pre-treatments (*p<0.05, ***p<0.0001).

5.3 Discussion

The relevance of the role of extracellular matrix/cell adhesion proteins in many tissues, including bone, is well established (Seitz et al., 1982)(Albelda and Buck, 1990)(Wilson et al., 2005). In particular Fn, thanks to its high concentration in serum, can serve as an immediate adhesion molecule to attach cells to ceramics. After this first step, however, cells can start synthesizing their own attachment machinery that may include Fn and/or other adhesion molecules. This mechanism is part of a complex system of events at the material-cell interface, which is due to the truly dynamic characteristic of the *in vivo* environment: this means that cells can not only start synthesizing their own adhesion molecules (Bagambisa et al., 1994), (Chou et al., 1995) but that they can also alter the density and the distribution of adhesion molecules receptors on the cell membrane (Singer et al., 1988)(Hormia and Könönen, 1994), change the differentiation state of the cell (Clover et al., 1992), (Siebers et al., 2005), and change the protein composition over time due to fibrin clot formation, remodelling, desorption of existing proteins and synthesis of new ones.

For all of these reasons detailed prediction of the events happening at the cell-material interface *in vivo* is difficult. Many studies report the importance of Fibronectin in mediating the attachment process (Kilpadi et al., 2001), (Seitz et al., 1982), (Yamada and Olden, 1978). However, it is still unclear how Fn is able to mediate this process, and also how material properties can affect its function, and subsequently influence the cell response. Other groups have tried to analyze the role that Fn has in modulating cell adhesion on these materials. A study from Schonmeyr (Schönmeyr et al., 2008a) reported significantly higher osteoblast adhesion on hydroxyapatite discs if these were pre-coated with a solution of Fn in fetal calf serum (FCS) compared to Fn only pre-coating or FCS alone. However, the Fn solutions were prepared at a concentration of only 0.04 mg/ml, and cell attachment was tested after 48 hours from incubation. These parameters, especially Fn concentration, are believed to be critical in determining Fn behaviour and can be hypothesized

that in such a lower concentration compared to the one used in this study, Fn was more able to change its conformation to an active state, and therefore increase cell adhesion compared to a solution with a higher concentration of the protein. 0.04 mg/ml of Fn in FCS could potentially be, therefore, the right concentration to use in order to have an increased cell adhesion promoted by Fn and at the same time no steric constraint in the solution could act as an obstacle to Fn conformational change.

Another work by Pendegrass (Pendegrass et al., 2012) investigated the attachment of dermal fibroblasts on titanium alloy, hydroxyapatite and Fn-coated hydroxyapatite (HA-Fn). The results showed a significant increase in cell attachment on HA-Fn substrate compared with the other materials at all time points: 1, 4 and 24 hours. In this study Fn was diluted in PBS, and each surface was treated with 0.02mg/ml of Fn. Furthermore, it should be taken into account that dermal fibroblasts could respond differently from human osteoblasts, and also that the conditioning temperature was not specified, which has been shown to be important in regulating protein adsorption (Mafina et al., 2013).

A work from Sawyer (Sawyer et al., 2005) demonstrates that, covering HA surfaces with an increasing number of RGD peptides (typical tri-peptide present in Fn), did not result in a linear increase in Mesenchymal Stem Cells adhesion, even if an increase in Fn was following the increase in RGD concentration. This proves that cell attachment is attenuated by mechanisms different to lack of Fn at the surface, therefore Fn alone is not able to directly influence cell adhesion.

Another work that points out the non-correlation between Fn concentration and cell adhesion is the one by El-Ghannam (El-Ghannam et al., 1999) which highlights how HA, even if showed to be able to adsorb more serum proteins compared to bioglass, showed a lower capacity to attach osteoblasts compared to the other surface after covering it with a calcium phosphate-rich layer.

The aim of the present study was to further understand the interactions between Fn adsorption, material chemistry and material strut porosity through comparison between the response of cell attachment to BARE, SCM, Fn1 and

Fn2 in PBS or SCM treatment groups: in this way it is possible to investigate the role that serum proteins and Fn have in modulating cell adhesion. As a first step however the effect of time on cell attachment was studied, primarily to identify an appropriate incubation period for the full study.

5.3.1 Investigation of incubation time

The number of cells attached to the samples was partially influenced by the incubation time. More specifically, for samples in the BARE and SCM treatment groups the cell attachment was constant during the three time points. However, with the presence of Fn1, the cell attachment was found to fluctuate with time. In particular, the conditioning with Fn1 pushed the cell attachment to peak at the earliest time point on HAG80/20, showing a significantly higher cell attachment compared to BARE and SCM, which then became significantly lower than BARE and similar to SCM treatments at the other two time points (Figure 5-1). On SAG80/20 cell adhesion showed a similar trend, where cell attachment to BARE and SCM treatments didn't substantially change with time while Fn1 treatment, after reaching a peak at 30 and 60 minutes, significantly lowered at 90 minutes (
Figure 5-2: number of cells attached to SAG80/20 after 30, 60 and 90 minutes incubation from BARE, SCM and Fn1 treatment groups.
). Interestingly, SAG80/30 didn't show a similar trend but the number of cells attached didn't significantly change over time for any of the three treatments (Figure 5-3), suggesting that a cell attachment to 30% strut porosity is more stable.

The finding that with BARE and with SCM pre-treatments there is no relevant change in number of cells attached to the samples at different time points suggests that this kind of system is able to rapidly reach an equilibrium, where cells can easily stay adhered to their substrate with no major changes at least until 90 minutes past seeding. Conversely the addition of Fn to SCM appeared to make this environment more dynamic, where the specific presence of Fn, together with serum proteins, was able to initially significantly increase cell attachment to samples with 20% strut porosity a more rapid (30 minutes for HAG80/20 and 30 and 60 minutes for SAG80/20). But with time this effect

appeared to be diminished or even reversed. This evaluation suggests that the pre-conditioning of the samples with Fn creates a more dynamic environment than no preconditioning (BARE) or pre-conditioning with SCM (SCM), environment which is sensed by the cells who then are able to respond in accordance. This suggests that Fn has a major role in influencing the adhesion of cells on the surface of BGS, as already showed by other studies (Klebe et al., 1981b), but also that, given the dynamic environment, there is a temporal element and that the quality (conformation) rather than the quantity of the protein could influence this behaviour (hypothesis further supported by the results in Chapter 4).

To summarize, these results show differences in the stability of cell attachment with time, as a function of pre-conditioning treatment, material chemistry and material porosity.
On BARE, SAG80/20 showed a greater fluctuation over time, with cell attachment dropping at later time points as compared to the other samples. The strut porosity didn't seem to influence significantly cell attachment on BARE, while greater attachment was supported by the HA chemistry as compared to SA (Figure 5-4).
On SCM treated samples, cell attachment didn't show any difference over time, The HA chemistry showed again a greater cell attachment than SA, and the 30% was better than the 20% strut porosity (Figure 5-5).
On Fn1 pre-conditioning there was a significant fluctuation of cell attachment, especially on HA (Figure 5-6). This finding can be correlated with the results of the previous chapter, were HA showed a greater Fn desorption as compared to SA (Figure 4-19b). In general, HA chemistry showed to be much more sensitive to fluctuation than SA.

5.3.2 The role of serum proteins and Fn on cell attachment

Having selected an incubation period of 60 minutes a series of experiments were performed to further investigate the relative influence of substrate chemistry, morphology and preconditioning environment on cell attachment. While HAD didn't show any significant difference in cell adhesion between the treatments (Figure 5-7), SAD showed a significantly higher number of cells

attached after pre-treatment with Fn2 PBS compared to Fn2 SCM (Figure 5-8). It is therefore possible to hypothesize that the presence of Si promotes sensitivity to pre-conditioning with Fn; however two relevant acknowledgments have to be made: the presence of Fn doesn't improve cell adhesion significantly (BARE vs Fn pre-treatments are not significantly different), and also that when there are serum proteins involved in the pre-conditionings (SCM and Fn1 and Fn2 in SCM) the number of cells attached was significantly reduced compared to the Fn2 PBS or BARE (in which there is no presence of competitive species) (Figure 5-8). Results of Fn adsorption experiments in Chapter 4 showed that Fn adsorption on SAD was inhibited by the presence of the serum proteins, (MEM vs MEM+FCS experiments), suggesting therefore that it is likely that this effect has led to the different cell attachment behaviour between Fn in PBS and Fn in SCM.
A critical discussion about how the chemistry of SA can affect differently the biological response as compared to HA can be found in Chapter 4.4.3.

Looking at the results on HAG80/20 (Figure 5-9), the only significant difference in cell adhesion was seen on BARE samples compared to the Fn2 SCM pre-treatment suggesting, again, that when Fn pre-coat the substrate in the competitive presence of serum the cell adhesion drops and lowers compared to a non pre-treated substrate.

Also for the granules, as seen for the dense discs, the presence of the Si increases the sensitivity of the material to pre-treatments. The SAG80/20 in fact (Figure 5-10) showed that Fn1 SCM has higher cell attachment not only compared to Fn2 SCM but also compared to BARE and SCM, suggesting that the presence of Fn is indeed fundamental at the material-cell interface in order to support cell attachment, and also that its concentration is also relevant. The finding that the pre-conditioning with Fn2 SCM significantly lowers the number of cells attached compared to Fn1 SCM, suggests that a higher amount of Fn doesn't relate to an higher amount of cells attached. Moreover, another interesting finding is that Fn2 PBS showed a significantly higher number of cells attached compared to Fn2 SCM: this result further support the hypothesis that Fn, especially at higher concentration (Fn2) is subject to physical

constraints and the further presence of competitive species in the solution (SCM) makes it harder for the protein to assume the exact conformation in order to support cell attachment.

The same observations can be made for SAG80/30 (Figure 5-11) which, similarly to SAG80/20, showed that the pre-treatment with Fn in PBS supports greater cell attachment than same pre-treatment with Fn in SCM: however on SAG80/20 this difference is found between the two Fn2 concentration solutions, while on SAG80/30 it is found between the two Fn1 concentration solutions. On SAG80/30, moreover, the cell attachment on BARE granules was significantly greater than on Fn1 and Fn2 SCM which, together with the evidence that Fn2 SCM showed a significantly lower cell attachment compared to all the other groups in the study, suggests a negative effect that SCM and a higher concentration of Fn has in the presence of an SA porous granules with a higher (30%) percentage of strut porosity.

All these results support the hypothesis that Fn could be affected by a conformational change which influence its effect on cell attachment. This hypothesis was already mentioned in the discussions of Chapter 4. The results of the previous set of experiments on PG in fact, showed a relatively higher amount of Fn adsorbed form the lower Fn concentration solution (Fn1) as compared to the higher, which could suggest that the presence of higher amount of Fn in the solution, or of other serum proteins, makes it harder for Fn to assume a specific conformational change needed for its adsorption on the surface of the biomaterials, probably for a physical constrain.

To summarize, pre-conditionings had the following general effects on cell attachment:

- On HAD: no statistically significant differences but a definite trend where pre-treatment with any SCM inhibited attachment, whereas Fn supplemented PBS rescued attachment to same as BARE.
- On SAD: similarly to HA, a definite trend where pre-treatment with any SCM inhibited attachment, but Fn2 supplemented PBS rescued attachment to same as Bare and significantly better than SCM Fn2.

- On HAG80/20: no statistically significant differences but a definite trend where any pre-treatment inhibited cell attachment, this time Fn2 supplemented PBS and Fn1 supplemented SCM rescued attachment slightly.
- On SAG80/20: very different behaviour – this time only pre-treatment with Fn2SCM inhibited attachment, trend to pre-treatment with 'low total protein concentration' solutions that contained Fn (Fn1 PBS, Fn2PBS and Fn1SCM) to support greater attachment.
- On SAG80/30: pre-treatment with any SCM inhibited attachment, Fn supplemented PBS rescued attachment to same as Bare

These effects seem to suggest that in general pre-conditioning with SCM inhibits cell attachment and serum proteins compete more strongly with Fn to dominate the character of the protein interlayer.

5.3.3 The influence of chemistry on cell adhesion

The presence of the Si has been shown to be relevant for the biological activity of BGS (Gibson et al., 2002a) (Rashid et al., 2008), (Botelho et al., 2006), (Guth et al., 2006b), (Campion et al., 2011), (Coathup et al., 2012) (Coathup et al., 2011)(Chan et al., 2012a)). However, it has not been identified yet through which mechanisms the substitution of phosphate ions for silicate ions in the crystal structure of hydroxyapatite influences the cell response.

Looking at the results of this set of experiments, it's possible to identify a role that silicate substitution has in its influence on cell attachment to the substrates. A previous study from Guth (Guth et al., 2010c), looking at the effect of Si substitution in HA on cells attachment, showed a non significant difference in human osteoblast-like cells attachment (HOS-TE85, suspended in a SCM) between HA and SA microporous discs. This result is in accordance with the present BARE treatment group results, where HA and SA supported the same level of cell attachment (Figure 5-4).

In Guth's study was also analyzed the effect of the pre-treatment of the discs with SCM at different time points. Her results this time showed a significant

difference in cell attachment between HA and SA microporous discs (with SA showing higher level of attachment) after one hour of SCM pre-treatment and 60 minutes of incubation from cell seeding. However, the cell solution this time was a serum-free media instead of a SCM, which can indeed influence cell attachment and could explain this discrepancy of results.

Given that the cell attachment on both BARE and on SCM pre-treatment group is the same between HA and SA in both studies, but that it changes between HA and SA if the cells are seeded in a serum-free media, then it is possible that greater cell attachment on SA compared to HA is favored by the pre-treatment with proteins on the surface of the material (in either the amount, conformation or both), but then further opportunity for dynamic modification of the protein interlayer through interaction with serum proteins in the media abolishes this preference making the final number of cells attached the same between HA and SA; whereas when cells are seeded in a serum-free media the initial favorable presence of the pre-treatment proteins on the SA is directly translated into a greater number of cells attached. Given the greater biological activity of SA compared to HA in *in vivo* studies, these results could suggest that the serum proteins act as “intermediary” only at a step before cells arrive at the implant site and start to attach, and that these two events don’t happen simultaneously.

Similar results to the BARE pre-treatment group are shown in Figure 5-5 from the SCM pre-treatment group (slightly higher cell attachment on HA, even though not significant).

As for the effect that Fn has in mediating cell attachment between HA and SA, this protein appears to play a relevant role in translating differences in chemistry into differences in attached cell number. More specifically, cell attachment was significantly higher on SA as compared to HA from the Fn2 PBS and Fn1 SCM groups (Figure 5-12). As previous results showed that the amount of Fn adsorbed on the SAG was significantly higher than the amount adsorbed on HA from Fn2 SCM concentration solution but not from Fn1 SCM (Figure 4-7), it is then hypothesized that it is not the amount of Fn adsorbed on the surface of the material to influence the cell attachment. Moreover, the opposite evidence comes from the Fn in PBS pre-conditionings: higher

number of cells attached to SA with Fn2 PBS, but no significant difference between HA and SA with Fn1 PBS pre-treatment. The evidence that Fn2 PBS showed a stronger effect as compared to Fn1 PBS on cell attachment, and that Fn1 and Fn2 in SCM showed exactly the opposite behavior, suggests that the role of Fn in directing cell adhesion can be influenced not only by its concentration level in the pre-treatment solution but also by the presence of competitive serum proteins in this solution.

It has already been shown that Fn has a weaker character in competitive conditions (Grinnell and Feld, 1982) and the present study highlights a particular aspect of this competition: the hypothesis is that Fn has a “physical constraint” which results in its inability to move freely in the environment to assume the specific, active conformation required by cells for attachment, when in the presence of other proteins or its greater concentrations. This could explain why, with the presence of serum proteins in the environment, Fn1 showed a better response in terms of cell attached than Fn2. Conversely, in a solution of PBS (free from competitive, sterically hindranced environment) Fn2 PBS was able to give a better cell response than the respective lower concentration (Fn1 PBS).

A study from (Rashid et al., 2008) shows that the presence of Si in the HA structure influences the biological response probably through the effect that surface charge and surface energy have on the interaction with serum proteins. Their study in fact showed that SA was able to absorb more Fn and to bind more cells than HA, however the amount of total proteins was interestingly similar between the samples, suggesting that it was not the quantity of adsorbed proteins that enhanced the greater cell attachment. Once again, it is possible to hypothesize that Fn could undergo different conformational changes which then would drive differently the cell behavior: a number of previous studies have demonstrated that parameters such as chemical species available at binding sites, polarity, surface charge, and their combined influence, are able to influence the conformation rather than the quantity of Fn at the binding sites (García et al., 1999)(Grinnell and Feld, 1982). Moreover, the findings of Grinnell and Feld demonstrated that, when Fn is in contact with two different surfaces, it is possible that it can assume

different conformations of which the more active is promoted on the more hydrophilic surface: in our study, this is represented by SA.

5.3.4 The influence of strut porosity on cell adhesion

The relevant influence that ceramic strut porosity (microporosity) has in influencing *in vitro* (Bignon et al., 2003) (Annaz et al., 2004) and *in vivo* (Hing et al., 2005) (Hing et al., 2004), (Yuan et al., 1999) bone formation is well established. Some studies demonstrated that it is the precise shape and geometrical structure of the micropores to influence *in vivo* osteoinductivity (Magan and Ripamonti, 1996), (Campion et al., 2011) (Coathup et al., 2011) (Chan et al., 2012b) (Coathup et al., 2012) and some others showed that the faster *in vivo* bone apposition rate is linked to the rate of development of the new vascular network (Hing et al., 2005) (Campion et al., 2011)(Hing et al., 2004).

It is in fact supposed that the presence of microporosity helps events fundamental to achieve osteointegration and osteoregeneration to happen: these events are for example the penetration of bone tissue, bone marrow and blood vessels inside the scaffold (as autografts and allografts already do).

The results of the present study showed that on the 20% strut porosity granules cell attachment is higher than the 30% with both Fn1 and Fn2 SCM, while the opposite (30% strut porosity showing higher cell attachment than 20%) was found from BARE, SCM and Fn1 and Fn2 PBS treatment groups, even if on the latter the difference was not statistically significant (Figure 5-13).

Moreover, looking at the results from the time-course study, the sample with 20% strut porosity showed a fluctuating trend of cell attachment, differently from the 30% strut porosity sample which instead showed a more stable trend (Figure 5-2, Figure 5-3).

Furthermore, results of Fn adsorption from the previous chapter didn’t show a significant difference of protein adsorbed when using Fn1 concentration (Figure 4-10d), and a significantly higher Fn adsorption on the 20% strut porosity sample only after 15 minutes of incubation using the Fn2 concentration solution (Figure 4-11).

Taking these results together, the evidence that there is a higher cell attachment on the 20% strut porosity sample after 60 minutes only with Fn1 and Fn2 SCM pre-treatments, and on the same sample a more fluctuating cell attachment over time, suggest that serum proteins together with Fn influence the cell attachment, and that this event is probably dependent on these proteins adsorption/desorption behaviours over time, but only when the material presents a relatively low percentage of strut porosity.

The results of these experiments suggest that features of the material which showed to be relevant and significantly improve the biological response *in vivo* and in clinic (like the presence of the Si and the increase in strut porosity from 20 to 30%), are able to make these materials more sensitive to Fn and serum proteins modulation of cell attachment

5.4 Conclusions

To summarize, the results of this chapter show that:

Firstly, there were differences in the stability of cell attachment with time, as a function of pre-conditioning treatment, material chemistry and material porosity. On SCM treated samples, cell attachment didn't show any difference over time. However cell attachment on BARE showed a greater fluctuation over time, especially on SAG80/20. On Fn1 pre-conditioning there was the greatest fluctuation of cell attachment over time, especially on HA. In general, HA chemistry showed to be much more sensitive to fluctuation than SA.

The presence of a competitive environment influenced also cell attachment, and material properties mediated differently this effect. In general, while on HAD, SAD and HAG80/20 there was a trend where pre-treatment with any SCM inhibited attachment (even if not statistically significant), the presence of the silicon together with a porous morphology (SAG) affected the role of the competitive environment: on SAG80/20 the pre-treatment with 'low total protein concentration' solutions that contained Fn (Fn1 PBS, Fn2PBS and Fn1SCM) supported greater attachment, and on SAG80/30 the pre-treatment

with Fn supplemented PBS rescued the lower cell attachment due to the SCM to same as Bare.

The chemistry appeared to play a relative role in mediating cell attachment: a higher number of cells on SA compared to HA was found only after pre-treatment with either Fn2 PBS or Fn1 SCM, suggesting that Fn and serum proteins mediate the effect of chemistry, where generally the presence of the silicon seems to positively influence cell behaviour.

Finally, the strut porosity looked to play a relevant role in mediating cell attachment, and this effect was differently influenced by Fn and serum proteins: in general, a lower strut porosity looked to be more influenced by the adsorption/desorption of Fn and serum proteins over time, while attachment on a higher strut porosity was positively supported by pre-conditioning of Fn without competitive species, only serum proteins and BARE.

6 HMSC Proliferation and Differentiation on SA, HA and HA-TCP Dense Discs and the role of chemical and mechanical treatments in modulating surface roughness and consequent cell response

6.1 Experimental background

In this chapter HMSCs cell proliferation and differentiation were analyzed on three chemically different ceramics discs: a biphasic calcium phosphate composed of hydroxyapatite/tri-calcium phosphate in a 60/40 ratio (HA/TCP), phase pure stoichiometric hydroxyapatite (HA), and silicate-substituted hydroxyapatite (SA). Furthermore, to test HMSCs' sensitivity to surface roughness, each disc was subject to one of three different treatments (one chemical and two mechanical) in order to increase or decrease significantly the surfaces roughness on each disc. The chemical treatment consisted of acid-etching the samples with a solution of phosphoric acid for a specific length of time, whereas the two mechanical treatments comprised hand grinding of the disc surfaces with two different grades of silicon carbide paper. Mechanical interlock has long been recognized as important to implant performance in both orthopedics and dentistry, particularly in the use of inert materials such as Titanium, PEEK and PMMA, and many studies have looked at the effect that either acid etching of metal implants surfaces (both *in vitro* (Martin et al., 1995) (Olivares-Navarrete et al., 2012) and *in vivo* (Buser et al., 2004), (Klokkevold et al., 1997)) or mechanically roughening a surface, has in directing bone regeneration (Boyan et al., 1996) (Lampin et al., 1997) (Anselme, 2000). However, there have been few systematic studies on hydroxyapatite and its derivatives (Rouahi et al., 2006) (Dos Santos et al., 2008). The hypothesis behind the set of experiments described in this chapter was to test whether roughening a material surface would aid cell attachment and development independently of the underlying disc chemistry, and whether or not any textural variation in roughness as a result of the different mechanisms selected for the two treatment processes (acid etching or mechanical grinding) played a role in cell response.

6.2 Experimental methodology

6.2.1 Materials

Phase pure, stoichiometric hydroxyapatite (HA) and silicate-substituted hydroxyapatite (SA) dense discs were prepared as previously described (Chapter 3, Section 3.2.1.1).

HA/TCP discs were purchased from Strauman (MA, United States) and were nominally composed of 60% HA and 40% Tricalcium-phosphate (TCP).

6.2.1.1 Disc treatments

All three discs were subject to 3 different treatments: acid etching, hand grinding with an 80Grit Silicon Carbide (SiC) paper and hand grinding with a 1000Grit SiC paper (Figure 6-1) (Struers UK). The treatments were carried out as described below:

Acid Etching (AE)

Initially the as pressed and sintered HA and SA discs and the as received HA/TCP discs were treated with a 2.5 v/v % of phosphoric acid for 30 seconds. However, results showed that this procedure was not aggressive enough and a higher percentage of phosphoric acid was subsequently used. Discs were therefore treated with a 37 wt/v % aqueous solution of phosphoric acid for 30 seconds, and after etching the discs were flooded with 100ml of cold double distilled (dd) H_2O to stop the reaction, washed twice with 10 ml ddH_2O and finally air dried.

80 Grit Hand Grinding (80Grit)

Discs were hand ground for one minute per surface using 80 grit silicon carbide paper, Figure 6-1, (ROTAR 40400059, Struers, UK) with ddH_2O as a lubricant, washed with ddH_2O and air dried.

1000 Grit Hand Grinding (1000Grit)

Discs were hand ground for one minute per surface using 1000 grit silicon carbide paper, Figure 6-1, (ROTAR 40400021, Struers, UK) with ddH_2O as a lubricant, washed with ddH_2O and air dried.

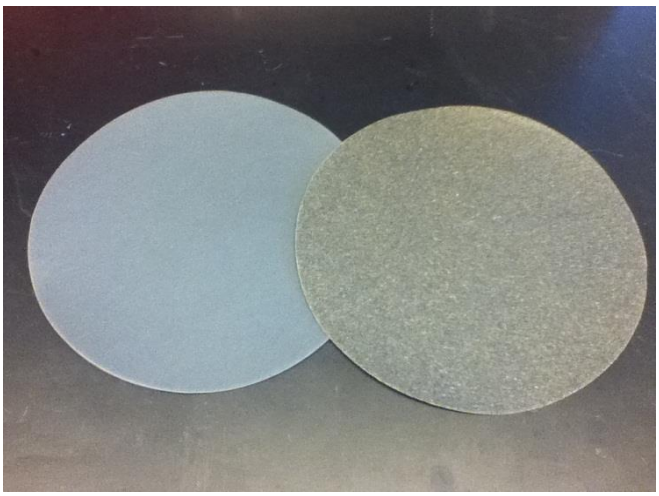

Figure 6-1: ***Silicon carbide papers for wet grinding: 1000 and 80 grit***

6.2.2 Materials characterization

6.2.2.1 Wettability measurements

Hydrophilic/hydrophobic properties of the materials were tested by contact angle measurements using the Ramé-Hart goniometer (Figure 6-2) (model 250-F1, NJ, USA). Images were analyzed with DROPimage CA software package (Ramé-Hart Instrument Co., Netcong, NJ).

Figure 6-2: Contact Angle measurement instrument in the Marcus Nanotechnology Centre at GeorgiaTech (Ramé-Hart, USA)

A single 4 micron drop of distilled water was added to the samples surface and contact angle was measured every 5 seconds for 20 seconds. Samples were run in triplicates, and five drops were tested on each sample.

6.2.2.2 Surface Roughness Analysis

Roughness of the discs was assessed using the material confocal microscope Olympus LEXT 3DV (Olympus America Inc., PA). The microscope uses a fixed wavelength of 405nm and has different magnification ranges. The magnifications used to characterize the samples were 20X and 100X, making possible to analyze an area of 0.413 cm^2 and 0.017 cm^2 respectively. Roughness results were evaluated using the LEXT OLS4000 software (Olympus).

To assess surfaces characteristics, it was decided to test not only surface roughness (Sa, average roughness), but also 3 other different parameters:

- Ra (average roughness profile),
- Ssk (Skewness of the 3D surface) and
- Sku (Kurtosis of the 3D surface).

Ssk is the “Skewness of the 3D surface”: an Ssk value <0 indicates a predominance of valleys; an Ssk value >0 indicates a predominance of peaks on the surface of the specimen.

Sku is called “Kurtosis of the 3D surface” and is a parameter which measures how regular/irregular the distribution of peaks and valleys on the surface is. A Sku value <3 indicates normally distributed heights; an Sku value >3 indicates irregularly distributed peaks/valleys on the surface.

Ten different points were analyzed on each sample and analysis were run in triplicates (n=3).

6.2.2.3 Chemical Analysis

X-ray Photoelectron Spectroscopy (XPS) was used to determine semi-quantitative chemical characterization of the samples. XPS is an analytical technique that directs a monochromatic beam of X-rays onto a sample and detects the characteristic electrons that are ejected: energies and number of these electrons can be used to determine the elements present on the surface. XPS measurements were performed on a Thermo K-Alpha (Thermo Fisher Scientific Inc., MA).

Three points were analyzed for their chemical characterization on each sample and analysis were run in triplicates (n=3).

XPS results were evaluated using the Thermo Advantage 4.43 software package provided by Thermo Fisher Scientific, Inc.

6.2.2.4 Surface Morphology Analysis

Discs surface morphology was qualitatively assessed by scanning electron microscopy (SEM) using an Ultra 60 field emission (FE) microscope (Carl Zeiss SMT Ltd., Cambridge, UK). The Hummer Sputtering System was used to prepare non-conductive samples by coating those with Au/Pd. Once coated, the samples were then mounted on aluminium stubs and analyzed for their surface characteristics from the micro to the nano scale using the Zeiss Ultra60 FE-SEM at magnifications ranging from 500X to 30,000X, with an accelerating voltage of 5KeV and a working distance between 4.6 and 11.1 mm.

6.2.1 Human Mesenchymal Stem Cell Incubation and Response

6.2.1.1 Culture of HMSCs and discs seeding

Bone marrow HMSCs (Lonza, Walkersville, MD) were used for this experiment. Basal MSC growth media (MSCGM, Lonza) was used to seed and expand them in sterile plastic flasks to passage 3 or 4. The media is designed to support mesenchymal stem cell growth without inducing

differentiation and is composed of basal stem cell media supplemented with 10% mesenchymal growth serum, 5% L-Glutamine and 1% Gentamicin sulphate/Amphotericin-B. At passage 3 or 4 cells were then seeded on the different samples.

Cells were cultured in a 5% CO_2 humidified atmosphere at 37˚C. HMSCs at passage number 3 or 4 were trypsinized, counted and then plated at 5000 cells/cm^2 on TCPS, HA-TCP, HA and SA surfaces in a 24 well plate (n=6). Basal growth media was changed after 24 hours and then every 48 hours until day 7. At day 7 media was changed and then collected after 24hours to be assayed for production of Osteoprotegerin (OPG), Vascular Endothelial Growth Factor (VEGF) and Osteocalcin (OCN). Adherent cells on the disc surfaces were twice rinsed with 1ml PBS prior to being lysed in 0.05% of Triton X-100 and sonicated at amplitude 60 for 60 seconds. Lysates were then assayed for total DNA, total protein and ALP activity.

6.2.1.2 Protocol for the determination of DNA content

DNA content from the samples was calculated using the Quant-iT PicoGreen dsDNA Assay Kit (Life Technologies, UK). Its reagent, the PicoGreen dye, is able to bind with high sensitivity to double-stranded DNA in solution and, due to its highly fluorescence emission when compared to the free dye in solution, enables quantification of DNA content in samples discriminating from RNA of single-strand DNA contaminations (see Chapter 2.1.1 for the theory behind Fluorescence Spectroscopy). For the analysis, standards were prepared using serial dilutions of the 2mg/ml DNA stock solution in TE buffer giving an 8-point fold calibration from 1 to 0.0078125mg/ml of DNA (Table 6-1). 100µl of each sample (from the lysed solution, n=6) and standards (n=3) were added into a 96-well black fluorescence plate and 100µl of PicoGreen reagent in Tris-EDTA buffer were added to each well. Plates were protected from light and incubated for 2 minutes at room temperature. Fluorescence intensity was then analyzed (excitation at 485nm, emission at 538nm) using the FLUOstar OPTIMA fluorometer (Figure 2-3) and unknown sample DNA content determined using the calibration curve. (For calibration curves see Appendix, Figure 9-8)

Table 6-1: DNA concentration in standard calibration samples

No	STD Concentration (μg/ml)
1	1
2	0.5
3	0.25
4	0.125
5	0.0625
6	0.03125
7	0.015625
8	0.0078125

6.2.1.3 Protocol for the determination of Total Protein

Total protein content was assessed using the colorimetric Marco BCA Protein Assay Kit (Thermo Scientific, UK). Total protein amount in each well was then used to normalize Alkaline Phosphatase specific activity. The presence of proteins in solution causes the reduction of Cu^{2+} to Cu^{+}, which then is able to chelate with two molecules of bicinchoninic acid (BCA) in the working solution giving a water soluble, purple solution which exhibits a strong absorbance at 562nm. The absorbance is linear to the protein concentration over a broad working range (20-2000μg/ml), enabling calculation of protein concentration by absorbance intensity analysis. The kit contains two reagents (A and B) and Bovine Serum Albumin (BSA), which was used as a control to prepare standard protein solutions. Firstly, Reagent A (containing sodium carbonate, sodium bicarbonate, bicinchoninic acid and sodium tartrate) was mixed with Reagent B (containing 4% cupric sulphate) in a 50/1 ratio to make up the necessary volume of working solution (0.2ml needed for each sample). Then, standard solutions were prepared adding sample diluent (0.05% of Triton X-100) to Albumin Standard solution (2mg/ml) as shown in Table 6-2.

Table 6-2: preparation of BSA standard solutions for the calibration of the total protein assay

No	Sample Diluent (µl)	Albumin Standard (µl)	Concentration (µg/ml)
1	200	0	0
2	195	5	50
3	190	10	100
4	180	20	200
5	160	40	400
6	140	60	600
7	120	80	800
8	100	100	1000
9	80	120	1200

Then, 25µl of standard (n=3) and samples (n=6) were added to a clear 96-well plate after vortexing. 200µl of the already-prepared working solution were then added to each well and the plate left to incubate at 37°C for 30 minutes. After incubation, the plate was allowed to cool down to room temperature and any bubbles in the wells of the plate were popped using a needle. Samples and standards were then analysed for their absorbance at 570nm using the FLUOstar OPTIMA fluorometer (Figure 2-3).

6.2.1.4 Protocol for the determination of ALP specific activity

ALP specific activity was assessed using a colorimetric assay (Abcam, UK) which enables the quantification of the activity of the enzyme by indirect measurement of an ALP product. A small volume of each sample (50µl) was added to each well of a clear 96-well plate, and the final volume was brought to 80µl with assay buffer. After adding 50µl of para-nitrophenyl phosphate

(pNPP) to each well, the reaction was incubated for 60 minutes at 25 degrees, protected from light. During this time, the ALP present in the samples dephosphorylates the pNPP which then turns yellow with an absorbance wavelength of 405 nm. To prepare the standard calibration curves, a 6-point serial dilution of 1mM pNPP standard solution was prepared, transferred in triplicates to the plate and then was added a standard volume of the standard ALP enzyme provided by the manufacturer (Table 6-3). The solutions were incubated for 60 minutes at 25 °C, protected from light and all the reactions were then stopped by adding 20µl of stop solution. At this point the optical density (OD) was measured at 405 nm using a microplate reader (FLUOstar OPTIMA fluorometer Figure 2-3).

Table 6-3: preparation of ALP standard solutions for the calibration of ALP specific activity assay

No	**1**	**2**	**3**	**4**	**5**	**6**
pNPP (µl)	0	4	8	12	16	20
Assay buffer (µl)	20	16	12	8	4	0
ALP solution (µl)	10	10	10	10	10	10
Concentration (µmol/ml)	0	4	8	12	16	20

6.2.1.5 Protocol for the determination of OPG and VEGF in media

Human OPG and Human VEGF were quantified, at each time point from the media collected from each sample, using an enzyme-linked immunosorbent assay (ELISA) kit (R&D Systems, UK) (see Chapter 2.1.5 for the theory behind ELISA). The whole assay consists of two steps: a plate preparation step and an assay procedure step. The plate preparation was done the night before the assay procedure, and consists of coating the 96-well microplate with 100µl per well of the diluted capture antibody provided by the manufacturer. Leaving the

plate overnight at room temperature allows the capture antibody to be linked to the bottom of each well of the plate. The day after, three washes with the wash buffer provided (400µl) are required in order to eliminate any residual non-linked capture antibody, and a reagent diluent (300µl) 1-hour step is required to block any free residual binding site in each well. Then, after repeating the wash step again to eliminate any residual non-linked reagent diluent, the plate was ready to pass to the second step of assay procedure. The assay procedure step consists of adding the samples to the plate and, using a detection antibody and a conjugate detector, to quantify the amount of OPG or VEGF using calibration curves prepared with standards provided by the manufacturer. The standard curve was made using a 7-point calibration from 62.5 to 4000 pg/ml for OPG (see Appendix, Figure 9-3) and from 31.25 to 2000 pg/ml for VEGF (see Appendix, Figure 9-4).

Firstly, 100µl of samples (or standards for the calibration) diluted in reagent diluent (1:1 ratio) are added to each well and left at room temperature for two hours: this allows the OPG (or VEGF) present in the samples and in the standards to be recognised and captured by the capture antibody. After another wash step, 100µl of reagent containing the biotinylated detection antibody was added to each well and incubated for two hours at room temperature to allow it to recognise the protein of interest and bind to it. Then, 100µl of a conjugate of streptavidin and horseradish-peroxidase (HRP) was added to each well after the usual wash step. Streptavidin is a protein with extraordinary affinity for biotin: being one of the strongest non-covalent interactions known in nature. This property is used in many biotechnology assays to detect or purify biomolecules. In the ELISA assays the streptavidin binds with high affinity to the biotin linked to the detection antibody and, after the addition of the substrate solution (made of hydrogen peroxide that acts as oxidizing agent on HRP), it was possible to quantify the characteristic colour change which is detectable by spectrophotometric methods. Optical density (OD) in each well is immediately measured using a microplate reader (Figure 2-3: FLUOstar OPTIMA, example of microplate reader used for fluorescence and optical density analysis.Figure 2-3) set at 405 nm. (For calibration curves see Appendix, Figure 9-3 and Figure 9-4).

6.2.1.6 Protocol for the determination of OCN in media

See Chapter 7, Section 7.1.2

6.2.2 Statistical Analisys

For material characterization analysis (wettability, surface roughness, and chemical analysis) the sample size was n=3, and mean and standard error were calculated for each sample. For cellular response analysis, the sample size was n=6. Variations in responses of cell behavior were assessed statistically by using a one-way analysis of variance. Differences were evaluated by using Bonferroni post testing. All statistical tests were run by using KaleidaGraph statistical software (v 4.0, Synergy Software, Reading, PA, USA) at a significance level of α=0.05.

6.1 Results

6.1.1 Wettability measurements

Wettability of the discs, as measured by analysis of the water drop contact angle, found HA/TCP discs to be the most hydrophobic, and HA discs to be the most hydrophilic. The acid etching treatment made all disc surfaces more hydrophilic than in the as received/as sintered condition, as also did the treatment with 80Grit SiC paper. The treatment with 1000Grit SiC paper, conversely, increased hydrophobicity on the HA and SA discs but not on HA/TCP discs. Overall, HA/TCP as received and 1000Grit SiC treated discs were the most hydrophobic, while HA and SA acid etched and 80Grit SiC treated discs were the most hydrophilic (Table 6-4). The appearance of typical water drops on as sintered HA and SA discs and as received HA/TCP discs are shown in Figure 6-3 a-c, respectively.

Table 6-4: ***contact angle values for HA, SA and HA-TCP before and after each treatment***

	HA	**SA**	**HA-TCP**
Original	45.11±0.75	58.23±0.09	82.72±0.52

Acid Etched	29.06±0.75	34.24±2.97	41.12±4.28
80 Grit	39.53±0.83	11.9±1.84	52.97±1.25
1000 Grit	69.95±2.23	64.87±2.48	74.05±3.28

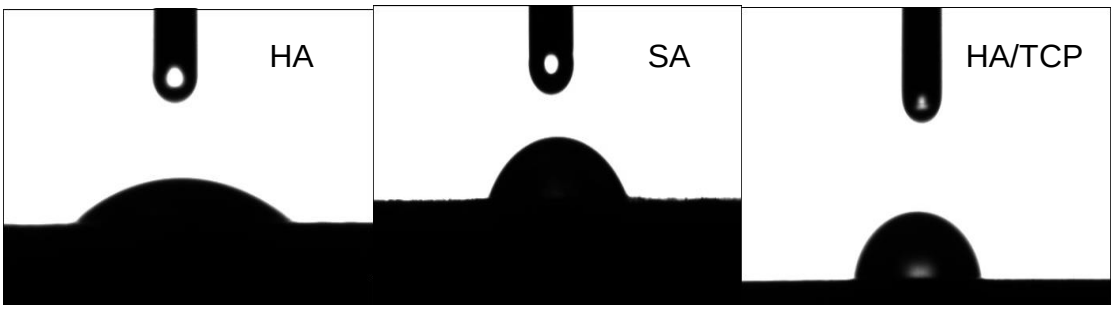

Figure 6-3: Appearance of water drops during contact angle measurement on as sintered HA and SA discs and HA/TCP as received discs.

6.1.2 Surface roughness

Acid etching with a 2.5% solution of phosphoric acid did not significantly increase the surface roughness of all the discs (Figure 6-4). Moreover, it was found to significantly reduced surface roughness of SA discs as assessed at 20X magnification and only significantly increased surface roughness of HA/TCP discs as assessed at both 20X and 100X. However, as can be seen in Figure 6-5A, acid etching with a 37% solution of phosphoric acid resulted in significant increases in surface roughness for all disc chemistry types as assessed at a magnification of 20x, although at a magnification of 100x (Figure 6-5B) only the surface roughness of HA/TCP was significantly increased.

In contrast, hand grinding with 80Grit SiC paper significantly increased the surface roughness for all disc chemistry types, as assessed at magnifications of both 20x and 100x (Figure 6-5), while the treatment with 1000Grit decreased the surface roughness for all disc chemistry types as assessed at both magnifications, but only significantly so for HA and SA discs.

Of particular interest was the disparity seen between assessment at the low magnification of 20X (area of 640X640µm, Figure 6-5A), and the higher magnification (130X130µm area, Figure 6-5B): this may be a result of the fact that at the higher magnification the size of the roughness 'features' may be approaching the size of the assessment area.

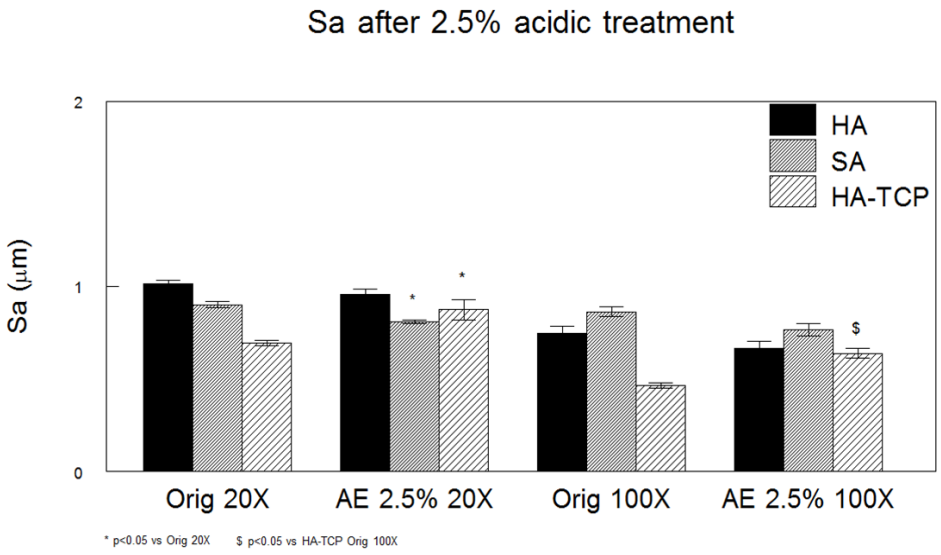

Figure 6-4: Surface roughness (Sa) values before and after acid etching with 2.5% of phosphoric acid at 20X and 100X magnification

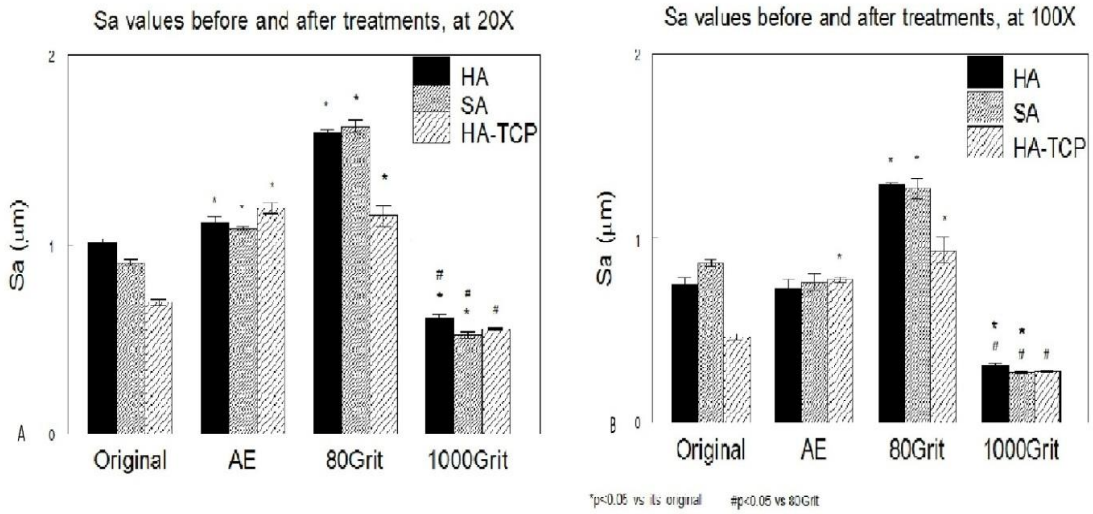

Figure 6-5: ***Sa values for all the discs before and after the three treatments at a magnification of 20X (A) and 100X (B) (*p<0.05 vs its original, #p<0.05 vs 80Grit).***

Figure 6-6A, B shows the results of the average roughness profile (Ra) for all the discs. Ra increased as Sa increased at 20X (Figure 6-6A), however at 100X it decreased on all the discs apart from HA/TCP AE, which showed a statistically significant increase at 100X (Figure 6-6B).

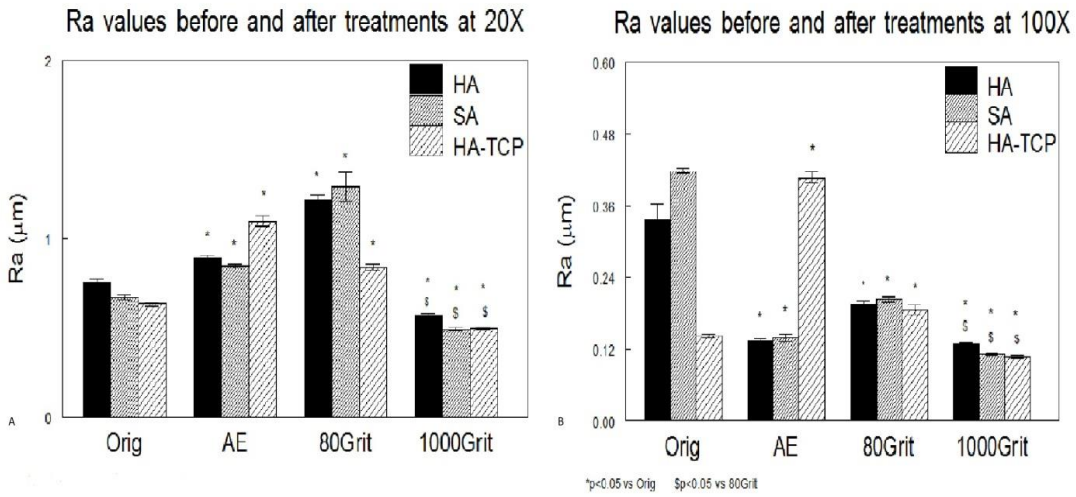

Figure 6-6: ***Ra values for all the discs before and after the three treatments at a magnification of 20X (A) and 100X (B) (*p<0.05 vs its original, $p<0.05 vs 80Grit).***

Figure 6-7 shows the Ssk values of the discs. Almost all the discs showed a predominance of valleys, apart for HA/TCP 80Grit as assessed at both 20X and 100X magnifications and the HA original disc at 100X, which instead showed a slightly higher presence of peaks. Furthermore, discs after AE and 80Grit treatments exhibited a lower presence of valleys compared to the other groups (statistically significant different at 20X).

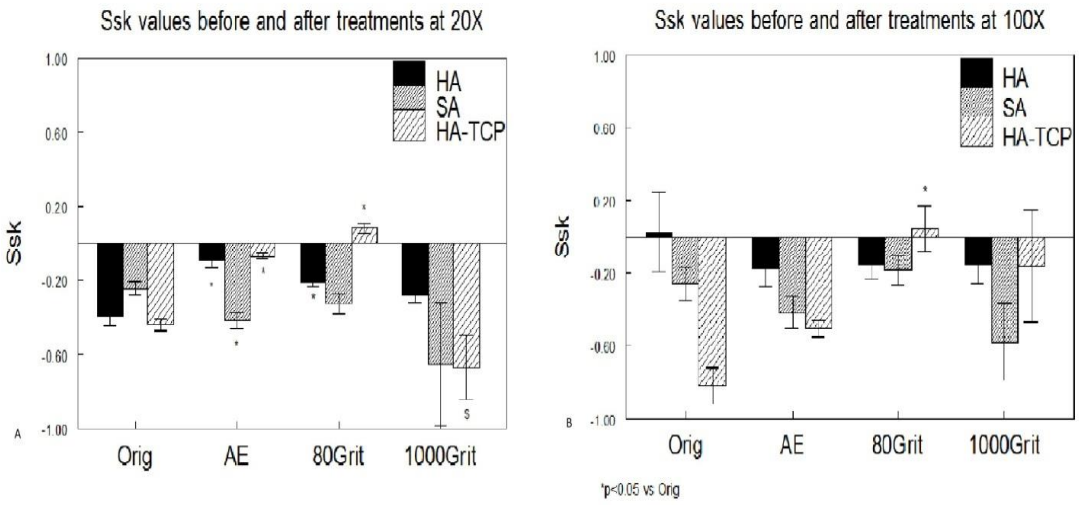

Figure 6-7: ***Ssk values for all the samples before and after the three treatments at a magnification of 20X (A) and 100X (B) (*p<0.05 vs its original).***

Figure 6-8 shows the Sku values of the discs. All the discs showed a prevalence of unordered peaks and valleys, with the 1000Grit discs at both the magnifications presenting the highest amount compared to the rest of the discs (statistically significant different at 100X).

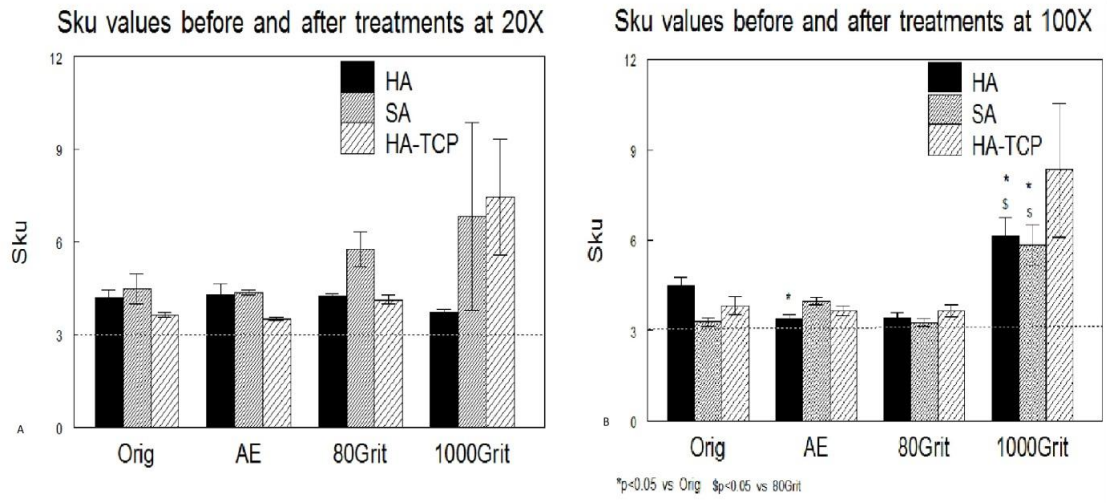

Figure 6-8: ***Sku values for all the discs before and after the three treatments at a magnification of 20X (A) and 100X (B) (*p<0.05 vs its original, $p<0.05 vs 80Grit).***

In order to show how these different surfaces look and how the differences found in Sa, Ra, Ssk and Sku are translated into the surface's cues, Figure

6-9, Figure 6-10 and Figure 6-11 show 3D representations at the confocal microscope of the surfaces for HA, SA, and HA/TCP respectively before and after each treatment at a magnification of 100X. From the images it is possible to note the similarity in roughness between HA and SA as sintered discs (Figure 6-9a and Figure 6-10a) and the respective AE (Figure 6-9b and Figure 6-10b). The as-received, AE HA/TCP discs surface (Figure 6-11b) showed conversely many, relatively small troughs and peaks which were more regularly distributed compared to HA and SA AE. Moreover, in all the discs there was a distinct difference between the originals, the 80Grit and 1000Grit surfaces: the 80Grit showed a very irregular surface, with few, irregular but relatively high peaks mixed with valleys. The 1000Grit showed a more smooth and regular surface.

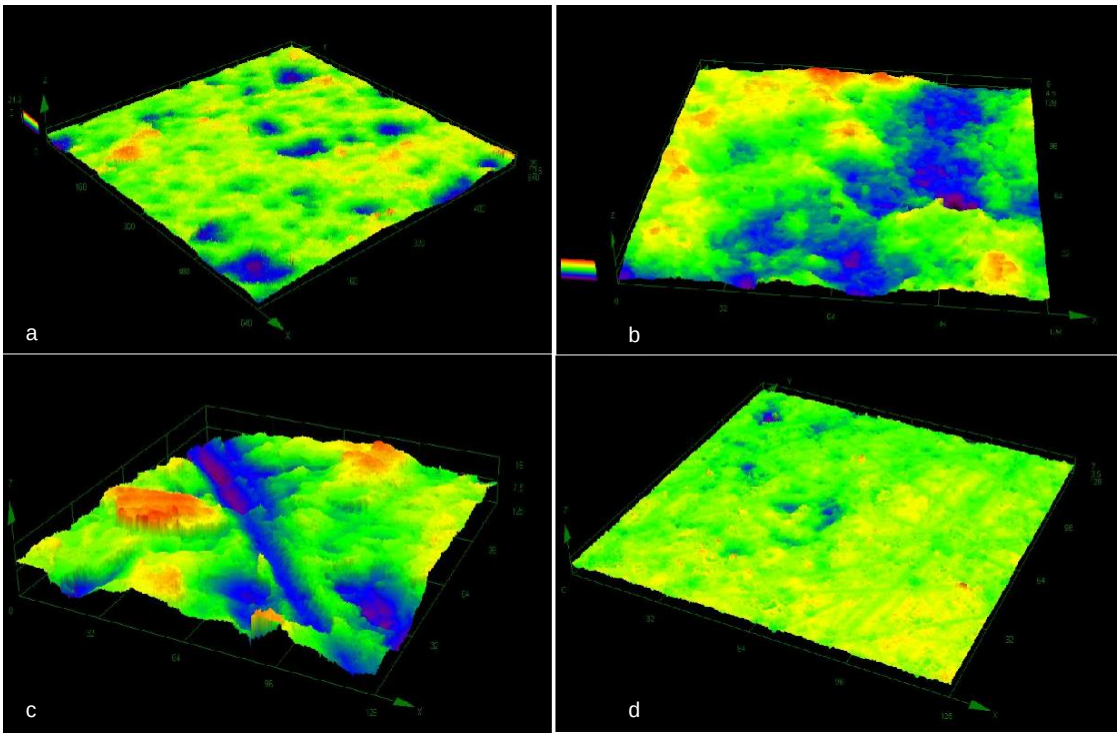

Figure 6-9: 3D images of the surfaces of HA original (a), AE (b), 80Grit (c) and 1000Grit (d) respectively at 100X magnification.

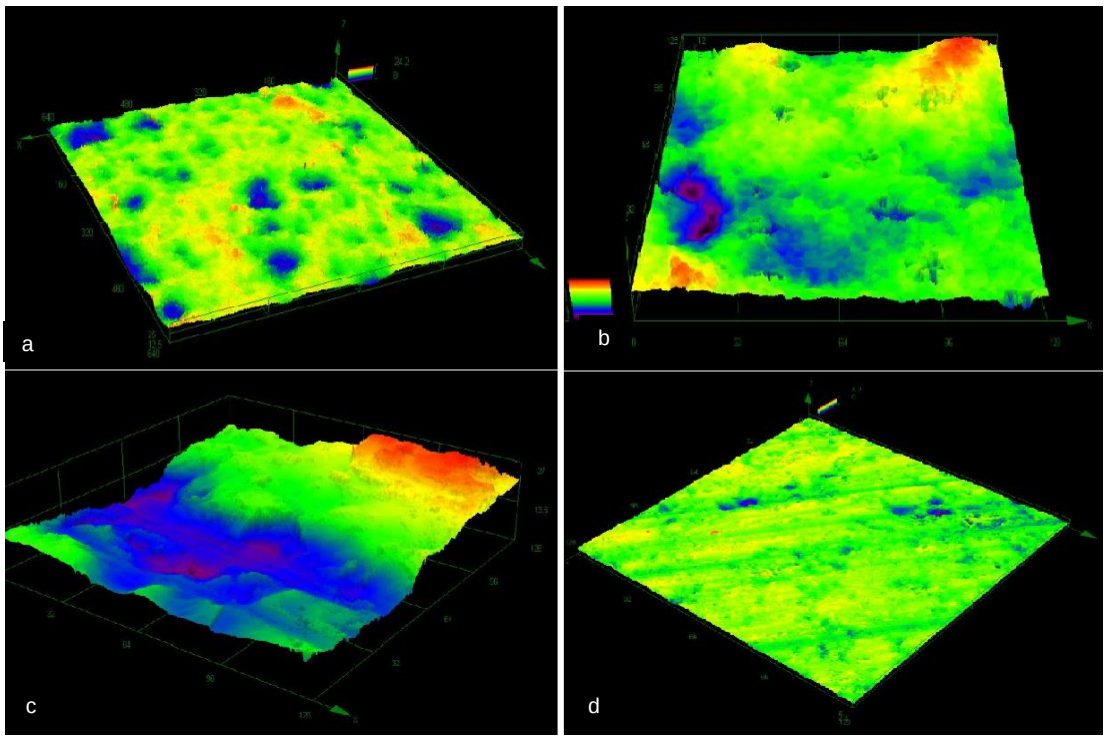

Figure 6-10: 3D images of the surfaces of SA original (a), AE (b), 80Grit (c) and 1000Grit (d) respectively at 100X magnification.

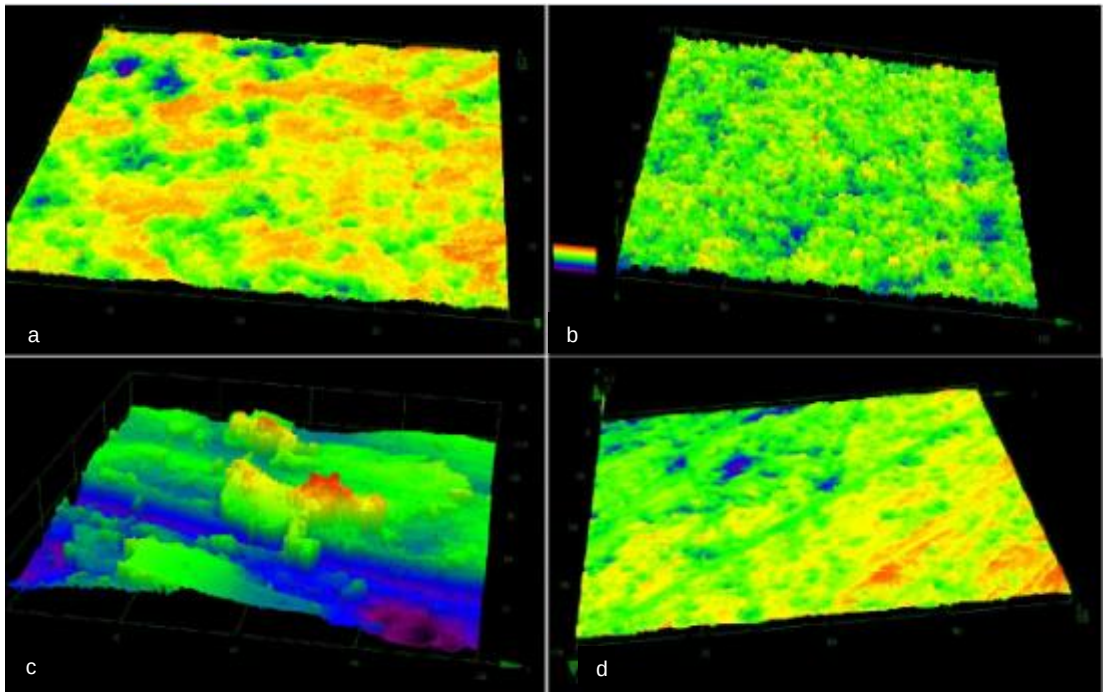

Figure 6-11: 3D images of the surfaces of HA-TCP original (a), AE (b), 80Grit (c), and 1000Grit (d) at 100X magnification.

6.1.3 Surface Morphology

Scanning electron microscopy was used to characterize qualitatively the discs surfaces microstructure, before and after both the chemical and mechanical treatments.

Micrographs of HA taken at a magnification of 1,000X (Figure 6-12) and 10,000X (Figure 6-13) show a more homogeneous and even surface structure after acid etching (Figure 6-12b and Figure 6-13b) and after treatment with the 1000Grit SiC paper (Figure 6-12d and Figure 6-13d) treatments; the surface structure instead appears more un-even and disordered after the treatment with the 80Grit SiC paper (Figure 6-12c and Figure 6-13c), on which it is also possible to identify grooves and scratches due to the mechanical forces.

SA discs showed similar characteristics to the HA discs (Figure 6-14, Figure 6-15), moreover, at the higher magnification it is possible to identify grain boundaries on both the as sintered HA and SA discs (Figure 6-13a, Figure 6-15a). The grain boundaries were even more pronounced after the AE treatment (Figure 6-13b and Figure 6-15b).

HA/TCP discs also demonstrated similar trends after the different treatments, with more clearly defined grain boundaries after AE (Figure 6-16b and Figure 6-17b); un-even grooves and structures were present after treatment with 80Grit SiC paper (Figure 6-16c and Figure 6-17c) and a relatively ordered and even surface after treatment with 1000Grit SiC paper (Figure 6-16d and Figure 6-17d). Differently from HA and SA discs, the grain boundaries couldn’t be clearly seen on the original as-received discs of HA/TCP (Figure 6-16a and Figure 6-17a).

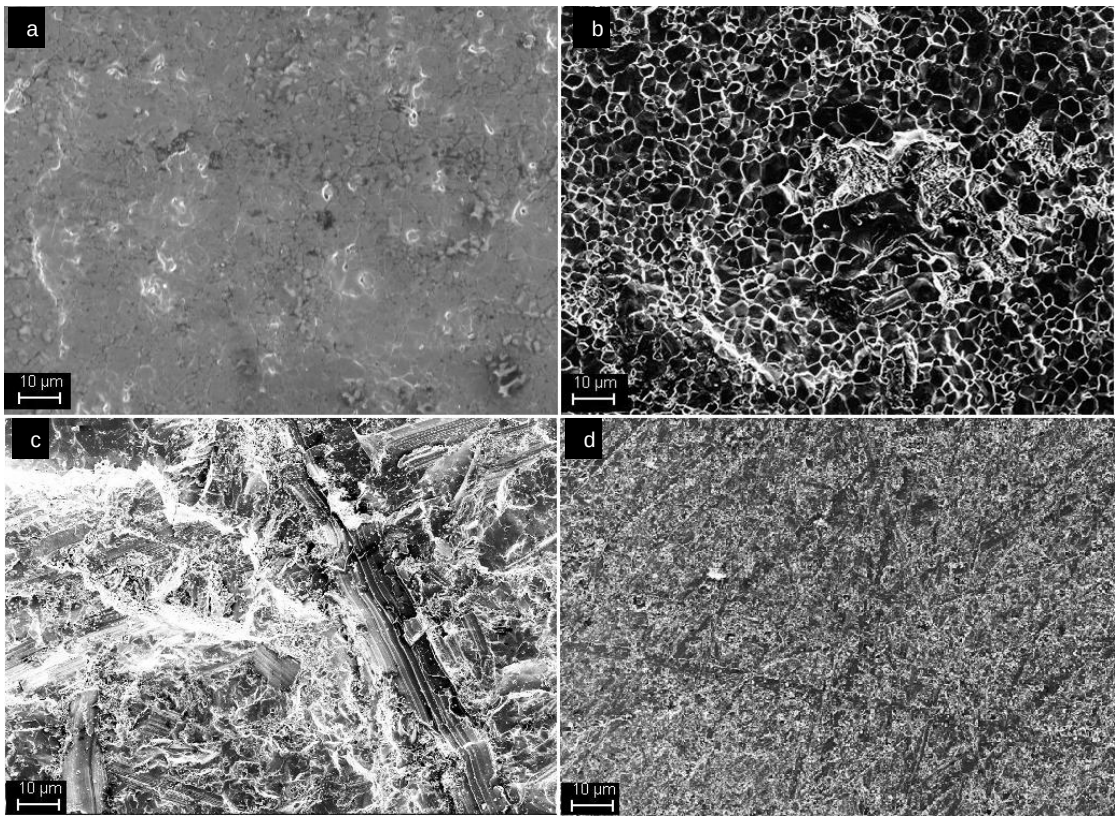

Figure 6-12: SEM images of the HA original as sintered (a), AE (b), 80Grit (c) and 1000Grit (d) disc surfaces at 1K magnification

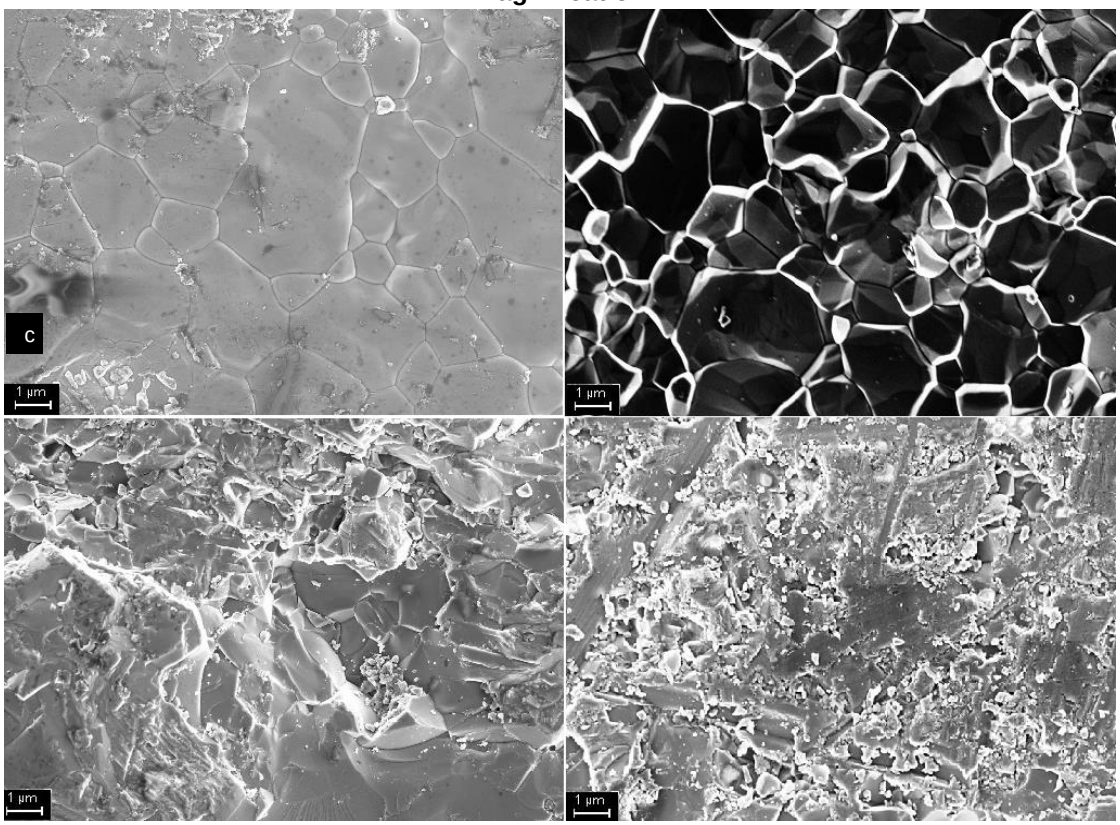

Figure 6-13: SEM images of the HA original as sintered (a), AE (b), 80Grit (c) and 1000Grit (d) disc surfaces at 10K magnification

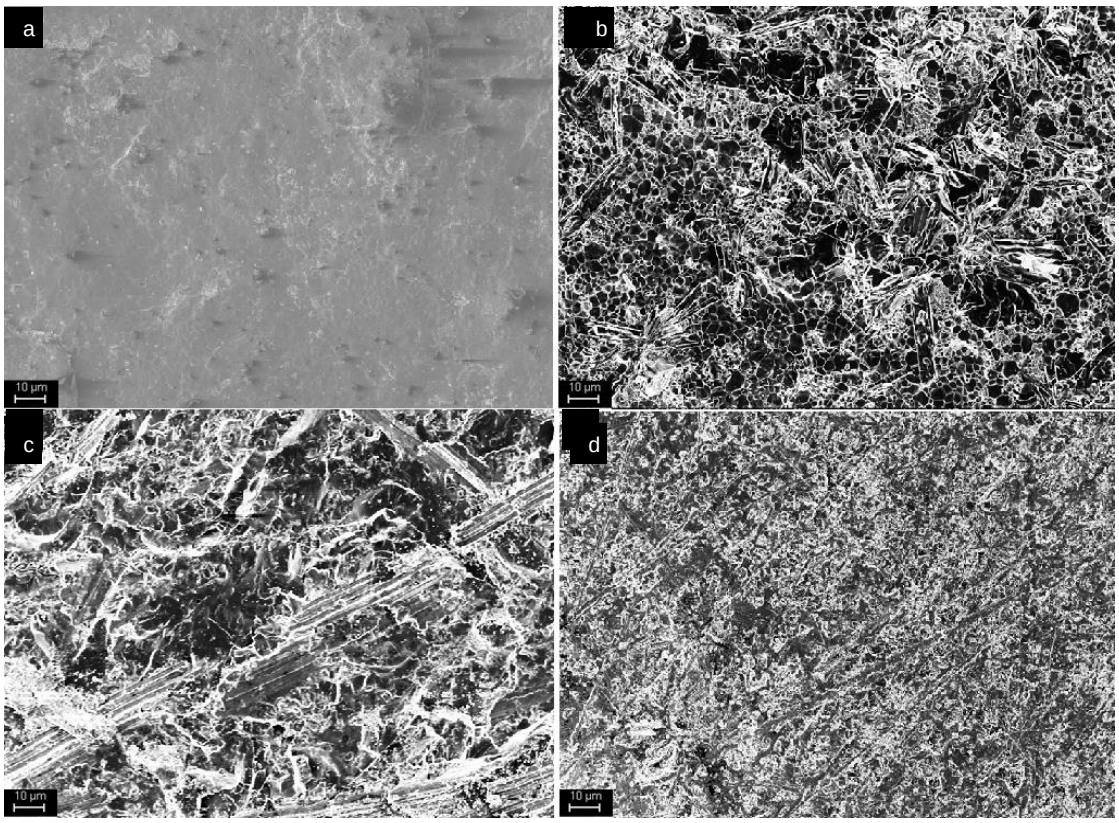

Figure 6-14: SEM images of the SA original as sintered (a), AE (b), 80Grit (c) and 1000Grit (d) disc surfaces at 1K magnification

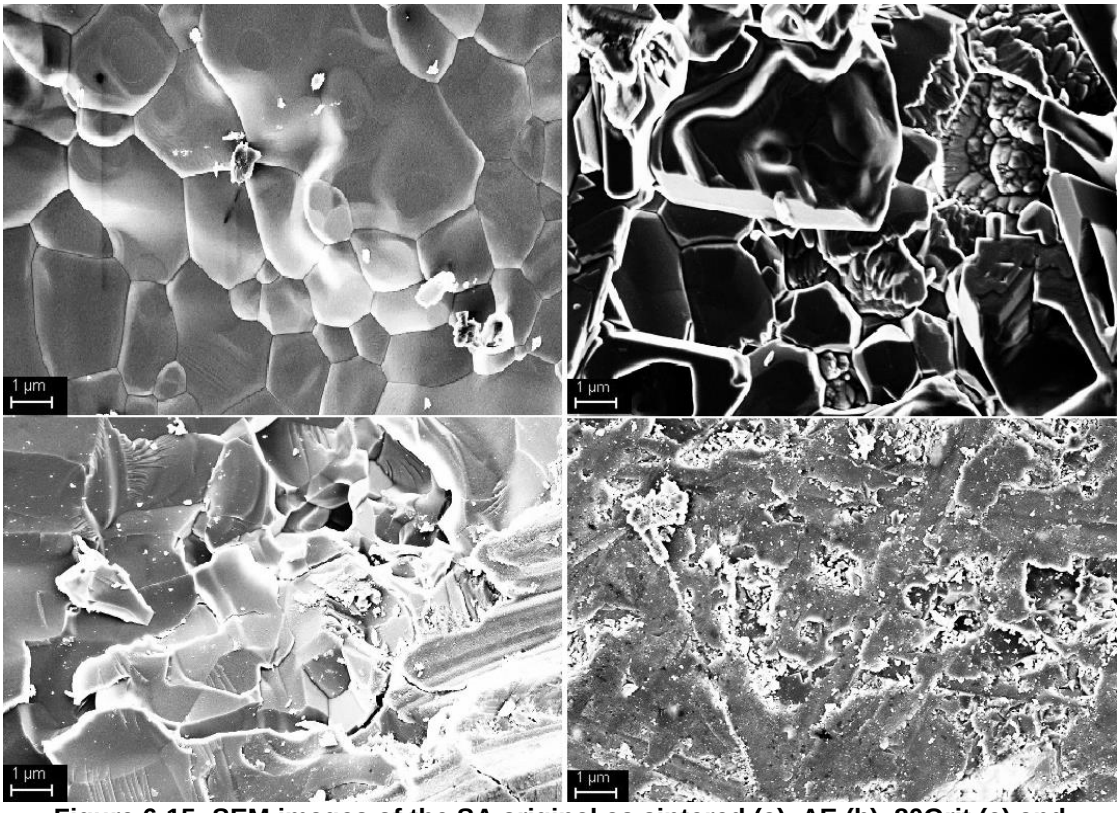

Figure 6-15: SEM images of the SA original as sintered (a), AE (b), 80Grit (c) and 1000Grit (d) disc surfaces at 10K magnification

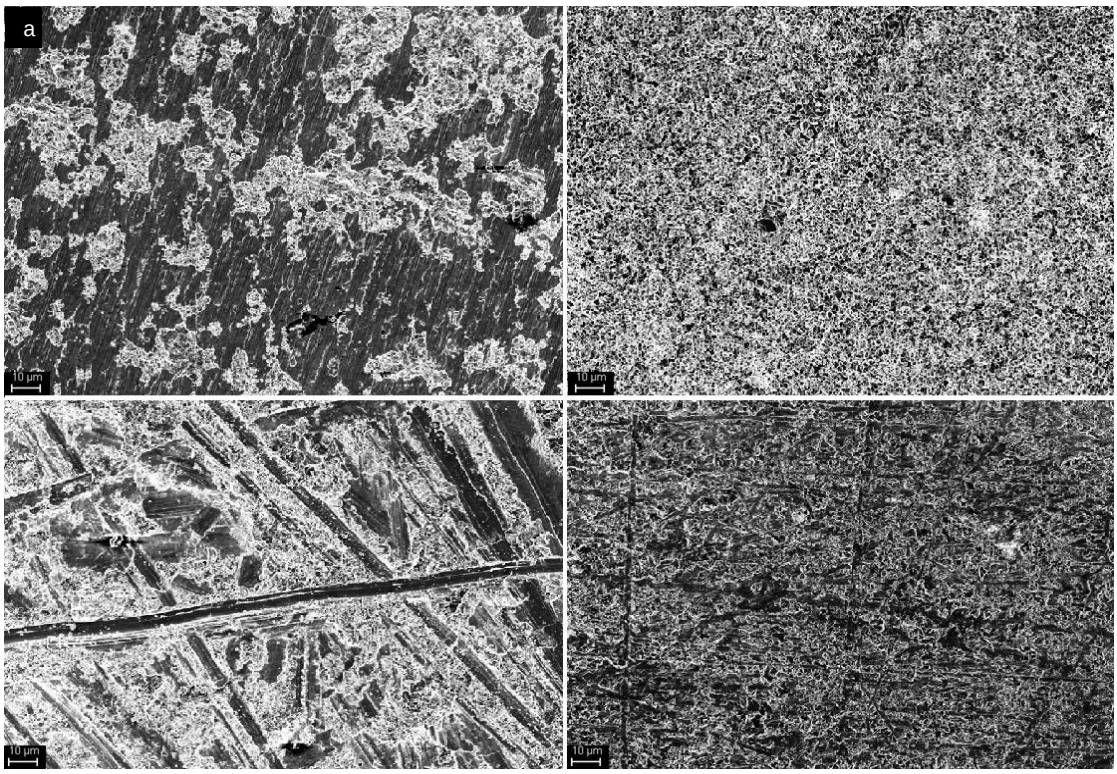

Figure 6-16: SEM images of the HA-TCP original as received (a), AE (b), 80Grit (c) and 1000Grit (d) disc surfaces at 1K magnification

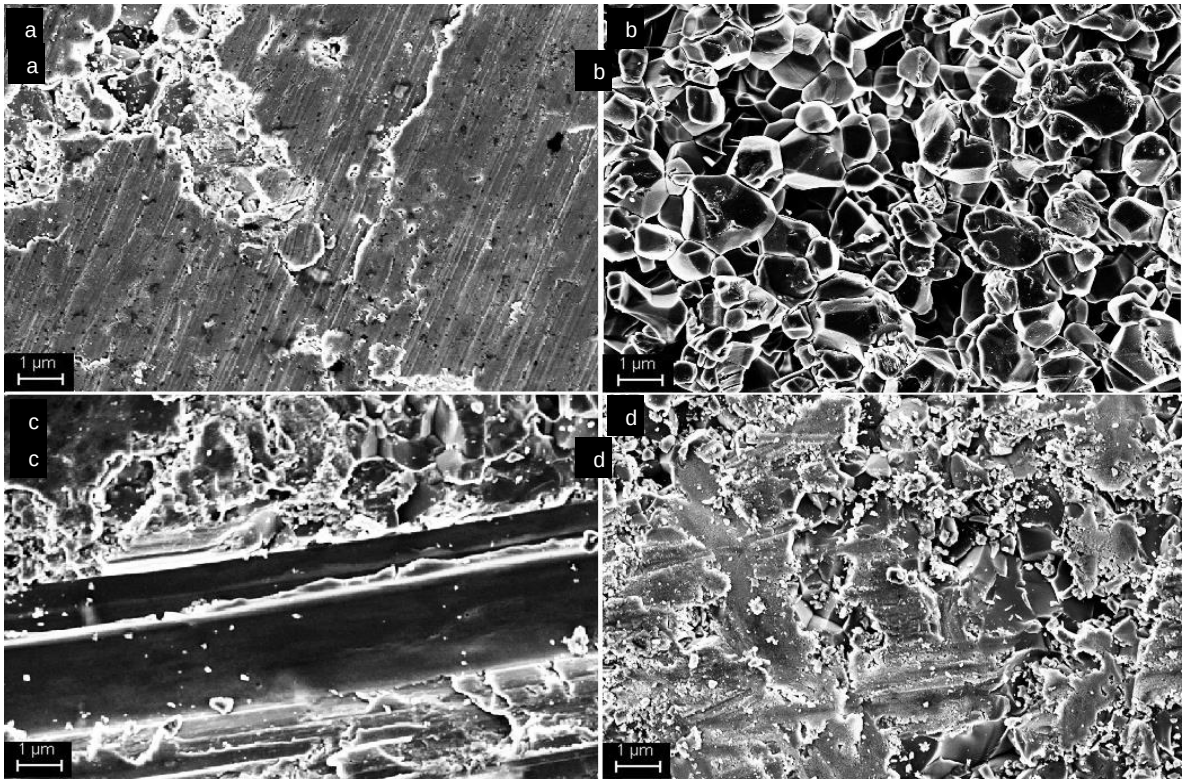

Figure 6-17: SEM images of the HA-TCP original as received (a), AE (b), 80Grit (c) and 1000Grit (d) disc surfaces at 10K magnification

6.1.4 X-Ray Photoelectron Spectroscopy

Semi-quantitative chemical analysis of disc surfaces before and after treatments, as evaluated by XPS, was expressed in terms of atomic percentage.

On HA and SA discs after all treatments (apart from hand grinding of HA discs with 80Grit SiC paper) there were marginally lower levels of oxygen, carbon, and phosphorus as compared to the as-sintered surfaces, whereas higher levels of carbon were observed on all HA and SA disc surfaces after all treatments (Table 6-5, Table 6-6). Analysis of silicon levels at the surfaces of SA discs demonstrated higher levels of silicon at SA disc surfaces after all treatments as compared to the as-sintered discs.

A different behaviour was observed on HA/TCP discs where an increase in the level of oxygen, carbon and phosphorus was detected while the level of carbon at the disc surfaces appeared to decreased after all treatments as compared to the as-received HA/TCP discs (Table 6-7).

Table 6-5: ***atomic percentage of oxygen, carbon, phosphorus and calcium on the surface of HA discs before and after treatments***

	O1s	Ca2p	P2p	C1s
HA	48.3±1.47	21.47±0.63	14.47±0.45	11.27±0.06
HA-AE	42.68±2.71	16.82±1.69	13.35±0.70	26.35±4.55
HA-80Grit	47.05±0.33	20.05±0.50	14.39±0.35	17.93±0.95
HA-1000Grit	40.17±2.55	15.59±1.48	11.87±0.88	30.11±4.37

Table 6-6: ***atomic percentage of oxygen, carbon, phosphorus, calcium and silicon on the surface of SA discs before and after treatments***

	O1s	Ca2p	P2p	C1s	Si2p
SA	48.2±1.50	20.77±0.07	14.52±0.42	14.52±2.69	0.095±0.06
SA-AE	41.29±2.36	15.27±0.89	12.56±0.77	28.51±3.82	0.47±0.33
SA-80Grit	33.42±8.7	12.27±3.61	7.97±1.71	43.78±13.7	0.90±0.64

SA-1000Grit	33.65±0.62	12.67±0.47	9.02±0.17	42.47±0.27	1.55±0.76

Table 6-7: ***atomic percentage of oxygen, carbon, phosphorus and calcium on the surface of HA-TCP discs before and after treatments***

	O1s	**Ca2p**	**P2p**	**C1s**
HA-TCP	29.51±1.22	8.7±0.59	6.97±0.52	52.17±1.33
HA-TCP-AE	37.64±2.52	14.02±1.56	10.45±1.25	36.77±4.83
HA-TCP-80Grit	45.75±0.55	18.15±1.02	13.17±3.06	22.55±2.86
HA-TCP-1000Grit	39.97±0.20	15.73±0.23	14.70±1.40	28.50±2.31

6.1.5 Human Mesenchymal Stem Cell Incubation and Response

Human Mesenchymal stem cells were incubated on all as received HA/TCP, as sintered HA and SA and treated (AE, 80Grit and 1000Grit) discs surfaces and assayed for various markers for cell proliferation and differentiation over a period of 7 days.

In order to assess the effects of surface treatment and roughness, statistics were performed between the four different surfaces for each single chemistry.

In order to compare the effects of disc chemistry statistics were performed between the 1000Grit treated HA/TCP, HA and SA discs as, from surface morphological analysis by SEM (Figure 6-13d, Figure 6-15d and Figure 6-17d), this treatment resulted in the most similar surface characteristics within the chemistries, as compared to the other two surface treatments and the as received/ as sintered discs.

6.1.5.1 Total DNA

Total DNA was generally found to increase on HA and HA/TCP discs with a greater surface roughness (Figure 6-18), indicating that higher surface roughness has a positive effect on cell proliferation for these disc chemistries.

This effect, however, was abolished on SA discs where no significant difference in total DNA was observed between the different surface treatments.

Moreover, there was no significant difference observed between the HA, SA and TCP/HA discs treated with 1000grit SiC paper, suggesting no significant effect of chemistry on cell proliferation on these relatively smooth surfaces.

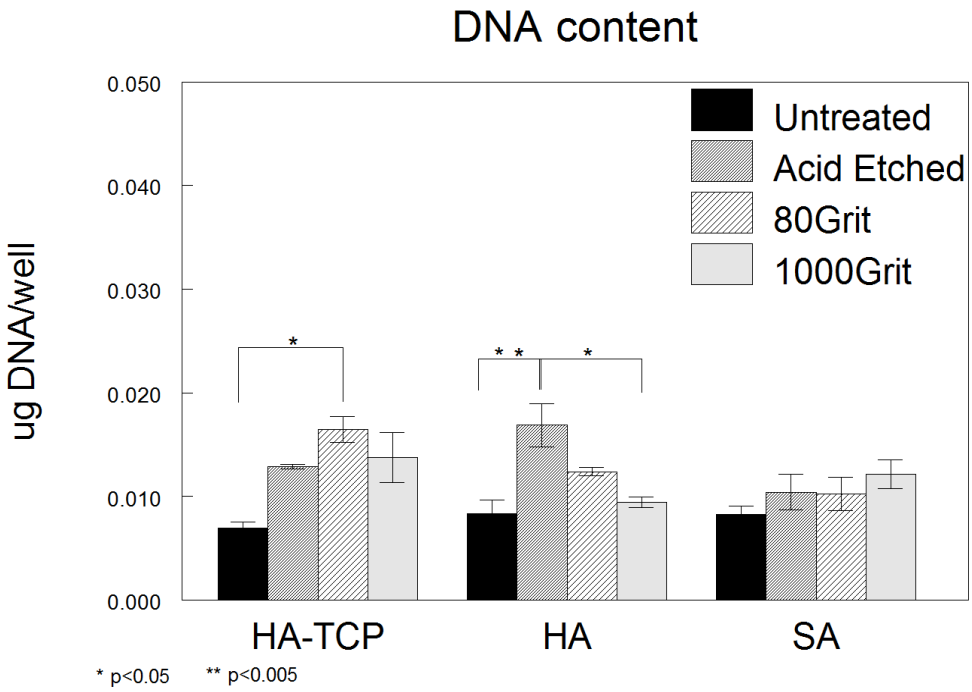

Figure 6-18: ***µg of DNA per well on different surfaces***

6.1.5.2 ALP activity

Alkaline phosphatase is an early marker of osteoblast maturation which peaks just before the mineralization phase. Its activity, normalized by total DNA amount, was significantly higher on the as-sintered HA discs as compared to the 1000Grit sample. There was no significant difference between surfaces on

either HA-TCP and SA, and also no significant effect of chemistry between the three different chemistries, 1000Grit treated discs (Figure 6-19).

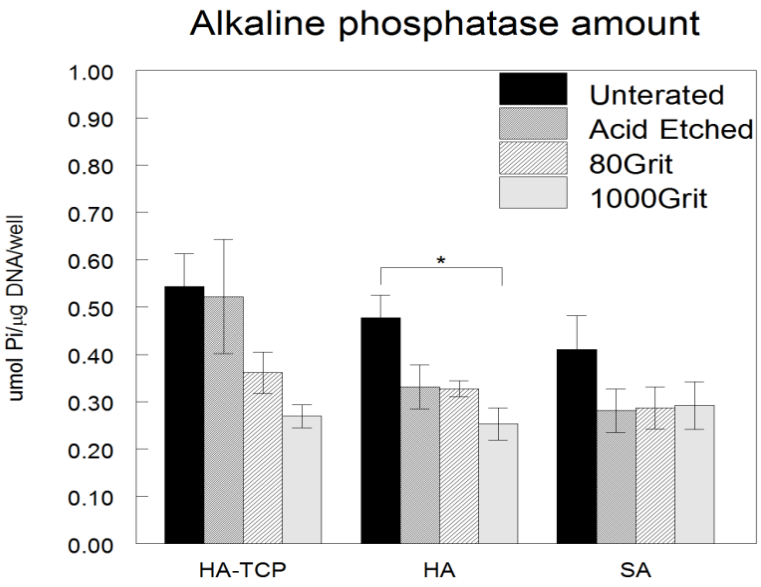

Figure 6-19: ***ALP specific activity normalized by Total DNA***

6.1.5.3 Osteocalcin Production

Figure 6-20 shows OCN amount, normalized by DNA, analyzed from the treated and un-treated discs. HA/TCP and SA supported significantly higher OCN production from the untreated disc surfaces compared to all the other three treated. As sintered HA discs and 1000Grit treated HA discs supported similar levels of OCN production, both of them significantly higher than the AE treated HA discs. In general, acid etching seemed always to show a significant decrease in OCN amount, while 80Grit and 1000Grit treatments showed a significant decrease only on HA/TCP and SA compared to their original surfaces.

Comparing discs chemistry, HA supported significantly higher OCN production as compared to SA, but there was no significant difference between HA and HA/TCP or between HA/TCP and SA.

.

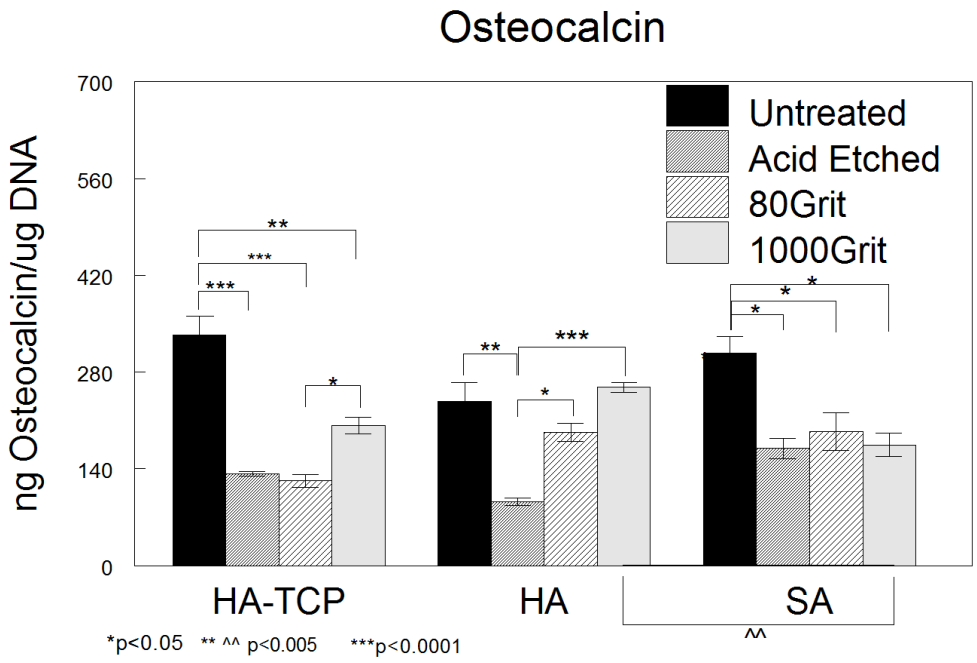

Figure 6-20: ***Osteocalcin amount normalized by Total DNA***

6.1.5.4 Osteoprotegerin Production

Osteoprotegerin is an important protein involved in the balance between bone formation and resorption, by regulating osteoclast activity. In the present study, the pattern of OPG production was similar between HA and SA discs: after 1000Grit SiC paper treatment supported significantly higher OPG production as compared to their respective untreated and AE surfaces.

In contrast, as received HA/TCP discs supported significantly higher OPG production as compared to all three treatments.

Disc chemistry was found to regulate OPG production, with significantly higher levels of protein production on both HA and SA as compared to HA/TCP (Figure 6-21).

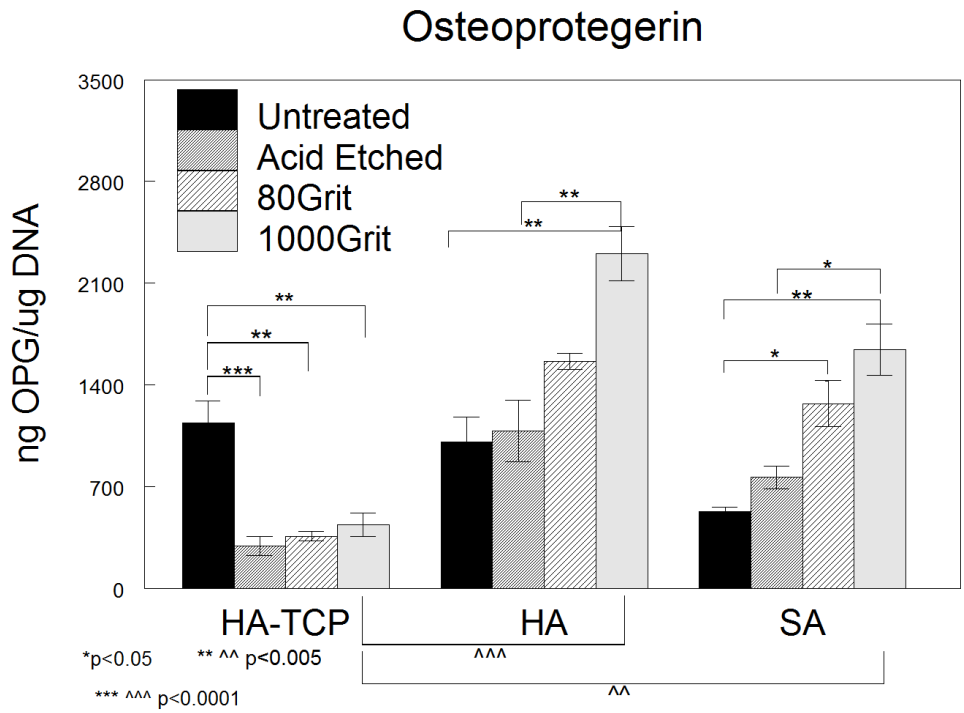

Figure 6-21: ***Osteoprotegerin amount normalized by Total DNA***

6.1.5.5 VEGF Production

VEGF production in response to the different disc treatments and chemistries is shown in Figure 6-22. VEGF is a growth factor key to the development of blood vessels, where adequate revascularization is a prerequisite to osteogenesis.

Interestingly, variation in surface morphology appeared to only regulate VEGF production on HA discs, where 1000Grit treated HA supported higher VEGF production as compared to AE and 80Grit surfaces, suggesting a role of roughness in directing VEGF synthesis.

Also chemistry appeared to have a significant effect on VEGF production. HA 1000Grit discs supported significantly higher protein production as compared to both HA/TCP and SA 1000Grit discs, while SA 1000Grit treated discs supported significantly higher protein production as compared to HA/TCP 1000Grit discs (Figure 6-22).

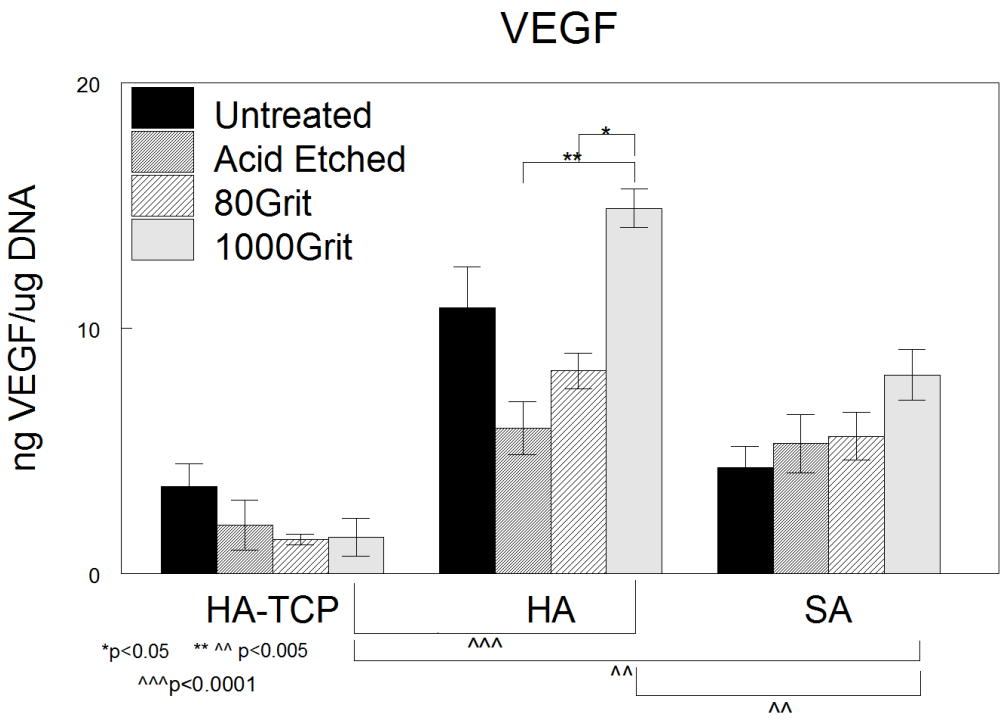

Figure 6-22: VEGF amount normalized by Total DNA

6.1 Discussion

6.1.1 The effect of chemistry

In this experiment the effect of the chemistries was analyzed by comparing HA-TCP, HA and SA after treatment with 1000Grit SiC papers, treatment which gave the smoothest roughness (Figure 6-5) and the most similar surface microstructure (Figure 6-13d, Figure 6-15d and Figure 6-17d).

DNA amount

Few studies have previously reported the analysis of differences in cell response between HA, SA and HA-TCP. When evaluating and comparing results from these different studies, however, it is important to note that differences in implants' properties like shape, size, amount of micro or macro porosity (which all affect in one way or another cell response and which can be different from study to study) can confound the actual effect of chemistry. Keeping this in mind, some *in vivo* studies showed a better ability of HA-TCP to stimulate early bone formation than HA.

In one of these (Sulaiman et al., 2013a) a 20/80 ratio of HA-TCP granules showed a higher osteogenic potential than pure HA after 8 weeks implantation in nude mice. Another work (Ng et al., 2008) using materials with the same granule size and HA-TCP ratio of Sulaiman's study, showed similar results. However, in both the studies the materials were implanted only after the seeding of induced sheep marrow cells and human osteoprogenitor cells respectively.

Another study by Hing *et al.* (Hing et al., 2007) compared instead dense calcium sulfate, ultra porous β-TCP and porous SA, and showed that both β-TCP and SA supported early bone apposition (<1 week), with SA showing also to be more stable and to support better angiogenesis.

Very few *in vitro* studies have been performed: in 2006 Jalota studied the cell viability (after 72 hours) and protein concentration (after 7 days) of osteoblasts on the surface of HA, β-TCP and HA-TCP, showing significant difference only in cell viability between HA and β-TCP, but not between HA and HA-TCP (Jalota et al., 2006).

In the present study, the HA-TCP ratio was 60/40, and the samples were all dense discs. The cell proliferation was not influenced by the chemistry, as seen by Figure 6-18, where all the samples showed very similar DNA amount. This is in accordance with the findings of Jalota *et al.* regarding HA and HA-TCP comparison.

ALP and OCN

Osteogenic differentiation, as a mean of ALP specific activity, was also found to be similar between the three chemistries (Figure 6-19).

The production of Osteocalcin, a protein fundamental for the process of new bone formation, therefore a marker for osteogenesis, was not seen to be significantly different between HA-TCP and either HA or SA, but it was significantly higher on HA compared to SA discs.

A study from Botelho (Botelho et al., 2006) showed no significant difference in OCN production between HA and SA discs after 7 days, however the values of the protein were not normalized by total DNA, which makes it difficult to get an indication of the actual protein synthesized per cell, and thus to make a rigorous comparison between studies. A possible explanation of the higher OCN synthesis on HA compared to SA, in contrast to previous reports in literature which suggest that SA has a higher biological activity than HA, could be study limitations associated with the fact that the assays were performed at 7 days, therefore missing a temporal shift in protein production.

OPG

OPG synthesis was found to be significantly higher on HA and SA compared to HA-TCP (Figure 6-21). This is in agreement with a recent study reporting the *in vivo* higher gene expression of both OCN and OPG from bovine HA in sinus lift of rabbits, as compared to autologus bone graft (Chaves et al., 2012). An interesting work from Wang *et al*., investigating any difference in cell proliferation and/or protein expression and protein production from HA, TCP and HA-TCP discs with different ratios, found that cell proliferation was not significantly different between samples, and that ALP and OCN mRNA

expression levels didn't show significant differences, which is in line with the present results (Wang et al., 2004a). Moreover, another study from Wang (Wang et al., 2004b) showed not significantly different OPG gene expression between HA, TCP, and HA-TCP with a 70/30 and a 35/65 ratio. These findings are in agreement with the comparison between original (Untreated) surfaces in the present work, where no significant difference was shown between the three materials (Figure 6-21).

Thus it is interesting to see how, by decreasing the roughness of the HA (or SA) surfaces, is possible to increase significantly the production of OPG, and that the inclusion of TCP abolishes the effect of the roughness showed by HA.

VEGF

VEGF synthesis was found to be significantly different between all the samples: HA-TCP showed a significantly lower synthesis compared to both HA and SA, and HA showed a significantly higher synthesis compared also to SA (Figure 6-22).

Many studies describe the positive effect that the localized delivery of VEGF (Riva et al., 2010) or VEGF gene transfer techniques (Duan et al., 2012) or the incorporation of exogenous VEGF with cells and scaffolds (Lee et al., 2012, Sever et al., 2012) have in promoting bone formation. However, few studies have been done aiming to look at the *in vitro* VEGF synthesis from cells in contact with BGSs.

A very interesting and recent work from Ghanaati (Ghanaati et al., 2012b), describes the differences of the *in vivo* tissue reactions between HA, TCP and a 60/40 ratio of HA-TCP granules: results show a significantly greater vessels area and vessels density with HA-TCP granules compared to HA after 3 days of subcutaneous implantation, while no significant difference between them at day 10. As the present study analyzed VEGF synthesis only at day 7, it is possible that an earlier and greater protein production by HA-TCP was missed by that time, but the improved HA synthesis was quite substantial. It is also possible that the implant topography (discs in the present study, granules in the Ghanaati study) strongly influenced the cell response, therefore changing the effect on vascularization.

Another work by Hing (Hing et al., 2007) looking at Capillary Index (CI) in rabbits femoral implantation of calcium sulfate, ultra porous β-TCP and porous SA, showed (at week 1) a higher CI from the SA implant compared to β-TCP, even if not statisticallysignificant.
The complexity, however, of comparing and interpreting results from these different studies lays also in the difficulties of translating results between *in vitro* and *in vivo* studies.

Some of the results in this study seem to be in contrast with different works demonstrating the higher *in vivo* biological activity of SA compared to HA. One possible reason to explain this discrepancy is that this could be due to the different dissolution behaviors which occurs *in vivo* between HA, SA and HA-TCP, which are evidently influenced by the physiological environment, but that can hardly be exactly reproduced in *in vitro* studies. Another possible explanation can be that the form actually used *in vivo* is different by the dense disc form which is instead used for the present *in vitro* study: consequences are that this influences the cellular response more than how much chemistry does, therefore shifting the higher biological activity of SA compared to HA.

6.1.2 The effect of surface roughness

Surface roughness is considered one of the material characteristics that mostly influences the biological response. This happens because cells and proteins are able to “feel” differences in surface roughnesses, and thereafter respond consequently to them.

In this study the cell behaviour (proliferation and differentiation) on four different surface roughness characteristics was analyzed: the one on the original samples (Untreated), the one given by the acid-etching treatment of the samples with an in 37% phosphoric acid for 30 seconds (AE), the one given by hand grinding the discs for one minute per surface on a grit 80 SiC paper (80Grit), and the one given by using the same method but on a grit 1000 (1000Grit). Materials were then tested for their properties and ensured that the methods were reproducible. Statistics were performed in order to see any significant difference between the four roughness for each of the three chemistries.

Different studies looked at the material's surface roughness and its effect on cell behaviour. However, while some of them looked at the osteoclasts response (Costa-Rodrigues et al., 2012, (Müller-Mai et al., 1990), many others studied the influence that roughness of the HA coating on titanium implants has on cell behaviour (Hayashi et al., 1994) (da Silva et al., 2003). Other studies look instead at differences in the influence of roughness between HA and Ti on cell response (Korovessis and Deligianni, 2002), (Borsari et al., 2005).

HA chemistry

A study from Missirilis (Missirlis, 2000) showed human bone marrow stromal cells proliferation and differentiation on HA discs with three different surface roughness values. After 8 days in culture, cell proliferation was slightly higher on the roughest surface, while ALP didn't show significant differences between samples. However, in the study it was not specified which was the area analyzed or the magnification used to assess roughness values, which makes it difficult to certainly estimate the results and compare them with the present or any other study. Moreover, cell proliferation was assessed by number of cells per unit of surface. This assessment makes the cell number subject to the surface area of the material as well, which can be differently influenced by the type of material, the methods used to change the roughness and the mechanical properties.

The results from Deligianni study are in agreement with the ones in the present study. The cell proliferation, analyzed by total amount of DNA per well, was found to be significantly higher on the AE sample (which in the present study is the roughest) compared to both the Untreated and the 1000Grit ones (Figure 6-18).

Stem cell differentiation was analysed through ALP specific activity and OCN production. The ALP specific activity, as in the Deligianni study, was not found to be significantly influenced by differences in surface roughness. Another work by Xia *et al.* looked at the *in vitro* and *in vivo* influence of differences in topography on HA macroporous scaffolds (Xia et al., 2013). Topographies were represented by either nanosheets, nanorods and micro-nano hybrids and

were compared to a control of dense HA discs. Even if roughness analyses was not performed, it is possible to assume that the presence of any of the three topographies represents an increase in surface roughness compared to the one of the dense discs. Results showed a greater cell proliferation on all the three topographies compared to control HA, which is in agreement with the results of the present study.
Comparisons between these two studies, however, needs to take into consideration that there are some crucial differences in the experimental set up: first, the materials used for the present study were all discs, while in Xia's study were macroporous scaffolds, and second that the cells used for Xia's experiments were rat bone marrow stromal cells instead of Human mesenchymal stem cells.

Nonetheless, these results show the influence that topography plays in directing stem cells proliferation and differentiation on these ceramics.

In the present study, cell differentiation was also assessed through analysis of OCN production. The results on the HA samples show an OCN content significantly lower on the AE compared to all the other samples, and significantly higher from 1000Grit compared to 80Grit. These results suggest that the roughness definitely has a strong effect on the protein's production. The smoothest surface was able to increase its production significantly compared to rough surfaces, while the roughest between all of them consistently showed the lowest amount (Figure 6-20).

Osteoprotegerin production was also analysed on the samples to check their osteogenic capacity. On HA discs its amount was, like for OCN, highest on the 1000Grit sample, with significance compared to the Untreated and the AE, but not with 80Grit, which has a roughness higher than the Untreated but lower than the AE (Figure 6-21). This result could be due to the fact that the mechanical treatment which was used to create the 1000 and the 80Grit roughnesses produced a different surface microstructure compared to the chemical treatment and the original surfaces, as clearly seen by the SEM images (Figure 6-13). It is possible to hypothesise therefore that OPG

production is more sensitive to the surface microstructure than how much it is for the surface roughness.

VEGF production was also analyzed from the samples. Its content was as well significantly higher on the HA 1000Grit than on the AE and 80Grit. For VEGF the synthesis seems to be positively influenced by smoother surfaces (Figure 6-22).

These results suggest that stem cell proliferation and differentiation into the osteoblast lineage are not influenced in the same way by differences in HA surface roughness: while cells seem to proliferate better on rougher surfaces, they also look to synthesize more osteoblastic markers like OPG and OCN and new tissue formation markers like VEGF on smoother surfaces.

SA chemistry

The Silicate-substituted HA showed to be the chemistry that was influenced the least by surface roughness.

Looking at the effect on cell proliferation, the DNA content was not significantly influenced by changes in surface roughness. Furthermore, what is possible to point out comparing HA and SA chemistries, is that the presence of the Si in the HA structure doesn't influence at all the DNA content on the Untreated, 80 or 1000Grit samples, but only on the AE one (Figure 6-18), revealing a potential important role of Si ions in abolishing the effect of surface roughness.
It is possible to hypothesize at least two different explanations for this behaviour. First, it is possible that the AE treatment increases DNA content on both HA and SA, and meanwhile that the presence of the silicon ions increases cell proliferation at earlier time-points than 7 days: in this case at day7 would be too late to see the higher DNA content from SA.
Second, it is also possible that the acid etching treatment, uniquely changes either the quantity of silicate or the SA structure in a way that influences cell proliferation.

The ALP activity was analysed to study cell differentiation on SA samples. The results showed no significant difference between samples, which is the same effect shown on the HA samples. It is possible to hypothesize that, being ALP a recognised early marker for osteoblasts differentiation, it is promptly more active at earlier time points than 7 days, where the influence that topography may have on its activity is then vanished.

OCN amount was also studied for cell differentiation. On SA discs it was found to be, as on HA, higher on the Untreated surface compared to all the other samples. However it is interesting to note that, while the SA and HA Untreated surfaces showed a very similar protein production, the 1000Grit SA surface showed an opposite behaviour compared to the same HA surface: which is a significant decrease compared to the Untreated surface, suggesting a possible negative influence of the Silicate only after smoothing the surface of SA.
Similarities in OCN amount after 7 days of culture between HA and SA was found also from a study of Botelho (Botelho et al., 2006) in which dense discs of HA and 0.8wt% Silicate-substituted HA were seeded with human osteoblasts cells and OCN amount was detected by enzyme immunoassay.

OPG amount showed to be significantly higher from the smoothest surface compared to Untreated and AE, and also from the 80Grit surface compared only to the Untreated. This result seems to suggest that rather than the roughness in itself, are more likely to influence OPG production the characteristics of the microstructure of the surface (dictated by the type of treatment used), as the smoothest (1000Grit) and the second roughest (80Grit) surfaces showed better protein amount on both HA and SA.

Finally the VEGF amount was also analysed. Its production was higher on the smoothest surface 1000Grit, however this increase was not significantly different. On both the Untreated and the 1000Grit samples SA showed to promote a lower amount of VEGF compared to HA which, supposing a correlation between VEGF and bone ingrowths, is in contrast with different

studies showing a higher bone formation promoted by SA compared to HA. Again, a possible reason why this happened could be that HMSCs promoted a higher VEGF amount from the SA compared to HA at an earlier time-point than 7 days, which would be in line with *in vivo* studies showing an earlier bone formation promoted by SA.

HA-TCP

HA-TCP 60/40 was influenced by surface roughness more similarly to HA than to SA. Few studies have been done looking at the influence that the roughness of the surface has on *in vitro* cell proliferation and differentiation.
In the present study, the DNA amount on HA-TCP increased after all the three treatments. However, this increase was significant only on the mechanically-treated, rough surface 80Grit.

ALP specific activity was analysed for cell differentiation potential. It was found to be influenced in a very similar manner to HA, however the effect showed a lower magnitude. The results show a very similar ALP specific activity from the Untreated and the AE samples, and a much lower from the 80 and 1000Grit samples. This difference, even though non statistically significant, could suggest that mechanical treatment, or the samples morphology after the mechanical treatment, negatively influence ALP activity (Figure 6-19). As the fact that neither the chemistry (no differences between HA-TCP, HA or SA) nor the treatment (no differences between the different roughness) seemed to influence significantly ALP activity, it may be possible that any effect happened earlier than 7 days.

Regarding HMSCs' proteins production, both OCN and OPG showed a significantly higher amount from the Untreated surface compared to all the other surfaces (Figure 6-20, Figure 6-21). However, OCN was also produced significantly more from the 1000Grit compared to the 80Grit surface: this could suggest that after 7 days of culture OCN production is not influenced only by roughness, but also by micro-structural characteristics of the surface or by

other material properties not analyzed in the present study. OPG production, as said, also showed to be lowered significantly from the three treated surfaces: the original showed to produce more OPG than the other samples.

Finally, VEGF amount was seen to not be significantly influenced by the surface roughness (Figure 6-22), being very similar between samples.

6.2 Summary

The following is a summary of the effect that differences in chemistries and surface roughness between HA-TCP, HA and SA have on stem cell proliferation and differentiation.

The results show that chemistry didn't have a significant effect on cell proliferation and ALP activity. However, it significantly influenced OCN, OPG and VEGF production. The HA chemistry showed to be particularly good in enhancing proteins production, compared to SA for OCN and VEGF, and to HA-TCP for OPG and VEGF. SA showed to produce significantly higher level of proteins compared to HA-TCP for OPG and VEGF.

Regarding the effect of roughness, results showed that its effect was not the same on the different chemistries. On HA, a very smooth surface was able to enhance significantly different cell markers for osteoblast differentiation, like OCN, OPG and VEGF.
On SA, a smooth surface roughness influenced significantly OPG production.
On HA-TCP, neither an increase nor a decrease of surface roughness (compared to the as-received material) significantly influenced the cell response.
The increase in roughness in itself (which precludes the same effect given from both AE and 80Grit samples) didn't seem to influence significantly cellular response.

Taken together, the results of this experiment suggest that the effect of surface roughness is never the same comparing different materials, and that chemistry and surface roughness influence each other in their effect on

cellular response. Therefore, *in vitro* studies aimed to clarify the mechanisms of actions of the biological response to bone graft substitutes, should be performed on materials that resemble as close as possible the characteristics of the actual bone grafts used in the market, especially in terms of chemistry and surface properties. Moreover, a time-course study would be more useful to clarify differences in cell proliferation and differentiation between samples.

7 HMSC Proliferation and Differentiation on SA and HA Microporous Bone Graft Substitute Granules and the role of Fibronectin in Modulating Response to Chemistry and Microporosity

The influence of material properties on modulating stem cell response has been increasingly recognised as a key factor in directing subsequent cell mitogenesis and morphogenesis. Different material properties have been studied over the years, but substrate chemistry and porosity have been nominated as most fundamental in directing cell response. This study investigates HMSC response to two porous scaffolds with matched macro and micro porosity but varied chemistry and two porous scaffolds with matched chemistry and macro porosity but varied micro porosity, in order to clarify the direct effect of chemistry and microporosity on subsequent cellular proliferation and differentiation. Moreover, as the role of adsorbed Fn in cell attachment has previously been established (Chapter 5), the influence of sample pre-conditioning was also investigated, in order to see how serum proteins and/or Fn interacted with these parameters.

7.1 Experimental Methodology

Human Mesenchymal Stem Cells (Lonza ltd, USA) were used for this experiment. Basal MSC growth media (MSCGM, Lonza ltd, USA) was used to seed and expand the cells in sterile plastic flasks to passage 3 or 4. The media is designed to support mesenchymal stem cell growth without inducing differentiation and is composed of basal stem cell media supplemented with 10% mesenchymal growth serum, 5% L-Glutamine and 1% Gentamicin sulphate/Amphotericin-B. At passage 3 or 4 cells were then seeded on the different samples.

Three different samples were used as described in Table 7-1 and four different groups (n=6 for each group) for each sample were prepared (see Table 7-2). Samples were either hydroxyapatite (HA) or 0.8wt% Silicate substituted HA

(SA), and were characterized as described in Chapter 3. Cells were also plated on Tissue Culture Polystyrene (TCPS) to be used as a control.

Table 7-1: Types of granule samples used during this study

Sample description	Acronyms
Hydroxyapatite porous granule 80% total and 20% strut porosity	HAG80/20
Silicate-substituted hydroxyapatite 80% total and 20% strut porosity	SAG80/20
Silicate-substituted hydroxyapatite 80% total and 30% strut porosity	SAG80/30

Table 7-2: Sample treatment groups used during this study

Preparation of sample	Acronyms
No pre-conditioning	BARE
Pre-conditioning with Mesenchymal Stem Cell Growth Media (MSCGM, media supplemented with 10% FCS)	MSCGM
Pre-conditioning with 0.10mg/ml of Fibronectin in MSCGM	Fn1
Pre-conditioning with 0.25mg/ml of Fibronectin in MSCGM	Fn2

Apart from the control samples TCPS, in order to avoid unintended cell attachment to the well plate bases, Ultra-Low attachment 24-well plates (Sigma-Aldrich) were used for the experiment. 0.3g of porous granules (size between 1 and 2 mm) were added to each well in 6 replicates for each

treatment group, for each sample type, and sterilized under UV light. Then, various pre-conditioning solutions were added to selected wells and left to incubate for 60 minutes, at 37 °C in a CO_2 controlled incubator. After the incubation time, pre-conditioning solutions were discarded and samples washed twice with fresh, sterile PBS. HMSC were plated on TCPS or samples surfaces at 10,000cells/cm^2 ($2x10^4$cells/sample) density in 24well plates. One ml of fresh media was changed in each well after 24 hours, and then every 48 hours. At 1, 2, 3, 4, 7, 10 and 14 days cells were incubated with fresh media for 24 hours and then media was collected to measure Osteocalcin (OCN), Osteoprotegerin (OPG), Vascular Endothelial Growth Factor (VEGF), Calcium release (Ca) and type I C-terminal collagen propeptide (CICP). Cells were harvested by washing the attached monolayer twice with fresh PBS, lysing them in 0.05% Triton X-100 and sonicating at amplitude 60 for 60 seconds. After collection samples were stored at -20 ˚C in 1ml aliquots to facilitate analysis of all time points simultaneously. Alkaline Phosphatase (ALP) specific activity was measured from cell lysates as was total protein and DNA content. The other cell markers were analysed from the collected media.

7.1.1 Protocol for the determination of Calcium release

Calcium release from the samples was assessed using a QuantiChrom Calcium Assay Kit (BioAssay Systems, USA) via analysis of the collected media. Aliquots of 5µl per sample (n=6) were added to a clear 96-well plate. 5µl (n=3) of standard solution of calcium in water ranging in concentration from 20 to 0 mg/dL (Table 7-3) was added to wells to determine calibration curves. The assay works using colorimetric principles (see Chapter 2.1.4 for the theory behind Colorimetry): a phenolsulphonephthalein dye in the working solution, subsequently added to standards and samples, forms a very stable blue colour when specifically bound to free calcium. The intensity of the colour, measured at 612 nm, is directly proportional to the amount of calcium in the sample. Samples and standards were left to incubate for 3 minutes at room temperature and the optical density was measured at 570-650nm with the FLUOStar OPTIMA fluorometer (Figure 2-3). (For calibration curves see Appendix, Figure 9-7)

Table 7-3: Standard solution dilutions for calibration curves to determine Ca amount in the samples

No	STD+H_2O	Vol (µl)	Ca (mg/dL)
1	100µl + 0µl	100	20
2	80µl + 20µl	100	16
3	60µl + 40µl	100	12
4	40µl +60µl	100	8
5	30µl + 70µl	100	6
6	20µl + 80µl	100	4
7	10µl + 90µl	100	2
8	0µl + 100µl	100	0

7.1.2 Protocol for the determination of DNA content

See Chapter 6, Section 6.2.1.2

7.1.3 Protocol for the determination of Total Protein

See Chapter 6, Section 6.2.1.3

7.1.4 Protocol for the determination of ALP specific activity

See Chapter 6, Section 6.2.1.4

7.1.1 Protocol for the determination of OPG and VEGF in media

See Chapter 6, Section 6.2.1.5

7.1.2 Protocol for the determination of OCN and CICP in media

Quantification of OCN and CICP in the samples collected media was also performed using an enzyme-linked immunosorbent assay (ELISA) (Quidel, USA). These ELISA kit differs from the ones from R&D Systems in that these provide strip wells pre-coated with capture antibodies. 25µl of standards (6-point standard curve from 0 to 74.5ng/ml for CICP, and 6-point standard curve from 0 to 29ng/ml for OCN) and 50µl of unknown samples were transferred to

each well; after the addition of 125µl of OCN (or CICP) antibody the plate was left for 2 hours at 20-25 degree. After incubation, three washes with buffer were needed to eliminate any non-bound protein and/or antibody, and 150µl of enzymatic conjugate (antibody conjugated with alkaline phosphatase, ALP) was added to the wells. The plate was incubated for 60 minutes at 20-25 °C to allow the conjugated antibody to recognise the OCN or CICP antibody. After this incubation time and three additional washing steps, a 150µl solution of p-nitrophenol (pNPP) was added to each well and left for 35-40 minutes at 20-25 °C. During this time, the ALP conjugated with the antibody dephosphorilates the pNPP giving a characteristic coloration. The OD in the wells of the samples was analysed by a spectrophotometric microplate reader (Figure 2-3), and the relative amount of OCN or CICP in the samples calculated from the appropriate calibration curve (see Appendix, Figure 9-6 and Figure 9-5 respectively).

Note: as seen from the graphs in Figure 9-5 and Figure 9-6 the calibration curves were not linear. However, the values of OD of the unknown samples were ranging always in a range between 0.3 and 1.1 for CICP and 0.2 and 0.4 for OCN.

7.1.3 Statistical Analisys

The sample size for each sample material was n=6. Variations in cellular response between chemistries (HA vs SA), strut porosities (20% vs 30%), or pre-treatments (BARE, MSCGM, Fn1, Fn2) were assessed statistically by using a one-way analysis of variance. Differences were evaluated by using Bonferroni post testing. All statistical tests were run by using KaleidaGraph statistical software (v 4.0, Synergy Software, Reading, PA, USA) at a significance level of α=0.05.

7.2 Results

Human mesenchymal stem cells have been analyzed for their proliferation (DNA content), osteoblast differentiation and mineralization ability (ALP specific activity and OCN production), bone turnover ability (OPG), collagen synthesis (CICP) and blood vessel formation (VEGF). Moreover, samples were tested for their ability to release calcium in the surrounding media. These markers were then correlated to the different experimental conditions used and to the material properties tested in order to assess the influence of

chemistry, strut porosity and serum proteins (MSCGM group) or Fn (Fn1 or Fn2 groups) in a 14-days time course study. In the figures, the statistics were calculated between the four pre-treatment groups. In the tables, the statistics were calculated between HAG80/20 and SAG80/20 (to compare chemistry) and SAG80/20 and SAG80/30 (to compare strut porosity). In both figures and tables the colour represents the group with the significantly higher marker level, and in the figures the signs represent: $p<0.05$ vs * BARE, ^ MSCGM, % Fn1 or $ Fn2.

7.2.1 Calcium release

The release of calcium from the material is important in determining the relative amount of this ion in the biological environment, influencing the cells and therefore their response. The release of calcium from the samples showed to be influenced by the pre-treatments. On HAG80/20 its release was significantly higher on the BARE group compared to the other pre-treatment groups at day 1, 2, 4, and 10, and it showed a high peak at day4 (Figure 7-1a). Also on SAG80/20 the BARE group showed the highest calcium release, significant at day1, 2, and 7, but this time peaking at day1 Figure 7-1b). Finally on SAG80/30 calcium release showed to be significantly higher on BARE at day4 and day10 and on MSCGM pre-treatment group at day2 and day10 Figure 7-1c). Table 7-7 shows the comparisons in calcium release between HAG80/20 and SAG80.20, and SAG80/20 and SAG80/30: this enables us to detect the effect that chemistry and strut porosity singularly have on calcium release. Results showed a late effect (day10 and day14) of chemistry on the BARE group where HAG80/20 released significantly higher calcium than SAG80/20; on the same treatment group the strut porosity had a significant effect only at day7 where the lower strut porosity percentage (20%) showed higher calcium release. The pre-treatment with MSCGM didn't influence the effect of the chemistry which was the same of the BARE group, as was also the effect from the strut porosity with the addition of a significantly higher ($p<0.0001$) calcium release from the 30% strut porosity at day14. The effect of the strut porosity in the presence of either Fn1 or Fn2 pre-treatment was the same, where again the 20% strut porosity sample showed significantly higher calcium release at day10 and day14. Finally the effect of chemistry didn't

significantly influence calcium release after Fn1 pre-treatment while affected it after Fn2 pre-treatment where at day14 was higher from the SAG80/20.

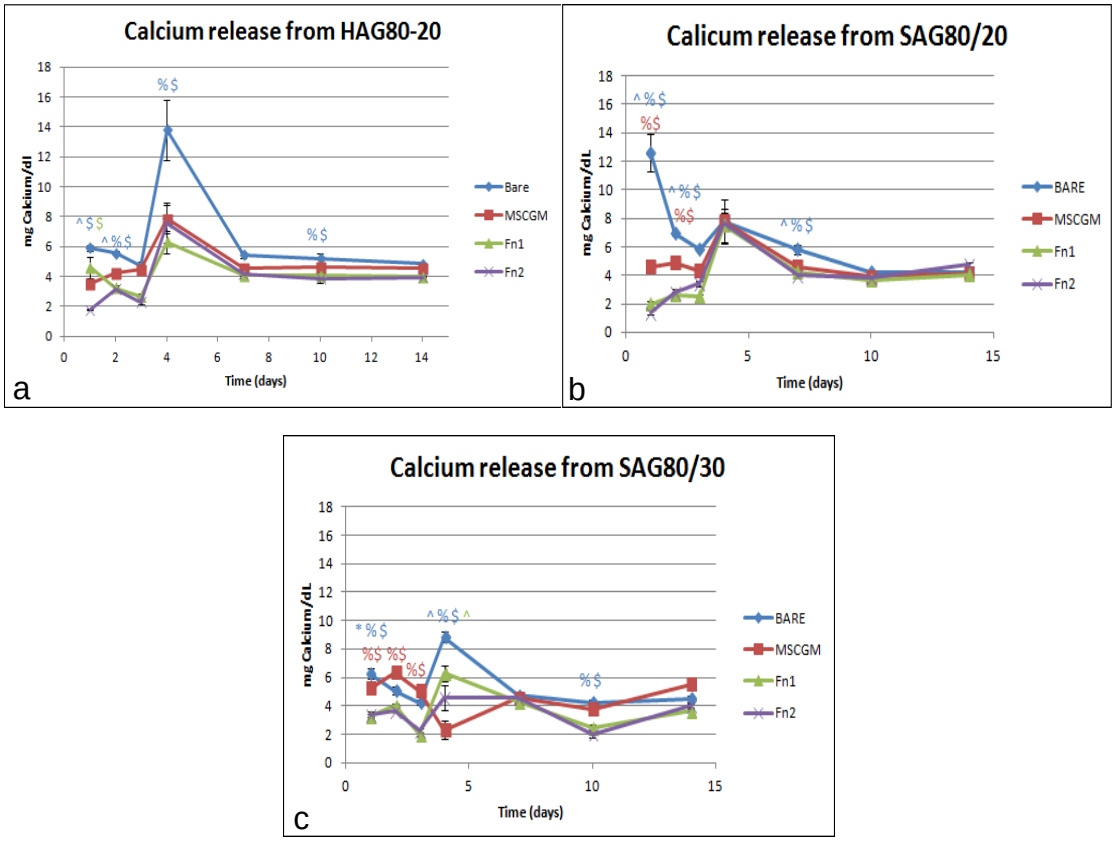

Figure 7-1: Effect of pre-treatment on HMSC Calcium release from (a) HAG80/20, (b) SAG80/20 and (c) SAG80/30 granules over a period of 14 days.

Table 7-4: Significant differences between chemistry (HA80/20 vs SA80/20) and porosity (20% vs 30% strut porosity on SA) for Calcium amount (*p<0.05, **p<0.005, ***p<0.0001. The colour refers to the higher value).

	Comparison	Day1	Day2	Day3	Day4	Day7	Day 10	Day 14
BARE	HA vs SA	-	-	-	-	-	*	**
	20% vs 30%	-	-	-	-	*	-	-
MSCGM	HA vs SA	-	-	-	-	-	**	*
	20% vs 30%	-	-	-	*	-	-	***
Fn1	HA vs SA	-	-	-	-	-	-	-
	20% vs 30%	-	-	-	-	-	**	*
Fn2	HA vs SA	-	-	-	-	-	-	*

	20% vs 30%	*	-	-	-	-	**	*

7.2.2 DNA content

Figure 7-2 shows the DNA content from HAG80/20, SAG80/20 and SAG80/30. On HAG80/20 cell proliferation was significantly higher on the BARE group samples at day4 and 7, peaking high at day14 (Figure 7-2a). SAG80/20 showed a similar trend, having the BARE treatment group with a significantly higher cell proliferation at day1, 7 and 10, and peaking at day10 (Figure 7-2b). SAG80/30 instead showed little significant difference between pre-treatments, with Fn1 (day1 and 3) and BARE (day10) promoting significantly higher cell proliferation compared to the other groups (Figure 7-2c). The DNA content in general peaked at late time points, between day 10 and day 14 on all the samples.

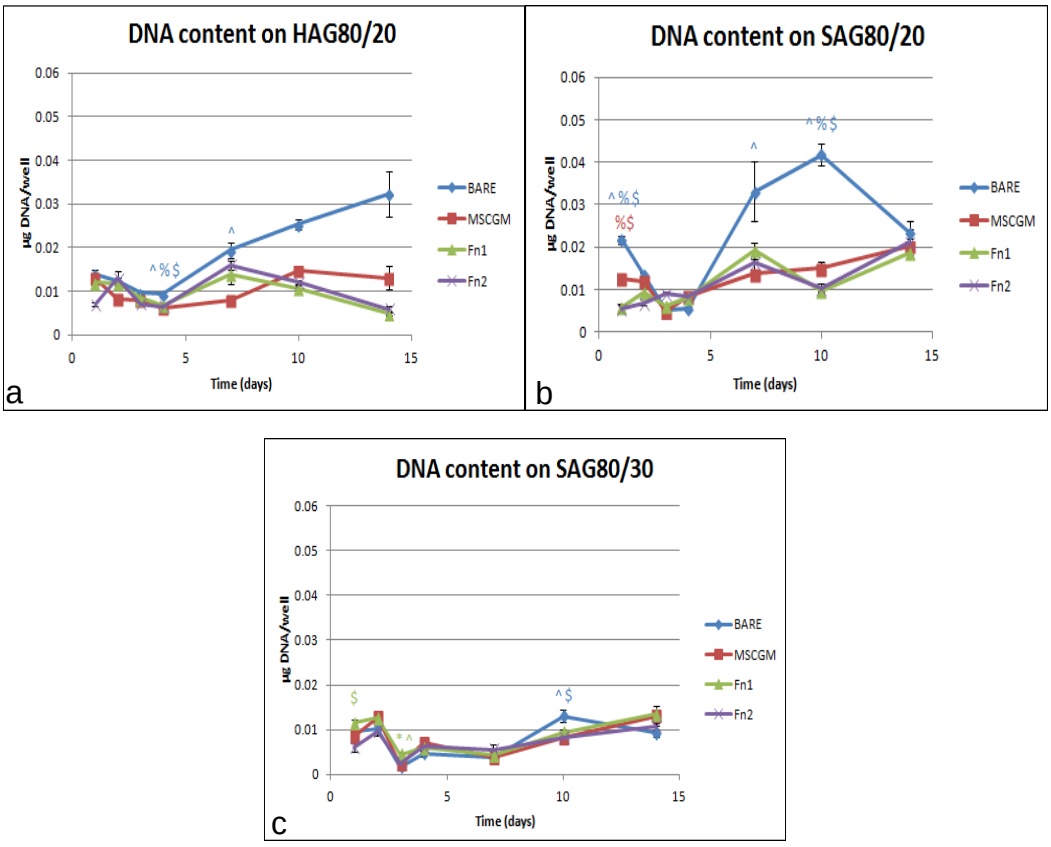

Figure 7-2: Effect of pre-treatment on HMSC proliferation as measured by total DNA on (a) HAG80/20, (b) SAG80/20 and (c) SAG80/30 granules over a period of 14 days.

Table 7-5 shows the specific effect of chemistry and strut porosity on DNA amount. On the BARE group the silicon-substituted HA (SAG) showed

significantly higher cell proliferation at day1, but at day3 and day4 was HAG to promote higher proliferation. The effect that strut porosity has on cell proliferation was instead more pronounced: at all the time points analyzed a part for day4, DNA amount was significantly higher on the 20% strut porosity percentage. The same effect is seen after pre-treatment with MSCGM, even if just at day1, 3, 7 and 10. While the effect of chemistry in this treatment group was showing again a succession of HA and SA significantly higher values at different time points. The effect that chemistry and strut porosity had in the Fn1 and Fn2 pre-conditioned groups was the same: early HA and later (from day3) SA higher DNA amount for the effect of chemistry, while strut porosity promoted an early 30% and later (from day3 again) 20% higher cell proliferation. The key result seen is that the BARE samples, together with the Silicon substitution of HA and a 20% strut porosity showed to promote better cell proliferation.

Table 7-5: Significant differences between chemistry (HA80/20 vs SA80/20) and porosity (20% vs 30% strut porosity on SA) for DNA (*p<0.05, **p<0.005, ***p<0.0001. The colour refers to the higher value).

	Comparison	Day1	Day2	Day3	Day4	Day7	Day 10	Day 14
BARE	HA vs SA	**	-	**	**	-	-	-
	20% vs 30%	***	*	*	-	*	*	*
MSCGM	HA vs SA	-	**	*	-	**	-	-
	20% vs 30%	*	-	*	-	*	*	-
Fn1	HA vs SA	*	-	-	*	-	-	**
	20% vs 30%	**	-	*	-	**	-	-
Fn2	HA vs SA	-	*	**	**	-	-	**
	20% vs 30%	-	*	***	-	*	-	-

7.2.3 Total protein

Figure 7-3 shows the amount of total protein analyzed from the cell lysate over the whole time frame 1-14 days for each of the three different granules. On HAG80/20 the four different treatment groups didn't show significant differences in values and/or trend apart for day3, where the BARE group showed significant higher amount of total protein compared to the other three pre-treatment groups (Figure 7-3a). SAG80/20 as well showed a similar trend of total protein production over the time frame between the treatment groups. However, showed also significantly higher values on BARE and MSCGM pre-treatment groups compared to Fn1 and Fn2 groups at day2, and on Fn2 pre-treatment group compared to BARE and MSCGM and BARE only at day3 and 14, respectively (Figure 7-3b). SAG80/30 instead didn't show any significant difference in total protein between treatments over the 14-days time course. Furthermore, the different pre-treatment groups followed a very similar trend between each other, where total protein peaked strongly at day3 (Figure 7-3c).

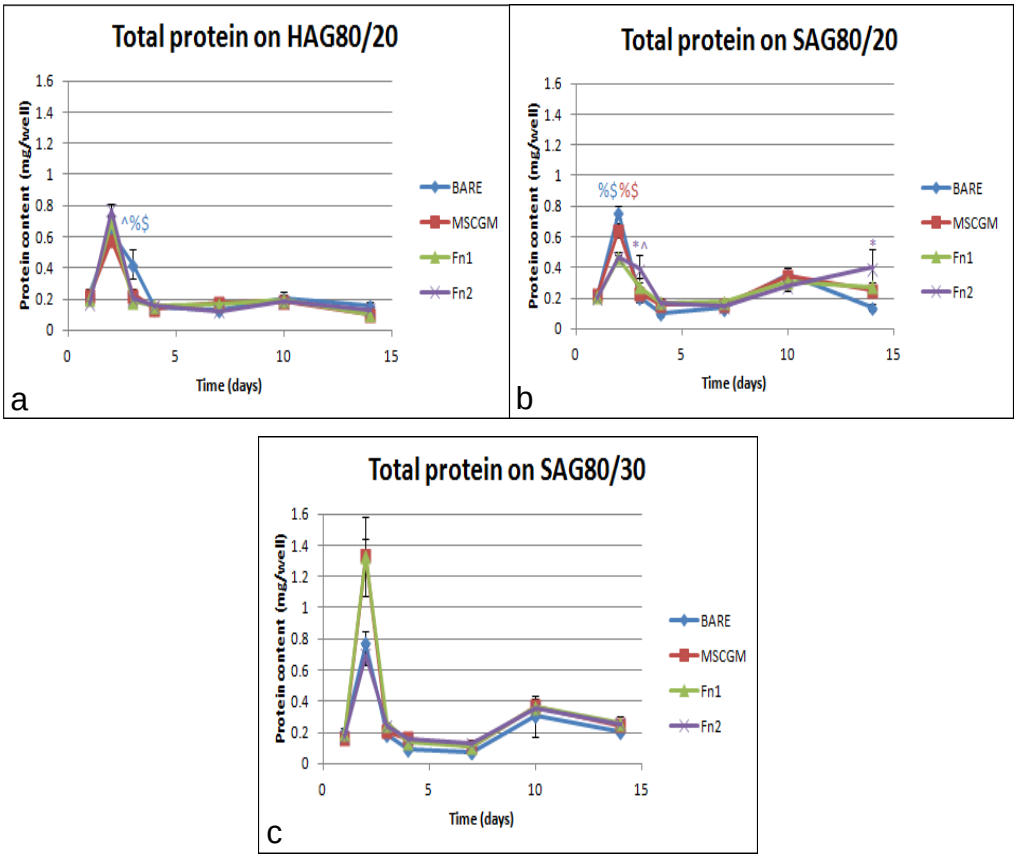

Figure 7-3: Effect of pre-treatment on HMSC total protein production on (a) HAG80/20, (b) SAG80/20 and (c) SAG80/30 granules over a period of 14 days.

Table 7-6 shows instead the influence of chemistry and strut porosity on total protein production for each treatment group. HAG80/20 promoted early (day2, 3 or 4) significantly higher amount of total protein production, while SAG80/20 did the same only at later time points (day7, 10 and/or 14). This effect was showed by all the pre-treatment groups apart for MSCGM, which instead showed only SAG80/20 supporting significantly higher protein production and only at day10 and 14. Also the strut porosity did influence total protein production, however the effect seen did not show one of the two topographies to be exclusively better compared to the other: both the samples showed to support significantly higher protein production at different time points in all the four pre-treatment groups.

Table 7-6: Significant differences between chemistry (HA80/20 vs SA80/20) and porosity (20% vs 30% strut porosity on SA) for total protein (*p<0.05, **p<0.005, ***p<0.0001. The colour refers to the higher value).

	Comparison	Day1	Day2	Day3	Day4	Day7	Day 10	Day 14
BARE	HA vs SA	-	-	**	**	-	**	-
	20% vs 30%	-	-	-	-	**	-	**
MSCGM	HA vs SA	-	-	-	-	-	**	***
	20% vs 30%	-	**	-	-	-	-	-
Fn1	HA vs SA	-	**	*	-	-	**	***
	20% vs 30%	-	*	-	-	*	-	-
Fn2	HA vs SA	**	***	**	-	*	**	**
	20% vs 30%	-	*	*	-	-	*	-

7.2.4 ALP specific activity

Figure 7-4 shows ALP specific activity normalized by total DNA for each of the three samples. On HAG80/20 ALP activity was significantly higher after the pre-treatments with Fn2 only at day1, and the pre-treatments with MSCGM and Fn1 at day7 and 10, and day 1, 10 and 14 respectively. Highest peaks

were shown at day7 from MSCGM and day14 from Fn1 pre-treatment groups (Figure 7-4a). On SAG80/20 ALP activity was significantly higher from all the pre-treatment groups at different time points: on BARE at day3, on MSCGM pre-treatment group at day3 and 7, on Fn1 at day1 and 10 and on Fn2 at day1 only. ALP activity peaked at day3 and day 7 from MSCGM and day10 from Fn1 pre-treatments (Figure 7-4b). Finally, on SAG80/30 ALP activity showed very high peaks at day3 and at day7. It was significantly higher from the MSCGM pre-treatment group at day1, 3 and 10 and from the BARE group at day3 (Figure 7-4c). In Table 7-7 are shown the comparisons of ALP specific activity between HAG80/20 and SAG80/20 to study the effect of chemistry, and between SAG80/20 and SAG80/30 to study the effect of strut porosity. With the exception of the BARE group, where both HAG (day1 and 2) and SAG (day3 and 14) showed significantly high peaks, all the pre-treatments showed a significantly higher ALP activity only on the HA chemistry compared to the SA one, and only on the 30% strut porosity compared to the 20%. These results show that SAG80/30 sample and the pre-treatment with MSCGM was the best combination to promote high ALP specific activity.

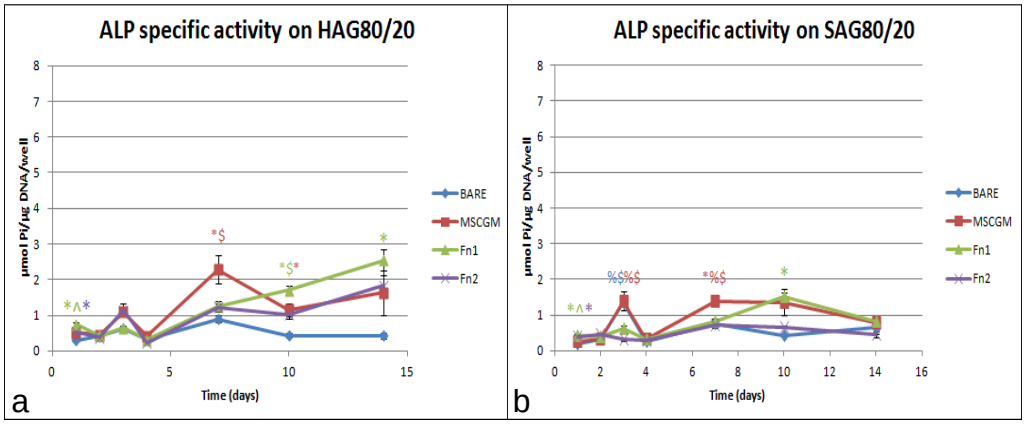

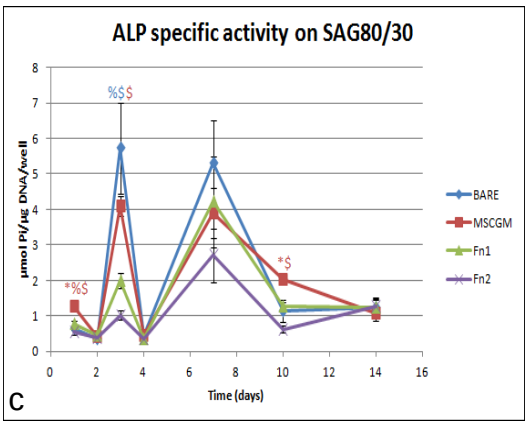

Figure 7-4: Effect of pre-treatment on HMSC differentiation as measured by ALP specific activity on (a) HAG80/20, (b) SAG80/20 and (c) SAG80/30 granules over a period of 14 days.

Table 7-7: Significant differences between chemistry (HA80/20 vs SA80/20) and porosity (20% vs 30% strut porosity on SA) for ALP amount normalized by DNA (*p<0.05, **p<0.005, ***p<0.0001. The colour refers to the higher value).

	Comparison	Day1	Day2	Day3	Day4	Day7	Day 10	Day 14
BARE	HA vs SA	*	***	**	-	-	-	*
	20% vs 30%	***	*	*	*	*	-	-
MSCGM	HA vs SA	**	**	-	**	-	-	-
	20% vs 30%	***	*	**	**	*	-	*
Fn1	HA vs SA	**	-	-	-	*	-	**
	20% vs 30%	**	-	**	-	*	-	-
Fn2	HA vs SA	-	-	**	-	**	*	**
	20% vs 30%	-	-	**	*	*	-	*

7.2.5 Osteocalcin content

Figure 7-5 shows the amount of OCN product on each of the three samples. The content of OCN on HAG80/20 changed significantly on the different pre-treatments during the time frame studied. At early time points the BARE (day3) and MSCGM (day2, day4, day7) samples showed significantly higher OCN than the other pre-treatment, while at late time points (day10 and day14) the pre-treatment with Fn1 increased the protein's production. Moreover OCN content peaked at day3 on the BARE treatment group (Figure 7-5a). The presence of the silicon in the lattice structure changed this effect: on SAG80/20 OCN was shown to be significantly higher on samples pre-treated with Fn1 (at day1 and day10) and Fn2 (at day1 and day14), and OCN content peaked again at day3 but without significant difference between treatments (Figure 7-5b). Finally, the SAG80/30 showed significantly higher OCN amount on the BARE group at day2, 3 and 4, showing a peak again at day3 (Figure 7-5c).

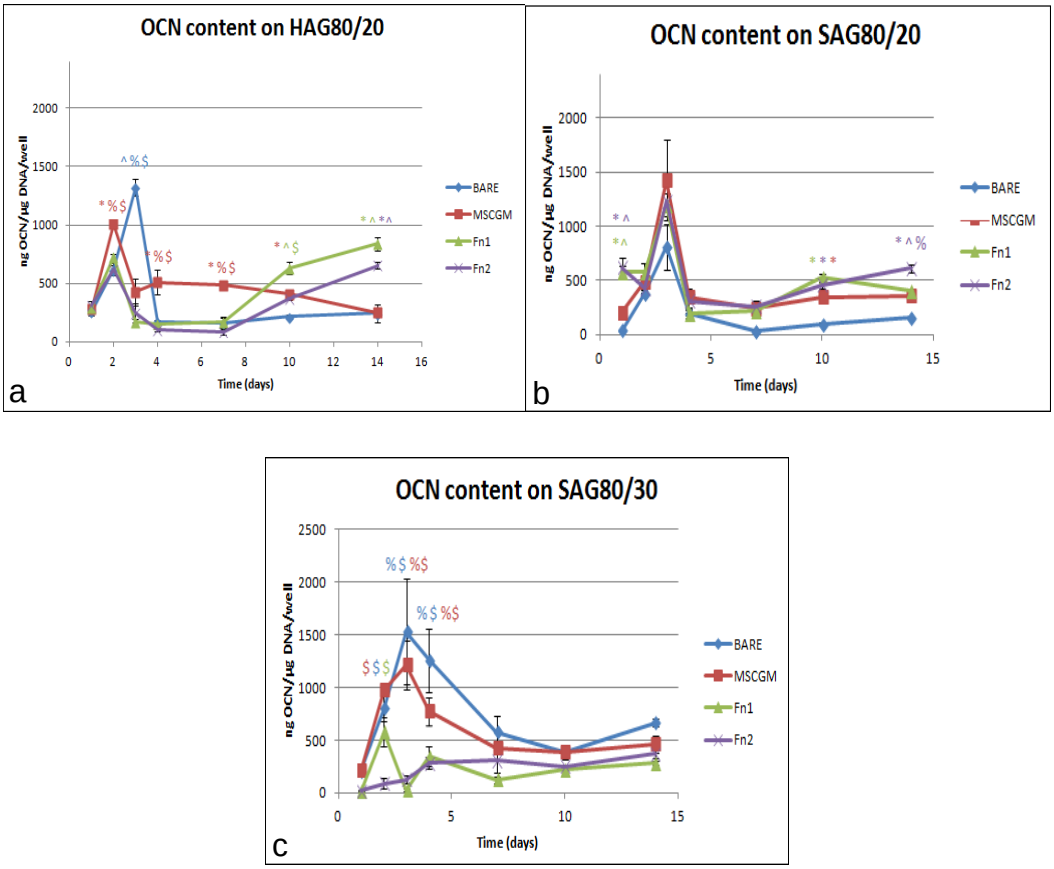

Figure 7-5: Effect of pre-treatment on HMSC differentiation and mineralization as measured by OCN production on (a) HAG80/20, (b) SAG80/20 and (c) SAG80/30 granules over a period of 14 days.

Table 7-8 shows the differences in OCN production between HAG80/20 and SAG80/20 (in order to compare chemistry) and SAG80/20 and SAG80/30 (in order to compare the effect of strut porosity). The results show that BARE and MSCGM treatment groups showed very similar results between each other, however opposed to Fn1 and Fn2 ones. In particular HA chemistry supported significantly higher OCN production than SA at day1, 2 and 10 for the BARE group and day2 and 7 for the MSCGM group. As soon as the pre-treatment change with either Fn1 or Fn2 however SA chemistry shows now significantly higher OCN production at day1 and 3 for Fn1 and day1, 3 and 4 for Fn2. HA kept showing the highest OCN amount only at day14 (for Fn1 group) and day14 (for the Fn2 group). Regarding the effect of strut porosity, on the BARE and MSCGM 30% strut porosity showed significantly higher OCN production at day1, 2, 4, 10 and 14 for BARE and day2, 4 and 7 for MSCGM. After the pre-treatment with Fn, however, the effect of the strut porosity, as the one of

the chemistry, changes: in both the Fn1 and Fn2 pre-treatment groups the 20% strut porosity promotes significantly higher production of OCN. These results together show that OCN production peaks at day3 on all the samples, and that the chemistry, strut porosity and presence of Fn significantly influence the production of this protein: while without Fn the HA chemiatry and the 30% strut porosity seem to support higher protein production, after Fn pre-treatment (irrespective of its concentration) the SA chemistry and 20% strut porosity become the best combination to promotes the protein production.

Table 7-8: Significant differences between chemistry (HA80/20 vs SA80/20) and porosity (20% vs 30% strut porosity on SA) for OCN amount (*p<0.05, **p<0.005, ***p<0.0001. The colour refers to the higher value).

	Comparison	Day1	Day2	Day3	Day4	Day7	Day 10	Day 14
BARE	HA vs SA	**	**	-	-	-	**	-
	20% vs 30%	***	*	-	*	-	**	***
MSCGM	HA vs SA	-	***	-	-	***	-	-
	20% vs 30%	-	***	-	*	*	-	-
Fn1	HA vs SA	**	-	***	-	-	-	**
	20% vs 30%	***	-	***	-	-	**	**
Fn2	HA vs SA	*	*	**	*	-	-	-
	20% vs 30%	**	**	**	-	-	**	**

7.2.1 Osteoprotegerin content

Figure 7-6 shows the OPG production from the samples after the different pre-treatments. HAG80/20 and SAG80/20 showed a very similar trend, where OPG amount was significantly higher after Fn2 pre-conditionings at almost all the time points analysed, showing a peak at day4 (on HAG80/20) and at day7 (on SAG80/20). Fn1 pre-treatment group also showed high OPG production (however lower than Fn2) which was significantly higher than the other two groups at day7 and 10 for HAG, and at day3 and 4 for SAG (Figure 7-6a and

b). On SAG80/30 OPG was significantly higher on the BARE group at day1 and 4 and on MSCGM at day3 compared only to Fn1 group. The protein production peaked at day7 but there was not significant difference between pre-treatment groups (Figure 7-6c). These results suggest that Fn2 pre-treatment is able to increase significantly OPG production only on the 20% strut porosity samples.

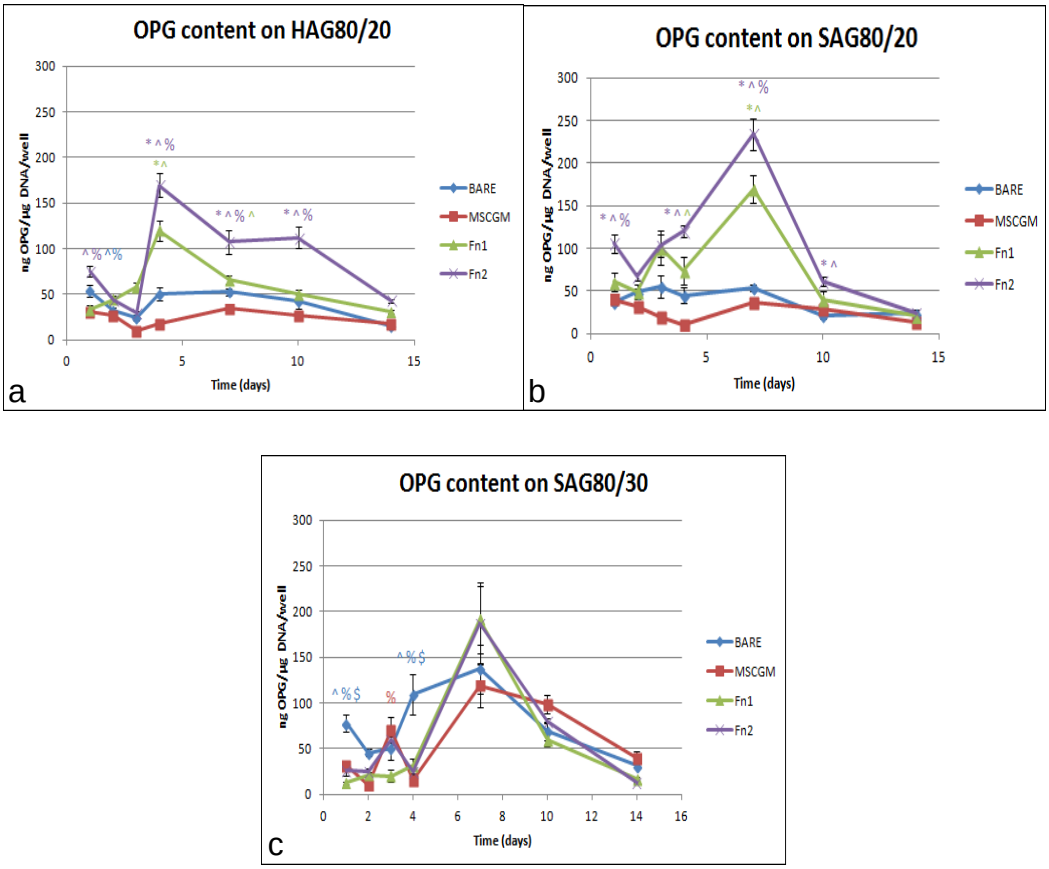

Figure 7-6: Effect of pre-treatment on HMSC OPG production on HAG80/20 (a), SAG80/20 (b) and SAG80/30 (c) granules over a period of 14 days.

Table 7-9 shows significant differences in OPG production affected by chemistry or strut porosity. The chemistry showed a significant influence in OPG amount only in the presence of Fn2 pre-treatment: in this case SAG promoted significantly higher OPG at 4 time points, and HAG did the same at the remaining 3. The strut porosity had a stronger influence in OPG production: in BARE conditions 30% strut porosity was significantly better in promoting the protein's production, while on MSCGM and Fn2 there was an early positive effect from the 20% and a late one from 30%. Finally the Fn1 pre-treatment showed only the 20% sample being better in supporting OPG

production. These results taken together suggest that while the chemistry doesn't have a significant influence, the 30% strut porosity is better in promoting OPG production; however the presence of Fn (especially Fn1) changes completely this scenario, showing the SA chemistry and the 20% strut porosity being the best to support OPG production.

Table 7-9: Significant differences between chemistry (HA80/20 vs SA80/20) and porosity (20% vs 30% strut porosity on SA) for OPG amount (*p<0.05, **p<0.005, ***p<0.0001. The colour refers to the higher value).

	Comparison	Day1	Day2	Day3	Day4	Day7	Day 10	Day 14
BARE	HA vs SA	-	*	-	-	-	*	-
	20% vs 30%	*	-	-	*	*	**	-
MSCGM	HA vs SA	-	-	-	-	-	-	-
	20% vs 30%	-	***	*	-	*	**	*
Fn1	HA vs SA	-	-	-	-	**	-	*
	20% vs 30%	**	*	*	*	-	-	-
Fn2	HA vs SA	*	**	**	*	**	*	**
	20% vs 30%	**	**	*	***	-	*	*

7.2.1 CICP content

Figure 7-7 shows the CICP amount on each of the three groups of samples. On all the samples, the BARE and MSCGM pre-treatment groups showed significantly higher protein produced. In particular, on HAG80/20 at day1 BARE showed significantly higher levels compared to the other groups, and MSCGM and Fn2 compared to Fn1; at day2 only from the BARE groups the level was significantly higher, while at day3 it was from both BARE and MSCGM groups compared to Fn2. At day4, however, this values dropped and Fn2 instead showed higher CICP production compared to BARE and MSCGM and at day7 compared only to MSCGM (Figure 7-7a). On SAG80/20 there is a very similar trend: BARE showed significantly higher levels of protein at day2,

3, 4 and 14; MSCGM group showed higher values at day3 and Fn2 at day7 (Figure 7-7b). SAG80/30 showed similar effect of BARE and MSCGM pre-treatments, which supported higher CICP amount at day1, 3, 4 and 7 (BARE) and day1 and 3 (MSCGM); no high later CICP amount was now found from Fn2 (Figure 7-7c). The CICP production peaked on all the three samples at day3.

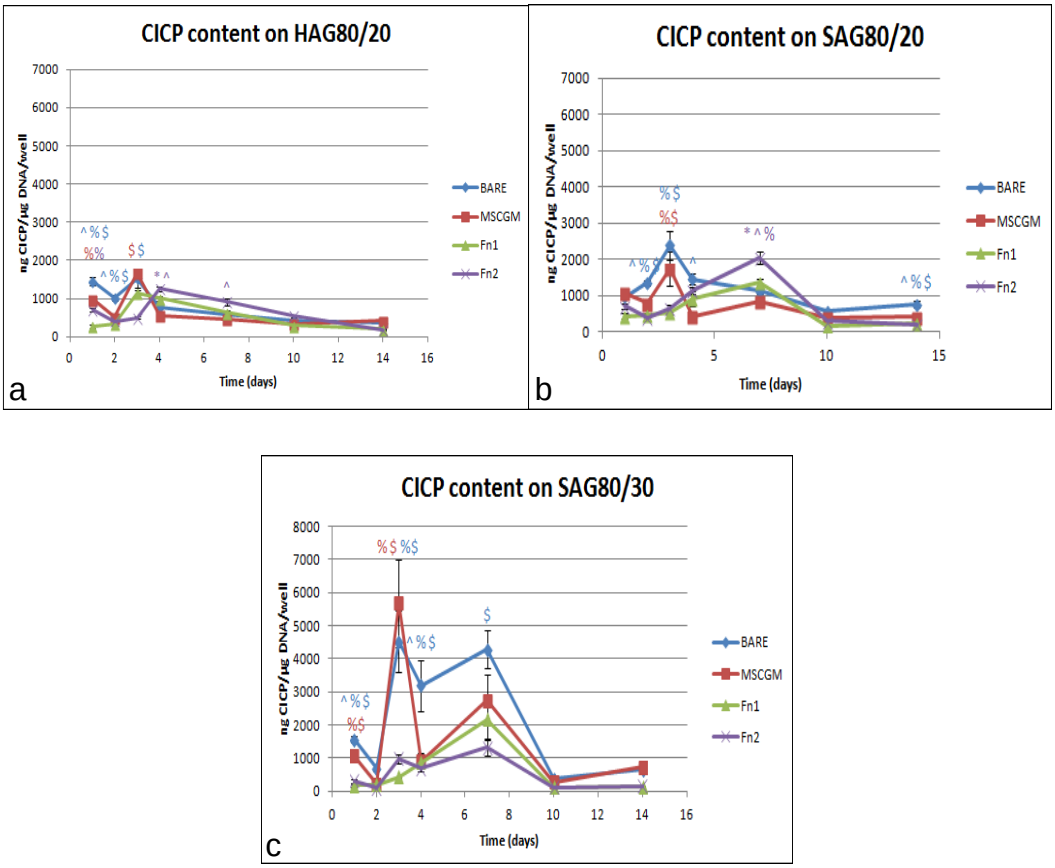

Figure 7-7: Effect of pre-treatment on HMSC extracellular matrix production as measured by CICP production on (a) HAG80/20, (b) SAG80/20 and (c) SAG80/30 granules over a period of 14 days.

Table 7-10 instead shows the effect of chemistry and strut porosity on CICP for each pre-treatment group. Regarding the effect of chemistry, on all the groups the samples seemed to produce the same amount of protein. Strut porosity on BARE and MSCGM was found to support higher protein synthesis on the higher strut porosity, while after Fn1 and Fn2 pre-treatments there was a similar effect between 20% and 30% strut porosity. Taken together these results show that the strut porosity significantly influence CICP production (30% higher than 20%), more than how much the chemistry does. However,

the presence of Fn1 and Fn2 pre-treatments demolished the favourable effect of high strut porosity on CICP production.

Table 7-10: Significant differences between chemistry (HA80/20 vs SA80/20) and porosity (20% vs 30% strut porosity on SA) for CICP amount (*p<0.05, **p<0.005, ***p<0.0001. The colour refers to the higher value).

	Comparison	Day1	Day2	Day3	Day4	Day7	Day 10	Day 14
BARE	HA vs SA	*	-	-	*	-	-	-
	20% vs 30%	**	**	**	**	**	-	-
MSCGM	HA vs SA	-	-	-	*	-	-	-
	20% vs 30%	-	**	**	*	*	-	**
Fn1	HA vs SA	-	-	**	-	**	-	-
	20% vs 30%	-	-	-	-	*	-	-
Fn2	HA vs SA	-	-	-	-	**	**	-
	20% vs 30%	-	-	-	-	*	-	-

7.2.2 VEGF production

Figure 7-8 shows VEGF production from HAG80/20, SAG80/20 and SAG80/30. On HAG80/20 it was significantly higher on the Fn2 pre-treatment group at day1 (compared to the other three groups), day4 (compared to MSCGM and BARE), day10 and day14 (compared only to BARE). At day14 also Fn1 group showed significantly higher production than BARE (Figure 7-8a). On SAG80/20 VEGF production differently influenced by the pre-treatments, depending by the time: at day1 Fn2 pre-treatment showed significantly higher amount than the other groups, at day3 and 4 BARE showed higher amount (compared to Fn1 and Fn2 and to MSCGM respectively), and at day10 was significantly higher from MSCGM, Fn1 and Fn2 compared to BARE (Figure 7-8b). SAG80/30 showed less sensitivity to pre-treatments on VEGF production: there was a significantly higher amount of protein from the BARE, MSCGM and Fn2 compared to Fn1 at day1, and at day4 from the BARE compared to the other groups (Figure 7-8c). Furthermore VEGF production peaked at day3 on SAG80/20 and SAG80/30 but didn't

show a particular peak at any time point on HAG80/20. Table 7-11 shows the effect of chemistry and strut porosity on VEGF production after each pre-treatment. Chemistry showed to not influence significantly VEGF production, in any pre-treatment conditions. Strut porosity instead showed to significantly influence VEGF production and to be sensitive to the pre-treatments with Fn: results showed a significantly higher amount of protein from the 30% strut porosity sample in BARE and MSCGM conditions, but the opposite or not significant difference from Fn1 and Fn2 pre-treatment groups. These results together suggest that strut porosity and pre-treatment conditions significantly influence VEGF production.

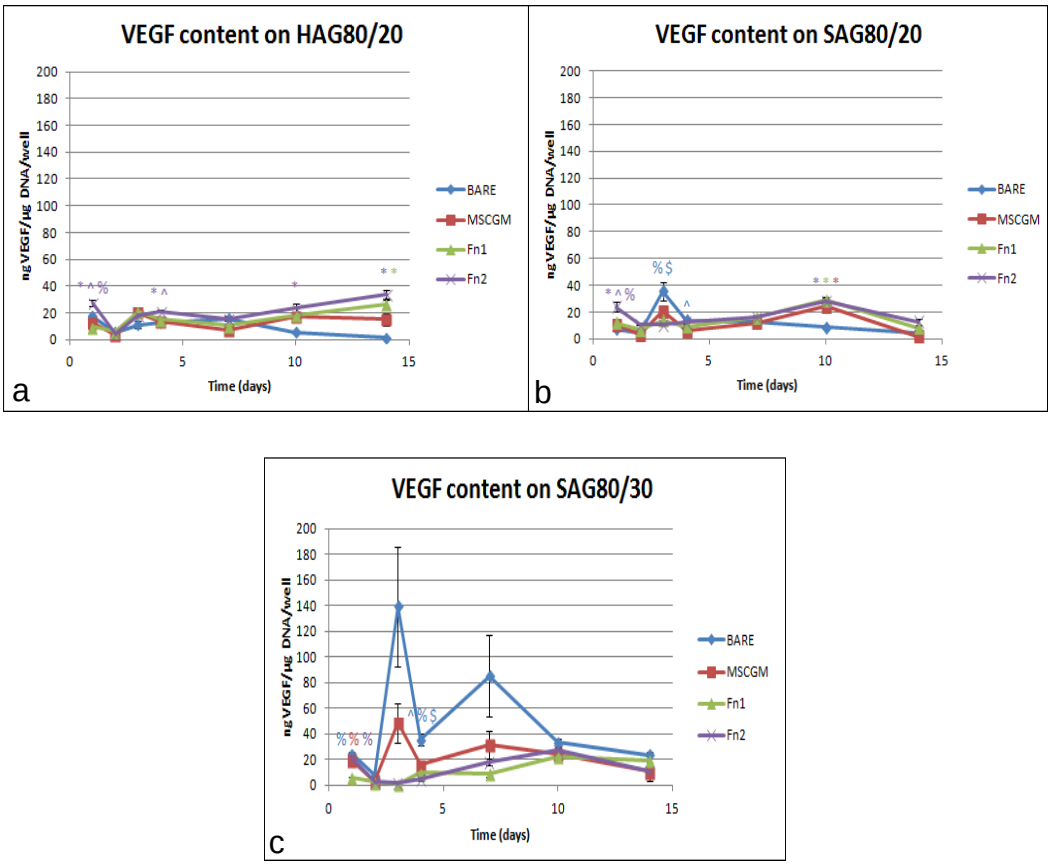

Figure 7-8: Effect of pre-treatment on HMSC angiogenentic potential as measured by VEGF production on (a) HAG80/20, (b) SAG80/20 and (c) SAG80/30 granules over a period of 14 days.

Table 7-11: Significant differences between chemistry (HA80/20 vs SA80/20) and porosity (20% vs 30% strut porosity on SA) for VEGF amount (*p<0.05, **p<0.005, ***p<0.0001. The colour refers to the higher value).

	Comparison	Day1	Day2	Day3	Day4	Day7	Day 10	Day 14
BARE	HA vs SA	*	-	*	-	-	-	-
	20% vs 30%	***	*	-	**	-	***	**
MSCGM	HA vs SA	-	-	-	-	-	-	-
	20% vs 30%	**	-	-	*	-	-	-
Fn1	HA vs SA	-	-	-	-	-	-	*
	20% vs 30%	-	-	*	-	-	-	-
Fn2	HA vs SA	-	*	-	-	-	-	**
	20% vs 30%	-	*	*	-	-	-	-

7.1 Discussion

7.1.1 The influence of chemistry

Calcium release

As previously discussed (Chapter 1, Section 1.5) calcium is the most abundant ion in the body, and bone represents the body's calcium reservoir. Its presence affects bone modeling and remodeling processes and many studies have been focused on identifying the role that calcium ions released from BGS have in directing the bone remodeling process. A study from Matsuoka dated 1999 (Matsuoka et al., 1999) for example showed that an increasing concentration of extracellular calcium ions promotes osteogenic differentiation *in vitro* by increasing ALP activity in a dose-dependent manner up to 1.6-fold, and ALP, OCN and TGF-β gene expression from osteoblastic cells. Similar results were shown also from other studies: extracellular calcium ions were found to positively stimulate DNA synthesis and ALP activity of osteoblasts via monocytes in bone remodelling and osteoblasts proliferation, directly and indirectly via monocytes (Kanatani et al., 1991). Regarding the effect that calcium ions released directly from the BGS have in influencing the material-mediated bone formation, an interesting work from Guth (Guth et al., 2011) looked at the release of ions from HA and SA discs under static and semi-dynamic (SD) conditions, and using serum-free media (SFM) or serum-containing media (C-MEM). The work showed that calcium ions were released only with C-MEM, from SA under both static and SD conditions, while on HA there was calcium depletion from the media but only under SD conditions. This suggested that serum proteins support this ionic exchange, and that SA more easily facilitates ion exchange between the material and the physiological environment compared to HA. Moreover, a net release of calcium from the materials was not seen, suggesting that the high bioactivity of these materials is not a result of significant Ca ion dissolution.

The results of the present study showed that the chemistry did influence calcium release especially on BARE samples where the presence of the silicon shifted the release of this ion from day4 to day1 (Figure 7-1a, b). In

general, on BARE and on MSCGM HA showed significantly more release of Ca compared to SA, but only at late time points. Furthermore, while with Fn1 pre-treatment there was no significant difference between HA and SA, with Fn2 pre-treatment SA showed significantly higher Ca release than HA (only at day14). These results suggest that: firstly, in normal conditions (BARE) HA is better able to release high amount of calcium than SA, even if this difference is seen only at late time points (day10 and day14); secondly, that serum proteins are not able to influence and/or change this effect of chemistry in influencing calcium release; thirdly, that high concentrations of Fn are able to invert the effect that chemistry has in modulating Ca release by promoting higher Ca release from SA rather than HA (Table 7-4). Moreover, Fn1 conditionings seem to cover any differential influence that chemistry has in modulating Ca release.

Compared with the study from Guth, these results are in disagreement. However, while her study was conducted on microporous discs and over a period of 28 days, the present study was conducted on porous granules and over a 14-days period. It is possible that these differences, especially the discs rather then the porous granules, play a role in influencing calcium release. Another difference between the studies is that in the present study the experiment was run in conjunction with cell culture, which is very likely to have influenced the release of the ion from the samples and therefore influenced the final results. Some other studies have revealed a greater biomimetic precipitation of a bone-like apatite on Si-substituted CaP materials (where bone-like apatite is defined as a biologically equivalent carbonated HA) and the relative ability of a surface to support its nucleation has been associated with a greater biological activity. This greater biological activity is thought to be due to a more favorable adsorption and incorporation of biological species at the surface of the implant that helps the subsequent attachment of cells (Ducheyne and Qiu, 1999). Si-substituted calcium phosphate materials are thought to show an enhanced biomimetic precipitation through different mechanisms: by increasing the solubility of the material by the creation of defects in the lattice (Porter, 2006) (Reid et al., 2005), by generating a more electronegative surface (Vandiver et al., 2005), and by generating a smaller

grain size, facilitating an increased dissolution at the surface (Porter, 2006). Calcium release can be seen as a preliminary step for biomimetic precipitation and in the present study it was seen to be enhanced preferably on the HA, in disagreement with the mentioned studies. A possible explanation for this discordance can be that the presence of stem cells on the surface influenced the ionic release from the material, supporting a higher release of calcium from HA in BARE and MSCGM conditions, and a higher one from SA after pre-treatment with Fn2 at late time points (day14).

Cell proliferation: DNA content and Total Protein

The positive effect that the presence of the silicon has on cell proliferation has previously been demonstrated (Rashid et al., 2008)(Botelho et al., 2006) (Guth et al., 2010c). Looking at the effect that chemistry seemed to have on DNA amount comparing HAG80/20 and SAG80/20, the present results are in fact in agreement with the previous studies (using dense discs instead of porous granules) which demonstrated higher cell number on SA compared to HA (Botelho et al., 2006). The reasons why the presence of silicon in the HA structure has a positive effect towards osteogenesis has long been debated, as discussed in Chapter 4 Section 4.4.3. In the present study, HA and SA porous granules were compared for their ability to stimulate cell proliferation by means of both DNA content and Total Protein production. In terms of variation with chemistry results of the two analyses are consistent. In both of them, chemistry did not appear to influence cell proliferation dramatically, affecting more the timing rather than the absolute amount of DNA or total protein produced. The DNA amount (Table 7-5) on BARE samples was significantly influenced by the presence of the silicon at a very early time point (day1) when SA showed greater cell proliferation than HA; after that HA also showed at two later time points higher DNA amount. The pattern of total protein production was very different to that of total DNA, peaking at day2 rather than increasing with time, suggesting that it may not be a reliable indicator of cell proliferation. This difference could suggest that DNA and total protein are not 100% comparable, therefore that there could be some differences between the actual number of cells (given by the DNA amount) and their activity (given by the level of total protein).

The effect of pre-treatments on DNA amount and protein production didn't show to change substantially the results. These results suggest that the chemistry was able to influence cell proliferation more in its time course than in its absolute value, with the presence of the silicon supporting a faster higher cell proliferation than HA, effect which was moreover independent by the presence of serum proteins or Fn.

Cell differentiation: ALP specific activity and Osteocalcin production

Alkaline Phosphatase is an enzyme whose activity is highly expressed in differentiated osteoblasts cells, and its role in bone mineralization has been extensively proved (Chapter 1, Section 1.6.1). For this reason, the specific activity of this enzyme has been extensively used as a marker for osteoblast differentiation. In the present experiments, ALP specific activity was normalized by DNA amount, analyzed and then statistically compared between samples with differences in chemistry, strut porosity or pre-treatments.

Osteocalcin is a protein present in the organic part of bone matrix, and plays an essential role the process of bone formation. Its synthesis is vitamin-K-dependent and its activity is Ca-dependent. Because of its role in bone formation and because it is synthesized by osteoblasts, it is widely used as a marker for osteoblasts differentiation.

The present results show that chemistry has a relevant effect on osteoblast differentiation. A significantly higher ALP activity was observed on HA at early time points, and on SA at later time points on BARE samples; however, this effect was abolished by the presence of serum proteins or Fn, which instead showed a significantly higher ALP activity only on HA (Table 7-7). Regarding OCN production, it was found to be significantly higher on HA on both BARE and MSCGM groups, but after Fn1 or Fn2 pre-treatments SA supported higher production of the protein at different time points (Table 7-8). These results are in relative discordance with previous studies showing instead the higher cell differentiation potential from SA rather than HA materials. A study from Botelho for example (Botelho et al., 2006), comparing the cell behavior of

human osteoblasts cells between HA, 0.8wt% and 1.5wt% silicon substituted HA, showed higher ALP activity at day7 from 0.8wt% SA compared to HA, and higher OCN levels in the media from the same chemistry at day1 and day5. However, the materials used for the latter study were dense discs. Also, the cells used were human OBS and not mesenchymal stem cells: this detail could have played a fundamental role in the discrepancy of the results, as HOB cells were received from donors between 55 and 65 years of age, which makes the cultures of these cells more differentiated than HMSC at an equivalent passage. Furthermore, the media used was supplemented with 30μg/ml of vitamin C, which definitely has an influence in bone formation and could have affected the influence of chemistry on cell behavior. Moreover, in Botelho's study, ALP was normalized by Collagen I amount, which makes harder the comparison between the two studies.

The present results therefore suggest that HA porous granules were a better candidate to stimulate cell differentiation on BARE samples (by means of ALP and OCN) in the present conditions and incubation in HMSCGM. Pre-treatment with either Fn1 or Fn2 was able to shift the effect on SA for ALP, and support higher OCN production on SA compared to HA, irrespectively of Fn concentration.

Bone turnover: Osteoprotegerin and CICP production

Osteoprotegerin (OPG) is a protein involved in the regulation of the skeletal development and homeostasis. It is a cytokine receptor for the RANKL, and intervenes in the inhibition of the differentiation of ostoclast precursors into mature osteoclasts, thus altering the bone turnover. As a result of its role in regulating the bone turnover, OPG is often used as a marker for osteogenic differentiation. CICP represents the C-terminal propeptide of the type-1 collagen, which is related to Collagen I production and thus to bone matrix production. In the present study, the media was analyzed for OPG and CICP production from HMSC and correlated to chemistry and strut porosity of the materials and different pre-treatment conditions. Regarding the effect of chemistry, results showed a significantly higher OPG production on the Silicon-substituted HA at day1, and on HA at the later time point of day7 on the BARE group (Table 7-9), suggesting that chemistry may have had a

temporal effect only temporal on OPG production. However, when pre-treating the samples with serum proteins (MSCGM group), the effect of chemistry disappeared and there was no significant difference between HA and SA chemistries on OPG production at any time point analyzed. The presence of Fn changed the results: while using Fn1 pre-treatment cells followed the same behavior as on BARE samples but slightly delayed, using Fn2 pre-treatment SA supported significantly increased OPG production as compared to HA.

Regarding CICP production, the presence of the silicon significantly increased the protein production only at few time points on BARE and MSCGM as compared to HA; the pre-treatment with serum proteins instead normalizes this behavior so that SA showed the same amount of CICP compared to HA (Table 7-10).

The effect of the chemistry on protein production of cells in contact with HA or SA has already been studied by different groups. Botelho *et al.* (Botelho et al., 2006) reported higher CICP amount from cells (HOBS) in contact with SA compared to HA at all the time points analyzed up to 25 days; results which are in accordance also with another study from Reffitt *et al.* (Reffitt et al., 2003a) which showed how orthosilicic acid stimulates collagen 1 synthesis in HOBS and enhances osteoblastic differentiation. The positive effect that Silicate ions have when incorporated in a CaP (this time TCP instead of HA), has also been shown already by other studies like Fielding *et al.* (Fielding and Bose, 2013) where Si-substituted TCP showed to promote higher OCN, COL I levels and blood vessels density compared to pure TCP *in vivo*. These results suggest that the presence of the silicon in the apatite lattice favorites an earlier OPG production from HMSC on un-treated samples, and that a high concentration of Fn on the implant surface supports a greater production of this protein from the SA chemistry. Moreover, while CICP is only slightly increased by the presence of the silicon in the apatite structure, the pre-treatment with serum proteins and Fn slightly balances the sensitivity to chemistry of protein production in HA and SA.

Blood vessel formation: VEGF production

VEGF is a key regulator in angiogenesis. High VEGF values are related to high blood vessel formation, which supports nutrients and oxygen supply, which in turn sustains new tissue formation. Its presence therefore is fundamental for the development of a new bone, and it is often used as a marker for new tissue vascularization, and therefore development. VEGF production was not significantly influenced by the chemistry of the materials: as shown in Table 7-11, its production was significantly higher on HA and SA respectively at day1 and day3 on BARE samples, and not significantly different at the other time points; after pre-treatment with either serum proteins, Fn1 or Fn2, there wasn't any significant difference in VEGF production between the two chemistries.

Summary

To summarize the effect of chemistry in directing cell response to BGS, the present results showed that HA performed better than SA in terms of ALP specific activity, OCN production and calcium release (only at late time points); meanwhile the presence of the silicon instead supported more rapid cell proliferation and OPG production compared to HA. The pre-treatment which was found to influence most significantly the effect of chemistry was Fn2, which favored an increase in calcium release, OPG and OCN production from SA samples.

7.1.2 The influence of strut porosity

Calcium release

There is little literature about the effect of microporosity on calcium release from HA and SA ceramics during cell culture. In the previous section we observed a positive effect that HA had on promoting significantly more calcium release than SA, and also that Fn2 pre-treatment can change this effect. Now we are looking at the effect of two different strut porosities (20% and 30%) on calcium release from silicon substituted hydroxyapatite samples: SAG80/20

and SAG80/30. Table 7-4 shows that the lower strut porosity (20%) promoted significantly higher calcium release compared to SA PG samples with 30% strut porosity, at one time point from the BARE pre-treatment group at day7, from MSCGM treated samples at day4 and from Fn1 and Fn2 pre-treatment groups at days 10 and 14; however, MSCGM and Fn2 pre-treatments also increased the calcium release significantly from the 30% microporosity sample at days 14 and 1 respectively. Analyzing these results it seems complex to get an idea of the effect of microporosity and pre-treatments on calcium release. It could be possible that the presence of serum proteins hasten the calcium release from both the samples compared to the BARE group. However, the presence of Fn looks to play a role in influencing calcium response in dependence of its concentration: at sub-physiological concentration it significantly influenced release from the samples only from the 20% microporosity at day10 and day14, while Fn2 pre-conditioning promoted significantly higher release of calcium from the 30% microporosity compared to the 20% as early as day1. This could suggest that high concentrations of Fn support an initial burst in release of calcium from 30% microporosity compared to 20%, and that at later time points promotes sustained Ca release from lower percentage (20%) strut porosity granules. In general, there was a trend towards greater Ca release from the 20% strut porosity granules.

Cell proliferation: DNA amount and Total Protein

It has been clearly demonstrated that microporosity significantly affects the post-implantation response of porous HA scaffolds (Hing et al., 2005). An *in-vitro* study from Annaz (Annaz et al., 2004) showed that cells are able to sense the microporosity and respond to this with protrusion of filipodia oriented towards the micropores, a rounded cellular morphology and extension of lamellipodia with a subsequent and organized cytoskeletal arrangement. In an *in vivo* study Holmes demonstrated that HA microporous implants can act as a bone graft substitute successfully as autografts (Holmes and Hagler, 1988). Looking at differences in levels of microporosities, some *in vivo* studies have found that a higher level of microporosity enhances osteointegration (Hing et al., 2004) (Campion et al., 2011). In our *in-vitro* study, however, we found that the lower microporosity (20%) enhanced a better cell proliferation response

compared to the higher. DNA amount was significantly higher on the 20% than on the 30% for 6 and 4 out of 7 time points, on the BARE and MSCGM treated groups respectively (Table 7-5). The presence of Fn slightly changed the response, where the 30% strut porosity supported significantly higher DNA at early time points (day1 and day2) for Fn1 and Fn2 groups respectively, although the 20% still supported higher results at day3 and day7. These results suggest that the presence of Fn in some way could mediate the higher biological activity of the granules with increased strut porosity by enhancing the cell proliferation earlier than on those with a lower porosity.

The effect of strut porosity on total protein production was marked with a stronger peak at day2, however no pre-treatment significantly enhanced the total protein production between one of the two samples (Table 7-6). This kind of pattern of total protein production, however, suggests that it may not be a reliable indicator of cell proliferation (as already mentioned in the previous section). Moreover, pre-conditioning the samples with either MSCGM or Fn1 was only found to support higher levels of DNA on SAG80/30 at early time points, which could indicate the role of these proteins in cell attachment.

The results of this study, which show that cell proliferation is inhibited by an increase in strut porosity, seem to contradict *in vivo* literature. However, it is possible that the post-implantation biological response can not be directly correlated to an isolated cell proliferation response *in vitro*.
This contradictory behavior has previously been observed, for instance, from Cerroni *et al.*, who measured osteoblast-like cells proliferation and ALP activity on three different HA granules: one with 30-40%, and one with 50-60% total porosity and a commercially available coralline derived porous HA, whose percentage of porosity was not specified (Cerroni et al., 2002). The latter material supported significantly lower cell proliferation than the other sample. These results suggest that there could be other additional events at the implant interface that we were not able to reproduce *in vitro* and that influence further the *in vivo* response.

In summary there was trend towards higher levels of cell proliferation on the 20% strut porosity sample, but total protein did not show a significant sensitivity to strut porosity.

Cell differentiation: ALP specific activity and Osteocalcin production

In vivo studies previously demonstrated the higher osteogenic potential of a silicon-substituted HA with higher strut porosity (Hing et al., 2004) (Campion et al., 2011)(Coathup et al., 2011)(Coathup et al., 2012)(Chan et al., 2012a). The results of ALP activity and OCN production are not only in line with these previous observations, but also help elucidate a clear effect that Fn has in mediating cellular response. Looking at Table 7-7 it is clear that strut porosity has a significant effect on ALP specific activity: the SAG80/30 sample, with high strut porosity, always showed a significantly higher activity, irrespectively of pre-treatment and of time point.

Regarding OCN production, on BARE and MSCGM pre-treatments the results again demonstrated that higher strut porosity supports significantly higher OCN production. However, the pre-treatment with Fn completely changed the effect: on Fn1 and Fn2 pre-treatments lower strut porosity SAG80/20 sample supported significantly higher OCN production than SAG80/30 sample (Table 7-8). These results clearly support the hypothesis that Fn is involved in mediating the biological activity of CaP based BGS ceramics.

In general it is possible to conclude that strut porosity has a relevant effect on cellular differentiation of HMSC, with higher strut porosity enhancing it and with Fn supporting a higher biological response from a lower microporosity, but not supporting further differentiation on HAG80/30.

Bone turnover: Osteoprotegerin and CICP production

Microporosity was found to significantly affect OPG production. In Table 7-9 it can be seen that OPG production was significantly higher on the 30% strut porosity sample in 4 out of 7 time points on both BARE and MSCGM pre-treatments. The presence of Fn was observed to significantly influence this response: after Fn1 and Fn2 pre-treatments the 20% strut porosity supported a significantly greater OPG production at 4 and 5 time points respectively.

Table 7-10 shows the statistical analysis of the CICP production: here the 30% strut porosity sample supported significantly higher collagen production compared to the 20% on BARE and MSCGM groups; after pre-treatment with Fn1 and Fn2, however, CICP production was not found significantly different between 20 and 30% strut porosity samples.

These results suggest that in normal conditions higher strut porosity enhances higher OPG and CICP production. Moreover, that the effect of microporosity is deeply influenced by the presence of Fn, which was determinant in improving the OPG production from the lower strut porosity sample (20%).

The fact that Fn was able to increase protein production from the 20% strut porosity sample rather than from the 30%, effect which was already seen also for OCN production, suggests that the activity of this protein is influenced by the microtopography of the material, in particular by its strut porosity. This could be due to the fact that Fn, in the presence of a higher presence of porous interconnectivity, can't easily assume its active (or more active) conformation which then mediate the response to the stem cells. The presence of a lower (20%) percentage of strut porosity would instead facilitate the change of conformation of Fn and, by that, indirectly stimulate a higher biological response from the cells. The hypothesis that Fn undergoes a change of conformation after contact with materials has been well reported by different studies (Grinnell and Feld, 1982) (Michael et al., 2003) (García et al., 1999b) and previously investigated in the present thesis (Chapter 4).

Blood vessel formation: VEGF production

The same effect of strut porosity seen on the production of OPG and OCN is also seen for the production of VEGF. Table 7-11 shows that, also for VEGF, the amount of the protein was significantly higher on the 30% microporosity sample compared to the 20%, after BARE and MSCGM pre-treatments; however, after pre-treatment with either Fn1 or Fn2, the amount of protein produced decreased significantly. This inhibitory effect, however, was not seen from the 20% microporosity sample.

These results suggest that, when there is no pre-treatment, a higher percentage of strut porosity supports a better cellular response than a lower strut porosity: this could be due to the fact that pores interconnectivity is

fundamental to help the formation of a vascular network, essential to support new bone formation. These results are in accordance with previous *in vivo* studies which demonstrated that faster bone apposition in microporous scaffolds with >20% strut porosity was linked to the rate of blood vessels development (Hing et al., 2005). The evidence that Fn was able to influence the cell response only from a specific material microporosity pattern (20% strut porosity) suggests that the mechanisms which undergo its activity are quite complex.

The topography of the material surface can influence the adsorption of proteins (thus their effect on cell response) in different ways: it can either be that the higher surface area, due to an increase in interconnectivity between pores, influences the quantity of the proteins adsorbed, or it can be that the different topography of the materials influences the way proteins interact and are adsorbed on its surface. Fn could, for example, need a conformational change in order to mediate the cell response between materials and cells: it could be possible that this conformational change cannot easily happen if the percentage of microporosity is too high (due to steric constrains, for example), which would consequently lead to affect only the materials with a lower percentage of microporosity (20%).

The cellular response to bioactive glass

Bioactive glasses are an extensively studied group of biomaterials which contain the silicate group along with other ionic groups. The surface reactions of these materials in biological media is initiated by the rapid loss of sodium ions from the surface and this loss of ions leads to the localized breakdown of the silica network forming silianol groups, which repolymerizes into a silica-rich porous surface layer. The loss of soluble silica from the surface of these materials has been implicated in the proliferation of osteoblasts at the surface of the glass. Bioactive glasses are infact thought to be able to stimulate bone regeneration as much as bioactive ceramics do. A lot of research is therefore currently ongoing in order to make these materials reaching their commercial potential, and a number of available present a range of compositions with varying solubility. As for bioactive ceramics, also for bioactive glasses one of the main objectives of the current research is to identify how materials' cues

and properties influence the cellular response, and the chemistry of the material is one of the most studied properties. *In vitro* studies indicate that their osteogenic properties are due to their dissolution products stimulating osteoprogenitor cells at the genetic level.

Different studies have looked at the interaction of these materials with osteoblasts *in vitro*: Silver in 2001 demonstrated that neither osteoblastic cell proliferation nor cellular metabolic activity changed significantly between three different bioactive glasses (Silver et al., 2001); Human primary osteoblasts when cultured on foamed bioglass 58S exhibited attachment, proliferation and mineralised nodule formation (Gough et al., 2004); The ionic dissolution products of Bioglass™ 45S5 (solutions containing Na, Ca, P and Si ions) when mixed with culture medium resulted in a 155% increase in proliferation of osteoblast in comparison to the control (Xynos et al., 2000); Zeolite A (sodium aluminiumsilicate) was shown to increase proliferation and differentiation when normal adult human osteoblasts-like cells were cultured on these materials (Keeting et al., 1992).

Reffitt et al (Reffitt et al., 2003b) studied the effects of soluble silicon on three forms of early osteoblastic cell lines (human osteosarcoma cell line MG63, primary osteoblast cells derived from human bone marrow stromal cells and osteoblast precursor HCCI cell line) . They demonstrated that with the addition of 5-20μM of orthosilicic acid (0.28- 0.56 μg.ml-1 Si) to the culture medium increased the production of type 1 procollagen liberated in all cell lines. The effect was highly significant in the MG-63 cell line (1.75 fold increase). However, addition of orthosilicic acid at supraphysiological levels of 50 μM (1.4 μg.ml-1 Si) lead to a smaller increase in collagen type 1 synthesis in the MG-63 and HCCI cell lines. Silicon addition to the culture at physiological levels also enhanced the production of bone formation markers such as alkaline phosphatase activity and osteocalcin synthesis.

Summary

To summarize the effect of strut porosity, from the results of this study it is clear that a lower strut porosity percentage (20%) supported better calcium release and cell proliferation, while a higher strut porosity (30%) positively

influenced cell differentiation, and synthesis of important proteins like OCN, OPG, CICP and VEGF.

7.1.1 The influence of pre-treatment with proteins

Calcium release

Figure 7-1 shows the effect of pre-treatment on the release of calcium from each sample. On HAG80/20 the BARE group showed significantly higher release of calcium compared to the other groups at 4 time points out of 7; SAG80/20 showed significantly higher Ca release from the BARE and also from the MSCGM pre-treatment group at early time points (day1 and day2). Similarly, SAG80/30 showed significantly higher Calcium release from the BARE and MSCGM groups, at day1, 4 and 10 and day1, 2 and 3 respectively.

The evidence that BARE conditioning showed a better Ca release irrespectively of chemistry and microporosity, could suggest that the presence of species pre-adsorbed at the surface of the implant negatively influence the ion release): this could potentially be a mere physical interference of the adsorbed proteins that obstacle the release of ions from the implant surface. However, the MSCGM pre-conditioning supported higher levels released only from the two SAG samples, but non from the HAG. It is possible to hypothesize that the calcium release from a surface pre-treated with MSCGM is significantly relevant only Silicate substituted HA, because of the higher protein-binding character of the silicate substituted HA.

In general it is possible to say that on HA the pre-treatment with proteins lowered calcium release, while on SA sample the pre-treatment with MSCGM equalized the effect of BARE in the release of calcium. Pre-treatments with Fn instead didn't show to enhance significantly calcium release.

Cell proliferation: DNA amount and Total Protein

Looking at the effect that pre-conditioning with proteins had on DNA amount, HAG80/20 and SAG80/20 showed a significantly higher cell proliferation only from the BARE pre-treatment group at day4 and 7 and at day1, 7 and 10 respectively (Figure 7-2). Differently, on SAG80/30 the DNA amount was found to be very similar between treatment groups, with a significantly higher value only from the Fn1 pre-treatment group at day1 and 3 (Figure 7-2c). These results suggest that the presence of additional proteins on the surface of the materials prevents the proliferative effect present in BARE conditions. However, in the presence of a higher strut porosity, the pre-treatment with sub-physiological concentrations of Fn supports a greater cell proliferation.

The total protein analyses, on the other hand, showed to be only slightly influenced by proteins. While SAG80/30 didn't show any significant difference in total protein amount between pre-treatment groups (Figure 7-3c), HAG80/20 and SAG80/20 showed a significantly higher peak from the BARE and BARE and MSCGM groups respectively (Figure 7-3a, b).
These results suggest that the total protein doesn't reflect properly the cell proliferation, as it is also suggested by the fact that the total protein peaked as early as day2 and then showed lower values until day14.

In general, SAG80/30 was found to be sensitive to sub-physiological concentrations of Fn, while there was no influence of protein pre-conditioning on samples with a lower strut porosity (HAG80/20 and SAG80/20).

Cell differentiation: ALP specific activity and Osteocalcin production

Figure 7-4 shows the ALP specific activity: on both HA and SA granules 80/20 it was significantly higher after pre-conditioning with MSCGM and Fn1 solutions (Figure 7-4a, b), while on SAG80/30 was shown to be significantly higher from the MSCGM pre-treatment group (Figure 7-4c). Moreover, ALP activity peaked earlier on silicon-substituted samples (day3) than on HA (day7).
These results support the ones of OCN production (Figure 7-5), which showed to be significantly higher after MSCGM and Fn1 pre-treatments on HAG08/20,

after Fn1 and Fn2 pre-treatments on SAG 80/20, and from BARE and MSCGM on SAG80/30. These results suggest that the pre-conditioning with Fn significantly increases ALP activity and OCN production from HAG80/20 and SAG80/20, while SAG80/30 showed significantly higher cell differentiation in either BARE conditions or after the pre-treatment with serum proteins.

Bone turnover: Osteoprotegerin and CICP production

Figure 7-6 shows that on both HAG80/20 and SAG80/20 OPG amount was significantly higher after pre-treatments with either Fn1 or Fn2; however, on SAG80/30 Fn didn't show any effect, but the BARE and the MSCGM pre-treatments showed a significant higher production of the protein (Figure 7-6c). Fn seems to play a role in mediating the influence that strut porosity has towards OPG synthesis, in particular increasing cell response on the sample with the lower microporosity (20%). Conversely, when the strut porosity increases, the presence of Fn diminishes OPG production.

Figure 7-7 shows the results for CICP production: SAG80/30 showed significantly higher protein production from the BARE and the MSCGM pre-treatment groups. A similar effect was found from SAG80/20 sample, while the CICP production from the HAG80/20 was significantly higher from the BARE and Fn2 pre-treatment groups. Moreover, all the samples showed the same trend of collagen production over time, with peak of CICP production as early as day3 and after a slightly lower level of protein production. These results suggest, again, that Fn supports a better cell response only from granules with a lower strut porosity (20%), and that a strut porosity of 30% shows to perform better without the presence of either serum proteins or Fn pre-conditionings.

Blood vessel formation: VEGF production

Figure 7-8 shows that Fn played an important role in enhancing VEGF production from the HA and SA 80/20 granules compared to the other pre-treatment groups. However, on SAG80/30 VEGF production was higher from the BARE group (Figure 7-8c), and also was found to be the highest VEGF amount between the three samples.

These results suggest that Fn plays a significant role in mediating the effect of material properties on cell response only on the lower strut porosity samples (20%). The fact that the highest VEGF production was still seen from the SAG80/30 sample, suggests that the strut porosity is the property of the material which plays a bigger role compared to chemistry.

These results, moreover, reflect the same effect seen for the OPG, OCN and CICP production and ALP specific activity, suggesting that the presence of the silicon, together with a high strut porosity is able to mediate a higher biological activity *in vitro*.

Summary

The **Error! Reference source not found.** summarizes how material properties (chemistry and microporosity) and pre-treatments influenced the different cell markers analysed in the present study. These results show that the effect of proteins pre-treatments resulted following two different trends: in one, which was seen on calcium release and on cell proliferation, the serum proteins and Fn1 pre-treatments enhanced the cell response on the sample with the highest strut porosity SAG80/30. The second, which was seen for OCN, OPG, CICP and VEGF production, showed that Fn pre-treatments support greater cellular response on HA and SA 80/20 granules, while SAG80/30 shows a higher cell response in BARE conditions.

Table 7-12: Summary of the effects of conditions and parameters that had a positive effect on cell behaviour

	Pre-treatment	Chemistry	Microporosity
Ca	BARE	HA	20%
DNA	BARE		20%
ALP	MSCGM	HA	30%
OCN	MSCGM, Fn1, Fn2	HA (BARE, MSCGM) SA (Fn1, Fn2)	30% (BARE, MSCGM) 20% (Fn1, Fn2)

OPG	Fn2, BARE		30% (BARE, MSCGM) 20% (Fn1, Fn2)
CICP	BARE, MSCGM, Fn2		30% (BARE, MSCGM)
VEGF	Fn2, BARE		30% (BARE, MSCGM) 20% (Fn1, Fn2)

These results therefore suggest that the presence of a protein layer of either serum proteins or serum proteins with Fn, is able to improve cell proliferation on SAG80/30 and cell differentiation on HA and SA 80/20 granules, while the higher biological activity shown by the SAG80/30 sample is not entirely mediated by the presence of this protein layer.

7.2 Conclusions

To summarize, the present results showed that chemistry plays a secondary role in influencing cell response, where a higher effect on ALP activity, OCN production and calcium release was found from the HA chemistry.The higher percentage of strut porosity responded better than the lower one, especially in terms of cell differentiation and proteins production. Furthermore, Fn showed to be able to positively influence cell response only on granules with a 20% strut porosity, irrespectively by the chemistry.

8 Executive Summary and Future Work

8.1 Executive Summary

8.1.1 Material properties

The effect of material chemistry, morphology and strut porosity influenced differently the response of Fn adsorption and cell attachment, proliferation and differentiation.

The following tables (Table 8-1, Table 8-2) summarize how chemistry and microporosity influenced Fn adsorption, and cell attachment, proliferation and differentiation in dependence of different pre-treatments.

Chemistry:

Table 8-1: The effect of chemistry on Fn adsorption and cell response in dependence of pre-treatments

	Fn Adsorption	**Cell Attachment**	**Cell Proliferation**	**Cell Differentiation**
BARE	-	=	=	HA
MSCGM	-	=	=	HA
Fn1	=	SA	=	HA (ALP) SA (OCN)
Fn2	SA	=	SA	HA (ALP) SA (OCN)

Microporosity:

Table 8-2: The effect of microporosity on Fn adsorption and cell response in dependence of pre-treatments

	Fn Adsorption	**Cell Attachment**	**Cell Proliferation**	**Cell Differentiation**

BARE	-	30%	20%	30%
MSCGM	-	30%	20%	30%
Fn1	=	20%	=	30% (ALP) 20% (OCN)
Fn2	=	20%	=	30% (ALP) 20% (OCN)

The presence of the silicon was found to favour Fn adsorption but only in non competitive conditions, and cell attachment only if Fn was present as a pre-treatment in particular concentrations. The stoichiometric HA chemistry was actually found to promote a greater cell response in terms of differentiation. The morphology of the materials was found to influence strongly the responses: the PG always performed better in terms of Fn adsorption and cell attachment compared to DD, and, as the response between DD and PG and between samples with same chemistry but different surface roughness was found to be significantly different, it is suggested that in *in vitro* studies aimed to clarify the mechanisms of actions of the biological response to bone grafts biomaterials, should always use samples that resemble as closely as possible the actual bone grafts morphology/topography used in the market. The strut porosity showed to be a relevant factor in mediating the bone grafts biological response: a higher percentage of strut porosity seemed to promote a better cell attachment and stem cell differentiation towards the osteoblast lineage, without the use of any protein pre-treatment. Differently, a lower strut porosity percentage supported a better cell attachment and cell response only after pre-treatment with Fn and serum proteins.

8.1.2 The Role of Fn

The role of Fn in mediating the effects of bone grafts material properties in the biological response *in vitro,* showed to be dependent by different factors.

Firstly, its adsorption on the surface of the materials showed to be dependent by its own concentration, suggesting that in *in vitro* studies aimed to clarify its mechanisms of actions should always be used physiological concentration of this protein. Secondly, its adsorption was also found to be dependent by the simultaneous presence of other protein species: its adsorption on the surface on the materials was diminished by their presence, suggesting a possible competition at the binding sites which should be taken into consideration when performing *in vitro* Fn assessment studies. Thirdly, even if its adsorption showed to be non dependent by material strut porosity, its pre-treatment on 20 and 30% strut porosity bone grafts influenced differently the cellular response. This evidence, together with the confirmation of a change in the protein secondary structure after contact with either HA or SA samples, suggests that sterical effects can be involved in the Fn-mediated bone grafts cell response, and that it is possible to hypothesize that it's the protein's conformation (quality) rather than its quantity to affect bone grafts biological response.

8.1.3 Study Limitations

One of the limitations of the present study regards the protein conformation analysis done on Fn using Circular Dichroism technique. This analysis was performed on Fn solution after contact with the materials, but not on the protein actually adsorbed on their surfaces. Unfortunately this technique enables to analyse conformational properties only from proteins in clear solutions, and there are not alternative techniques that enable a quick and easy conformational change analysis like CD.

Another study limitation is the fact that the effect of chemistry and roughness of the materials on cellular response, whose experiments are described in Chapter 6, was only analysed at one time point. This didn't allow the analysis of any possible effect of chemistry, roughness, or their combined effect on the timing of the cellular response. Moreover there are possibilities that the highest expression of relevant cell markers were missed because didn't necessarily happen at day 7. For this reason, and to enable a better understanding of material's properties on cellular response, the next experimental studies (Chapter 7) were carried out on a period as long as 14-days, enabling the analysis at seven different time-points.

Another study limitation regards the cell study set up. Experiments were carried out in static conditions, which could mislead the effect that the material properties analysed have in a real physiological environment to the cellular resonse. It has infact been established that mechanical stimuli, constant hoxygen and nutrient supply, and other physiological cues that can only be reproduced by dynamic cell culture conditions, are a more realistic representation of the real physiological environment.

8.2 Future Work

The results of this study further highlight the complex and intriguing dependence of the cellular response to both organic (proteins) and inorganic (bone grafts material properties) cues when in contact with BGS. The evidence of these findings opens the doors to the need to further analyze this dependence firstly, *in vitro*, and subsequently *in vivo*.

- Further work is required to determine whether the cellular attachment of HMSC to SA and HA porous granules chemistry and strut porosity shows the same trends seen from the MG63 osteoblasts-like cells.

- The role of serum proteins in mediating the cellular response to bone graft substitutes should be further investigated. For this purpose, cell culture in a serum-free media could help to define more precisely which proteins are involved in modulating the cellular response, and which are the mechanisms of actions of this modulation.

- The study of the biological response could be further investigated by extending cell culture experiments to multiple time points.

- Further cell morphology studies are required in order to elucidate how material properties influence the cells' shape, and if and how this has an effect on the cellular response

- Additional cellular markers could be analysed to clarify further the biological response to BGS. For example the analysis of markers involved in the physiological inflammatory response during bone

healing (such as IL-6, IL-8, TNF-α) could be useful to determine wether or not BSG are able to influence this process.

- Finally, many studies show the increasing evidence of a need to reproduce *in vitro* an environment which resemble the *in vivo* conditions as close as possible: for this reason it is essential to try to develop any further *in vitro* work in dynamic (or at least, semi-dynamic) conditions

9 Appendix

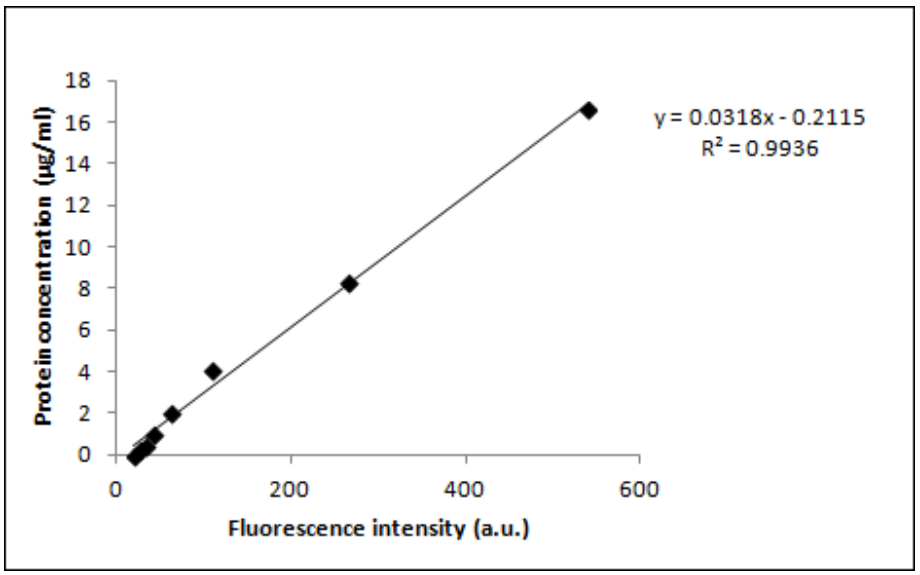

Figure 9-1: Calibration curve of several dilutions of SR101-Fn in MEM solution, from 0 to 16.65 µg/ml of protein concentration

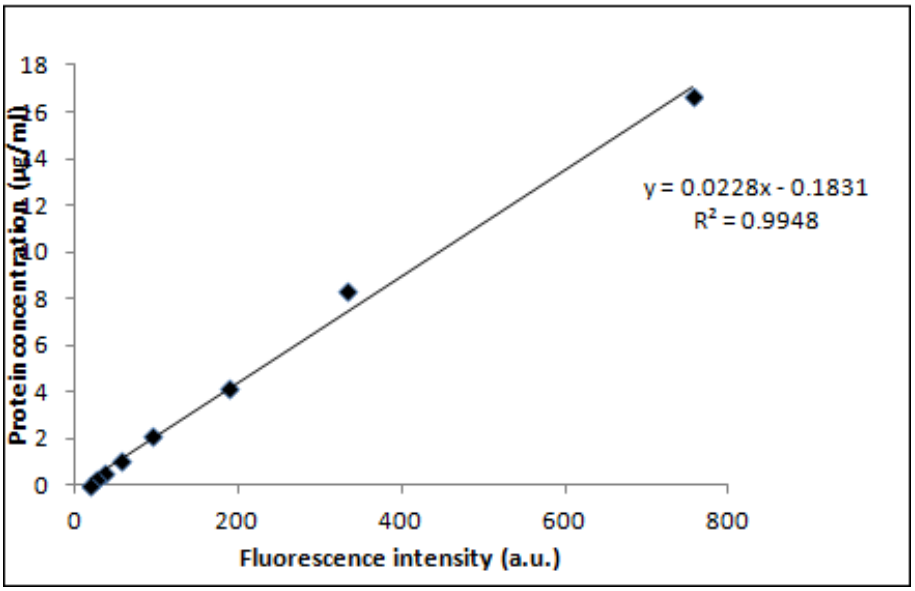

Figure 9-2: Calibration curve of several dilutions of SR101-Fn in MEM+10% of FCS solution, from 0 to 16.6 µg/ml of protein concentration

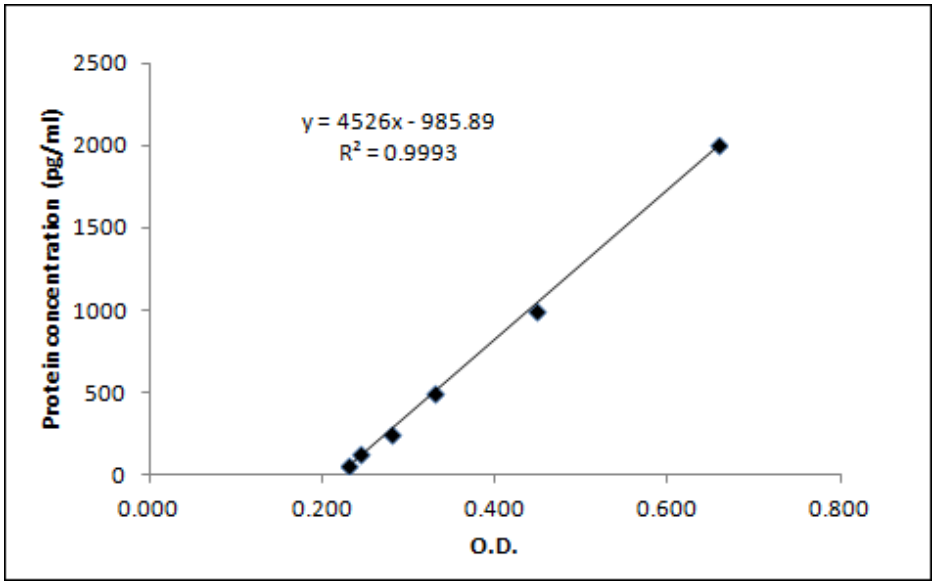

Figure 9-3: Calibration curve of OPG amount versus optical density at Day 2

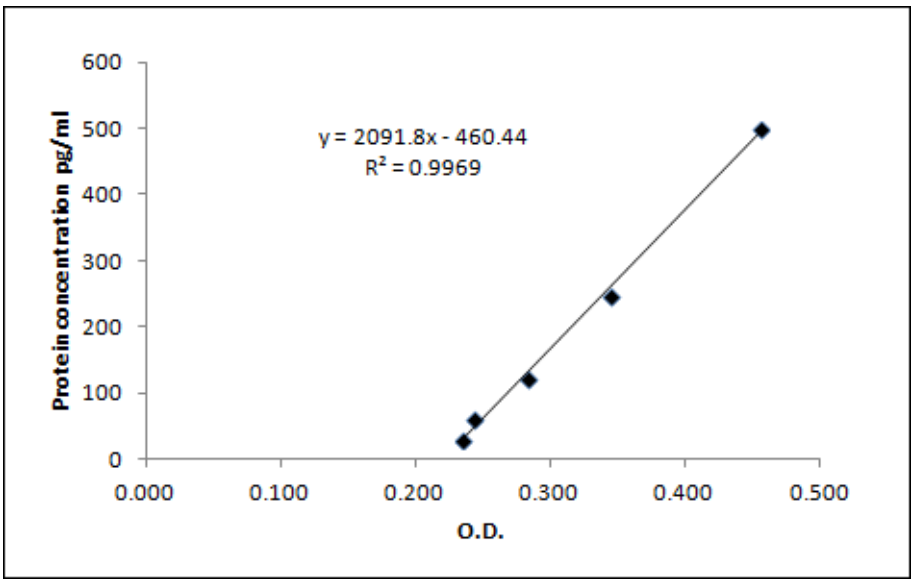

Figure 9-4: Calibration curve of VEGF amount versus optical density

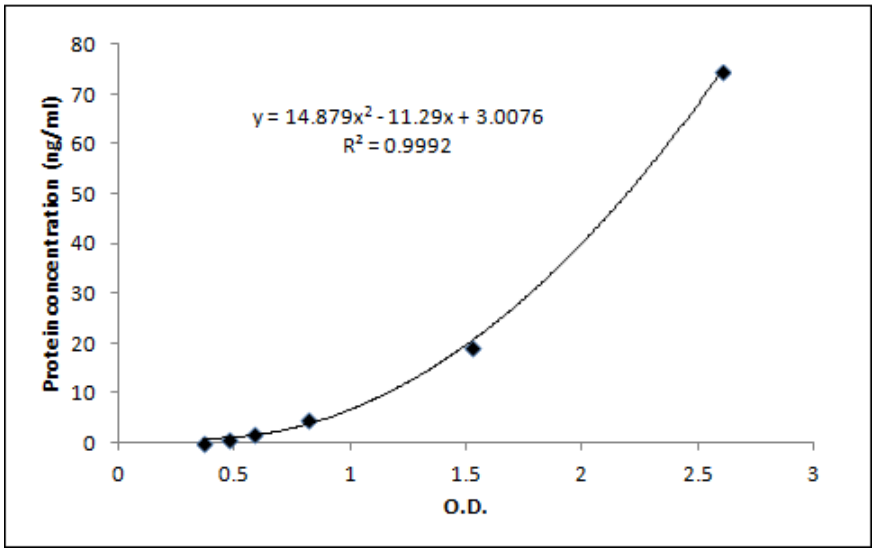

Figure 9-5: Calibration curve of CICP amount versus optical density

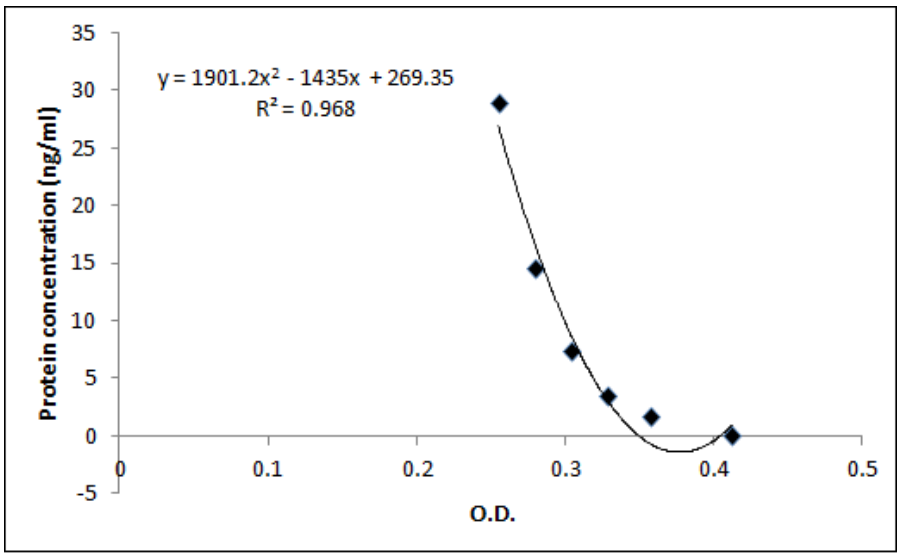

Figure 9-6: ***Calibration curve of OCN amount versus optical density***

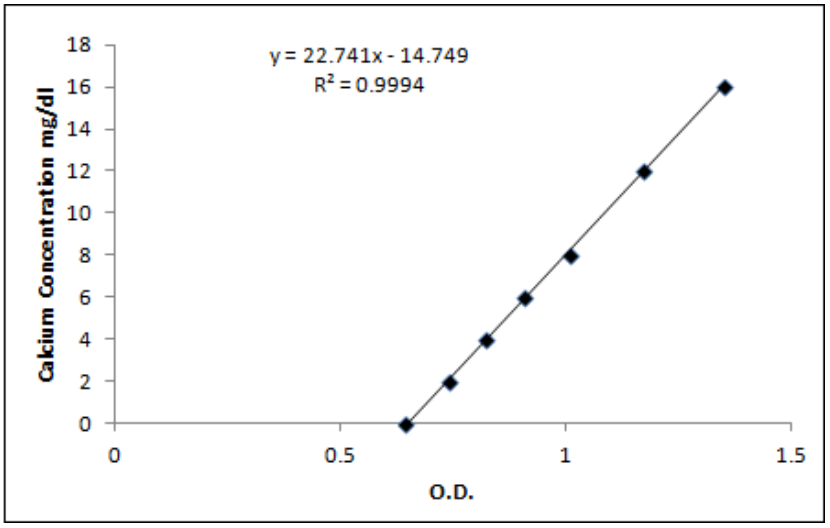

Figure 9-7: Calibration curve of Ca amount versus optical density

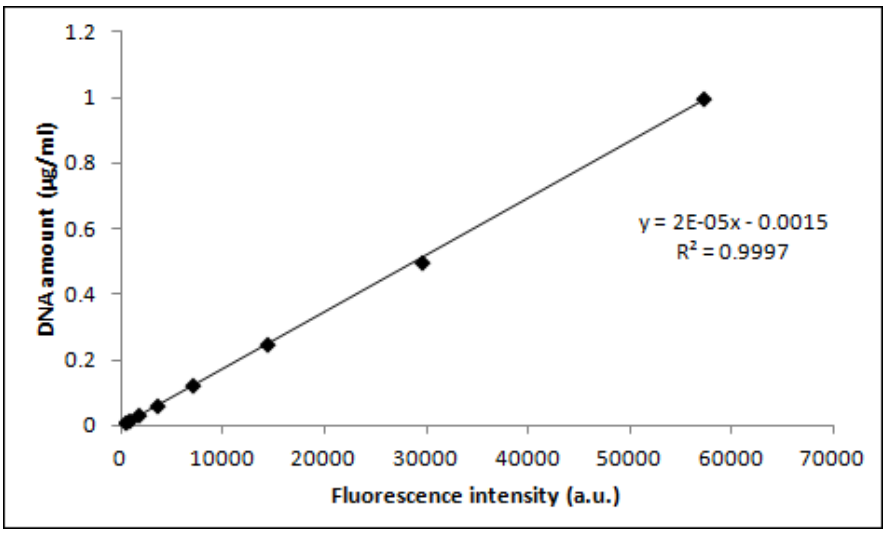

Figure 9-8: Calibration curve of DNA amount versus fluorescence intensity

10 Bibliography

Abiko, O. (2004). Differentiation of the human mesenchymal stem cells derived from bone marrow and enhancement of cell attachment by fibronectin. Journal of Oral Science *46*, 207–213.

Akao, M., Aoki, H., and Kato, K. (1981). Mechanical properties of sintered hydroxyapatite for prosthetic applications. Journal of Materials Science *16*, 809–812.

Albelda, S.M., and Buck, C.A. (1990). Integrins and other cell adhesion molecules. FASEB J *4*, 2868–2880.

Albrektsson, T., and Johansson, C. (2001). Osteoinduction, osteoconduction and osseointegration. European Spine Journal *10*, S96–S101.

Altankov, G., and Groth, T. (1994). Reorganization of substratum-bound fibronectin on hydrophilic and hydrophobic materials is related to biocompatibility. J Mater Sci: Mater Med *5*, 732–737.

Anderson, H.C. (2003). Matrix vesicles and calcification. Current Rheumatology Reports *5*, 222–226.

Annaz, B., Hing, K., Kayser, M., Buckland, T., and Di Silvio, L. (2004). Porosity variation in hydroxyapatite and osteoblast morphology: a scanning electron microscopy study. JOURNAL OF MICROSCOPY-OXFORD *215*, 100–110.

Anselme, K. (2000). Osteoblast adhesion on biomaterials. Biomaterials *21*, 667–681.

Van Apeldoorn, A., Aksenov, Y., Stigter, M., Hofland, I., De Bruijn, J., Koerten, H., Otto, C., Greve, J., and Van Blitterswijk, C. (2005). Parallel high-resolution confocal Raman SEM analysis of inorganic and organic bone matrix constituents. Journal of The Royal Society Interface *2*, 39–45.

Arcos, D., Greenspan, D., and Vallet-Regi, M. (2002). Influence of the stabilization temperature on textural and structural features and ion release in SiO2-CaO-P2O5 sol-gel glasses. Chemistry of Materials *14*, 1515–1522.

Arrington, E.D., Smith, W.J., Chambers, H.G., Bucknell, A.L., and Davino, N.A. (1996). Complications of iliac crest bone graft harvesting. Clinical Orthopaedics and Related Research *329*, 300–309.

Bagambisa, F.B., Kappert, H.F., and Schilli, W. (1994a). Cellular and molecular biological events at the implant interface. Journal of Cranio-Maxillofacial Surgery *22*, 12–17.

Bagambisa, F.B., Kappert, H.F., and Schilli, W. (1994b). Cellular and molecular biological events at the implant interface. Journal of Cranio-Maxillofacial Surgery *22*, 12–17.

Balas, F., Pérez-Pariente, J., and Vallet-Regí, M. (2003). In vitro bioactivity of silicon-substituted hydroxyapatites. Journal of Biomedical Materials Research Part A *66A*, 364–375.

Balasubramaniam, R. (2007). Callister'S Materials Science And Engineering: Indian Adaptation (W/Cd) (John Wiley & Sons).

Barkmeier, W.W., Gwinnett, A.J., and Shaffer, S.E. (1985). Effects of enamel etching time on bond strength and morphology. Journal of Clinical Orthodontics: JCO *19*, 36.

Baron, M., Main, A.L., Driscoll, P.C., Mardon, H.J., Boyd, J., and Campbell, I.D. (1992). Proton NMR assignment and secondary structure of the cell adhesion type III module of fibronectin. Biochemistry *31*, 2068–2073.

Bauer, T.W., and Muschler, G.F. (2000). Bone graft materials: an overview of the basic science. Clinical Orthopaedics and Related Research *371*, 10–27.

Beer, A. (1852). Bestimmung der Absorption des rothen Lichts in farbigen Flüssigkeiten. Annalen Der Physik *162*, 78–88.

Best, S., Sim, B., Kayser, M., and Downes, S. (1997). The dependence of osteoblastic response on variations in the chemical composition and physical properties of hydroxyapatite. Journal of Materials Science: Materials in Medicine *8*, 97–103.

Bignon, A., Chouteau, J., Chevalier, J., Fantozzi, G., Carret, J.-P., Chavassieux, P., Boivin, G., Melin, M., and Hartmann, D. (2003). Effect of micro- and macroporosity of bone substitutes on their mechanical properties and cellular response. Journal of Materials Science: Materials in Medicine *14*, 1089–1097.

Bodhak, S., Bose, S., and Bandyopadhyay, A. (2009). Role of surface charge and wettability on early stage mineralization and bone cell–materials interactions of polarized hydroxyapatite. Acta Biomaterialia *5*, 2178–2188.

Bonewald, L.F. (1999). Establishment and characterization of an osteocyte-like cell line, MLO-Y4. Journal of Bone and Mineral Metabolism *17*, 61–65.

Bonewald, L., and Mundy, G. (1990). Role of transforming growth factor-beta in bone remodeling. Clinical Orthopaedics and Related Research *250*, 261–276.

Borsari, V., Giavaresi, G., Fini, M., Torricelli, P., Salito, A., Chiesa, R., Chiusoli, L., Volpert, A., Rimondini, L., and Giardino, R. (2005). Physical characterization of different-roughness titanium surfaces, with and without hydroxyapatite coating, and their effect on human osteoblast-like cells. Journal of Biomedical Materials Research Part B: Applied Biomaterials *75*, 359–368.

Botelho, C. M., Lopes, M. A., Gibson, I. R., Best, S. M., and Santos, J. D. (2002). Structural analysis of Si-substituted hydroxyapatite: zeta potential and X-ray photoelectron spectroscopy. Journal of Materials Science: Materials in Medicine *13*, 1123–1127.

Botelho, C. M., Brooks, R.A., Kawai, T., Ogata, S., Ohtsuki, C., Best, S. M., Lopes, M. A., Santos, J.D., Rushton, N., and Bonfield, W. (2005a). In vitro analysis of protein adhesion to phase pure hydroxyapatite and silicon substituted hydroxyapatite. Key Engineering Materials *284*, 461–464.

Botelho, C. M., Brooks, R. A., Best, S. M., Lopes, M. A., Santos, J. D., Rushton, N., and Bonfield, W. (2006). Human osteoblast response to silicon-substituted hydroxyapatite. Journal of Biomedical Materials Research Part A *79A*, 723–730.

Botelho, C.M., Brooks, R.A., Best, S.M., Lopes, M.A., Santos, J.D., Rushton, N., and Bonfield, W. (2004). Biological and Physical-Chemical Characterization of Phase Pure HA and SI-Substituted Hydroxyapatite by Different Microscopy Techniques. Key Engineering Materials *254-256*, 845–848.

Botelho, C.M. da C.F., da Silva Santos, J.D., Lopes, M.A.F., and Porto, U. do (2005b). Silicon-substituted hydroxyapatite for biomedical applications.

Boyan, B.D., Hummert, T.W., Dean, D.D., and Schwartz, Z. (1996). Role of material surfaces in regulating bone and cartilage cell response. Biomaterials *17*, 137–146.

Boyce, T., Edwards, J., and Scarborough, N. (1999). Allograft bone: the influence of processing on safety and performance. Orthopedic Clinics of North America *30*, 571–581.

Brahms, S., and Brahms, J. (1980). Determination of protein secondary structure in solution by vacuum ultraviolet circular dichroism. Journal of Molecular Biology *138*, 149–178.

Brash, J.L., and Horbett, T.A. (1995). Proteins at interfaces. (ACS Publications), pp. 1–25.

Brodsky, B., and Persikov, A.V. (2005). Molecular structure of the collagen triple helix. Advances in Protein Chemistry *70*, 301–339.

Brown, K.L., and Cruess, R.L. (1982). Bone and cartilage transplantation in orthopaedic surgery. A review. The Journal of Bone and Joint Surgery. American Volume *64*, 270.

Bruck, S. (1979). The behavior of three different types of materials in vitro and in the dynamic physiological environment: review and analyses of critical parameters. The International Journal of Artificial Organs *2*, 31–34.

Bruijn, J. d, Dalmeijer, R., and Groot, K. d (1999). Osteoinduction by microstructured calcium phosphates. In ANNUAL MEETING-SOCIETY FOR BIOMATERIALS IN CONJUNCTION WITH THE INTERNATIONAL BIOMATERIALS SYMPOSIUM, pp. 235–235.

Brunauer, S., Emmett, P.H., and Teller, E. (1938). Adsorption of gases in multimolecular layers. Journal of the American Chemical Society *60*, 309–319.

Buck, B., Malinin, T.I., and Brown, M.D. (1989). Bone transplantation and human immunodeficiency virus: an estimate of risk of acquired immunodeficiency syndrome (AIDS). Clinical Orthopaedics and Related Research *240*, 129–136.

Burchardt, H. (1987). Biology of bone transplantation. The Orthopedic Clinics of North America *18*, 187–196.

Burge, R.T., Worley, D., Johansen, A., Bhattacharyya, S., and Bose, U. (2001). The cost of osteoporotic fractures in the UK: Projections for 2000-2020. Journal of Medical Economics *4*, 51–62.

Burr, D. (2002). Targeted and nontargeted remodeling. Bone *30*, 2–4.

Buser, D., Broggini, N., Wieland, M., Schenk, R., Denzer, A., Cochran, D., Hoffmann, B., Lussi, A., and Steinemann, S. (2004). Enhanced bone apposition to a chemically modified SLA titanium surface. Journal of Dental Research *83*, 529–533.

Campion, C.R., Chander, C., Buckland, T., and Hing, K. (2011). Increasing strut porosity in silicate-substituted calcium-phosphate bone graft substitutes enhances osteogenesis. Journal of Biomedical Materials Research Part B: Applied Biomaterials *97B*, 245–254.

Cantor, C.R. (1980). Biophysical chemistry: Part II: Techniques for the study of biological structure and function (Macmillan).

Carano, R.A., and Filvaroff, E.H. (2003). Angiogenesis and bone repair. Drug Discovery Today *8*, 980–989.

Carlisle, E.M. (1970). Silicon: a possible factor in bone calcification. Science *167*, 279–280.

Carlisle, E.M. (1972). Silicon: an essential element for the chick. Science *178*, 619–621.

Carlisle, E.M. (1978). Essentiality and function of silicon. In Biochemistry of Silicon and Related Problems, (Springer), pp. 231–253.

Carlisle, E.M. (1981). Silicon: a requirement in bone formation independent of vitamin D1. Calcified Tissue International *33*, 27–34.

Carsons, S.E. (1989). Fibronectin in health and disease (CRC Press).

Cazalbou, S., Combes, C., Eichert, D., and Rey, C. (2004). Adaptative physico-chemistry of bio-related calcium phosphates. Journal of Materials Chemistry *14*, 2148–2153.

Center for History and New Media Zotero Quick Start Guide.

Cerroni, L., Filocamo, R., Fabbri, M., Piconi, C., Caropreso, S., and Condò, S.. (2002). Growth of osteoblast-like cells on porous hydroxyapatite ceramics: an in vitro study. Biomolecular Engineering *19*, 119–124.

Chan, O., Coathup, M.J., Nesbitt, A., Ho, C.-Y., Hing, K.A., Buckland, T., Campion, C., and Blunn, G.W. (2012). The effects of microporosity on osteoinduction of calcium phosphate bone graft substitute biomaterials. Acta Biomaterialia *8*, 2788 – 2794.

Chaves, M.D., de Souza Nunes, L.S., de Oliveira, R.V., Holgado, L.A., Matsumoto, M.A., Ribeiro, D.A., and others (2012). Bovine hydroxyapatite (Bio-Oss< sup>®</sup>) induces osteocalcin, RANK-L and osteoprotegerin expression in sinus lift of rabbits. Journal of Cranio-Maxillofacial Surgery *40*, e315–e320.

Chen, J.-T., Hosoda, K., Hasumi, K., Ogata, E., and Shiraki, M. (1996). Serum N-terminal osteocalcin is a good indicator for estimating responders to hormone replacement therapy in postmenopausal women. Journal of Bone and Mineral Research *11*, 1784–1792.

Chen, P., Satterwhite, J.H., Licata, A.A., Lewiecki, E.M., Sipos, A.A., Misurski, D.M., and Wagman, R.B. (2005). Early changes in biochemical markers of bone formation predict BMD response to teriparatide in postmenopausal women with osteoporosis. Journal of Bone and Mineral Research *20*, 962–970.

Chou, L., Firth, J.D., Uitto, V.J., and Brunette, D.M. (1995). Substratum surface topography alters cell shape and regulates fibronectin mRNA level, mRNA stability, secretion and assembly in human fibroblasts. J Cell Sci *108*, 1563–1573.

Christophy, C., Rashid, N., DiSilvio, L., and Hing, K.A. (2009). Encouraging nature with ceramics: The roles of surface roughness and physio-chemistry on cell response to substituted apatites. Advances in Science and Technology *57*, 22–30.

Clover, J., Dodds, R.A., and Gowen, M. (1992). Integrin subunit expression by human osteoblasts and osteoclasts in situ and in culture. J. Cell. Sci. *103 (Pt 1)*, 267–271.

Coathup, M.J., Samizadeh, S., Fang, Y.S., Buckland, T., Hing, K.A., and Blunn, G.W. (2011). The osteoinductivity of silicate-substituted calcium phosphate. The Journal of Bone & Joint Surgery *93*, 2219–2226.

Coathup, M.J., Hing, K.A., Samizadeh, S., Chan, O., Fang, Y.S., Campion, C., Buckland, T., and Blunn, G.W. (2012). Effect of increased strut porosity of calcium phosphate bone graft substitute biomaterials on osteoinduction. Journal of Biomedical Materials Research Part A *100A*, 1550–1555.

Cohen, B.E., McAnaney, T.B., Park, E.S., Jan, Y.N., Boxer, S.G., and Jan, L.Y. (2002). Probing protein electrostatics with a synthetic fluorescent amino acid. Science *296*, 1700–1703.

Conget, P.A., and Minguell, J.J. (1999). Phenotypical and functional properties of human bone marrow mesenchymal progenitor cells. Journal of Cellular Physiology *181*, 67–73.

Coombes, A., and Meikle, M. (1994). Resorbable synthetic polymers s replacements for bone graft. Clinical Materials *17*, 35–67.

Costa-Rodrigues, J., Fernandes, A., Lopes, M.A., and Fernandes, M.H. (2012). Hydroxyapatite surface roughness: Complex modulation of the osteoclastogenesis of human precursor cells. Acta Biomaterialia *8*, 1137 – 1145.

COVENTRY, M.B., and TAPPER, E.M. (1972). Pelvic instability a consequence of removing iliac bone for grafting. The Journal of Bone & Joint Surgery *54*, 83–101.

Cowley, S., and Anderson, L. (1983). Hernias through donor sites for iliac-bone grafts. J Bone Joint Surg Am *65*, 1023–1025.

De Crombrugghe, B., Lefebvre, V., and Nakashima, K. (2001). Regulatory mechanisms in the pathways of cartilage and bone formation. Current Opinion in Cell Biology *13*, 721–728.

Culav, E.M., Clark, C.H., and Merrilees, M.J. (1999). Connective tissues: matrix composition and its relevance to physical therapy. Physical Therapy *79*, 308–319.

Cummings, S.R., and Melton, L.J. (2002). Epidemiology and outcomes of osteoporotic fractures. The Lancet *359*, 1761–1767.

Curtis, A.S.G., and Wilkinson, C.D.W. (1998). Reactions of cells to topography. Journal of Biomaterials Science, Polymer Edition *9*, 1313–1329.

Damien, C.J., and Parsons, J.R. (1991). Bone graft and bone graft substitutes: a review of current technology and applications. Journal of Applied Biomaterials *2*, 187–208.

Deckers, M.M., van Bezooijen, R.L., van der Horst, G., Hoogendam, J., van der Bent, C., Papapoulos, S.E., and Löwik, C.W. (2002). Bone morphogenetic proteins stimulate angiogenesis through osteoblast-derived vascular endothelial growth factor A. Endocrinology *143*, 1545–1553.

Delaissé, J.-M., Andersen, T.L., Engsig, M.T., Henriksen, K., Troen, T., and Blavier, L. (2003). Matrix metalloproteinases (MMP) and cathepsin K contribute differently to osteoclastic activities. Microscopy Research and Technique *61*, 504–513.

Deligianni, D., Korovessis, P., Porte-Derrieu, M.C., and Amedee, J. (2005). Fibronectin Preadsorbed on Hydroxyapatite Together With Rough Surface Structure Increases Osteoblasts' Adhesion "In Vitro": The Theoretical Usefulness of Fibronectin Preadsorption on Hydroxyapatite to Increase Permanent Stability and Longevity in Spine Implants. Journal of Spinal Disorders & Techniques *18*.

DeLise, A., Fischer, L., and Tuan, R. (2000). Cellular interactions and signaling in cartilage development. Osteoarthritis and Cartilage *8*, 309–334.

Dennis, J., Haynesworth, S., Young, R., and Caplan, A. (1992). Osteogenesis in marrow-derived mesenchymal cell porous ceramic composites transplanted subcutaneously: effect of fibronectin and laminin on cell retention and rate of osteogenic expression. Cell Transplantation *1*, 23.

Desai, B.M. (2007). Osteobiologics. American Journal of Orthopedics (Belle Mead, NJ) *36*, 8–11.

Desai, T.A. (2000). Micro-and nanoscale structures for tissue engineering constructs. Medical Engineering & Physics *22*, 595–606.

Duan, C., Liu, J., Yuan, Z., Meng, G., Yang, X., Jia, S., Zhang, J., and Chen, S. (2012). Adenovirus-mediated transfer of VEGF into marrow stromal cells combined with PLGA/TCP scaffold increases vascularization and promotes bone repair in vivo.

Ducheyne, P. (1987). Bioceramics: material characteristics versus in vivo behavior. Journal of Biomedical Materials Research *21*, 219–236.

Ducheyne, P., and Qiu, Q. (1999). Bioactive ceramics: the effect of surface reactivity on bone formation and bone cell function. Biomaterials *20*, 2287 – 2303.

Ducheyne, P., Radin, S., and King, L. (1993). The effect of calcium phosphate ceramic composition and structure on in vitro behavior. I. Dissolution. Journal of Biomedical Materials Research *27*, 25–34.

Ebeling, P.R., Atley, L.M., Guthrie, J.R., Burger, H.G., Dennerstein, L., Hopper, J.L., and Wark, J.D. (1996). Bone turnover markers and bone density across the menopausal transition. The Journal of Clinical Endocrinology and Metabolism *81*, 3366–3371.

El-Ghannam, A. (2005). Bone reconstruction: from bioceramics to tissue engineering.

El-Ghannam, A., Ducheyne, P., and Shapiro, I.M. (1999). Effect of serum proteins on osteoblast adhesion to surface-modified bioactive glass and hydroxyapatite. Journal of Orthopaedic Research *17*, 340–345.

Emad, B., Sherif, E.-M., Basma, G.M., Wong, R.W., Bendeus, M., and Rabie, A.B.M. (2006). Vascular endothelial growth factor augments the healing of demineralized bone matrix grafts. International Journal of Surgery *4*, 160–166.

Endres, S., Wilke, M., Knöll, P., Frank, H., Kratz, M., Windler, M., and Wilke, A. (2005). [Comparative in vitro analysis of vacuum plasma-sprayed titanium implants–evaluation of OPG, Osteokalzin and AP expression]. Zeitschrift Fur Orthopadie Und Ihre Grenzgebiete *144*, 632–638.

Eriksen, E.F. (1986). Normal and Pathological Remodeling of Human Trabecular Bone: Three Dimensional Reconstruction of the Remodeling Sequence in Normals and in Metabolic Bone Disease*. Endocrine Reviews *7*, 379–408.

Eriksen, E.F., Axelrod, D.W., and Melsen, F. (1994). Bone histomorphometry (Raven Press New York).

Fabrizius-Homan, D.J., and Cooper, S.L. (1991). Competitive adsorption of vitronection with albumin, fibrinogen, and fibronectin on polymeric biomaterials. Journal of Biomedical Materials Research *25*, 953–971.

Fellah, B.H., Gauthier, O., Weiss, P., Chappard, D., and Layrolle, P. (2008). Osteogenicity of biphasic calcium phosphate ceramics and bone autograft in a goat model. Biomaterials *29*, 1177–1188.

Feng, J., Chong, M., Chan, J., Zhang, Z., Teoh, S.H., and San Thian, E. (2013). A scalable approach to obtain mesenchymal stem cells with osteogenic potency on apatite microcarriers. Journal of Biomaterials Applications 0885328213515734.

Fielding, G., and Bose, S. (2013). SiO2 and ZnO dopants in three-dimensionally printed tricalcium phosphate bone tissue engineering scaffolds enhance osteogenesis and angiogenesis in vivo. Acta Biomaterialia *9*, 9137 – 9148.

Fujisawa, R., Mizuno, M., Nodasaka, Y., and Yoshinori, K. (1997). Attachment of osteoblastic cells to hydroxyapatite crystals by a synthetic peptide (Glu< sub> 7</sub>-Pro-Arg-Gly-Asp-Thr) containing two functional sequences of bone sialoprotein. Matrix Biology *16*, 21–28.

Galbraith, C.G., Yamada, K.M., and Sheetz, M.P. (2002). The relationship between force and focal complex development. The Journal of Cell Biology *159*, 695–705.

García, A.J., Vega, M.D., and Boettiger, D. (1999). Modulation of cell proliferation and differentiation through substrate-dependent changes in fibronectin conformation. Mol. Biol. Cell *10*, 785–798.

Gauthier, O., Bouler, J.-M., Aguado, E., Legeros, R., Pilet, P., and Daculsi, G. (1999). Elaboration conditions influence physicochemical properties and in vivo bioactivity of macroporous biphasic calcium phosphate ceramics. Journal of Materials Science: Materials in Medicine *10*, 199–204.

Geesink, R.G. (2002). Osteoconductive coatings for total joint arthroplasty. Clinical Orthopaedics and Related Research *395*, 53–65.

Geiger, F., Bertram, H., Berger, I., Lorenz, H., Wall, O., Eckhardt, C., Simank, H.-G., and Richter, W. (2005). Vascular Endothelial Growth Factor Gene-Activated Matrix (VEGF165-GAM) Enhances Osteogenesis and Angiogenesis in Large Segmental Bone Defects. Journal of Bone and Mineral Research *20*, 2028–2035.

Genetos, W. (2012). Modulation of osteogenic differentiation in hMSCs cells by submicron topographically-patterned ridges and grooves. Biomaterials *33*, 128–136.

George, E.L., Georges-Labouesse, E.N., Patel-King, R.S., Rayburn, H., and Hynes, R.O. (1993). Defects in mesoderm, neural tube and vascular development in mouse embryos lacking fibronectin. Development *119*, 1079–1091.

Gerber, H.-P., Vu, T.H., Ryan, A.M., Kowalski, J., Werb, Z., and Ferrara, N. (1999). VEGF couples hypertrophic cartilage remodeling, ossification and angiogenesis during endochondral bone formation. Nature Medicine *5*, 623–628.

Ghanaati, S., Barbeck, M., Detsch, R., Deisinger, U., Hilbig, U., Rausch, V., Sader, R., Unger, R.E., Ziegler, G., and Kirkpatrick, C.J. (2012). The chemical composition of synthetic bone substitutes influences tissue reactions in vivo: histological and histomorphometrical analysis of the cellular inflammatory response to hydroxyapatite, beta-tricalcium phosphate and biphasic calcium phosphate ceramics. Biomedical Materials *7*, 015005.

Giacomelli, C.E., and Norde, W. (2001). The adsorption–desorption cycle. Reversibility of the BSA–silica system. Journal of Colloid and Interface Science *233*, 234–240.

Giannoudis, P.V., Dinopoulos, H., and Tsiridis, E. (2005). Bone substitutes: An update. Injury *36*, S20–S27.

Gibson, I. R., and Bonfield, W. (2002). Preparation and characterization of magnesium/carbonate co-substituted hydroxyapatites. Journal of Materials Science: Materials in Medicine *13*, 685–693.

Gibson, I. R., Best, S. M., and Bonfield, W. (1999). Chemical characterization of silicon-substituted hydroxyapatite. Journal of Biomedical Materials Research *44*, 422–428.

Gibson, I. R., Ke, S., Best, S. M., and Bonfield, W. (2001). Effect of powder characteristics on the sinterability of hydroxyapatite powders. Journal of Materials Science: Materials in Medicine *12*, 163–171.

Gibson, I. R., Huang, J., Best, S. M., and Bonfield, W. (1999). Enhanced in vitro cell activity and surface apatite layer formation on novel silicon-substituted hydroxyapatites.

Gibson, I.R., Hing, K.A., Revell, P.A., Santos, J.D., Best, S.M., and Bonfield, W. (2002). Enhanced In Vivo Response to Silicate-Substituted Hydroxyapatite. Key Engineering Materials *218-220*, 203–206.

Glorieux, F.H. (2005). Caffey disease: an unlikely collagenopathy. The Journal of Clinical Investigation *115*, 1142–1144.

Goldstein, J., Newbury, D.E., Joy, D.C., Lyman, C.E., Echlin, P., Lifshin, E., Sawyer, L., and Michael, J.R. (2003). Scanning electron microscopy and X-ray microanalysis (Springer).

Golub, E.E., and Boesze-Battaglia, K. (2007). The role of alkaline phosphatase in mineralization. Current Opinion in Orthopaedics *18*.

Gordon, D. (1995). Spectroscopic techniques. Principles and Techniques in Practical Biochemistry, Edited by K. Wilson and J. Walker, Cambridge University Press, Cambridge.

Greenfield, N.J. (2007). Using circular dichroism spectra to estimate protein secondary structure. Nature Protocols *1*, 2876–2890.

Grinnell, F., and Feld, M.K. (1982). Fibronectin adsorption on hydrophilic and hydrophobic surfaces detected by antibody binding and analyzed during cell adhesion in serum-containing medium. J. Biol. Chem. *257*, 4888–4893.

Groessner-Schreiber, B., and Tuan, R.S. (1992). Enhanced extracellular matrix production and mineralization by osteoblasts cultured on titanium surfaces in vitro. Journal of Cell Science *101*, 209–217.

Gugala, Z., and Gogolewski, S. (2004). Protein adsorption, attachment, growth and activity of primary rat osteoblasts on polylactide membranes with defined surface characteristics. Biomaterials *25*, 2341 – 2351.

Gullberg, B., Johnell, O., and Kanis, J. (1997). World-wide projections for hip fracture. Osteoporosis International *7*, 407–413.

Guth, K., Buckland, T., and Hing, K.A. (2006). Silicon dissolution from microporous silicon substituted hydroxyapatite and its effect on osteoblast behaviour. Key Engineering Materials *309*, 117–120.

Guth, K., Campion, C., Buckland, T., and Hing, K.A. (2010a). Effect of Silicate-Substitution on Attachment and Early Development of Human Osteoblast-Like Cells Seeded on Microporous Hydroxyapatite Discs. Advanced Engineering Materials *12*, B26–B36.

Guth, K., Campion, C., Buckland, T., and Hing, K.A. (2010b). Surface Physiochemistry Affects Protein Adsorption to Stoichiometric and Silicate-Substituted Microporous Hydroxyapatites. Advanced Engineering Materials *12*, B113–B121.

Guth, K., Campion, C., Buckland, T., and Hing, K.A. (2011). Effects of serum protein on ionic exchange between culture medium and microporous hydroxyapatite and silicate-substituted hydroxyapatite. Journal of Materials Science: Materials in Medicine *22*, 2155–2164.

Hämmerle, C.H., Olah, A.J., Schmid, J., Gogolewski, S., Winkler, J.R., Lang, N.P., and others (1997). The biological effect of natural bone mineral on bone neoformation on the rabbit skull. Clinical Oral Implants Research *8*, 198–207.

Hanein, D., Geiger, B., and Addadi, L. (1993). Fibronectin adsorption to surfaces of hydrated crystals. An analysis of the importance of bound water in protein-substrate interactions. Langmuir *9*, 1058–1065.

Harlow, E., and Lane, D. (1988). Antibodies: a laboratory manual (Cold Spring Harbor Laboratory).

Hayashi, K., Inadome, T., Tsumura, H., Nakashima, Y., and Sugioka, Y. (1994). Effect of surface roughness of hydroxyapatite—coated titanium on the bone-implant interface shear strength. Biomaterials *15*, 1187–1191.

Haynes, C.A., and Norde, W. (1994). Globular proteins at solid/liquid interfaces. Colloids and Surfaces B: Biointerfaces *2*, 517–566.

Hench, L.L. (1998). Bioactive materials: the potential for tissue regeneration. Journal of Biomedical Materials Research *41*, 511–518.

Hench, L.L., and Wilson, J. (1993). An introduction to bioceramics (World Scientific).

Hennessy, K.M., Pollot, B.E., Clem, W.C., Phipps, M.C., Sawyer, A.A., Culpepper, B.K., and Bellis, S.L. (2009). The effect of collagen I mimetic peptides on mesenchymal stem cell adhesion and differentiation, and on bone formation at hydroxyapatite surfaces. Biomaterials *30*, 1898–1909.

Hersel, U., Dahmen, C., and Kessler, H. (2003). RGD modified polymers: biomaterials for stimulated cell adhesion and beyond. Biomaterials *24*, 4385–4415.

Hing, C. (2008). Encouraging Nature with Ceramics: The roles of surface roughness and physio-chemistry on cell response to substituted apatites. Advances in Science and Technology *57*, 22–30.

Hing, K., Gibson, I., Di-Silvio, L., Best, S., and Bonfield, W. (1998). Effect of variation in Ca: P ratio on cellular response of primary human osteoblast-like cells to hydroxyapatite-based ceramics. In BIOCERAMICS-CONFERENCE-, pp. 293–296.

Hing, K., Best, S., and Bonfield, W. (1999). Characterization of porous hydroxyapatite. Journal of Materials Science: Materials in Medicine *10*, 135–145.

Hing, K.A., Saeed, S., Annaz, B., Buckland, T., and Revell, P.A. (2004). Microporosity Affects Bioactivity of Macroporous Hydroxyapatite Bone Graft Substitutes. Key Engineering Materials *254-256*, 273–276.

Hing, K.A., Annaz, B., Saeed, S., Revell, P.A., and Buckland, T. (2005). Microporosity enhances bioactivity of synthetic bone graft substitutes. J Mater Sci: Mater Med *16*, 467–475.

Hing, K.A., Revell, P.A., Smith, N., and Buckland, T. (2006). Effect of silicon level on rate, quality and progression of bone healing within silicate-substituted porous hydroxyapatite scaffolds. Biomaterials *27*, 5014 – 5026.

Hing, K.A., Wilson, L.F., and Buckland, T. (2007). Comparative performance of three ceramic bone graft substitutes. The Spine Journal *7*, 475 – 490.

Hoang, Q.Q., Sicheri, F., Howard, A.J., and Yang, D.S.C. (2003). Bone recognition mechanism of porcine osteocalcin from crystal structure. Nature *425*, 977–980.

Hock, J.M., CENTRELLA, M., and CANALIS, E. (1988). Insulin-Like Growth Factor I Has Independent Effects on Bone Matrix Formation and Cell Replication*. Endocrinology *122*, 254–260.

Hollinger, J.O., and Battistone, G.C. (1986). Biodegradable bone repair materials synthetic polymers and ceramics. Clinical Orthopaedics and Related Research *207*, 290–306.

Holmes, R., and Hagler, H. (1988). Porous hydroxyapatite as a bone graft substitute in maxillary augmentation: An histometric study. Journal of Cranio-Maxillofacial Surgery *16*, 199 – 205.

Horbett, T. (1996). Proteins: structure, properties, and adsorption to surfaces. Biomaterials Science: An Introduction to Materials in Medicine 133–141.

Horbett, T. (1999). The role of adsorbed adhesion proteins in cellular recognition of biomaterials. BMES Bull *23*, 5–9.

Horbett, T.A. (1994). The role of adsorbed proteins in animal cell adhesion. Colloids and Surfaces B: Biointerfaces *2*, 225–240.

Hormia, M., and Könönen, M. (1994). Immunolocalization of fibronectin and vitronectin receptors in human gingival fibroblasts spreading on titanium surfaces. Journal of Periodontal Research *29*, 146–152.

Hott, M., Noel, B., Bernache-Assolant, D., Rey, C., and Marie, P.J. (1997). Proliferation and differentiation of human trabecular osteoblastic cells on hydroxyapatite. Journal of Biomedical Materials Research *37*, 508–516.

Howlett, C.R., Evans, M.D.M., Walsh, W.R., Johnson, G., and Steele, J.G. (1994). Mechanism of initial attachment of cells derived from human bone to commonly used prosthetic materials during cell culture. Biomaterials *15*, 213 – 222.

Hynes, R.O. (1990). Fibronectins (Springer-Verlag).

Ikeuchi, M., Ito, A., Dohi, Y., Ohgushi, H., Shimaoka, H., Yonemasu, K., and Tateishi, T. (2003). Osteogenic differentiation of cultured rat and human bone marrow cells on the surface of zinc-releasing calcium phosphate ceramics. Journal of Biomedical Materials Research Part A *67*, 1115–1122.

Israelachvili, J., and Wennerström, H. akan (1996). Role of hydration and water structure in biological and colloidal interactions.

Itoh, D., Yoneda, S., Kuroda, S., Kondo, H., Umezawa, A., Ohya, K., Ohyama, T., and Kasugai, S. (2002). Enhancement of osteogenesis on hydroxyapatite surface coated with

synthetic peptide (EEEEEEEPRGDT) in vitro. Journal of Biomedical Materials Research *62*, 292–298.

Iuliano, D.J., Saavedra, S.S., and Truskey, G.A. (1993). Effect of the conformation and orientation of adsorbed fibronectin on endothelial cell spreading and the strength of adhesion. J. Biomed. Mater. Res. *27*, 1103–1113.

Jalota, S., Bhaduri, S.B., and Tas, A.C. (2006). In vitro testing of calcium phosphate (HA, TCP, and biphasic HA-TCP) whiskers. Journal of Biomedical Materials Research Part A *78*, 481–490.

James, J., and Tanke, H. (1991). Fluorescence microscopy. In Biomedical Light Microscopy, (Springer), pp. 50–66.

Jarcho, M. (1981). Calcium phosphate ceramics as hard tissue prosthetics. Clinical Orthopaedics and Related Research *157*, 259–278.

Jarcho, M., Bolen, C.H., Thomas, M.B., Bobick, J., Kay, J.F., and Doremus, R.H. (1976). Hydroxylapatite synthesis and characterization in dense polycrystalline form. Journal of Materials Science *11*, 2027–2035.

Jha, L., Best, S. M., Knowles, J. C., Rehman, I., SANTOS, J. D., and Bonfield, W. (1997). Preparation and characterization of fluoride-substituted apatites. Journal of Materials Science: Materials in Medicine *8*, 185–191.

Johnell, O., and Kanis, J. (2006). An estimate of the worldwide prevalence and disability associated with osteoporotic fractures. Osteoporosis International *17*, 1726–1733.

Jönsson, U., Ivarsson, B., Lundström, I., and Berghem, L. (1982). Adsorption behavior of fibronectin on well-characterized silica surfaces. Journal of Colloid and Interface Science *90*, 148–163.

Jørgensen, N.R., Teilmann, S.C., Henriksen, Z., Civitelli, R., Sørensen, O.H., and Steinberg, T.H. (2003). Activation of L-type calcium channels is required for gap junction-mediated intercellular calcium signaling in osteoblastic cells. Journal of Biological Chemistry *278*, 4082–4086.

Kanatani, M., Sugimoto, T., Fukase, M., and Fujita, T. (1991). Effect of elevated extracellular calcium on the proliferation of osteoblastic MC3T3-E1 cells: Its direct and indirect effects via monocytes. Biochemical and Biophysical Research Communications *181*, 1425 – 1430.

Kanis, J., and Johnell, O. (2005). Requirements for DXA for the management of osteoporosis in Europe. Osteoporosis International *16*, 229–238.

Kanis, J., Group, W.H.O.S., and others (2007). WHO technical report. University of Sheffield, UK *66*.

Karageorgiou, V., and Kaplan, D. (2005). Porosity of 3D biomaterial scaffolds and osteogenesis. Biomaterials *26*, 5474–5491.

Kikuchi, M., Ikoma, T., Itoh, S., Matsumoto, H.N., Koyama, Y., Takakuda, K., Shinomiya, K., and Tanaka, J. (2004). Biomimetic synthesis of bone-like nanocomposites using the self-organization mechanism of hydroxyapatite and collagen. Composites Science and Technology *64*, 819 – 825.

Kilpadi, K.L., Chang, P.L., and Bellis, S.L. (2001). Hydroxylapatite binds more serum proteins, purified integrins, and osteoblast precursor cells than titanium or steel. J. Biomed. Mater. Res. *57*, 258–267.

Klawitter, J., and Hulbert, S. (1971). Application of porous ceramics for the attachment of load bearing internal orthopedic applications. Journal of Biomedical Materials Research *5*, 161–229.

Klebe, R.J., Bentley, K.L., and Schoen, R.C. (1981). Adhesive substrates for fibronectin. J. Cell. Physiol. *109*, 481–488.

Klein, C., Driessen, A., De Groot, K., and Van Den Hooff, A. (1983). Biodegradation behavior of various calcium phosphate materials in bone tissue. Journal of Biomedical Materials Research *17*, 769–784.

Klein, C., Groot, K. de, Chen, W., Li, Y., and Zhang, X. (1994). Osseous substance formation induced in porous calcium phosphate ceramics in soft tissues. Biomaterials *15*, 31 – 34.

Klokkevold, P.R., Nishimura, R.D., Adachi, M., and Caputo, A. (1997). Osseointegration enhanced by chemical etching of the titanium surface. A torque removal study in the rabbit. Clinical Oral Implants Research *8*, 442–447.

Kohri, M., Miki, K., Waite, D.E., Nakajima, H., and Okabe, T. (1993). < i> In vitro</i> stability of biphasic calcium phosphate ceramics. Biomaterials *14*, 299–304.

Koole, R. (1994). Ectomesenchymal mandibular symphysis bone graft: an improvement in alveolar cleft grafting? The Cleft Palate-Craniofacial Journal *31*, 217–223.

Korovessis, P.G., and Deligianni, D.D. (2002). Role of surface roughness of titanium versus hydroxyapatite on human bone marrow cells response. Journal of Spinal Disorders & Techniques *15*, 175–183.

Kurtz, S.M., Ong, K.L., Schmier, J., Mowat, F., Saleh, K., Dybvik, E., Kärrholm, J., Garellick, G., Havelin, L.I., Furnes, O., et al. (2007). Future Clinical and Economic Impact of Revision Total Hip and Knee Arthroplasty. The Journal of Bone & Joint Surgery *89*, 144–151.

Kwon, S.-H., Jun, Y.-K., Hong, S.-H., Lee, I.-S., Kim, H.-E., and Won, Y.Y. (2002). Calcium phosphate bioceramics with various porosities and dissolution rates. Journal of The American Ceramic Society *85*, 3129–3131.

Kwon, S.-H., Jun, Y.-K., Hong, S.-H., and Kim, H.-E. (2003). Synthesis and dissolution behavior of β-TCP and HA/β-TCP composite powders. Journal of the European Ceramic Society *23*, 1039–1045.

L D Buttery, S.B. (2001). Differentiation of osteoblasts and in vitro bone formation from murine embryonic stem cells. Tissue Engineering *7*, 89–99.

Lakowicz, J.R. (2007). Principles of fluorescence spectroscopy (Springer).

Lampin, M., Warocquier-Clérout, R., Legris, C., Degrange, M., and Sigot-Luizard, M.F. (1997). Correlation between substratum roughness and wettability, cell adhesion, and cell migration. Journal of Biomedical Materials Research *36*, 99–108.

Landis, W. (1995). The strength of a calcified tissue depends in part on the molecular structure and organization of its constituent mineral crystals in their organic matrix. Bone *16*, 533–544.

Lane, J.M., Tomin, E., and Bostrom, M.P. (1999). Biosynthetic bone grafting. Clinical Orthopaedics and Related Research *367*, S107–S117.

LC, H., and M, S. (2004). CLinical implications of the osteoprotegerin/rankl/rank system for bone and vascular diseases. JAMA *292*, 490–495.

Lee, A.J., Hodges, S., Eastell, R., and others (2000). Measurement of osteocalcin. Annals of Clinical Biochemistry *37*, 432–446.

Lee, J.-H., Um, S., Jang, J.-H., and Seo, B.M. (2012). Effects of VEGF and FGF-2 on proliferation and differentiation of human periodontal ligament stem cells. Cell and Tissue Research *348*, 475–484.

Lee, N.K., Sowa, H., Hinoi, E., Ferron, M., Ahn, J.D., Confavreux, C., Dacquin, R., Mee, P.J., McKee, M.D., Jung, D.Y., et al. (2007). Endocrine regulation of energy metabolism by the skeleton. Cell *130*, 456–469.

LeGeros, R.Z. (1994). Biological and synthetic apatites. Hydroxyapatite and Related Materials”; BocaRaton: CRC Pres.

Lewandowska, K., Balachander, N., Sukenik, C.N., and Culp, L.A. (1989). Modulation of fibronectin adhesive functions for fibroblasts and neural cells by chemically derivatized substrata. Journal of Cellular Physiology *141*, 334–345.

Lietman, S.A., Tomford, W.W., Gebhardt, M.C., Springfield, D.S., and Mankin, H.J. (2000). Complications of irradiated allografts in orthopaedic tumor surgery. Clinical Orthopaedics and Related Research *375*, 214–217.

Lin, L., Chow, K.L., and Leng, Y. (2009). Study of hydroxyapatite osteoinductivity with an osteogenic differentiation of mesenchymal stem cells. Journal of Biomedical Materials Research Part A *89A*, 326–335.

Lindsay, R., Cosman, F., Zhou, H., Bostrom, M.P., Shen, V.W., Cruz, J.D., Nieves, J.W., and Dempster, D.W. (2006). A Novel Tetracycline Labeling Schedule for Longitudinal Evaluation of the Short-Term Effects of Anabolic Therapy With a Single Iliac Crest Bone Biopsy: Early Actions of Teriparatide. Journal of Bone and Mineral Research *21*, 366–373.

Liu, X.S., Ardeshirpour, L., VanHouten, J.N., Shane, E., and Wysolmerski, J.J. (2012). Site-specific changes in bone microarchitecture, mineralization, and stiffness during lactation and after weaning in mice. Journal of Bone and Mineral Research *27*, 865–875.

Locklin, R.M., Oreffo, R.O., and Triffitt, J.T. (1999). Effects of TGFβ and bFGF on the differentiation of human bone marrow stromal fibroblasts. Cell Biology International *23*, 185–194.

De LongJr, W.G., Einhorn, T.A., Koval, K., McKee, M., Smith, W., Sanders, R., and Watson, T. (2007). Bone grafts and bone graft substitutes in orthopaedic trauma surgeryA critical analysis. The Journal of Bone & Joint Surgery *89*, 649–658.

Lutolf, M., and Hubbell, J. (2005). Synthetic biomaterials as instructive extracellular microenvironments for morphogenesis in tissue engineering. Nature Biotechnology *23*, 47–55.

MacDonald, D., Deo, N., Markovic, B., Stranick, M., and Somasundaran, P. (2002). Adsorption and dissolution behavior of human plasma fibronectin on thermally and chemically modified titanium dioxide particles. Biomaterials *23*, 1269–1279.

Mackie, E.J., Ahmed, Y.A., Tatarczuch, L., Chen, K.-S., and Mirams, M. (2008). Endochondral ossification: How cartilage is converted into bone in the developing skeleton. The International Journal of Biochemistry & Cell Biology *40*, 46 – 62.

Mafina, M.-K., Hing, K.A., and Sullivan, A.C. (2013). Development of Novel Fluorescent Probes for the Analysis of Protein Interactions under Physiological Conditions with Medical Devices. Langmuir *29*, 1420–1426.

Magan, A., and Ripamonti, U. (1996). Geometry of porous hydroxyapatite implants influences osteogenesis in baboons (Papio ursinus). JOURNAL OF CRANIOFACIAL SURGERY *7*, 71–78.

Manavalan, P., and Johnson Jr, W.C. (1987). Variable selection method improves the prediction of protein secondary structure from circular dichroism spectra. Analytical Biochemistry *167*, 76–85.

Maniatopoulos, C., Sodek, J., and Melcher, D.A.H. (1988). Bone formation in vitro by stromal cells obtained from bone marrow of young adult rats. Cell Tissue Res. *254*, 317–330.

Manjubala, I., Sivakumar, M., Sureshkumar, R.V., and Sastry, T.P. (2002). Bioactivity and osseointegration study of calcium phosphate ceramic of different chemical composition. Journal of Biomedical Materials Research *63*, 200–208.

Martin, T.J., and Sims, N.A. (2005). Osteoclast-derived activity in the coupling of bone formation to resorption. Trends in Molecular Medicine *11*, 76–81.

Martin, J.Y., Schwartz, Z., Hummert, T.W., Schraub, D.M., Simpson, J., Lankford, J., Dean, D.D., Cochran, D.L., and Boyan, B.D. (1995). Effect of titanium surface roughness on proliferation, differentiation, and protein synthesis of human osteoblast-like cells (MG63). Journal of Biomedical Materials Research *29*, 389–401.

Matsuoka, H., Akiyama, H., Okada, Y., Ito, H., Shigeno, C., Konishi, J., Kokubo, T., and Nakamura, T. (1999). In vitro analysis of the stimulation of bone formation by highly bioactive apatite-and wollastonite-containing glass-ceramic: Released calcium ions promote osteogenic differentiation in osteoblastic ROS17/2.8 cells. Journal of Biomedical Materials Research *47*, 176–188.

Matsuura, T., Hosokawa, R., Okamoto, K., Kimoto, T., and Akagawa, Y. (2000). Diverse mechanisms of osteoblast spreading on hydroxyapatite and titanium. Biomaterials *21*, 1121–1127.

McFarland, C.D., Thomas, C.H., DeFilippis, C., Steele, J.G., and Healy, K.E. (2000). Protein adsorption and cell attachment to patterned surfaces. Journal of Biomedical Materials Research *49*, 200–210.

Meeder, P.-J., and Eggers, C. (1994). 1. The history of autogenous bone grafting. Injury *25*, SA2–SA4.

Michael, K.E., Vernekar, V.N., Keselowsky, B.G., Meredith, J.C., Latour, R.A., and García, A.J. (2003). Adsorption-induced conformational changes in fibronectin due to interactions with well-defined surface chemistries. Langmuir *19*, 8033–8040.

Missirlis, D. (2000). Effect of surface roughness of hydroxyapatite on human bone marrow cell adhesion, proliferation, di!erentiation and detachment strength. Biomaterials *22*, 87–96.

Moore, W.R., Graves, S.E., and Bain, G.I. (2001). Synthetic bone graft substitutes. ANZ Journal of Surgery *71*, 354–361.

Mosher, D., and Williams, E. (1978). Fibronectin concentration is decreased in plasma of severely ill patients with disseminated intravascular coagulation. The Journal of Laboratory and Clinical Medicine *91*, 729–735.

Mu, P., and Plummer, D.T. (1988). Introduction to practical biochemistry (Tata McGraw-Hill Education).

Müller-Mai, C., Voigt, C., Gross, U., and others (1990). Incorporation and degradation of hydroxyapatite implants of different surface roughness and surface structure in bone. Scanning Microscopy *4*, 613.

Murugan, R., and Ramakrishna, S. (2005). Development of nanocomposites for bone grafting. Composites Science and Technology *65*, 2385 – 2406.

Mygind, T., Stiehler, M., Baatrup, A., Li, H., Zou, X., Flyvbjerg, A., Kassem, M., and Bünger, C. (2007). Mesenchymal stem cell ingrowth and differentiation on coralline hydroxyapatite scaffolds. Biomaterials *28*, 1036–1047.

Nafie, L.A., Keiderling, T., and Stephens, P. (1976). Vibrational circular dichroism. Journal of the American Chemical Society *98*, 2715–2723.

Nakagawa, M., Kaneda, T., Arakawa, T., Morita, S., Sato, T., Yomada, T., Hanada, K., Kumegawa, M., and Hakeda, Y. (2000). Vascular endothelial growth factor (VEGF) directly enhances osteoclastic bone resorption and survival of mature osteoclasts. FEBS Letters *473*, 161–164.

Ng, A.M., Tan, K., Phang, M., Aziyati, O., Tan, G., Isa, M., Aminuddin, B., Naseem, M., Fauziah, O., and Ruszymah, B. (2008). Differential osteogenic activity of osteoprogenitor cells on HA and TCP/HA scaffold of tissue engineered bone. Journal of Biomedical Materials Research Part A *85*, 301–312.

Norde, W. (1996). Driving forces for protein adsorption at solid surfaces. (Wiley Online Library), pp. 5–18.

Norde, W., and Giacomelli, C.E. (1999). Conformational changes in proteins at interfaces: from solution to the interface, and back. (Wiley Online Library), pp. 125–136.

Norde, W., and Giacomelli, C.E. (2000). BSA structural changes during homomolecular exchange between the adsorbed and the dissolved states. Journal of Biotechnology *79*, 259–268.

Ohura, K., Nakamura, T., Yamamuro, T., Kokubo, T., Ebisawa, Y., Kotoura, Y., and Oka, M. (1991). Bone-bonding ability of P2O5-Free CaO· SiO2 glasses. Journal of Biomedical Materials Research *25*, 357–365.

OIKARINEN, J., and KORHONEN, L.K. (1979). The bone inductive capacity of various bone transplanting materials used for treatment of experimental bone defects. Clinical Orthopaedics and Related Research *140*, 208–215.

OKLUND, S.A., PROLO, D.J., GUTIERREZ, R.V., and KING, S.E. (1986). Quantitative comparisons of healing in cranial fresh autografts, frozen autografts and processed

autografts, and allografts in canine skull defects. Clinical Orthopaedics and Related Research *205*, 269–291.

Olivares-Navarrete, R., Gittens, R.A., Schneider, J.M., Hyzy, S.L., Haithcock, D.A., Ullrich, P.F., Schwartz, Z., and Boyan, B.D. (2012). Osteoblasts exhibit a more differentiated phenotype and increased bone morphogenetic protein production on titanium alloy substrates than on poly-ether-ether-ketone. The Spine Journal *12*, 265 – 272.

Olkarinen, J., and Korhonen, L.K. (1979). Repair of bone defects by bone inductive material. Acta Orthopaedica *50*, 21–26.

Oonishi, H. (1991). Orthopaedic applications of hydroxyapatite. Biomaterials *12*, 171 – 178.

Owen, T.A., ARONOW, M.S., Barone, L.M., BETTENCOURT, B., Stein, G.S., and Lian, J.B. (1991). Pleiotropic Effects of Vitamin D on Osteoblast Gene Expression Are Related to the Proliferative and Differentiated State of the Bone Cell Phenotype: Dependency upon Basal Levels of Gene Expression, Duration of Exposure, and Bone Matrix Competency in Normal Rat Osteoblast Cultures*. Endocrinology *128*, 1496–1504.

Palastanga, N., Field, D., and Soames, R. (2006). Anatomy and human movement: structure and function (Elsevier Health Sciences).

Paolella, G., Barone, M., and Baralle, F. (1993). Fibronectin. Extracellular Matrix. Chemistry, Biology and Pathobiology with Emphasis on the Liver," Zern, MA, and Reid, LM (eds). New York: Marcel Dekker 3–24.

Parfitt, A. (2002). Targeted and nontargeted bone remodeling: relationship to basic multicellular unit origination and progression. Bone *30*, 5–7.

Park, J., and Lakes, R.S. (2007). Biomaterials: an introduction (Springer).

Patel, N., Best, S., Bonfield, W., Gibson, I., Hing, K., Damien, E., and Revell, P. (2002). A comparative study on the in vivo behavior of hydroxyapatite and silicon substituted hydroxyapatite granules. Journal of Materials Science: Materials in Medicine *13*, 1199–1206.

Pendegrass, C.J., El-Husseiny, M., and Blunn, G.W. (2012). The development of fibronectin-functionalised hydroxyapatite coatings to improve dermal fibroblast attachment in vitro. J Bone Joint Surg Br *94-B*, 564–569.

Pittenger, M.F., Mackay, A.M., Beck, S.C., Jaiswal, R.K., Douglas, R., Mosca, J.D., Moorman, M.A., Simonetti, D.W., Craig, S., and Marshak, D.R. (1999). Multilineage potential of adult human mesenchymal stem cells. Science *284*, 143–147.

Pockwinse, S.M., Wilming, L.G., Conlon, D.M., Stein, G.S., and Lian, J.B. (1992). Expression of cell growth and bone specific genes at single cell resolution during

development of bone tissue-like organization in primary osteoblast cultures. Journal of Cellular Biochemistry *49*, 310–323.

Porter, A.E. (2006). Nanoscale characterization of the interface between bone and hydroxyapatite implants and the effect of silicon on bone apposition. Micron *37*, 681–688.

Porter, A.E., Best, S.M., and Bonfield, W. (2004). Ultrastructural comparison of hydroxyapatite and silicon-substituted hydroxyapatite for biomedical applications. Journal of Biomedical Materials Research Part A *68A*, 133–141.

Potts, J.R., and Campbell, I.D. (1994). Fibronectin structure and assembly. Current Opinion in Cell Biology *6*, 648–655.

Provencher, S.W., and Gloeckner, J. (1981). Estimation of globular protein secondary structure from circular dichroism. Biochemistry *20*, 33–37.

Qing, H., Ardeshirpour, L., Divieti Pajevic, P., Dusevich, V., Jähn, K., Kato, S., Wysolmerski, J., and Bonewald, L.F. (2012). Demonstration of osteocytic perilacunar/canalicular remodeling in mice during lactation. Journal of Bone and Mineral Research *27*, 1018–1029.

Rabie, A. (1997). Vascular endothelial growth pattern during demineralized bone matrix induced osteogenesis. Connective Tissue Research *36*, 337–345.

Rabie, A., and Hägg, U. (2002). Factors regulating mandibular condylar growth. American Journal of Orthodontics and Dentofacial Orthopedics *122*, 401–409.

Rabie, A., Dai, J., and Xu, R. (2007). Recombinant AAV-mediated VEGF gene therapy induces mandibular condylar growth. Gene Therapy *14*, 972–980.

Rashid, N., Harding, I.S., Buckland, T., and Hing, K.A. (2008). Nano-scale manipulation of silicate-substituted apatite chemistry impacts surface charge, hydrophilicity, protein adsorption and cell attachment. International Journal of Nano and Biomaterials *1*, 299–319.

RAY, R.D., and WARD Jr., A.A. (1951). A preliminary report on studies of basic calcium phosphate in bone replacement. Surgical Forum 429–434.

Reffitt, D.M., Ogston, N., Jugdaohsingh, R., Cheung, H.F.J., Evans, B.A.J., Thompson, R.P.H., Powell, J.J., and Hampson, G.N. (2003). Orthosilicic acid stimulates collagen type 1 synthesis and osteoblastic differentiation in human osteoblast-like cells in vitro. Bone *32*, 127–135.

Reid, J.W., Pietak, A., Sayer, M., Dunfield, D., and Smith, T.J.N. (2005). Phase formation and evolution in the silicon substituted tricalcium phosphate/apatite system. Biomaterials *26*, 2887 – 2897.

Riddle, D. (2006). Coral Coloration: Fluorescence: Part 1. Advanced Aquarist Magazine Online [serial Conline] *5*.

Riva, B.D. la, Sánchez, E., Hernández, A., Reyes, R., Tamimi, F., López-Cabarcos, E., Delgado, A., and Évora, C. (2010). Local controlled release of {VEGF} and {PDGF} from a combined brushite–chitosan system enhances bone regeneration. Journal of Controlled Release *143*, 45 – 52.

ROBINSON, R.A. (1952). An electron-microscopic study of the crystalline inorganic component of bone and its relationship to the organic matrix. The Journal of Bone & Joint Surgery *34*, 389–476.

Rochow, T.G., and Tucker, P.A. (1994). Introduction to microscopy by means of light, electrons, X-rays, or acoustics (Springer).

Roessler, S., Born, R., Scharnweber, D., Worch, H., Sewing, A., and Dard, M. (2001). Biomimetic coatings functionalized with adhesion peptides for dental implants. Journal of Materials Science: Materials in Medicine *12*, 871–877.

Roodman, G.D. (1999). Cell biology of the osteoclast. Experimental Hematology *27*, 1229–1241.

Rouahi, M., Gallet, O., Champion, E., Dentzer, J., Hardouin, P., and Anselme, K. (2006). Influence of hydroxyapatite microstructure on human bone cell response. Journal of Biomedical Materials Research Part A *78A*, 222–235.

Royer, A., Viguie, J., Heughebaert, M., and Heughebaert, J. (1993). Stoichiometry of hydroxyapatite: influence on the flexural strength. Journal of Materials Science: Materials in Medicine *4*, 76–82.

Rubin, C.T., and Lanyon, L.E. (1987). Osteoregulatory nature of mechanical stimuli: function as a determinant for adaptive remodeling in bone. Journal of Orthopaedic Research *5*, 300–310.

Rupp, H., and Weser, U. (1978). Circular dichroism of metallothioneins: a structural approach. Biochimica et Biophysica Acta (BBA)-Protein Structure *533*, 209–226.

Saadeh, P.B., Mehrara, B.J., Steinbrech, D.S., Dudziak, M.E., Greenwald, J.A., Luchs, J.S., Spector, J.A., Ueno, H., Gittes, G.K., and Longaker, M.T. (1999). Transforming growth factor-β1 modulates the expression of vascular endothelial growth factor by osteoblasts. American Journal of Physiology-Cell Physiology *277*, C628–C637.

Sanan, A., and Haines, S.J. (1997). Repairing holes in the head: a history of cranioplasty. Neurosurgery *40*, 588–603.

Dos Santos, E., Farina, M., Soares, G., and Anselme, K. (2008). Surface energy of hydroxyapatite and β-tricalcium phosphate ceramics driving serum protein adsorption and osteoblast adhesion. Journal of Materials Science: Materials in Medicine *19*, 2307–2316.

Sawyer, A.A., Hennessy, K.M., and Bellis, S.L. (2005). Regulation of mesenchymal stem cell attachment and spreading on hydroxyapatite by RGD peptides and adsorbed serum proteins. Biomaterials *26*, 1467–1475.

Schönmeyr, B.H., Wong, A.K., Li, S., Gewalli, F., Cordiero, P.G., and Mehrara, B.J. (2008). Treatment of Hydroxyapatite Scaffolds with Fibronectin and Fetal Calf Serum Increases Osteoblast Adhesion and Proliferation In Vitro. Plastic and Reconstructive Surgery *121*.

Schwartz, Z., Martin, J., Dean, D., Simpson, J., Cochran, D., and Boyan, B. (1996). Effect of titanium surface roughness on chondrocyte proliferation, matrix production, and differentiation depends on the state of cell maturation. Journal of Biomedical Materials Research *30*, 145–155.

Schwarz, K. (1974). Proceedings: Recent dietary trace element research, exemplified by tin, fluorone, and silicon. In Federation Proceedings, pp. 1748–1757.

Schwarz, K. (1978). Significance and functions of silicon in warm-blooded animals. Review and outlook. In Biochemistry of Silicon and Related Problems, (Springer), pp. 207–230.

Schwarz, K., and Milne, D.B. (1972). Growth-promoting effects of silicon in rats.

Schwarz, M., and Juliano, R. (1984). Surface activation of the cell adhesion fragment of fibronectin. Experimental Cell Research *153*, 550–555.

Scotchford, C.A., Cooper, E., Leggett, G.J., and Downes, S. (1998). Growth of human osteoblast-like cells on alkanethiol on gold self-assembled monolayers: The effect of surface chemistry. Journal of Biomedical Materials Research *41*, 431–442.

Scotchford, C.A., Gilmore, C.P., Cooper, E., Leggett, G.J., and Downes, S. (2002). Protein adsorption and human osteoblast-like cell attachment and growth on alkylthiol on gold self-assembled monolayers. Journal of Biomedical Materials Research *59*, 84–99.

Seitz, T.L., Noonan, K.D., Hench, L.L., and Noonan, N.E. (1982). Effect of fibronectin on the adhesion of an established cell line to a surface reactive biomaterial. J. Biomed. Mater. Res. *16*, 195–207.

Sever, C., Uygur, F., Kose, G.T., Urhan, M., Haholu, A., Kulahci, Y., Sinan, O., Cihan, S., Omer, O., and others (2012). Prefabrication of vascularized bone graft using an interconnected porous calcium hydroxyapatite ceramic in presence of vascular endothelial growth factor and bone marrow mesenchymal stem cells: Experimental study in rats. Indian Journal of Plastic Surgery: Official Publication of the Association of Plastic Surgeons of India *45*, 444.

Siebers, M.., ter Brugge, P.., Walboomers, X.., and Jansen, J.. (2005). Integrins as linker proteins between osteoblasts and bone replacing materials. A critical review. Biomaterials *26*, 137–146.

Da Silva, M.H.P., Soares, G.D., Elias, C.N., Best, S.M., Gibson, I.R., DiSilvio, L., and Dalby, M.J. (2003). In vitro cellular response to titanium electrochemically coated with hydroxyapatite compared to titanium with three different levels of surface roughness. Journal of Materials Science: Materials in Medicine *14*, 511–519.

Silver, I., Murrills, R., and Etherington, D. (1988). Microelectrode studies on the acid microenvironment beneath adherent macrophages and osteoclasts. Experimental Cell Research *175*, 266–276.

Silverstone, L. (1974). Fissure sealants. Caries Research *8*, 2–26.

Simon, L., Krane, S., Wortman, P., Krane, I., and Kovitz, K. (1984). Serum Levels of Type I and III Procollagen Fragments in Paget's Disease of Bone*. The Journal of Clinical Endocrinology & Metabolism *58*, 110–120.

Singer, I.I., Scott, S., Kawka, D.W., Kazazis, D.M., Gailit, J., and Ruoslahti, E. (1988). Cell surface distribution of fibronectin and vitronectin receptors depends on substrate composition and extracellular matrix accumulation. J Cell Biol *106*, 2171–2182.

Smit, T.H., Burger, E.H., and Huyghe, J.M. (2002). A case for strain-induced fluid flow as a regulator of BMU-coupling and osteonal alignment. Journal of Bone and Mineral Research *17*, 2021–2029.

Sogo, Y., Ito, A., Matsuno, T., Oyane, A., Tamazawa, G., Satoh, T., Yamazaki, A., Uchimura, E., and Ohno, T. (2007). Fibronectin-calcium phosphate composite layer on hydroxyapatite to enhance adhesion, cell spread and osteogenic differentiation of human mesenchymal stem cells in vitro. Biomed Mater *2*, 116–123.

Sreerama, N., and Woody, R.W. (1994). Poly (Pro) II helixes in globular proteins: Identification and circular dichroic analysis. Biochemistry *33*, 10022–10025.

Sreerama, N., Venyaminov, S.Y., and Woody, R.W. (2000). Estimation of protein secondary structure from circular dichroism spectra: inclusion of denatured proteins with native proteins in the analysis. Analytical Biochemistry *287*, 243–251.

Sreerama, N., Yu Venyaminov, S., and Woody, R.W. (2001). Analysis of protein circular dichroism spectra based on the tertiary structure classification. Analytical Biochemistry *299*, 271–274.

Van Staa, T., Dennison, E., Leufkens, H., and Cooper, C. (2001). Epidemiology of fractures in England and Wales. Bone *29*, 517–522.

Stanford, C., Keller, J., and Solursh, M. (1994). Bone cell expression on titanium surfaces is altered by sterilization treatments. Journal of Dental Research *73*, 1061–1071.

Steele, J.G., Dalton, B.A., Johnson, G., and Underwood, P.A. (1993). Polystyrene chemistry affects vitronectin activity: An explanation for cell attachment to tissue culture

polystyrene but not to unmodified polystyrene. Journal of Biomedical Materials Research *27*, 927–940.

Steele, J.G., Dalton, B., Johnson, G., and Underwood, P.A. (1995). Adsorption of fibronectin and vitronectin onto Primaria™ and tissue culture polystyrene and relationship to the mechanism of initial attachment of human vein endothelial cells and BHK-21 fibroblasts. Biomaterials *16*, 1057–1067.

Stephansson, S.N., Byers, B.A., and García, A.J. (2002). Enhanced expression of the osteoblastic phenotype on substrates that modulate fibronectin conformation and integrin receptor binding. Biomaterials *23*, 2527 – 2534.

Stokes, G.G. (1852). On the change of refrangibility of light. Philosophical Transactions of the Royal Society of London 463–562.

Van Straalen, J.P., Sanders, E., Prummel, M.F., and Sanders, G.T. (1991). Bone-alkaline phosphatase as indicator of bone formation. Clinica Chimica Acta *201*, 27–33.

Strong, D.M., Friedlaender, G.E., Tomford, W.W., Springfield, D.S., Shives, T.C., Burchardt, H., Enneking, W., and Mankin, H.J. (1996). Immunologic responses in human recipients of osseous and osteochondral allografts. Clinical Orthopaedics and Related Research *326*, 107–114.

Sugimoto, T., Kanatani, M., Kano, J., Kaji, H., Tsukamoto, T., Yamaguchi, T., Fukase, M., and Chihara, K. (1993). Effects of high calcium concentration on the functions and interactions of osteoblastic cells and monocytes and on the formation of osteoclast-like cells. Journal of Bone and Mineral Research *8*, 1445–1452.

Sulaiman, S.B., Keong, T.K., Cheng, C.H., Saim, A.B., and Idrus, R.B.H. (2013). Tricalcium phosphate/hydroxyapatite (TCP-HA) bone scaffold as potential candidate for the formation of tissue engineered bone. The Indian Journal of Medical Research *137*, 1093.

Taichman, R.S. (2005). Blood and bone: two tissues whose fates are intertwined to create the hematopoietic stem-cell niche. Blood *105*, 2631–2639.

Teitelbaum, S.L., Abu-Amer, Y., and Ross, F.P. (1995). Molecular mechanisms of bone resorption. Journal of Cellular Biochemistry *59*, 1–10.

Thomas, K.A. (1996). Vascular endothelial growth factor, a potent and selective angiogenic agent. Journal of Biological Chemistry *271*, 603–606.

Thomas, C.H., McFarland, C.D., Jenkins, M.L., Rezania, A., Steele, J.G., and Healy, K.E. (1997). The role of vitronectin in the attachment and spatial distribution of bone-derived cells on materials with patterned surface chemistry. Journal of Biomedical Materials Research *37*, 81–93.

Tomford, W., Malinin, T., Moore, T., Rodrigo, J., Strobos, J., and Woodcock, J. (1995). Symposium: Current concepts and controversies in tissue banking. Contemporary Orthopaedics *30*, 349–361.

Tortora, G.J., and Derrickson, B.H. (2008). Principles of anatomy and physiology (John Wiley & Sons).

Toth, J., Lynch, K., and Hackbarth, D. (1993). Ceramic-induced osteogenesis following subcutaneous implantation of calcium phosphates. Bioceramics *6*, 9–13.

Tracy, B.M., and Doremus, R.H. (1984). Direct electron microscopy studies of the bone—hydroxylapatite interface. Journal of Biomedical Materials Research *18*, 719–726.

Ubara, Y., Fushimi, T., Tagami, T., Sawa, N., Hoshino, J., Yokota, M., Katori, H., Takemoto, F., and Hara, S. (2003). Histomorphometric features of bone in patients with primary and secondary hypoparathyroidism. Kidney International *63*, 1809–1816.

Ubara, Y., Tagami, T., Nakanishi, S., Sawa, N., Hoshino, J., Suwabe, T., Katori, H., Takemoto, F., Hara, S., and Takaichi, K. (2005). Significance of minimodeling in dialysis patients with adynamic bone disease. Kidney International *68*, 833–839.

Underwood, P.A., and Bennett, F.A. (1989). A comparison of the biological activities of the cell-adhesive proteins vitronectin and fibronectin. Journal of Cell Science *93*, 641–649.

Urist, M.R. (1965). Bone: formation by autoinduction. Science *150*, 893–899.

Vaananen, H., Zhao, H., Mulari, M., and Halleen, J.M. (2000). The cell biology of osteoclast function. Journal of Cell Science *113*, 377–381.

Vacanti, J.P., Morse, M.A., Saltzman, W.M., Domb, A.J., Perez-Atayde, A., and Langer, R. (1988). Selective cell transplantation using bioabsorbable artificial polymers as matrices. Journal of Pediatric Surgery *23*, 3–9.

Valeur, B., and Berberan-Santos, M.N. (2013). Molecular fluorescence: principles and applications (John Wiley & Sons).

Van Apeldoorn, A., Aksenov, Y., Stigter, M., Hofland, I., De Bruijn, J., Koerten, H., Otto, C., Greve, J., and Van Blitterswijk, C. (2005). Parallel high-resolution confocal Raman SEM analysis of inorganic and organic bone matrix constituents. Journal of The Royal Society Interface *2*, 39–45.

Vandiver, J., Dean, D., Patel, N., Bonfield, W., and Ortiz, C. (2005). Nanoscale variation in surface charge of synthetic hydroxyapatite detected by chemically and spatially specific high-resolution force spectroscopy. Biomaterials *26*, 271 – 283.

Vogler, E.A. (1998). Structure and reactivity of water at biomaterial surfaces. Advances in Colloid and Interface Science *74*, 69–117.

Vroman, L., and Adams, A.L. (1986). Adsorption of proteins out of plasma and solutions in narrow spaces. Journal of Colloid and Interface Science *111*, 391–402.

Van Wachem, P.B., Vreriks, C.M., Beugeling, T., Feijen, J., Bantjes, A., Detmers, J.P., and van Aken, W.G. (1987). The influence of protein adsorption on interactions of cultured human endothelial cells with polymers. Journal of Biomedical Materials Research *21*, 701–718.

Wada, T., Nakashima, T., Hiroshi, N., and Penninger, J.M. (2006). RANKL–RANK signaling in osteoclastogenesis and bone disease. Trends in Molecular Medicine *12*, 17 – 25.

Wakitani, S., Kimura, T., Hirooka, A., Ochi, T., Yoneda, M., Yasui, N., Owaki, H., and Ono, K. (1989). Repair of rabbit articular surfaces with allograft chondrocytes embedded in collagen gel. Journal of Bone & Joint Surgery, British Volume *71*, 74–80.

Wang, C., Duan, Y., Markovic, B., Barbara, J., Howlett, C.R., Zhang, X., and Zreiqat, H. (2004a). Phenotypic expression of bone-related genes in osteoblasts grown on calcium phosphate ceramics with different phase compositions. Biomaterials *25*, 2507–2514.

Wang, C.Y., Duan, Y.R., Markovic, B., Barbara, J., Rolfe Howlett, C., Zhang, X.D., and Zreiqat, H. (2004b). Quantitative analysis of osteoprotegerin and RANKL expression in osteoblast grown on different calcium phosphate ceramics. Key Engineering Materials *254*, 713–716.

Wang, D.S., Yamazaki, K., Nohtomi, K., Shizume, K., Ohsumi, K., Shibuya, M., Demura, H., and Sato, K. (1996). Increase of vascular endothelial growth factor mRNA expression by 1, 25-dihydroxyvitamin D3 in human osteoblast-like cells. Journal of Bone and Mineral Research *11*, 472–479.

Weiss, M.J., Henthorn, P.S., Lafferty, M.A., Slaughter, C., Raducha, M., and Harris, H. (1986). Isolation and characterization of a cDNA encoding a human liver/bone/kidney-type alkaline phosphatase. Proceedings of the National Academy of Sciences *83*, 7182–7186.

Whitmore, L., and Wallace, B. (2004). DICHROWEB, an online server for protein secondary structure analyses from circular dichroism spectroscopic data. Nucleic Acids Research *32*, W668–W673.

Whitmore, L., and Wallace, B.A. (2008). Protein secondary structure analyses from circular dichroism spectroscopy: methods and reference databases. Biopolymers *89*, 392–400.

Wilson, C.J., Clegg, R.E., Leavesley, D.I., and Pearcy, M.J. (2005). Mediation of biomaterial-cell interactions by adsorbed proteins: a review. Tissue Eng. *11*, 1–18.

Wise, D.L., Trantolo, D.J., Lewandrowski, K.-U., Gresser, J.D., Cattaneo, M.V., and Yaszemski, M.J. (2000). Biomaterials engineering and devices: human applications (Springer).

Wolff, J. (1870). Ueber die innere Architectur der Knochen und ihre Bedeutung für die Frage vom Knochenwachsthum. Archiv Für Pathologische Anatomie Und Physiologie Und Für Klinische Medicin *50*, 389–450.

Xia, L., Lin, K., Jiang, X., Xu, Y., Zhang, M., Chang, J., and Zhang, Z. (2013). Enhanced osteogenesis through nano-structured surface design of macroporous hydroxyapatite bioceramic scaffolds via activation of ERK and p38 MAPK signaling pathways. Journal of Materials Chemistry B *1*, 5403–5416.

Yamada, K.M., and Olden, K. (1978). Fibronectins—adhesive glycoproteins of cell surface and blood. Nature *275*, 179–184.

Yamagami, S., Kawashima, H., Tsuru, T., Yamagami, H., Kayagaki, N., Yagita, H., Okumura, K., and Gregerson, D. (1997). Role of Fas-Fas ligand interactions in the immunorejection of allogeneic mouse corneal transplants. TRANSPLANTATION *64*, 1107–1111.

Yang, Y., Cavin, R., and Ong, J.L. (2003). Protein adsorption on titanium surfaces and their effect on osteoblast attachment. Journal of Biomedical Materials Research Part A *67*, 344–349.

Yaszemski, M.J., Payne, R.G., Hayes, W.C., Langer, R., and Mikos, A.G. (1996). Evolution of bone transplantation: molecular, cellular and tissue strategies to engineer human bone. Biomaterials *17*, 175–185.

Yoshikawa, T., Ohgushi, H., Dohi, Y., and Davies, J.E. (1997). Viable bone formation in porous hydroxyapatite: marrow cell-derived in vitro bone on the surface of ceramics. Bio-Medical Materials and Engineering *7*, 49–58.

Young, R.W. (1963). 14 Nucleic Acids, Protein Synthesis and Bone. Clinical Orthopaedics and Related Research *26*, 147–160.

Young, R.A., and Spooner, S. (1970). Neutron diffraction studies of human tooth enamel. Archives of Oral Biology *15*, 47 – 63.

Yuan, H., Yang, Z., Li, Y., Zhang, X., De Bruijn, J.D., and De Groot, K. (1998). Osteoinduction by calcium phosphate biomaterials. Journal of Materials Science: Materials in Medicine *9*, 723–726.

Yuan, H., Kurashina, K., Bruijn, J.D. de, Li, Y., Groot, K. de, and Zhang, X. (1999). A preliminary study on osteoinduction of two kinds of calcium phosphate ceramics. Biomaterials *20*, 1799 – 1806.

Zheng, X., Huang, M., and Ding, C. (2000). Bond strength of plasma-sprayed hydroxyapatite/Ti composite coatings. Biomaterials *21*, 841 – 849.

Zhu, X.D., Fan, H.S., Xiao, Y.M., Li, D.X., Zhang, H.J., Luxbacher, T., and Zhang, X.D. (2009). Effect of surface structure on protein adsorption to biphasic calcium-phosphate ceramics in vitro and in vivo. Acta Biomaterialia *5*, 1311 – 1318.

Zreiqat, H., Evans, P., and Howlett, C.R. (1999). Effect of surface chemical modification of bioceramic on phenotype of human bone-derived cells. Journal of Biomedical Materials Research *44*, 389–396.

Zreiqat, H., Valenzuela, S.M., Nissan, B.B., Roest, R., Knabe, C., Radlanski, R.J., Renz, H., and Evans, P.J. (2005). The effect of surface chemistry modification of titanium alloy on signalling pathways in human osteoblasts. Biomaterials *26*, 7579–7586.

Zur Nieden, N.I., Kempka, G., and Ahr, H.J. (2003). In vitro differentiation of embryonic stem cells into mineralized osteoblasts. Differentiation *71*, 18–27.